UNIVERSITA' DEL SALENTO

Dipartimento di Fisica

Dottorato di Ricerca in Fisica

Tesi di Dottorato

GROUND COLLECTED PM:

MASS CONCENTRATION AND COMPOSITION

Tutore:
Ch.ma Prof.ssa M.R. Perrone

DOTTORANDA:
Ilaria Carofalo

XX CICLO

CONTENTS

INTRODUCTION

Atmospheric particles are a complex mixture of organic and inorganic substances, suspended in the atmosphere as both liquid and solid (Seinfeld and Pandis, 1998). Individual aerosol particles vary considerably in size, shape, chemical composition and physical properties. They are crucially important in many issues but they represent also one of the poorly understood aspects of the atmosphere.

Atmospheric particles play important roles in climate change and human health. A series of epidemiologic studies have indicated associations between particulate matter (PM) and adverse human health effects (Dockery et al., 1993; Kunzli et al., 2000; Samet et al., 2000; Stieb et al., 2002). The PM fine fraction is particularly important, since smallest particles can penetrate deep into human lungs. In addition to their effects on human health, aerosols in the atmosphere contribute to the impairment of visibility and affect the global radiation balance. Atmospheric particles affect planetary energy balance in two ways: they scatter and absorb solar radiation both in cloud-free and cloudy conditions either directly or by acting as cloud condensation nuclei (CNN). In this second process aerosols modify the optical properties and lifetimes of clouds playing an important role in the process of cloud formation and precipitation.

The size of atmospheric particles ranging from a few tens of angstroms to several hundred micrometers (Seinfeld and Pandis, 1998) dictates their transport and chemical properties and is thus a critical parameter in a number of environmental and health issues.

In the atmosphere the concentration of aerosol particles depends upon factors such as location, annual and diurnal cycles of atmospheric conditions and presence of local sources, reaching sometimes up to 10^7 and 10^8 particles per cm^3 whether in urban or remote areas (Seinfeld and Pandis, 1998). Particles smaller than 1 μm in diameter generally have atmospheric concentration in the range between ten to several thousand particles per cm^3. Particles larger than 1 μm in diameter have usually concentration less than 1 particle per cm^3.

Aerosols are produced by both human activity and natural sources and subsequently modified by several processes. The chemical complexity of airborne particles requires a consideration of their composition and sources. It is well known that chemical contents influence the transport and transformation processes of atmospheric particles, thus the aerosol characterization of aerosols has an important role to better

understanding of their behaviour and properly assessing their effects on various issues. Particles of industrial origin mainly contain significant quantity of some trace elements that are potential dangerous not only for human health but also for climate, ecosystem, cultural and natural heritage which are sensitive to aerosol elemental and chemical composition.

The main objective of this PhD thesis is to contribute to the monitoring and characterization of atmospheric aerosols in central Mediterranean. To this end several measurements have been performed at the Physics Department of the University of Salento (40.33° N, 18.10° E) in order to investigate in particular the dependence of the atmospheric aerosol mass concentration and composition on particle size.

The observation site, located in a suburban area of the Salento Peninsula away from large sources of local pollution, is well suited to contribute to the aerosol characterization of the central Mediterranean basin that represents a unique area in terms of suspended particulate matter. Long-range transport processes from the different regions around the basin significantly affect the Mediterranean atmosphere in which different aerosol types can be found: desert dust from the Sahara desert and the arid regions in the Iberian Peninsula, polluted particles from urban and industrial areas of North- and East-Europe, marine aerosols from the Mediterranean itself or transported from the Atlantic, and biomass burning particles, often produced in forest fire.

In this PhD research several combined aerosol measurements have been carried out using different devices in order to investigate the properties of aerosol of different size. In particular an automatic dual sampler has been used to perform simultaneous aerosol sampling collections and a 7-stage cascade impactor has allowed the fractioning of collected particles in different size intervals. Moreover, in situ measurements of particles size distributions have been performed by an Aerodynamic Particle Sizer (APS) spectrometer.

To characterize the complex chemical composition of collected particles different techniques have been used:

- Scanning Electron Microscopy combined with the Energy Dispersive X-ray (EDX) technique has been used to characterize morphological properties of sampled atmospheric particles and to perform a semi-quantitative analysis of their elemental composition;
- Ion Chromatography (IC) and Inductively Coupled Plasma Atomic Emission Spectroscopy (ICP-AES) analyses have been performed to determine in the

collected particulate matter the mass concentration of the main ionic and metal species;

- Thermal-Optical Transmittance (TOT) technique has been applied to determine in collected samples the mass concentration of organic and elemental carbon.

In addition, the influence of long-range transported air masses over the sampling site and in particular on the ground level particulate matter concentration and composition have been investigated. To this end, analytical back-trajectories, which provide information on the aerosol origin observed at a particular location and on the dynamical patterns governing the air mass transport (Kazadzis et al, 2007), have been used.

In Chapter 1 of this thesis the main properties of atmospheric aerosols are presented and discussed with a particular attention to the method of mathematically characterizing the aerosol size distributions and the properties of the major ambient aerosol types.

In Chapter 2 the Aerodynamic Particle Sizer (APS) spectrometer are described and some examples of aerosol size distribution measurements performed at Lecce are presented and discussed.

In Chapter 3 a short presentation of the air quality legislation directives are provided and the particulate matter sampler devices used for this PhD work are described.

Chapter 4 discusses the Scanning Electron Microscopy (SEM) technique and the importance of its application in environmental studies. In particular, the morphological and elemental SEM/EDX results about some selected size-fractioned samples collected by a 7-stage cascade impactor at the Physics Department of Lecce are discussed.

In Chapter 5 the Thermal-Optical Transmittance (TOT) technique is described and organic and elemental carbon mass concentrations detected in fine particulate matter samples collected during the year 2008 at the Physics Department of Lecce are presented and discussed.

In Chapter 6 results about the Ion Chromatography (IC) and Inductively Coupled Plasma Atomic Emission Spectroscopy (ICP-AES) analyses performed on some particulate matter samples of different fraction collected during the year 2004 are provided

Chapter 7 reports results on the ionic and elemental composition of some fine particulate matter samples collected during the years 2004 and 2005. The study focuses in particular on the fine fraction PM characterization in order to deepen the knowledge on the main composition properties of small particles given the increasing interest to this particulate matter fraction and the scarcity of available data.

Chapter 8 discusses Ion Chromatography and organic/elemental carbon analysis results about some selected samples of different fraction collected during the year 2007. The study has been conducted in particular to investigate how mass concentration and chemical composition of the analyzed samples are affected by different long-range transport processes.

Finally, concluding remarks are provided.

CHAPTER 1

PROPERTIES OF ATMOSPHERIC AEROSOLS

1 PROPERTIES OF ATMOSPHERIC AEROSOLS

The behaviour of particulate matter in the atmosphere, its potential to affect human health, atmospheric visibility and the Earth's radiation budget are governed by physical and chemical properties of atmospheric particles which are closely dependent on the source type and on formation processes that particles undergo at the source or in the atmosphere.

The size of particles is a crucial parameter in characterizing the behaviour of particulate matter, since affects both aerosol properties and lifetime in the atmosphere. It has therefore been useful and convenient to develop a rigorous mathematical method for a correct description and interpretation of the aerosol size distribution which is fundamental to evaluate the dynamics of aerosol production processes, their size transformation and consequently their role on climate changes and air quality.

In this chapter the main properties of atmospheric particles are presented and discussed with a particular attention to the method of mathematically characterizing the aerosol size distributions and the features of the size distributions of the major ambient aerosol types.

1.1 Size of atmospheric particles

Airborne particulate matter including dust, dirt, liquid droplets, smoke, and soot may be a complex mixture of organic and inorganic substances. They may be characterized by their physical attributes and their chemical composition which are known to be crucially important in many issues that directly affect everyday life. Several terms have been used to describe types of particulate matter. Table 1.1 reports the common usage terms relating to the different atmospheric particles.

Particle size represents one of the most important key parameters that governs the transport and removal of atmospheric particles from air, the contribution to light extinction and the deposition within the respiratory system. The diameters of atmospheric particles cover a very wide range from a few nanometers to around 100 μm and they are generally separated in two distinct modes: the *fine mode* which refers to particles that are less than 2.5 μm in diameter, and *coarse mode* which refers to particles greater than 2.5 μm in diameter (Seinfeld and Pandis, 1998).

Fine particles differ from *coarse* ones in origin, chemistry, optical properties and in general the two different modes are transformed separately and removed from the atmosphere by different mechanisms (Seinfeld and Pandis, 1998). In fact combustion-generated particles such as those due to wood burning, automobiles and power generation can vary in size from a few nanometers to 1 μm. Photochemical processes produce in the atmosphere particles smaller than 1 μm. Conversely sea salts, pollens, plant fragments and wind-blown dust are generally larger than 1 μm.

Fine particles can often be divided in *nuclei* mode or *Aitken* mode and *accumulation* mode. The first mode refers to particles between 0.005 and 0.1 μm in diameter and rarely accounts for more than a few percent of the total mass of atmospheric particles. The *nuclei* mode particles are formed from the nucleation of atmospheric species to form fresh particles and from condensation of hot vapors during combustion processes.

Table 1. 1 - Terminology relating to atmospheric particles (Seinfeld and Pandis, 1998). D_p is the particle diameter.

Aerosols, aerocolloids, aerodisperse systems	Tiny particles dispersed in gases
Dusts	Suspensions of solid particles produced by mechanical disintegration of material such as crushing, grinding, and blasting. $D_p > 1$ μm.
Fog	A loose term applied to visible aerosols in which the dispersed phase is liquid. Usually, a dispersion of water or ice, close to the ground.
Fume	The solid particles generated by condensation from the vapour state, generally after volatilization from melted substances, and often accompanied by a chemical reaction such as oxidation. Often the material involved in noxious. $D_p < 1$ μm.
Hazes	An aerosol that impedes vision and may consist of a combination of water droplets, pollutants, and dust. $D_p < 1$ μm.
Mists	Liquid, usually water in the form of particles suspended in the atmosphere at or near the surface of the Earth; small water droplets floating or falling, approaching the form of rain, and sometimes distinguished from fog as being more transparent or as having particles perceptibly moving downward. $D_p > 1$ μm.
Particle	An aerosol particle may consist of a single continuous unit of solid or liquid containing many molecules held together by intermolecular forces and primarily larger than molecular dimensions (> 0.001 μm). A particle may also be considered to consist of two or more such unit structures held together by interparticle adhesive forces such that it behaves as a single unit in suspension or upon deposit.
Smog	A term derived from smoke and fog, applied to extensive contamination by aerosols. Now sometimes used loosely for any contamination of the air.
Smoke	Small gas-borne particles resulting from incomplete combustion, consisting predominantly of carbon and other combustible material, and present in sufficient quantity to be observable independently of the presence of other solids. $D_p \geq 0.01$ μm.
Soot	Agglomerations of particles of carbon impregnated with “tar”, formed in the incomplete combustion of carbonaceous material.

The *accumulation* mode instead refers to particles between 0.1 and 2.5 μm in diameter and generally accounts a significant percent of the total aerosol mass. Particles in *accumulation* mode are formed from condensation of vapors onto existing particles and from coagulation of particles in nuclei mode.

Aerosols of different size ranges are responsible for different atmospheric processes. Nuclei mode particles play a significant role in atmospheric electricity, accumulation mode aerosols influence the visible solar radiation and coarse mode aerosols can act as cloud condensation nuclei to form clouds.

Figure 1.1 (Whitby and Cantrell, 1976) shows an idealized schematic of the distribution of particle surface area of an atmospheric aerosol. A strong distinction between fine and course particles is revealed by figure 1.1: the sources, chemical and optical properties, transformation mechanisms, effects and deposition pathways are generally very different for the two classes of particles.

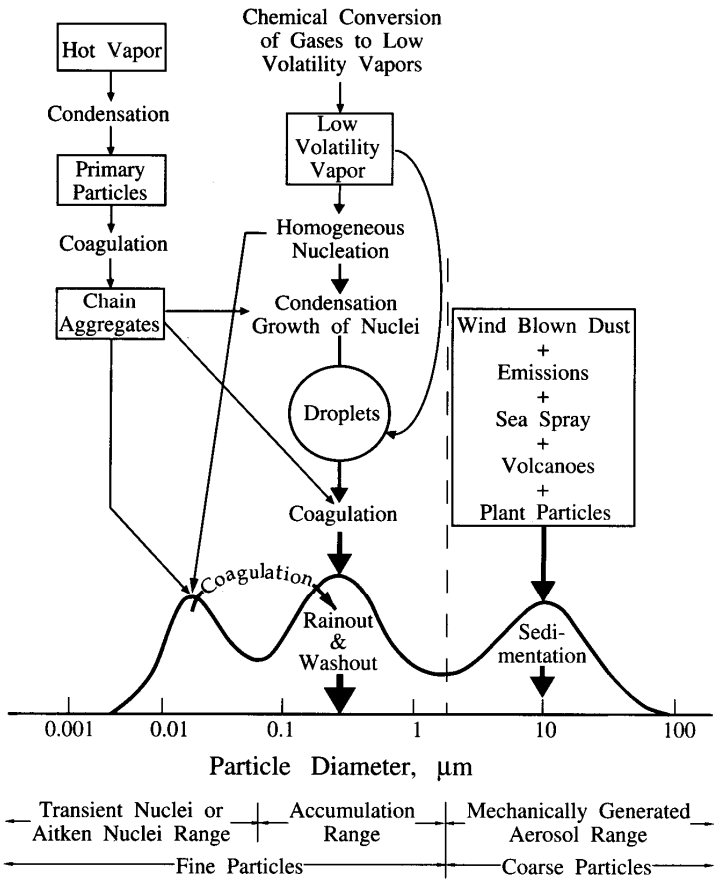

Figure 1.1 Idealized schematic of the distribution of particle surface area of an atmospheric aerosol (Whitby and Cantrell, 1976)

Besides the previous classification of airborne particles, some technical terms are generally used to describe the atmospheric aerosols: the Total Suspended Particulate (TSP) matter term refers to the particles smaller than 40 – 50 μm. Conversely PMx term is used to indicate the particulate matter with diameter smaller than x μm. Due to the close relation to adverse human health effects, PM2.5 and PM10 are the most monitored aerosol fractions.

1.2 Sources of atmospheric particulate matter

Airborne suspended particulate matter can be emitted directly into the atmosphere (*primary* particles) or formed in the atmosphere from gaseous species by either heterogeneous or homogeneous reactions (*secondary* particles). The different emission sources origin particles with different size distribution and chemical composition. Primary particles may result from natural or anthropogenic (human) activities. Significant natural sources include sea spray, biomass burning, soil and rock debris (terrestrial dust), volcanic actions, wildfires and reaction between natural gaseous emissions. Anthropogenic sources include fuel combustion, industrial processes, nonindustrial fugitive sources (roadway dust, constructions, etc.) and transportation sources (automobile, etc.).

Secondary particles are mainly present in fine fraction, and can also be of either anthropogenic or natural origin. Reactions involving precursor gases such as sulphur dioxide (SO_2), ammonia (NH_3), nitrogen oxides (NO_x) and other organic gases typically origin secondary particulate matter.

Coarse particles generally originate by mechanical processes either of natural or anthropogenic nature: soil dust, sea salt, tire wear particles, fly ash, etc.; while fine fraction consists mainly by primary particle from combustion sources and secondary aerosol material derived from chemical reactions.

Table 1.2 provides some estimates of the total global aerosol emission (Kiehl and Rodhe, 1995); a number of classes of aerosol are shown, and the size of the particles comprising the flux is also estimated.

Table 1.2 - Global emission estimates for major aerosol types (Kiehl and Rodhe, 1995).

	Estimated Flux (Tg yr^{-1})			
SOURCE	**Low**	**High**	**Best**	**Particle size category [a]**
NATURAL				
Primary				
Soil dust (mineral aerosol)	1000	3000	1500	Mainly coarse
Sea salt	1000	10000	1300	Coarse
Volcanic dust	4	10000	30	Coarse
Biological debris	26	80	50	Coarse
Secondary				
Sulphates from biogenic gases	80	150	130	Fine
Sulphates from volcanic SO_2	5	60	20	Fine
Organic matter from biogenic VOC [b]	40	200	60	Fine
Nitrates from NO_x	15	50	30	Fine and coarse
Total natural	2200	23500	3100	
ANTHROPOGENIC				
Primary				
Industrial dust, etc. (except soot)	40	130	100	Fine and coarse
Soot	5	20	10	Mainly fine
Secondary				
Sulphates from SO_2	170	250	190	Fine
Biomass burning	60	150	90	Fine
Nitrates from NO_x	25	65	50	Mainly coarse
Organics from anthropogenic VOC	5	25	10	Fine
Total anthropogenic	300	650	450	
Total	2500	24000	3600	

[a] Coarse and fine size categories refer to mean particle diameter above and below 1 μm, respectively.
[b] The term VOC (Volatile Organics Compounds) is used to denote the entire set of vapour-phase atmospheric organics excluding CO and CO_2.
Note: Sulphates and nitrates are assumed to occur as ammonium salts. Flux unit:Tg yr^{-1} (dry mass).

1.3 Atmospheric particle removal processes

Airborne particles can be eventually removed from the atmosphere by different mechanisms. The major processes removing aerosols from the atmosphere are dry deposition or sedimentation and wet removal. Dry deposition refers to the mechanisms that transport the airborne species (both gaseous and particulate) directly to the Earth's surface without the aid of precipitation. The gravitation settling is one of the most efficient removal dry mechanisms. The process refers to the fall of very large particles, reaching a terminal velocity. The particles falls at this rate until it strikes the surface.

Wet deposition is the name given to deposition pathways involving water. The atmospheric gases or the particles are transferred to the Earth's surface in aqueous form (rain, snow, fog). Two important wet deposition processes are rainout and washout. Rainout describes the removal of a cloud condensation nucleus. Atmospheric aerosol can act as nuclei for the condensation of cloud droplets; in clouds producing rain, some of these drops grow to such a large size that they fall as rain drops. The aerosol deposited in this way are said to have been rained out.

Washout describes the removal of aerosol by cloud droplets. A particle is said to have been washed if it is incorporated into an already existing cloud drop which grows large enough to fall as rain. It is important to note that the difference between washout and rainout is the required pre-existence of a collecting drop for washout.

1.4 The size distribution functions

A complete description of aerosol size distribution includes an accounting of the size of each particle. Airborne particle size may vary over several orders of magnitude; thus the multiplicity of the diameters of thousands of atmospheric particles that varies as a function of time and space makes very difficult a presentation of the size distribution considering the full aerosol size range; several details of the distribution structure could necessarily lost (Seinfeld and Pandis, 1998).

A first simplification in the accounting of the size of each atmospheric particle is obtained by the division of the particle size range in discrete intervals and the calculation of the number of particles in each size bin. However the description of a size distribution using bins with different widths could introduce biases. These complications involve a loss of information about the distribution in each size interval

and it makes often necessary the normalization of the distribution dividing the concentrations with the corresponding size range. Particle concentrations therefore are expressed in μm^{-1} cm^{-3} and the size distribution changes shape but the area below the curve is proportional to the number concentration.

In this work the effect of particle shape has been neglected and only spherical particles have been considered.

If the value of an aerosol distribution n_i for a size interval i is expressed as the ratio of the absolute aerosol concentration N_i of this interval and the size range ΔD_p (particle diameter); the absolute concentration N_i can be calculated by the equation:

$$N_i = n_i \, \Delta D_p \, .$$

In order to avoid biases in the descriptions of the size distribution using arbitrary intervals ΔD_p it is useful to take the limit $\Delta D_p \rightarrow 0$, considering ΔD_p infinitesimally small and equal to dD_p. At this limit, $n_N(D_p)\, dD_p$ represents the number of particles per cm^3 of air having diameters in the range D_p to $D_p + dD_p$. The units of the size distribution function $n_N(D_p)$ are μm^{-1} cm^{-3} and the total number of particles per cm^{-3}, N, is:

$$N = \int_0^\infty n_N(D_p)\, dD_p \, . \qquad (1.1)$$

It is useful to introduce also a normalized size distribution function:

$$\bar{n}_N(D_p) = n_N(D_p) / N \, , \qquad (1.2)$$

which is the fraction of the total number of particles per cm^3 having diameters in the range D_p *to* $D_p + dD_p$. The normalized size distribution function $\bar{n}_N(D_p)$ is expressed in μm^{-1} and can be considered as the probability that a randomly selected particle has a diameter between D_p and $D_p + dD_p$.

In the common notation the size distribution function $n_N(D_p)$ can also be written as:

$$n_N(D_p) = \frac{dN}{dD_p} \, , \qquad (1.3)$$

where $dN = n_N(D_p)\, dD_p$ is the number of particles in the size range $(D_p, D_p + dD_p)$.

In this discussion we assume that beyond a number of molecules around 100 the number distribution is a continuous function of the diameter D_p and not a discrete function of the number of molecules. It is important to note that the most of atmospheric particles have a diameter smaller than 0.1 μm, consequently the number distribution

function $n_N(D_p)$ generally peaks below 0.1 um. In figure 1.2 atmospheric aerosol number, surface and volume continuous distributions are plotted as a function of particle size. The diameter range between 0 and 0.5 μm is reported in the inset: we can observe the narrow spike near the origin often present in the number distribution.

Because aerosol properties depend on the particle surface area and volume distributions with respect to particle size, it is useful to define also these important functions. If we consider all atmospheric particles as spheres we define the aerosol surface area distribution $n_S(D_p)$ so as to $n_S(D_p)\,dD_p$ be the surface area of particles per cm^3 of air having diameters in the range D_p to $D_p + dD_p$.

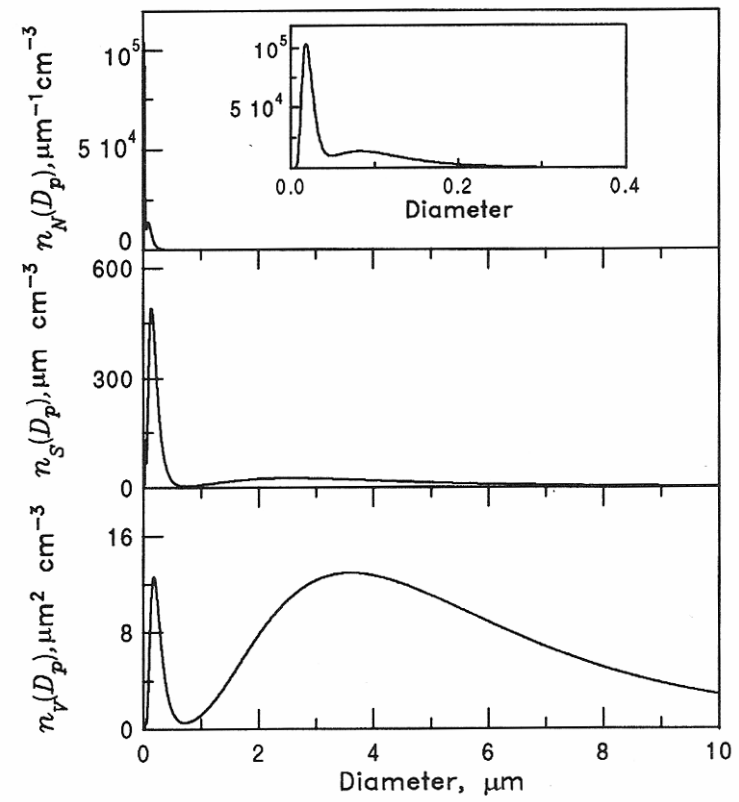

Figure 1. 2 – Atmospheric aerosol number, surface, and continuous volume distributions as function of particle size. The diameter range between 0 and 0.5 μm is shown in the inset (Seinfeld and Pandis, 1998).

In the infinitesimally size interval all particles have effectively the same diameter D_p and a surface area $\pi\, D_p^2$, thus if $n_S(D_p)\,dD_p$ is the number of particles in

the considered size range, $\pi D_p^2 n_S(D_p) dD_p$ is the surface area of all particles. By definition we can write the aerosol surface area distribution as:

$$n_S(D_p) = \pi D_p^2 n_N(D_p) . \quad (1.4)$$

The aerosol surface area distribution is expressed in μm cm^{-3} and the total surface area S of the aerosol per cm^3 of air is:

$$S = \pi \int_0^\infty D_p^2 n_N(D_p) dD_p = \int_0^\infty n_S(D_p) dD_p . \quad (1.5)$$

S is expressed in μm^2 cm^{-3} and is equal to the area below the curve $n_S(D_p)$ in figure 1.2. We can also define the aerosol volume distribution $n_V(D_p)$ so as to $n_V(D_p) dD_p$ be the volume of particles per cm^{-3} of air having diameters in the range D_p to $D_p + dD_p$ and therefore:

$$n_V(D_p) = \frac{\pi}{6} D_p^3 n_N(D_p) . \quad (1.6)$$

The aerosol volume distribution is expressed in μm^2 cm^{-3} and the total aerosol volume per cm^3 of air, V, is:

$$V = \frac{\pi}{6} \int_0^\infty D_p^3 n_N(D_p) dD_p = \int_0^\infty n_v(D_p) dD_p . \quad (1.7)$$

V is expressed in μm^3 cm^{-3} and is equal the area below the curve $n_V(D_p)$ in figure 1.2. The common notation for the number, surface and volume distributions is:

$$n_N(D_p) = \frac{dN}{dD_p} ; \; n_S(D_p) = \frac{dS}{dD_p} ; \; n_V(D_p) = \frac{dV}{dD_p} ,$$

where dN, dS and dV are the number, surface and volume differential of particles in the size range D_p to $D_p + dD_p$, respectively.

A useful distribution is also the distribution of particle mass with respect to particle size given by the equation:

$$n_M(D_p) = \left(\frac{\rho_p}{10^6}\right) n_V(D_p) = \left(\frac{\rho_p}{10^6}\right)\left(\frac{\pi}{6}\right) D_p^3 n_N(D_p) ;$$

we assumed that all particles have density ρ_p (g cm^{-3}) and the factor 10^6 is needed to convert the units of density from g cm^{-3} to μg μm^{-3} and to have the units for the distribution as μg μm^{-1} cm^{-3}.

As previously discussed, the atmospheric particle size can varies over several orders of magnitude, thus the use of the aerosol distributions $n_N(D_p)$, $n_S(D_p)$ and $n_V(D_p)$ could make some scale problems. To avoid these complications the most convenient way to represent the aerosol distributions is to express them as functions of ln D_p or log D_p. Because formally the logarithm can not be considered as a dimensional quantity, in this discussion we consider ln(D_p /1), where 1 μm is the "reference" diameter and it is not explicitly indicated. Therefore we define the number distribution function $n_N{}^e(\ln D_p)$ so as to $n_N{}^e(\ln D_p)\, d\ln D_p$ be the number of particles per cm^3 of air in the size range ln D_p *to* ln D_p + dD_p.

The notation $n_N{}^o(\log D_p)$ is used if we express the number distribution as function of log D_p.

The aerosol number distribution $n_N{}^e(\ln D_p)$ is expressed in cm^{-3} and the total number concentration of particles N is:

$$N = \int_{-\infty}^{+\infty} n_N{}^e(\ln D_p)\, d\ln D_p \ . \qquad (1.8)$$

The units of N are cm^{-3} and the independent variable ln D_p makes the limits of integration from $-\infty$ to $+\infty$.

Similarly to the aerosol number distribution, the aerosol surface area and volume distributions can also be expressed as functions of ln D_p (or log D_p):

$$n_S{}^e(\ln D_p) = \pi\, D_p{}^2 n_N{}^e(\ln D_p) \quad (n_S{}^o(\log D_p) = \pi\, D_p{}^2 n_N{}^o(\log D_p));$$

$$n_V{}^e(\ln D_p) = \frac{\pi}{6} D_p{}^3 n_N{}^e(\ln D_p) \ (n_V{}^o(\log D_p) = \frac{\pi}{6} D_p{}^3 n_N{}^o(\log D_p)).$$

Therefore the total surface area, S, and the total volume, V, can be written as:

$$S = \pi \int_{-\infty}^{+\infty} D_p{}^2 n_N{}^e(\ln D_p)\, d\ln D_p = \int_{-\infty}^{+\infty} n_S{}^e(\ln D_p)\, d\ln D_p \ ;$$

$$V = \frac{\pi}{6} \int_{-\infty}^{+\infty} D_p{}^3 n_N{}^e(\ln D_p)\, d\ln D_p = \int_{-\infty}^{+\infty} n_V{}^e(\ln D_p)\, d\ln D_p \ ,$$

The units of S and V are μm^2 cm^{-3} and μm^3 cm^{-3}, respectively.

The common notation for the number, surface and volume distributions as functions of ln D_p become respectively:

$$n_N{}^e(D_p) = \frac{dN}{d\ln D_p} \ ; \ n_S{}^e(D_p) = \frac{dS}{d\ln D_p} \ ; \ n_V{}^e(D_p) = \frac{dV}{d\ln D_p} \ .$$

An advantage of presenting the data in this form is that in the given size range the area under the curve of the distribution is proportional to the number, surface area or volume respectively.

1.5 Size distribution of aerosols of different type

The normal distribution for a quantity α defined from $-\infty$ to $+\infty$ is:

$$n(\alpha) = \frac{N}{(2\pi)^{1/2}\sigma_\alpha} \exp\left(-\frac{(\alpha - \overline{\alpha})^2}{2\sigma_\alpha^2}\right), \qquad (1.9)$$

where $\overline{\alpha}$ is the mean of the distribution, σ_α^2 is the variance and

$$N = \int_{-\infty}^{+\infty} n(\alpha)\, d\alpha .$$

A quantity α is *log-normal distributed* if its logarithm is normally distributed; either the natural or the base 10 logarithm can be used. Thus, an aerosol population is log-normally distributed if $\ln D_p$ (or $\log D_p$) satisfies the equation (1.9):

$$n_N{}^e(\ln dD_p) = \frac{dN}{d\ln D_p} = \frac{N}{(2\pi)^{1/2}\ln\sigma_g} \exp\left(-\frac{(\ln D_p - \ln \overline{D}_{pg})^2}{2\ln^2\sigma_g}\right),$$

where N is the total aerosol number concentration, $\overline{D}_{pg}$ and σ_g are the parameters of the distribution.

Atmospheric aerosol size distributions are often described by the sum of k log-normal distributions:

$$n_N{}^o(\log D_p) = \sum_{i=1}^{k} \frac{N_i}{(2\pi)^{1/2}\log\sigma_i} \exp\left(-\frac{(\log D_p - \log \overline{D}_{pi})^2}{2\log^2\sigma_i}\right),$$

where N_i is the number concentration, $\overline{D}_{pi}$ is the mean diameter and σ_i is the standard deviation of the i^{th} log-normal mode.

In the next sections the properties and the characteristics of the size distributions of the major aerosol types (urban, marine, desert, rural continental and remote continental aerosol) are presented and discussed.

1.5.1 Urban aerosol

Urban aerosols consist of a mixture of primary aerosol emissions from natural sources, industries, power generation, transportation, and secondary particulate formed by gas-to-particle conversion processes.

Fine and coarse mode particles in an urban aerosol have different sources. Coarse particles tend to be mechanically generated and are composed of materials such as soil dust, tyre wear particles and fly ash. Fine particles (accumulation and nucleation mode) tend to be produced either directly from combustion sources, or by gas to particle conversion involving reaction products of sulphates, nitrates, ammonium and organics.

Typical urban distributions have characteristic peaks visible in the three plots of number, area and volume distribution shown in figure 1.3.

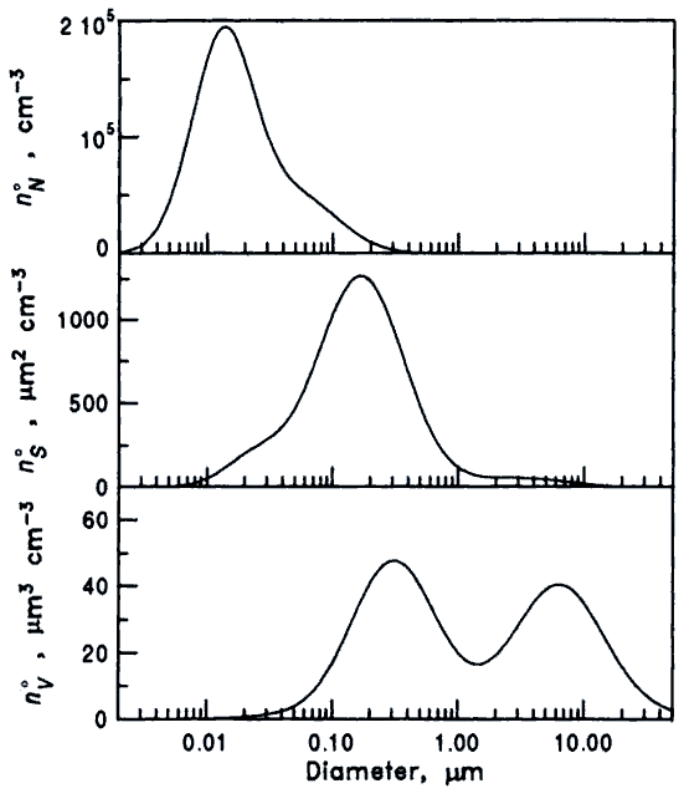

Figure 1.3 – Typical urban aerosol number, surface and volume distributions (Seinfeld and Pandis, 1998)

The urban aerosol number distribution consists principally by particles smaller than 0.1 μm; the most of the surface area is instead in the size range between 0.1 and 0.5

μm, finally the volume distribution has generally two distinct modes, one in the coarse size range and one in the submicron regime.

In an urban area the aerosol size distributions is variable: close to sources the number concentration of particles less than 0.1 μm in diameter is generally very high but decreases rapidly with distance from the source. Figure 1.4 shows the number distribution as a function of particles size for different categories of environment: average urban, urban influenced background, next to a freeway and for background conditions.

The distributions plotted in figure 1.4 have a different trend, mainly in the size range under 0.1 μm, in particular we can observe that about an order of magnitude more particles can be found close to a freeway with respect to the average urban aerosol.

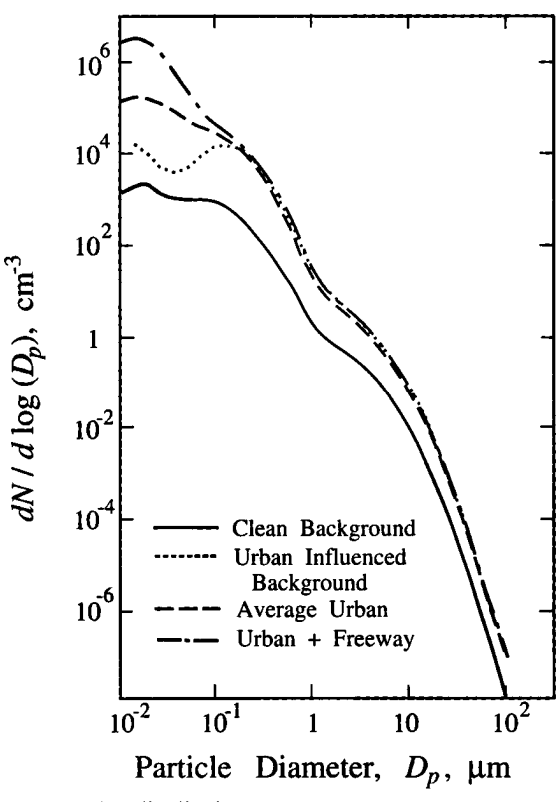

Figure 1.4 - Aerosol number distributions next to a source (freeway), for average urban, for urban influenced background, and for background conditions (Seinfeld and Pandis, 1998).

The volume distributions referring to these two different varieties of environment are reported in figure 1.5. We can note that in an urban area, although the most of the particles are less than 0.1 μm in diameter, the nuclei mode has a negligible

contribution to the volume distribution with the exception of area close to combustion sources. Therefore it is important to highlight that in the urban aerosol the mass concentration of the accumulation mode and coarse mode are generally comparable and that the most of the particle mass is to ascribe to particles with a diameter larger than 0.1 μm.

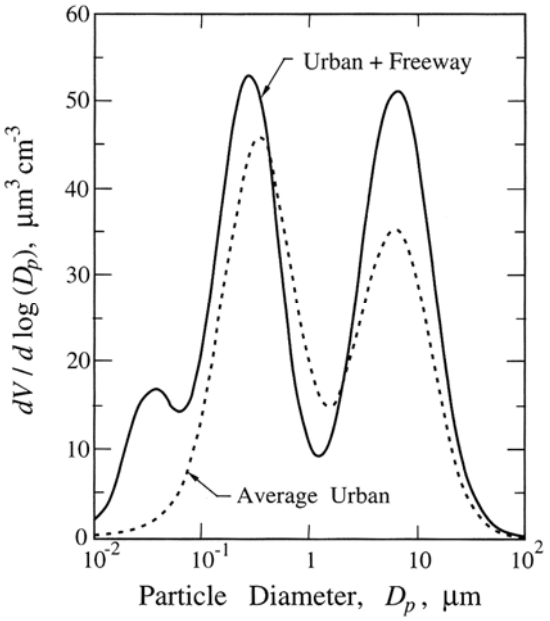

Figure 1.5 – Aerosol volume distributions next to a source (freeway) and for average urban conditions (Seinfeld and Pandis, 1998).

1.5.2 Marine aerosol

Particles in remote ocean environments are found at concentrations around 100 – 300 cm^{-3}. In the size distribution marine particles occupy three modes: the nuclei mode, the accumulation mode and the coarse mode (Fitzgerald, 1991). The course fraction generally contains about 95% of the total particulate mass, but low number concentration (from 5 to 10% of the particle number). The fine mode comprises the 90-95% of the particles but only a few percentages (about 5%) of the particle mass.

Coarse marine aerosols are mainly composed of salt from evaporated sea spray originated by wind-induced wave breaking or bursting bubbles (Blanchard and Woodcock, 1957; Monahan et al., 1983; Seinfeld and Pandis, 1998). Each bursting bubble produces about 1-10 jet drops with a radius less than 10 μm and hundreds of film

drops with a radius smaller than 1 μm (Woolf et al., 1988). Each drop can become sea salt particles or sea salt solution droplets. Particles larger than 10 μm in radius, generally known as spume drops, originate by the mechanical disruption of wave crests by wind; mainly at wind speed greater than 10 m/s (Wang and Street, 1978; Monahan et al., 1986).

Fine particles too are produced in the ocean environment, but from processes such as DMS (Dimethyl Sulphate produced over the oceans by several species of marine plankton) reaction product condensation (Kloster et al. 2006). Fine fraction consists mainly by non sea salt - sulphate (Fitzgerald, 1991).

The size distribution of marine atmospheric particles is typically characterized by three modes: the nuclei mode in the size range under 0.1 μm, the accumulation mode between 0.1 and 0.6 μm and the coarse mode in the regime over 0.6 μm. (Fitzgerald, 1991).

Figures 1.6 and 1.7 show a model marine aerosol size distribution (solid line) compared with the number and volume distributions (symbols) measured by several investigators in clean maritime air (Mészaros and Vissy, 1974; Haaf and Jaenicke, 1980; De Leeuw, 1986; Hoppel et al., 1989).

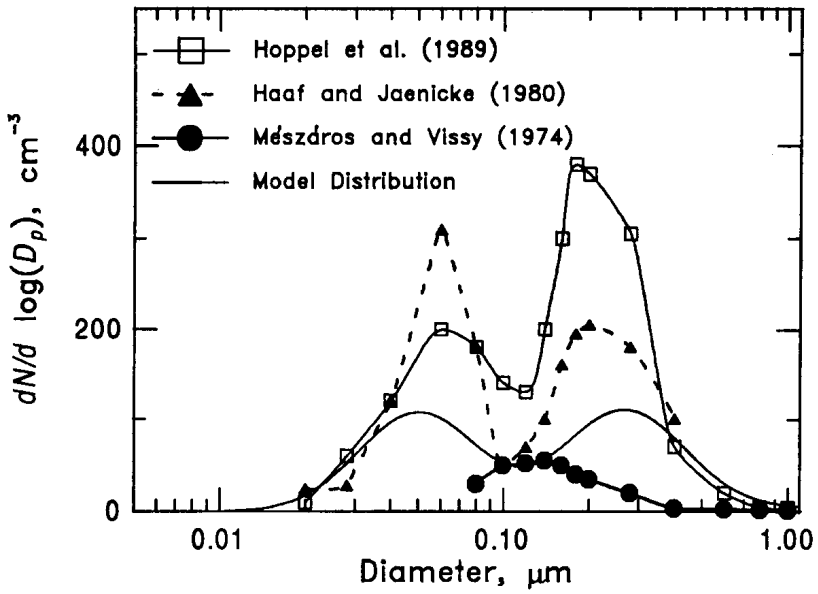

Figure 1.6 - Measured marine aerosol number distributions and a model distribution used to represent average conditions (Seinfeld and Pandis, 1998).

The distribution of Mészaros and Vissy (1974) is an average of distributions measured in South Atlantic and Indian Ocean at an average wind speed of about 12 m s^{-1}. Instead, the distributions of Hoppel et al. (1989) and De Leeuw (1986) were obtained at wind speeds less than 5 m s^{-1} in the subtropical and North Atlantic respectively. It is difficult to establish the uncertainties referring to the different measurement methods and to assess the contribution to the size distributions relative to the differences in sampling location and meteorological conditions, in particular in wind speed which mainly affects the concentrations of coarse particles.

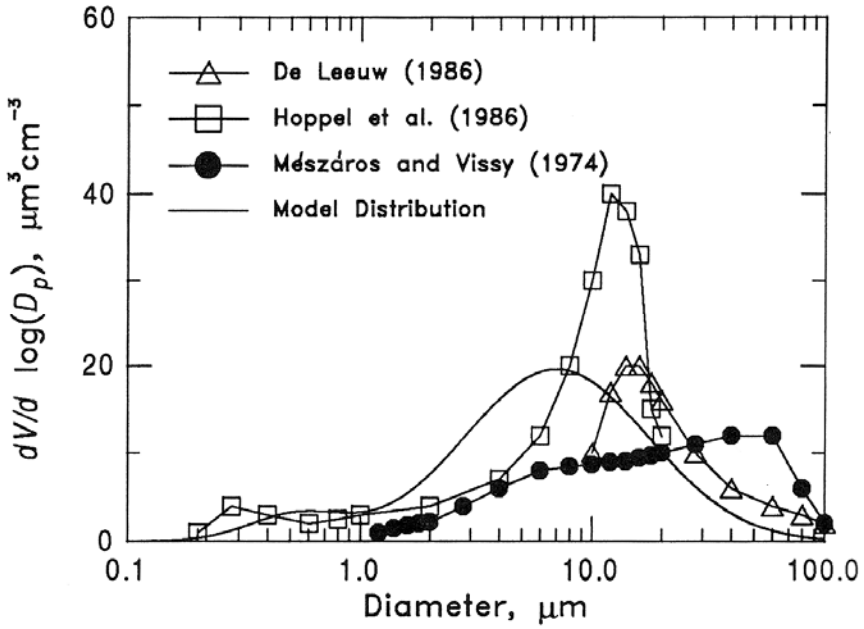

Figure 1.7 – Measured marine aerosol volume distributions and a model distribution used to represent average conditions (Seinfeld and Pandis, 1998).

In figure 1.6 we can observe the typical peaks of the marine aerosol number distribution in the nuclei and accumulation mode. Figure 1.7 shows the mode in coarse regime in the volume distribution. The figures explicitly show the significant contribution of coarse particles to the mass concentration and the evident secondary role of fine particles, which become crucial in number distribution.

1.5.3 Desert aerosol

Desert aerosol is a mixture of particles mainly composed by soils and crustal materials. The abundances of major elements present in these two kind of primary emissions are reported in table 1.3 (Warneck, 1988). The soil and crustal rock composition are similar, with the exception of the soluble elements such as Calcium (Ca), Magnesium (Mg) and Sodium (Na), which reach the lower relative concentration in soil material.

Table 1.3 – Average abundances of major elements in soil and crustal rock (Warneck, 1988).

	Elemental abundance (ppm by mass)	
Element	**Soil**	**Crustal Rock**
Si	330000	311000
Al	71300	77400
Fe	38000	34300
Ca	13700	25700
Mg	6300	33000
Na	6300	31900
K	13600	29500
Ti	4600	4400
Mn	850	670
Cr	200	48
V	100	98
Co	8	12

Desert dust aerosol originates mainly from large arid areas of the planet; the Sahara, the East Asian and Saudi Arabian deserts and others arid regions provide a significant amount of mineral dust emissions (Dentener et al., 1996; Husar et al., 1997). However, desert particles actually can extend considerably over lands and oceans adjacent to arid source regions (Jaenicke and Schutz, 1978; d'Almeida and Schutz, 1983; Li et al., 1996), especially during dust storms. Dust particles smaller than 10 μm in diameter can be transported over long distances often further than 5000 km; large

particles of about 100 μm in diameter generally are not transported at large distances out of the source regions (Seinfeld and Pandis, 1998).

Figure 1.8 shows the typical desert aerosol number, surface and volume distributions which generally are strongly dependent on the wind speed. The number function is characterized by three overlapping modes: one in the size interval less than 0.01 μm, the second at 0.05 μm and the third in the coarse range at about 10 μm (Jaenicke, 1993). The surface distribution exhibits its modes in the size region over 0.1 μm, while the volume distribution peaks in the coarse interval.

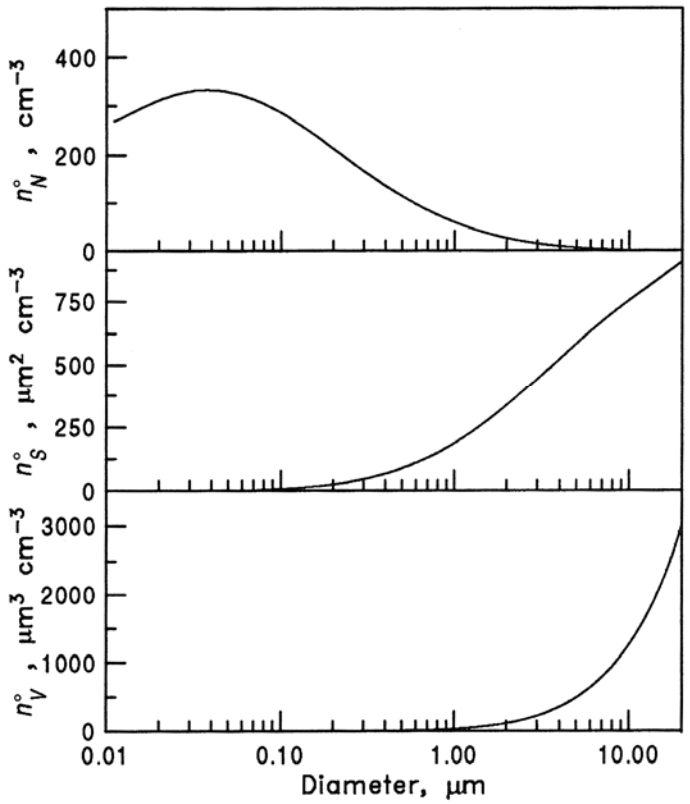

Figure 1.8 – Typical desert aerosol number, surface and volume distributions (Seinfeld and Pandis, 1998).

1.5.4 Rural continental aerosol

Rural aerosols primarily consist by materials of natural origin with a low influence of anthropogenic sources (Hobbs et al., 1985). The PM10 concentrations reach values around 20 μg cm^{-3} for rural only particles.

The typical rural continental number, surface and volume distributions are reported in figure 1.9. Two important modes at diameter values of about 0.02 and 0.08 μm respectively characterize the number distribution (Jaenicke, 1993); a mode at about 0.2 μm dominates the surface distribution; while the mass concentration peaks in the coarse range at about 7 μm. It is important to highlight that the mass concentration of continental aerosol not influenced by local sources has not a nuclei mode, but only a low peak in the accumulation mode.

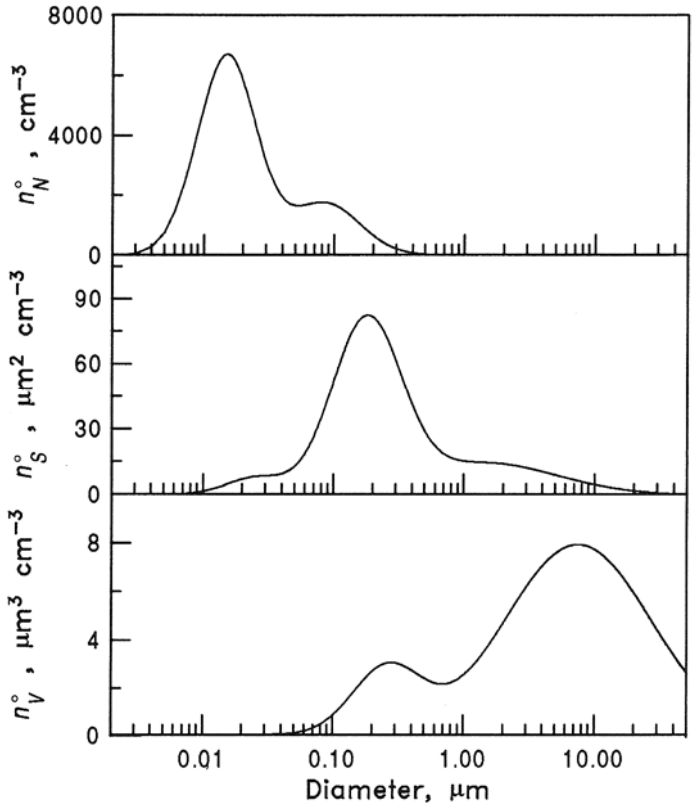

Figure 1.9 – Typical rural continental aerosol number, surface and volume distributions (Seinfeld and Pandis, 1998).

1.5.5 Remote continental aerosol

Remote continental aerosols are a mixture of primary particles and secondary oxidation products (Deepak and Gali, 1991). The PM2.5 fraction primarily consists of ammonium, sulphates and organics and represents 40 to 80 % of the PM10 mass which typically has an average value around 10 μg cm^{-3} (Bashurova et al., 1992; Koutsenogii et al., 1993; Koutsenogii and Jaenicke, 1994).

Figure 1.10 shows the typical remote continental aerosol number, surface and volume distribution. The aerosol number distribution is generally characterized by the same three modes as marine aerosol at diameter values around 0.02, 0.1 and 2 μm, but at number concentration around 2000-10000 particles cm^{-3}.

Table 1.4 summarizes the average number and mass concentration of the major aerosol types that have previously been described.

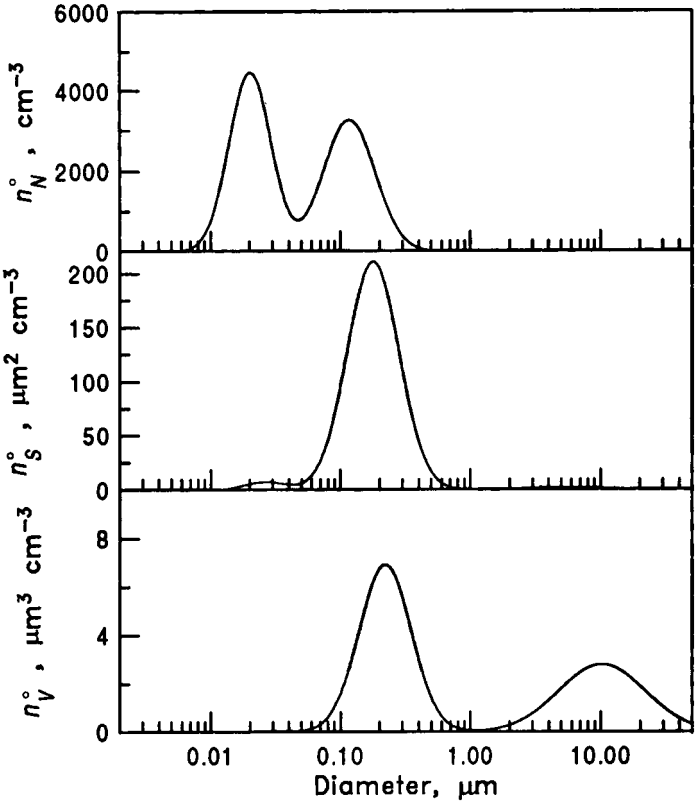

Figure 1.10 - Typical remote continental aerosol number, surface and volume distributions (Seinfeld and Pandis, 1998).

Table 1. 4 – Properties of atmospheric aerosol types (Seinfeld and Pandis, 1998).

Type	Number (cm^{-3})	PM_1 (μg cm^{-3})	PM_{10} (μg cm^{-3})
Urban (Polluted)	10^5 – 4 x 10^6	30 -150	100 - 300
Marine	100 - 400	1 - 4	10
Rural	2000 – 10000	2.5 - 8	10 - 40
Remote continental	50 – 10000	0.5 – 2.5	2 - 10

1.6 Aerosol chemical composition

Aerosols produced from different natural and anthropogenic activities are mixed together, thus each atmospheric particle is a composite of different chemical constituents. Sulphates, nitrates, ammonium, crustal species, sea salt, water, organic material and hydrogen ions are the major components of atmospheric aerosol particles (Seinfeld and Pandis, 1998).

Fine fraction particles mainly contain sulphates, ammonium and organic and inorganic carbon compounds. Although small particles generally originate from primary anthropogenic or secondary sources, forest fires are known to be a large natural source of particulate matter in fine fraction.

Coarse particles predominantly consist of crustal species (silicon, calcium, aluminium, magnesium and iron), sea salt spray (sodium and chloride) and biogenic organic particles (pollen, spores and plant fragments). Some chemical species such as nitrates and chloride may be found in both the fine and coarse fractions.

Fine nitrates usually originate from the nitric acid/ammonia reactions for the formation of ammonium nitrate; while coarse nitrate generally result from coarse particle (sea salt or aerosol crustal aerosol)/nitric acid reactions.

Figure 1.11 shows a typical urban aerosol distribution as a function of size particle (Wall et al., 1988): we can observe how different species are included in different particle modes. Nitrates, sulphates and ammonium have two important modes in the size range between 0.1 and 1 μm; a third evident peak is in the coarse range over 1 μm. From figure 1.11 it is worth noting that more than 50 % of nitrate, with most of the sodium and chloride is found in the coarse mode; however the chloride ion seems to have been involved in some reaction, redistributing it into fine fraction.

Sodium (Na^+) and chloride (Cl^-) ions are typically present in significant concentrations in sites close to seawater and generally they interact with several components with a consequent formation of different solid compounds (ammonium chloride, sodium sulphate and sodium bisulphate, sodium nitrate). In an urban aerosol some interesting reactions involving anthropogenic pollutants and naturally produced material can be place. In particular in addition of sea salt particles the reaction:

$$NaCl_{(s)} + HNO_{3(g)} \leftrightarrow NaNO_{3(s)} + HCl_{(g)}$$

of NaCl with HNO_3 produces a transfer of nitrate in aerosol phase and it is generally associated with coarse sea salt particles (Seinfeld and Pandis, 1998). This mechanism is considered the principal source of coarse particle nitrate.

It is important to note that during the reaction involving sea salt particles and nitric acid and that involving sulphuric acid too:

$$2\ NaCl_{(s)} + H_2SO_{4(g)} \leftrightarrow Na_2SO_{4(s)} + HCl_{(g)}$$

$$NaCl_{(s)} + H_2SO_{4(g)} \leftrightarrow NaHSO_{4(s)} + HCl_{(g)}$$

$HCl_{(g)}$ is released to the gas phase leading to a "chloride deficit" in the marine aerosol.

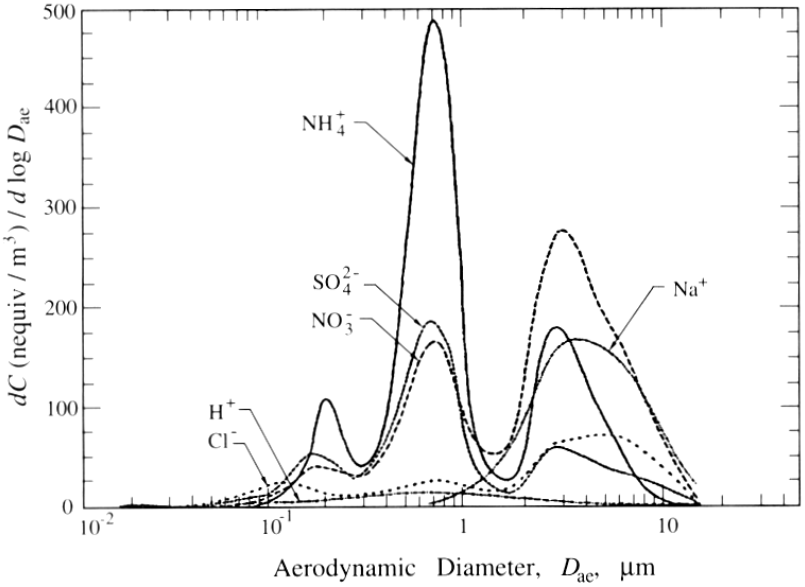

Figure 1.11 - Measured size distributions of aerosol sulphate, nitrate, ammonium, chloride, sodium and hydrogen in Claremont, CA (Wall et. al., 1988)

Sulphate is one of the predominant species in the fine mode. It may be formed in the atmosphere through the oxidation of SO_2 in the gas phase or aqueous phase. The reaction of gas-phase oxidation involves hydroxyl radical to form sulphuric acid gas (Atkinson and Lloyd, 1984). The low vapour pressure makes the nucleation of sulphuric acid gas in the presence of water vapour to form sulphuric acid droplets. Sulphuric acid gas can also condense on existing particles or react with ammonia to produce $(NH_4)HSO_4$ and $(NH_4)_2SO_4$. Gas to particles transformation is controlled by the production of the hydroxyl radical closely related to photochemistry (Calvert and Stockwell, 1983). Therefore, in summertime when the photochemistry is much more

active, the rate of transformation is higher. Aqueous phase oxidation by oxygen and hydrogen peroxide is another important pathway for sulphate production (Saxena and Seigneur, 1987). In the presence of fog or clouds, SO_2 may dissolve in droplets, where it undergoes aqueous reactions. In particular in the presence of ammonia H_2SO_4 is neutralized to form $(NH_4)_2SO_4$.

Ammonia is the most common alkaline component in the atmosphere. It neutralizes atmospheric gases such as HNO_3, H_2SO_4 and HCl to produce several salts including NH_4NO_3, NH_4HSO_4, $(NH_4)_2SO_4$ and NH_4Cl. The most significant sources of ammonia include combustion processes, refinery operations, chemical fertilizer manufacture and application, chemical plants, steel mill coke ovens and decomposing livestock wastes.

Organic carbon (OC) particulate matter is predominantly present in fine fraction (Van Vaeck and Van Cauwenberghe, 1978) and it is directly emitted in the atmosphere or produced from secondary gas to particle conversion processes.

Inorganic or elemental carbon (EC) also named graphitic or black carbon is primary in nature; it originates from incomplete combustion of carbon based materials in particular from fuel combustion and biomass burning (Penner et al., 1993). Several measurements shown that the size distribution of EC particles in ambient air and vehicular emissions is characterized by a bimodal trend with modes in the size ranges between 0.05 and 0.12 μm and 0.5 and 1 μm (Venkataraman and Friedlander, 1994).

In atmospheric particulate matter more than 40 trace elements are also present in either fine or the coarse fraction. They originate from numerous and different sources such as combustion of coal, wood burning, waste incineration, dust, boilers, steel furnaces, smelters and break wear. Products of combustions are generally found as oxides (Fe_2O_3, Fe_3O_4, Al_2O_3). Elements such as iron, copper and lead reach the highest concentration values; instead concentrations of elements such as mercury, cobalt and antimony are usually low.

CHAPTER 2

AEROSOL SIZE DISTRIBUTION ANALYSIS

2 AEROSOL SIZE DISTRIBUTION ANALYSIS

Aerosol size distributions are among the most important parameters to characterize an aerosol population (Penner et al., 1998). Micro-scale aerosol mechanisms (coagulation, condensation) and large scale atmospheric processes (rainfall, atmospheric circulation systems) product different signature in the size distribution (Moorthy et al., 1991; Smirnov et al., 1994). The particle size distribution is especially important in human health studies because it determines the regional deposition of inhaled aerosols in the different parts of the human respiratory tract (Hlavay et al., 1992; European Standard EN 481, 1993; Pui, 1996). Therefore characterization of the size distribution is valuable and can serve several purposes (Clarke and Whitby, 1967; Khemani et al., 1982).

Since particle size distributions can be measured with high time resolution, they can be used to distinguish between different air mass types, to identify particle formation and possibly transformation and removal processes. For a given location, they are useful in interpretation of the aerosol system in the analyzed air mass and they can be used to infer relative contributions to the aerosol from different sources, especially when combined with aerosol chemistry observations.

In this chapter in situ measurements of particles size distributions performed by an Aerodynamic Particle Sizer (APS) spectrometer are presented and discussed.

The particle size distribution of airborne particulate matter was also determined in this PhD work by a sampling system equipped with an inertial cascade impactor (chapter 3) that separates the particulate matter during sampling on the basis of the particle size. This second method has been used in this thesis to obtain additional results and to perform the chemical characterization of atmospheric size-fractionated particles by scanning electron microscopy (SEM) technique (chapter 4).

2.1 Measurement site

The aerosol size distribution measurements analyzed in this work have been performed at the Physic Department of the University of Salento, which is located in a suburban area of the Salento Peninsula, in South-East Italy, near Lecce (40.33° N, 18.10° E) at about 20 km from both Adriatic and Ionic sea (Figures 2.1, 2.2).

The measurements have been carried out at the top of the Physics Department building at about 10 m from ground, where is located the "Aerosol and Climate" laboratory (Figure 2.3).

Figure 2.1 – The Salento Peninsula, in the South-East Italy. The yellow indicator shows Lecce (40.33° N, 18.10° E) which is located at about 5 Km from the Physics Department of the University of Salento.

The site is in the Central Mediterranean area which is of great interest for global climate studies because aerosol composition and size distribution may exhibit large variations due to transport and mixing of air masses originating from different regions (Chester et al., 1993). The transport of polluted air masses from the North-East European industrialized countries is significant as well as the influence of sea spray from Atlantic Ocean and the Mediterranean itself. Moreover, due to the proximity to the Africa Continent, Saharan dust events are frequently observed (Kalivitis et al; 2007).

It is important to highlight that the observation site is in an area basically rural and totally flat; the Salento Peninsula in fact is essentially characterized by level land, sometimes spaced out by low hills (Murge Salentine) which extend from North to South and do not rise 200 m. Air masses coming from surrounding regions do not find geographical barriers, then in this area long-range transport effects easily could sum to the local influences (open-work caves, vegetative burning, marine aerosol, etc.). This

peculiarity makes complex the interpretation of measurement results and the discrimination among pollutants of different origin.

Figure 2.2 – Satellite image of the Physics Department of the University of Salento.

Figure 2.3 – The "Aerosol and Climate" laboratory located at the top of the Physics Department building of the University of Salento. The measurements are performed at about 10 m from ground.

2.2 Aerodynamic Particle Sizer (APS) spectrometer

In this work size distribution measurements have been performed by an Aerodynamic Particle Sizer (APS) spectrometer (TSI-Model 3321) in order to determine representative atmospheric particle size distributions and analyze them according to their potential source regions.

The TSI - APS spectrometer Model 3321 (Figure 2.4) sizes particles in the range from 0.5 to 20 μm using a sophisticated time of flight technique that measures aerodynamic diameter in real time.

Aerodynamic diameter is defined as the physical diameter of spherical particle having a density of 1 g cm^{-3} that settles through the air with a terminal velocity equal to that of the particle in question. It is one of the most important parameter because it determines the particle's behaviour in the atmosphere. Particles showing the same airborne behaviour have the same aerodynamic diameter, regardless of their composition, physical size, shape or density. Knowledge of the aerodynamic diameter allows determine: the human respiratory tracts where the particle will be deposited, how long the airborne particle will remain in the atmosphere, whether the particle will enter a sampling system, penetrate a filter or a pipe, tube, duct or channel.

Figure 2.4 – The Aerodynamic Particle Sizer (APS) spectrometer (TSI – Model 3321).

The functioning scheme of the APS is illustrated in figure 2.5. As particles exit the acceleration nozzle, they cross through two partially overlapping laser beams in the detection area. Light is scattered as each particle crosses through the overlapping beams. An elliptical mirror, placed at 90 degrees to the laser beam axis, collects the

light and focuses it onto an Avalanche Photodetector (APD) which converts the light pulses in electrical pulses. By electronically timing between the peaks of the pulses, the velocity can be calculated for each individual particle. Velocity information is stored in 1024 time of flight bins. Using a polystyrene latex (PSL) sphere calibration, which is stored in non-volatile memory, the APS converts each time of flight measurement to an aerodynamic particle diameter. For convenience this particle size is binned on a logarithm scale in 52 channels.

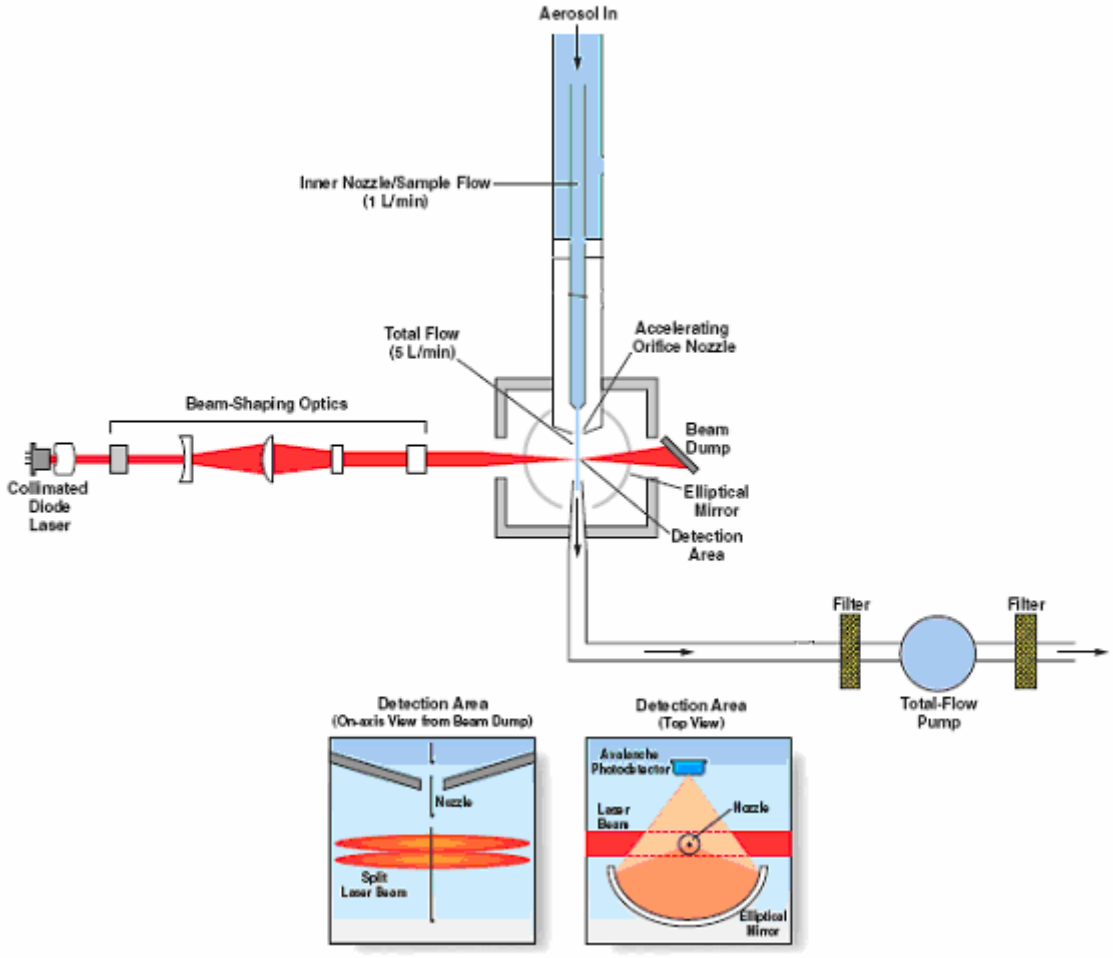

Figure 2.5 – Functioning scheme of the TSI - APS Model 3321.

The use of two partially overlapping laser beams allows obtaining for each particle a single two-crested signal (Figure 2.6). The time between the crests provides aerodynamic particle size information. Peak to peak time of flight is measured with 4 nanosecond resolution for aerodynamic sizing. The amplitude of the signal depends on

the light scattering intensity. After measurement the particle stream exits the optics chamber, drawn by the total flow pump.

The smaller particles generally origin only one detectable crest and therefore they are binned separately. The instrument displays these particles in the smallest size channel (less than 0.523 μm).

If more than one particle is in the viewing volume, more than two crests appear and the APD logs this separately as a coincidence event. In this case the particles are also binned separately, but they are not used to build aerodynamic size of light scattering distribution. Coincidence typically increases proportionally with particle concentration.

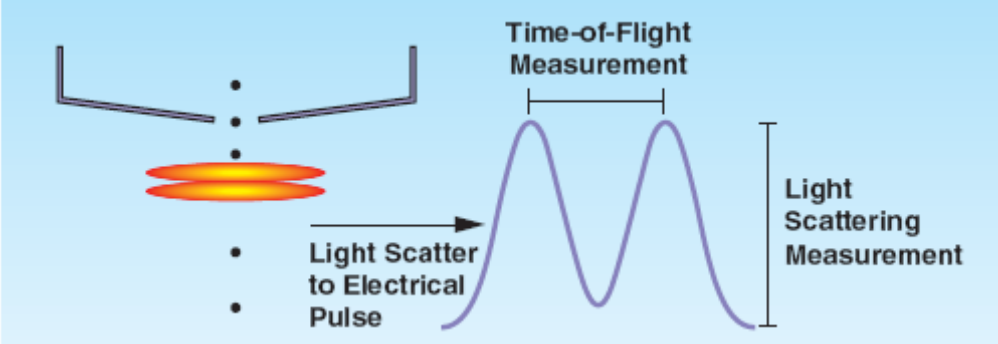

Figure 2.6 - The TSI - APS spectrometer Model 3321 uses a patented optical system to produce one double-crested signal for each particle, therefore it allows performing highly accurate measurements.

Every particle signal is processed in real time as one of four distinct events. The event 1 (Figure 2.7) occurs when the signal for a small particle cannot stay above the threshold and only one crest is detected. The measurement is aborted, and the time of flight of the particle is not recorded. However, the event is logged for concentration calculations and displayed in the lowest size channel.

The event 2 (Figure 2.8) is a valid particle measurement. The signal stays above the threshold and two crests are detected. The time of flight between the two crests is recorded and the events are included in the concentration calculations.

The event 3 (Figure 2.9) is caused by coincidence. Although the signal stays above the threshold, three or more crests are detected. Events of this type are logged but not recorded for concentration or time of flight.

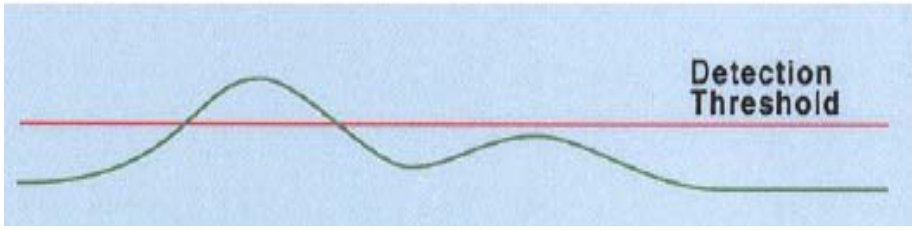

Figure 2.7 – Event 1 occurs when the signal of a small particle is below a certain threshold. The particle is put into the lowest size class (< 0.523 μm).

The event 4 (Figure 2.10) is outside the maximum range of the timer. The signal remains above the threshold until it moves outside the timer range, and only one crest is detected. A type 4 event is normally caused by large or recirculating particles. Again, the event is logged, but no time of flight is recorded.

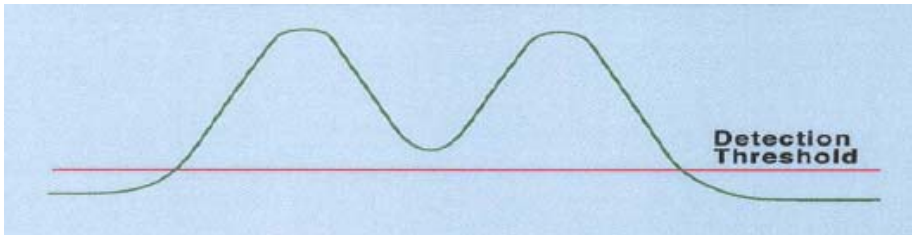

Figure 2.8 – Event 2 is a valid measurement. The particle is classified.

APS operates at flow rate of (5.0 ± 0.2) L/min. The maximum recommended concentration measured by the instrument is 1000 particles/cm^3 at 0.5 and 10 μm, with coincidence errors inferior to 5 % and 10 % respectively; while the minimum particle concentration is 0.001 particles /cm^3. The usable data reach values up to 10000 particles/cm^3.

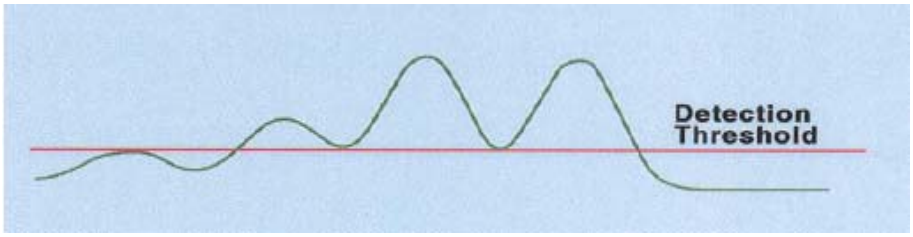

Figure 2.9 – Event 3 occurs due to coincidence. The particle is not classified, however, added to the total concentration.

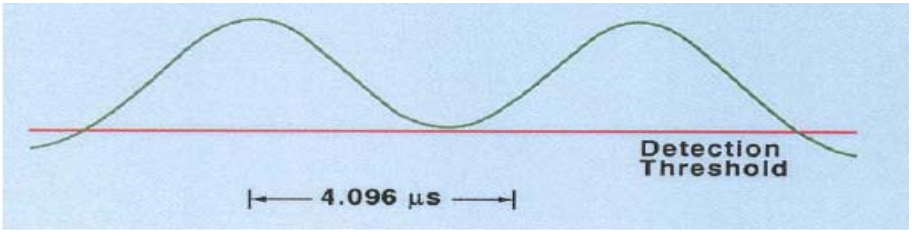

Figure 2.10 – Event 4 occurs when the time of flight is longer the maximum time. The reason therefore is usually due to a large or a recirculation particle. The particle is not classified, however, added to the total concentration.

2.3 Aerosol size distribution results

The most of size distribution observations analyzed in this work have been performed during particular advection patterns events, in order to better understand the variability of aerosols at the monitored site and to assess the impact of long-range transport from various regions on aerosol load and size. To this end the size distribution measurement analyses have been often combined with the study of the analytical 7-day back-trajectories provided by NASA for Lecce being an AERONET site. The trajectories provide important information on the air masses origin observed at a particular location and on dynamical patterns governing the air mass transport (Kazadzis et al., 2007). They are based on the trajectory Code 613.3 developed at NASA/Goddard – The Atmospheric Chemistry and Dynamics Branch* and are provide for distinct arrival pressure levels and for two arrival times (12:00 and 24:00 UTC) on a day-by-day basis.

The transport pathways from different regions can have different effects on aerosol size distribution. A pollution advection event from North-East-Europe can increase the concentration of fine particles since polluted air masses coming from continental countries usually transport particulate matter of secondary anthropogenic origin. Dust outbreaks instead typically have a significant influence on coarse fraction, transporting primary desert aerosols mainly composed by soil and rock particles.

For a given location the monitoring of aerosol size distribution is also important to define the main properties of local aerosol background, in order to better identify the influence of transfrontier air pollution.

Figure 2.11 shows an example of 24-h number size distribution measurement performed on 08 November 2006. The colour scale refers to the number concentration

* (http://croc.gsfc.nasa.gov/aeronet/index.html)

$dN/dlogD_p$ values expressed in cm^{-3}; D_p is the aerodynamic diameter of atmospheric particles. The temporal trend of the number size distribution shows a low particle number concentration during the day; in particular on 08 November at 13:00 hours (solar time) the number concentration reached the lower values. Instead a high number concentration of fine particles (less than 1 μm in aerodynamic diameter) has been recorded during the evening hours, mainly during the night (from 23:00 hours of 08 November to 05:00 hours of 09 November). During the following hours the number concentration decreased but the contribution of fine fraction remained dominant.

The temporal trend of particle size distribution reported in figure 2.11 seems to respond to the diurnal variation of the Planetary Boundary Layer (PBL) which is the region of the atmosphere governing transport and dispersion of pollutants (Senfiled and Pandis, 1998). The depth of the PBL is not constant: it extends upward from the surface to a height that ranges anywhere from 100 to 3000 m and it is directly influenced by the presence of the Earth's surface, responding to such forcings as frictional drag and solar heating.

At night and in the cool season the PBL tends to be lower in thickness while during the day and in the warm season it tends to have a higher thickness. Because the height of the PBL is so dependent on the energy budget of the layer, the diurnal change in surface temperature is one of the most significant factors influencing the PBL. The surface heating of the daytime increases the convective turbulence within the PBL, in a layer called “mixed layer”. At night the PBL contracts due to a reduction of rising thermals from the surface; the dramatic decrease in incoming energy allows the mixed layer to vanish with the sun as the thermally driven convection ceases.

The PBL begins to grow an hour after sunrise and the maximum PBL depth occurs near sunset; as the night progresses, the PBL usually collapses to a shallow layer (Stull 1988; Medeiros et al., 2005).

In figure 2.11 we can observe that at 13:00 hours the minimum value of particle number concentration could be ascribed to a high diurnal depth of PBL and a consequent more efficient atmospheric aerosol dispersion. During the following hours (night and sunrise) the nocturnal contraction of PBL favours a minor dispersion and the growth in particles concentrations.

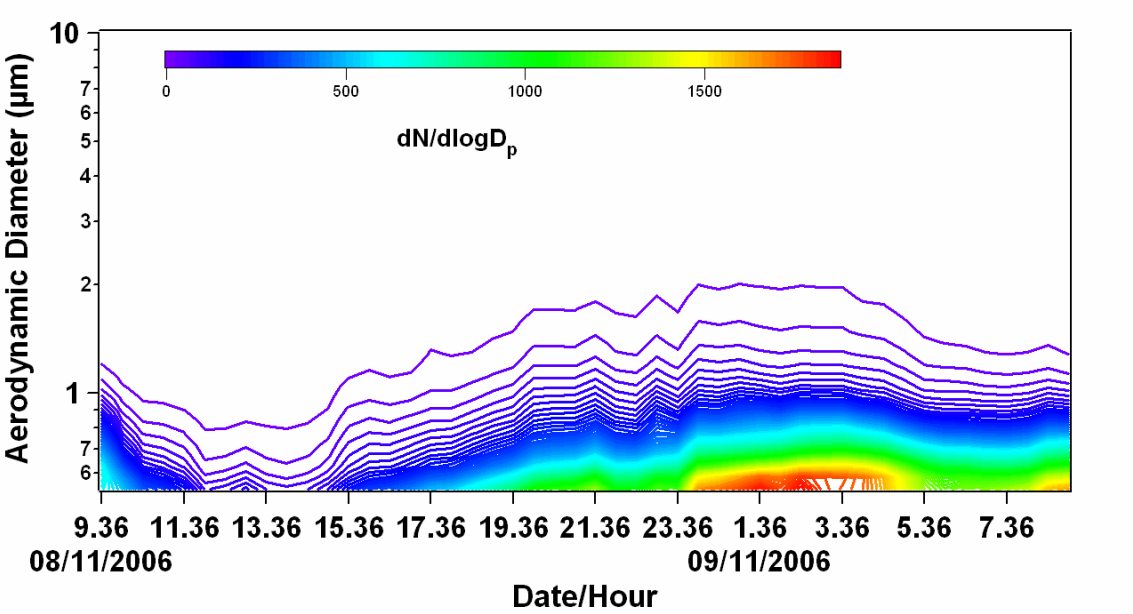

Figure 2.11 – Temporal trend (24-h) of the number size distribution observed at Physics Department of University of Salento on 08 November 2006. The colour scale refers to the $dN/dlogD_p$ values. D_p is the particle aerodynamic diameter.

Figures 2.12 shows the number concentration as a function of aerodynamic diameter at three particular times: 13:36 hours of 08 November (red line) when the number size distribution reached the lower value, 01:36 hours of 09 November (green line) when the concentration was highest and 07:36 hours of the same day (blue line) when the concentration assumed intermediate values. Figure 2.13 illustrates the corresponding volume distributions.

The plots clearly show that the most of particles are less than 1 µm in diameter while most of the particle mass is found in coarse particles (with aerodynamic diameter larger than 10 µm).

In accordance with the discussion reported in chapter 1, the volume distribution allows inferring at least a bimodal size distribution function with a mode in the fine fraction at about 0.6 µm and a second peak in the coarse size interval.

Figures 2.14 and 2.15 show the trajectories followed by the air masses during the 7 days before arriving to the observation site on 08 November at 12:00 UTC and on 09 November at 00:00 UTC respectively. The figures clearly illustrate that the dominant advection pattern coming from North - Europe did not change during the measurement period. This result suggests that the long-range transport process could have affected the

aerosol number concentration increasing the contribution of fine particles (up to 2000 cm^{-3}).

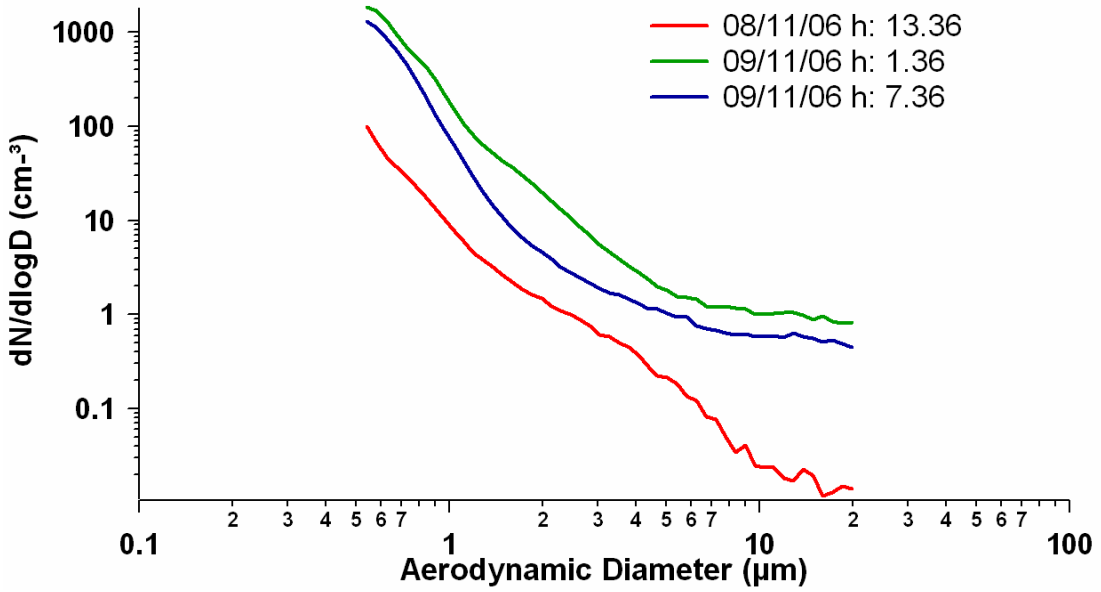

Figure 2.12 – The particle number distribution observed on 08 November 2006 at Physics Department of Lecce at three different times: 13:36 hours of 08 November (red line), 01:36 hours (green line) and 07:36 hours (blue line) of 09 November. The most of particles are smaller than 1 µm.

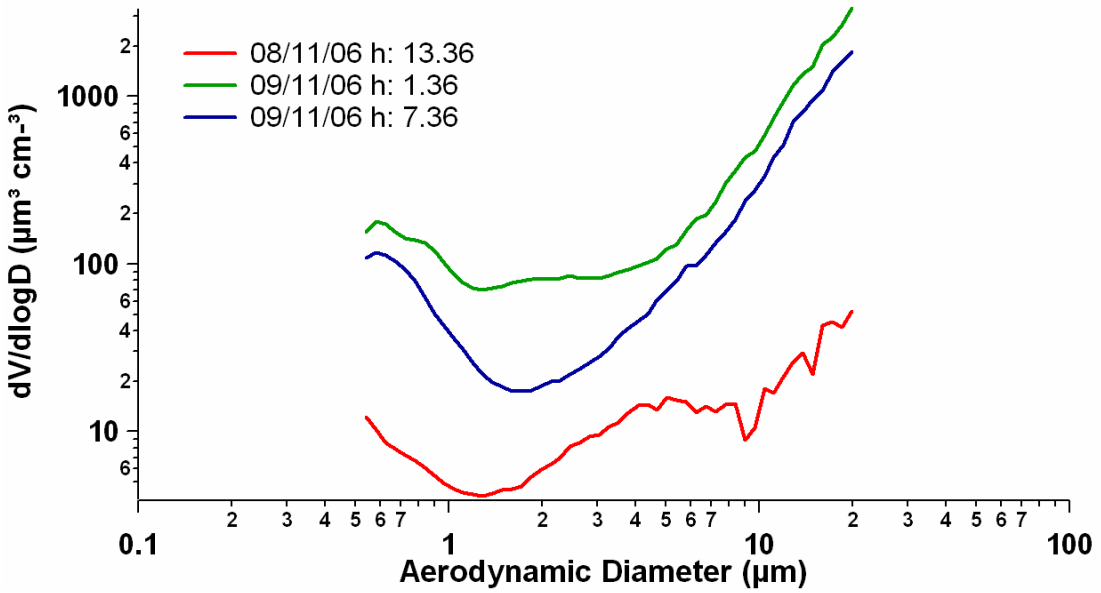

Figure 2.13 – The particle volume distribution observed on 08 November 2006 at Physics Department of Lecce at three different times: 13:36 hours of 08 November (red line), 01:36 hours (green line) and 07:36 hours (blue line) of 09 November. The most of particle mass is found in particles greater than 10 µm in diameter.

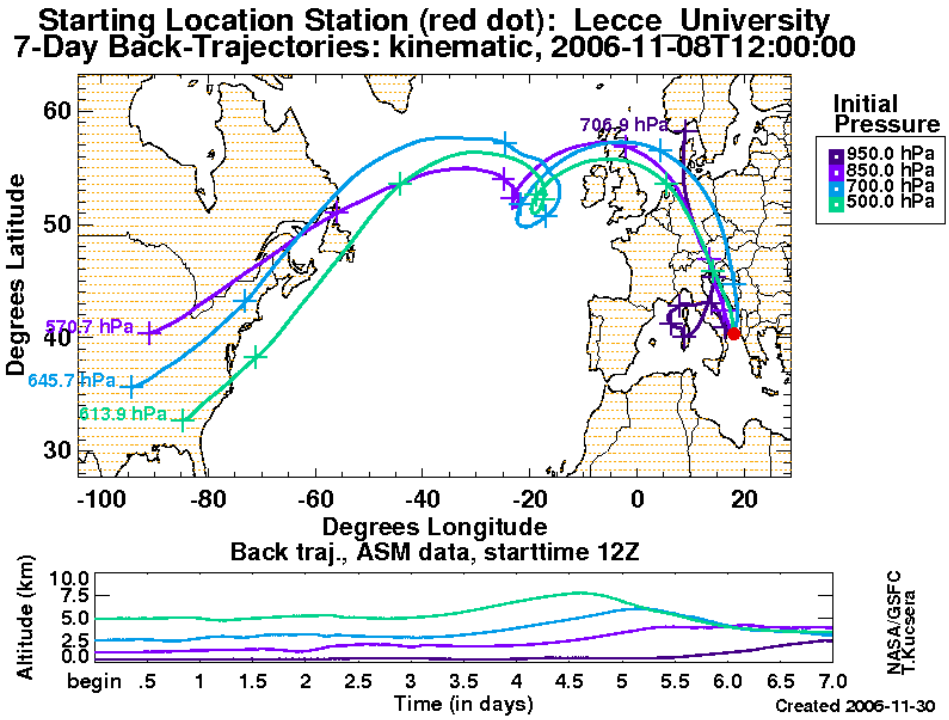

Figure 2.14 – 7-day analytical back - trajectories for the air masses reaching the observation site on 08 November 2006 (at 12:00 UTC) and pressure levels of each back trajectory as a function of time.

Another interesting set of examples of particle number distribution measurements is reported in figures 2.16-2.19. The contour plots show the chronological temporal trend (solar time) of the particle number distribution as a function of the aerodynamic diameter, observed during an intensive monitoring campaign (IMC) carried out from 06 to 10 February 2008 within the FIRS Project "Aeroclouds". The measurements have not been performed continually, but during different time intervals in accordance with the campaign scheduled measurement time intervals of the IMC. Each figure shows the results referring to the data collected during the single time interval. From figures 2.16-2.19 we can observe that the trend of the number size distribution and the concentration values vary day after day. At the beginning of the campaign, on 06 February, the number concentration values are quite high (up to 1300 cm^{-3}) and the fine fraction is dominant. During the following day, in particular from 13 hours of 07 February, the concentration values decrease (from 20 to 120 cm^{-3}) and particles with a higher aerodynamic diameter (up to 3 μm) appear in very low concentration.

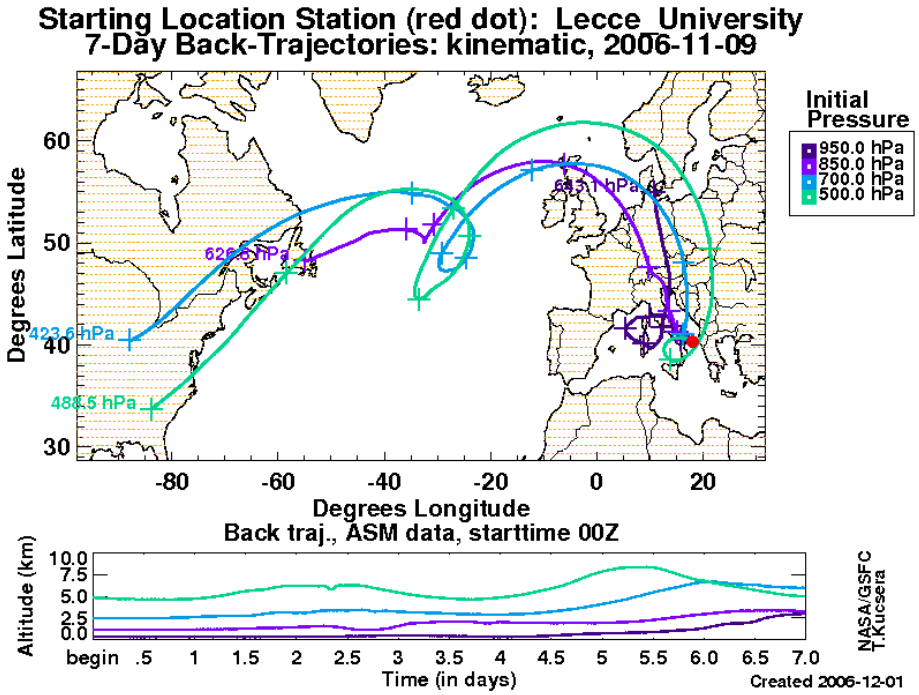

Figure 2.15 – 7-day analytical back - trajectories for the air masses reaching the observation site on 09 November 2006 (at 00:00 UTC) and pressure levels of each back trajectory as a function of time.

The size distribution observed on 08 February is characterized by very low particle concentrations for each aerodynamic diameter. During the night and the first hours of 09 February the contribution of fine particles increases again, although the concentration values remain low until the end of the campaign.

The analysis of analytical 7-day back-trajectories showed that the main long-range transport processes changed during the campaign. In particular on 07 February at 00:00 UTC two advection patterns dominated (Figure 2.20): from South at low pressure levels and from West at higher altitudes. This transport pathway remains unchanged until 08 February at 12:00 UTC (Figure 2.21), then it changed and the trajectories at low pressure levels arrived from East (Figures 2.22-2.23).

It is important to note that at the beginning of the campaign the contribution of coarse particles could be slightly influenced by the transport from South region; then the shift of the transport pathway on East-Europe could affected the concentration values of fine fraction particles. However these results show that during the observation period the main advection pattern over the monitoring site was essentially considered mixed. The lack of marked signs of clear advection pattern events and the very low concentration values make difficult the interpretation of results.

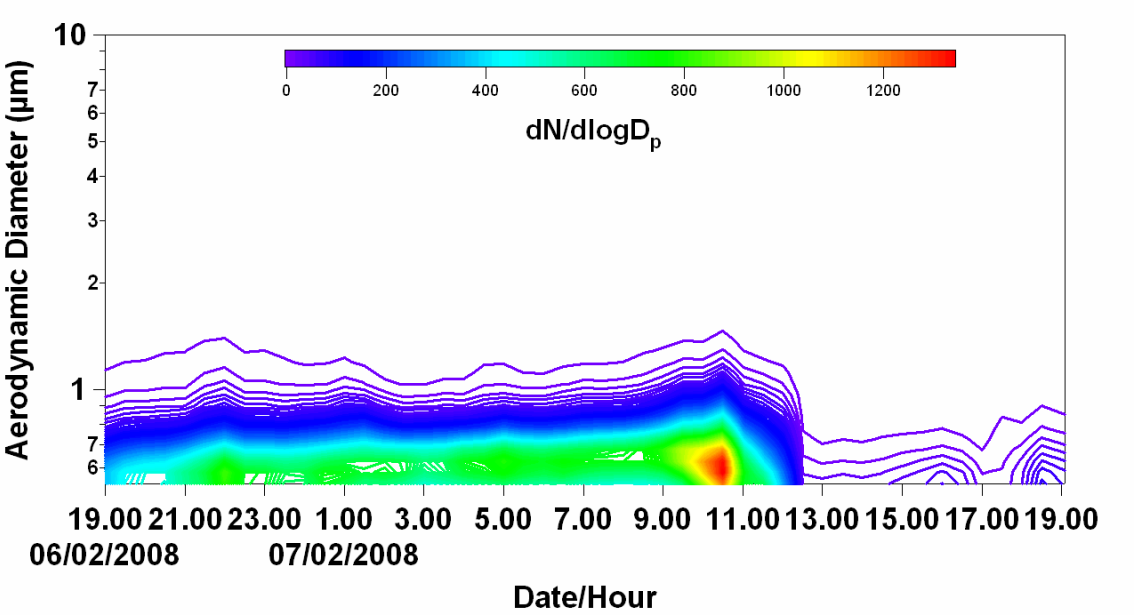

Figure 2.16 – Temporal trend of the number size distribution observed at Physics Department of University of Salento from 06 to 07 February 2008. The colour scale refers to the $dN/dlogD_p$ values. D_p is the particle aerodynamic diameter.

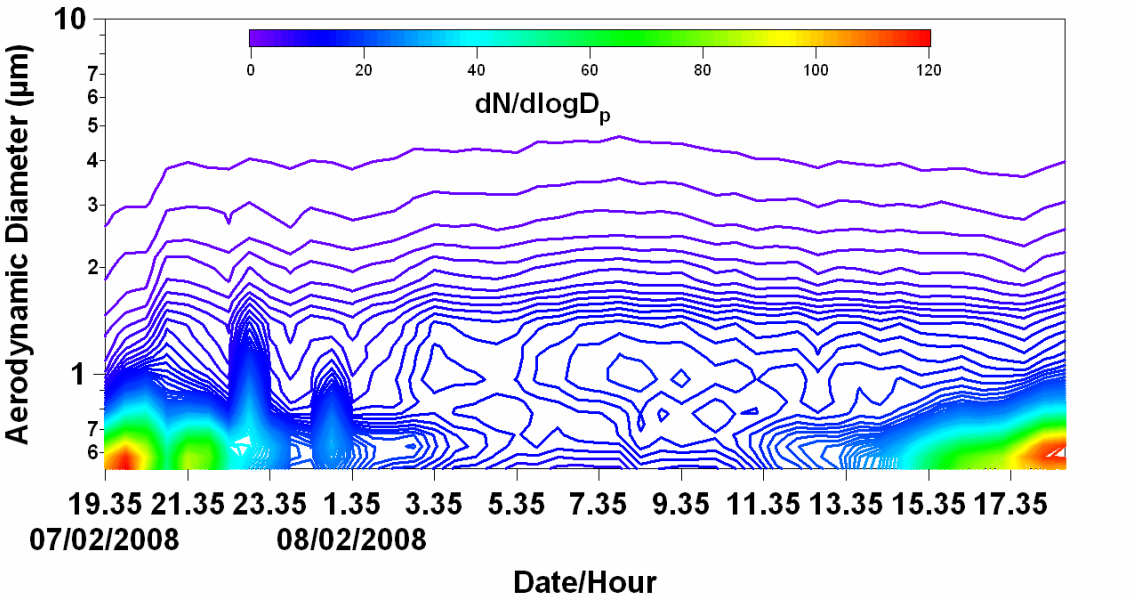

Figure 2.17 - Temporal trend of the number size distribution observed at Physics Department of University of Salento from 07 to 08 February 2008. The colour scale refers to the $dN/dlogD_p$ values. D_p is the particle aerodynamic diameter.

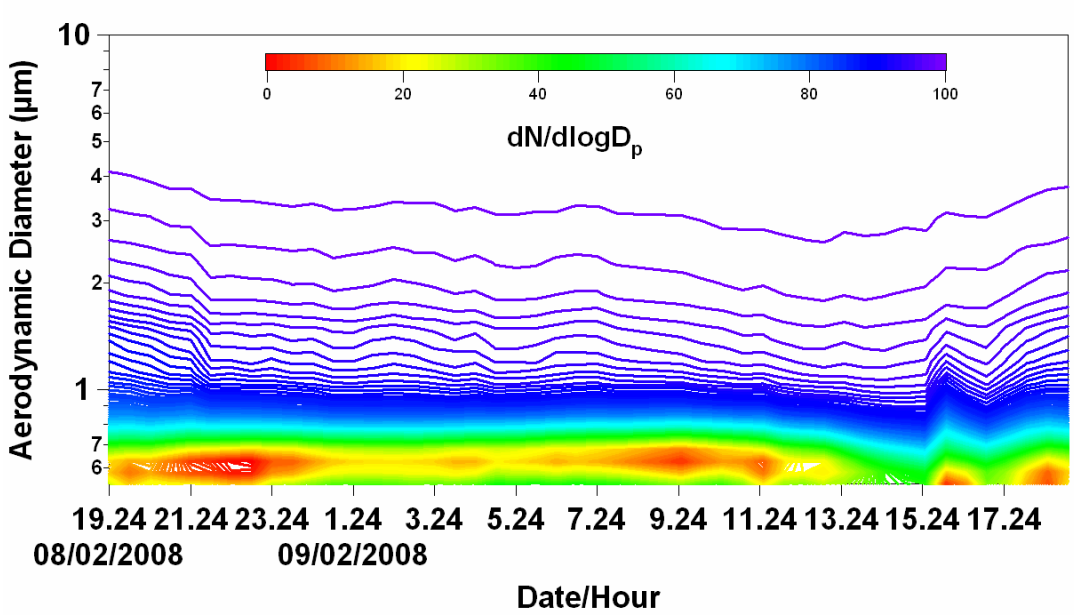

Figure 2.18 - Temporal trend of the number size distribution observed at Physics Department of University of Salento from 08 to 09 February 2008. The colour scale refers to the $dN/dlogD_p$ values. D_p is the particle aerodynamic diameter.

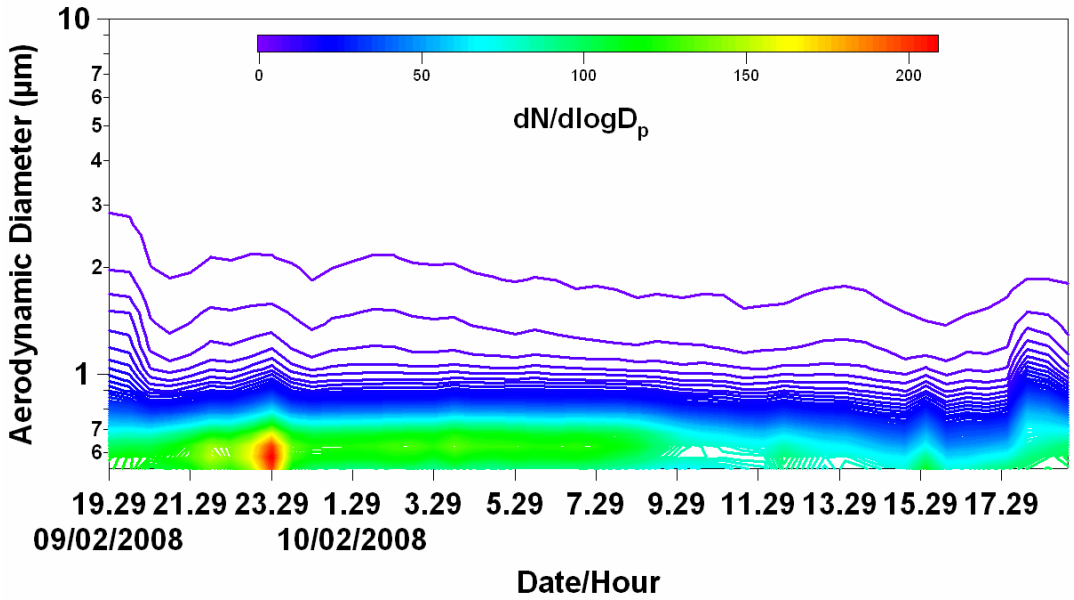

Figure 2.19 - Temporal trend of the number size distribution observed at Physics Department of University of Salento from 09 to 10 February 2008. The colour scale refers to the $dN/dlogD_p$ values. D_p is the particle aerodynamic diameter.

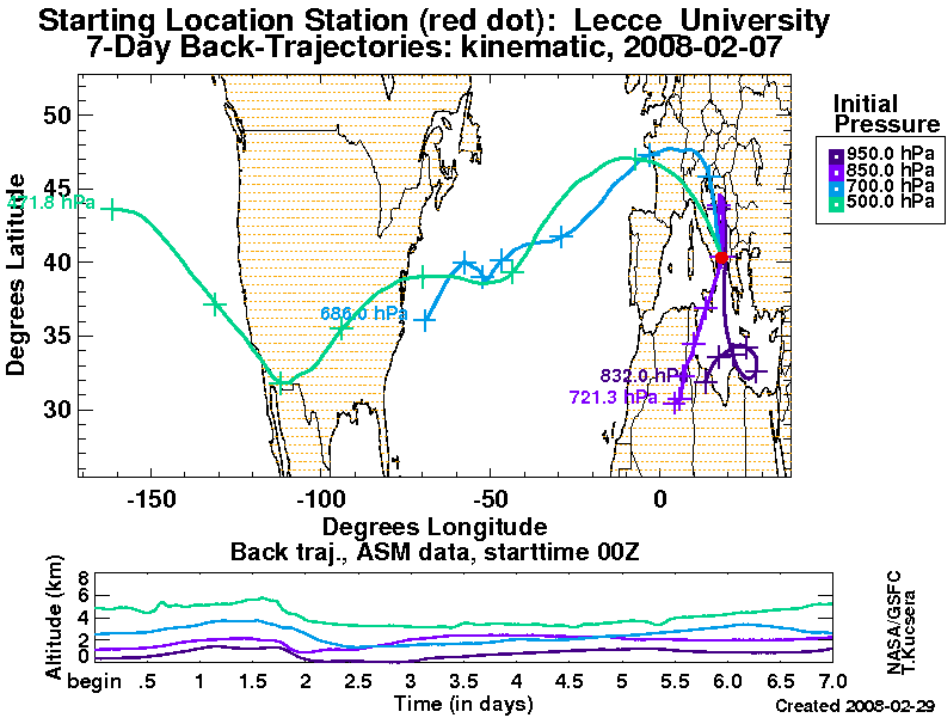

Figure 2.20 – 7-day analytical back - trajectories for the air masses reaching the observation site on 07 February 2008 at 00:00 UTC and pressure levels of each back trajectory as a function of time.

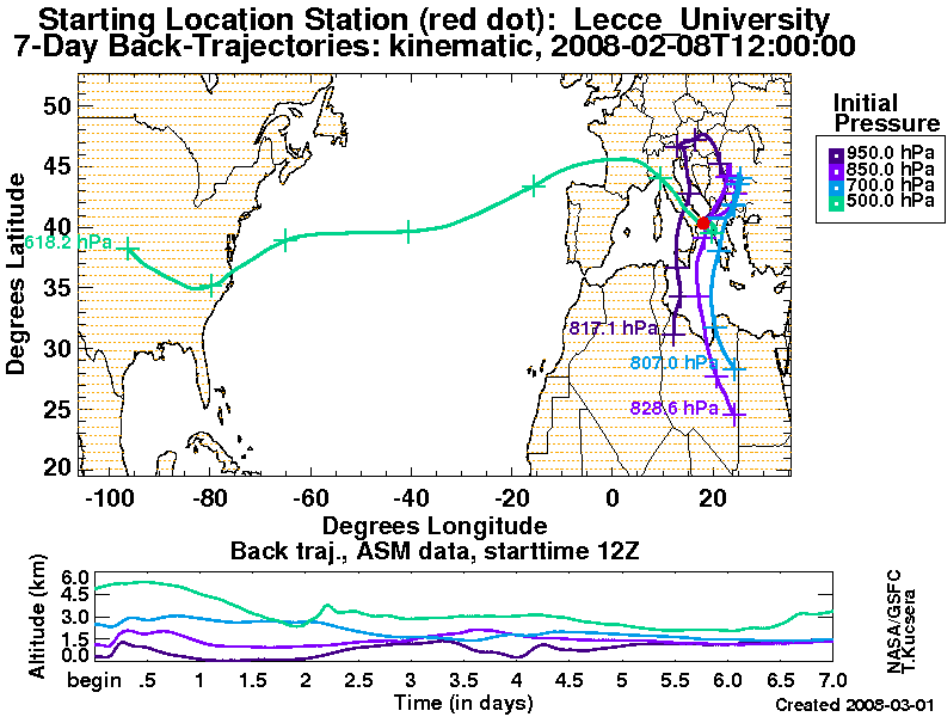

Figure 2.21– 7-day analytical back - trajectories for the air masses reaching the observation site on 08 February 2008 at 12:00 UTC and pressure levels of each back trajectory as a function of time.

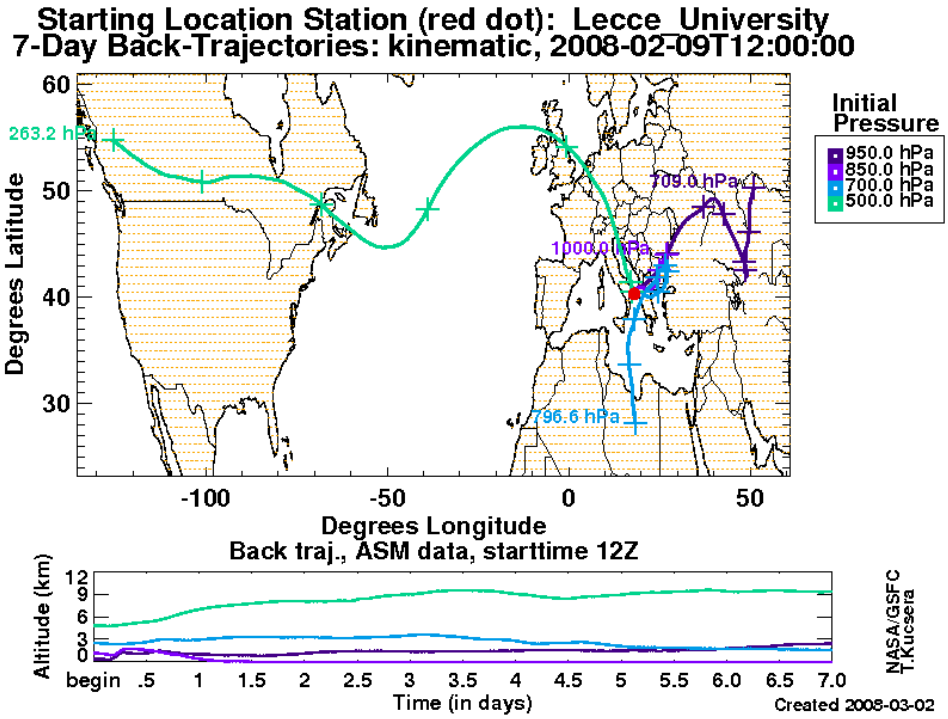

Figure 2.22 – 7-day analytical back - trajectories for the air masses reaching the observation site on 09 February 2008 at 12:00 UTC and pressure levels of each back trajectory as a function of time.

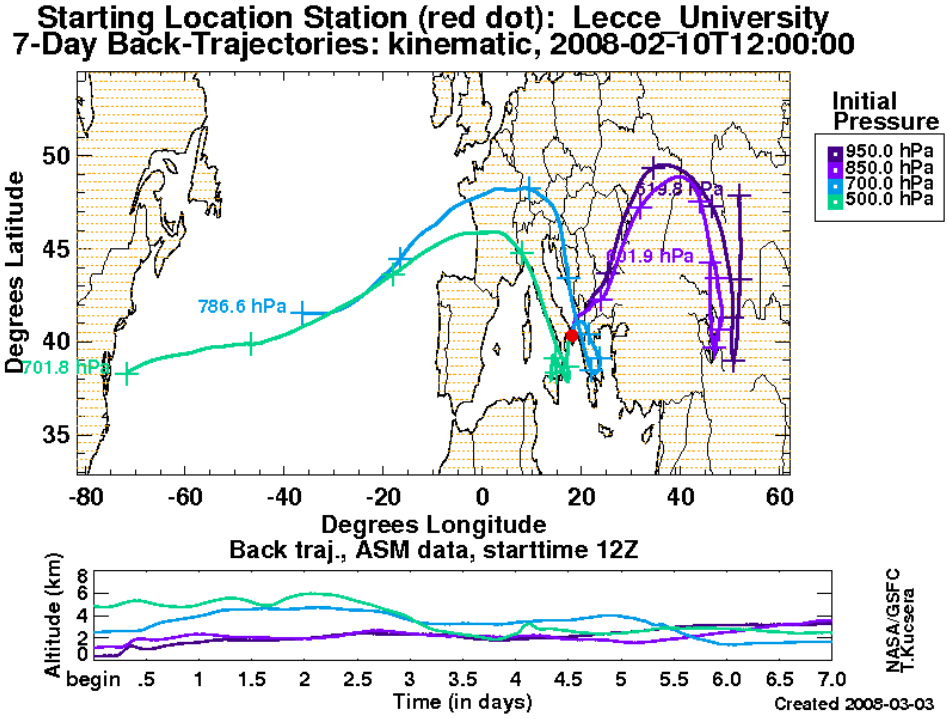

Figure 2.23 – 7-day analytical back - trajectories for the air masses reaching the observation site on 10 February 2008 at 12:00 UTC and pressure levels of each back trajectory as a function of time.

The PM10 mass concentration values obtained from sampling measurements performed during the IMC supported the particle number size distribution results. In fact, from 06 to 08 February 2008 the 24-h mass concentration value decreased from 38 to 19 $\mu m/m^3$; during the following day the mass concentration slightly increased to 32 $\mu m/m^3$ and decreased again at the end of the campaign reaching a value of about 21 $\mu m/m^3$.

The combined results made us to believe that during the campaign the contribution of long–range transport processes on ground level particulate matter concentration is negligible.

CHAPTER 3

PARTICULATE MATTER SAMPLING DEVICES

3 PARTICULATE MATTER SAMPLING DEVICES

In recent years the need to measure aerosol properties has increased, mainly because of the adverse effects they have on human health and environment and for the role they play in atmospheric processes and climate changes. Legislation requires measuring particle emissions and ambient particle mass and/or number concentrations and exposure times, to ensure that limits are met and the public is not exposed to undesirable concentrations of aerosols.

The mass concentration represents the most commonly monitored parameter to quantify the atmospheric particulate matter and it is routinely measured in monitoring stations in various locations around the world. A common used technique for measuring particulate mass concentration involves filtration (Chow, 1995; Spurny 1999; McMurry, 2000): atmospheric particles are collected on a filter using suction for offline gravimetric mass measurements.

The main goal of this PhD research work is to investigate the dependence of the particulate matter mass concentration and composition on particle size; to this end in situ measurements have been carried out using several sampling devices equipped with different PM inlets (TSP, PM10, PM2.5 and PM1). In this chapter after a short presentation of the air quality legislation directives, the particulate matter sampler devices used for this PhD work are presented and described.

3.1 Ambient air quality directives

Adverse effects of atmospheric aerosols on environment and principally on human health have stimulated many controlled studies of airborne particles and led to the establishment of ambient air-quality standards.

Authorities have attempted to place controls on the total amount of annual pollution and the magnitude of pollution episodes in order to reduce the health burden of atmospheric particulate.

The total suspended particulate (TSP) matter has been used at first as indicator of suspended particles in ambient air. In 1987, the monitoring of TSP has been replaced by PM10 measurements in the Unites States as a result of a review of the National Standards (US-EPA, 1986). In Europe, the Council Directive 1999/30/EC (1999)

established limit values for PM10 (Table 3.1) in ambient air to avoid, prevent or reduce the effects on human health and environment. PM10 is the particulate matter fraction, also called inhalable particles, which can pass into the upper airways of the respiratory system (nose and mouth) becoming a great concern for human health (Englert, 2004). Fuel oil and coal, cement factories, road traffic, combustion installations burning and waste incinerators are the major sources of these particles (WHO, 2003).

Table 3. 1– Limit value for PM10 (European Council Directive 1999/30/EC – D.M. n. 60 - 02/04/2002).

STAGE 1		
Averaging period	**Limit value PM10**	**Date by which limit value is to be met**
24 hours	50 μg/m^3 not to be exceeded more than 35 times a calendar year	1st January 2005
Calendar year	40 μg/m^3	1st January 2005

STAGE 2		
Averaging period	**Limit value PM10**	**Date by which limit value is to be met**
24 hours	50 μg/m^3 not to be exceeded more than 7 times a calendar year	1st January 2010
Calendar year	20 μg/m^3	1st January 2010

Attention has recently shifted to investigating ambient PM2.5 because fine particles that are dispersed through the atmosphere have a greater influence on health effects. Fine particles, generally called respirable particles, can penetrate and block the very small passages of the lungs. Of particular interest are sources of fossil fuel combustion because they have been hypothesized potentially contributing to the observed link between atmospheric particulate matter and health effects. Countries like Unites States introduced standards also for particles smaller than 2.5 μm in diameter (US-EPA, 1997) and last year in Europe the European Commission focused on the fine atmospheric particles levels and established a PM2.5 annual limit of 25 μg/m³ (Table

3.2) not to be exceeded in any site of E.U. from 1 January 2015 (Council Directive 2008/50/EC, 2008).

Table 3. 2– Limit value for PM2.5 (European Council Directive 2008/50/CE).

STAGE 1			
Averaging period	**Limit value PM2.5**	**Margin of tolerance**	**Date by which limit value is to be met**
Calendar year	25 μg/m^3	20% on 11 June 2008, decreasing on the next 1 January and every 12 months thereafter by equal annual percentages to reach 0% by 1 January 2015.	1st January 2015

STAGE 2$^{(*)}$			
Averaging period	**Limit value PM2.5**	**Margin of tolerance**	**Date by which limit value is to be met**
Calendar year	20 μg/m^3		1st January 2020

$^{(*)}$ Stage 2 – Indicative limit value to be reviewed by the Commission in 2013 in the light of further information on health and environment effects, technical feasibility and experience of the target value in Member States.

3.2 Particulate matter measurements

The volumetric mass concentration of particulate matter represents worldwide used parameter for environmental monitoring and control. Mass measurements may be made directly or indirectly.

Direct (or manual) measurements consist in collecting airborne particles using suction on a pre-weighed substrate over a specified period.

Indirect method implies the measurements of other particle properties closely related to particle mass.

In direct measurements the use of filters has become the most method of collecting airborne particulates. Advantages include low cost, simplicity, small space requirement for storage and a wide choice of available filter media and sizes.

An aerosol sampler comprises a suction system, an inlet system, a filter assembly and the associated instrumentation and control system. The suction system acts allows intaking the air to be sampled. The sucked air particles are then collected on the filter. The flow rate and the period of sampling are controlled by the suction system and the inlet system diverts the unwanted particles away from the path to the filter.

Particulate matter samplers are generally equipped with inlets that eliminate particles above a specified cut-off diameter.

The so-called high volume samplers with an air flow in the range of between 60–90 m^3/h or so-called low volume air samplers with an air flow of between 1–3 m^3/h are widely used: the flow of air varies depending on the filter material and its flow resistance, and on the efficiency of the sampler pump.

The procedure used for the determination of the suspended particle mass concentration by high and low volume samplers is usually based on the gravimetric method: filters are weighed under controlled temperature and relative humidity conditions before and after sampling, and mass concentrations are determined from the increase in filter mass and the volume of the sampled air.

Several mechanisms are involved in filtration. These include direct interception, inertial impaction, diffusion, electrical attraction, and gravitational forces.

Interception occurs when a particle following an air stream gets in contact with a surface, such as a filter fiber, and adheres to it.

Impaction occurs when a particle, due to its inertia, can not adjust quickly enough to the changing direction of the air stream. As the air stream deflects around an obstacle, the particle continues toward the object and impacts it. The particle's inertia is a function of its size, density and velocity and so impaction is a very important collection mechanism for larger particles that are collected more easily than smaller particles for their greater inertia.

Inertial impaction and interception are usually highly efficient for particles larger than 10 μm-diameter. They become progressively less effective as the size decreases. Impaction is not efficient for particles less than 0.5 μm-diameter due to their low inertia.

Very small particles (less than 0.5 μm-diameter) in a gas stream deflect slightly when gas molecules strike them. Transfer of kinetic energy from the rapidly moving gas molecule to small particles causes these deflections (Brownian diffusion).

The Brownian diffusion becomes an important collection mechanism for particles less than 0.5 μm-diameter and is especially significant for particles in the 0.01 to 0.1 μm size range.

Electrostatic attraction results when particles are attracted to a surface because of opposing electrical charges on the particles and surface. This can be due to natural charges or charges induced on the particle or collecting surface. In general, naturally occurring charges are not an important collection mechanism.

Deposition by gravitational settling occurs as a result of the influence of gravity on particles suspended in the air.

One or more of these mechanisms could predominate in a given case and depend on the flow rate, the nature of the filter and of the aerosol (Lippmann, 1978). With fibrous and membranes filters particles are removed from the air stream primarily by impaction and diffusion mechanisms. Direct interception and electrostatic deposition may also be present, but in the case of fiber and membrane filters, usually are less important.

Filter media used for the collection of particulate matter by high and low volume samplers are available in a wide variety of sizes and with different pore size: teflon membranes, polystyrene, cellulose acetate, polytetrafluoroethylene (PTFE) membranes, quartz, cellulose, cellulose ester, nitrocellulose, nylon, polystyrene, silver membranes, graphite, and glass fibre filters.

Teflon filters are generally composed of a thin, porous polytetrafluoroethylene (PTFE) teflon sheet stretched across a ring. They are commonly used for mass and elemental analysis (X-ray and proton-induced fluorescence). This type of filter is very chemical resistant and hydrophobic but not good for high flow rates because of the fragile filter structure.

Quartz filters that are made by woven quartz filaments are widely used for Ion Chromatography, carbon analyses, atomic absorption and particulate mass concentration measurements. The collection efficiency, the relative low moisture uptake and the low trace contaminant levels represent main advantages of quartz filters.

Nylon filters consist of porous nylon sheets and are generally used for collection of nitric acid.

Cellulose filters instead consist of tightly woven paper mat. They are inexpensive and allow a convenient extraction of particulates. In addition they are very

sensitive to humidity but they are not good for the collection of submicron sized particles.

The polycarbonate membrane filters are made by a thin polycarbonate sheet characterized by pores of uniform diameter. These filters are used for size selective measurements; they are good for analysis by electron microscopy but carry electrostatic charge.

Different methods for the determination of aerosol particle mass have been extensively tested. Since different methods may give rise to systematic differences in the results, standardisation is necessary as specified by the European Union and the European Standards Organisation.

The EN 12341 regulation defined in EU Directive 1999/30/EC (1999), specifies the reference method for the determination of PM10 mass concentration: it is required that the filters are equilibrated, at 20° C (±1) and 50% relative humidity (±5), for 48 hours. This equilibration must before the and after sampling. These precautions intend to minimize the liquid water absorbed by soluble compounds. Nominal values of relative humidity and temperature best conserve the particle deposit during sampling weighing.

Exposed filters should immediately be left to equilibrate, or stored in a fridge or cooling room (< 10^{o}C) prior to equilibration to reduce the losses by volatile species. Care must be taken to avoid condensation of water onto the filter.

The EN 12341 also gives detailed instructions with respect to comparisons, which are required to show that alternative samplers are equivalent to the reference methods for determination of PM10.

3.3 Descriptions of PM samplers

In this PhD thesis the determination of PM mass concentration has been performed using direct measurements. In order to obtain the major information from different combined measurements, several particulate matter sampling devices have been used. The attention has been focused mainly on the monitoring and characterization of fine particles which, as previously discussed, compose the most alarming PM fraction.

A low volume HYDRA (FAI – Instruments) automatic dual sampler and a manual low volume FH95KF (Thermo ESM Andersen) sampler have been used to

collect PM on filters and to determine mass concentrations by gravimetric measurements.

A 7-stages cascade impactor (OH – 610 – C, Kálmán System) has been used to collect size-segregated particulate matter. Subsequently some selected size-fractionated samples have been morphologically and compositionally characterized by the Scanning Electron Microscopy (SEM) technique.

Quartz fiber filters have been used in the most of gravimetric measurements for their very high efficiency, although their fibrous nature makes difficult morphological analyses of collected atmospheric particles.

In order to control and minimize uncertainties, the sampling of particulate matter and the weighing of filters have been carried out according to the standard operation procedures to assure high quality of sample processing. In fact each measurement contains a degree of uncertainty due to the limits of the measurement system and to the people using the equipment. The major sources of errors concerning the sampling and analyses of particulate matter samples include: loss of collected aerosol species during sampling or after sampling, artefacts or contamination of samples, sample handling, transport and storage, modification of samples during analyses and errors in data handling.

Following the European directive procedures filters have been weighed using a microbalance with a resolution of 10 μg located in a temperature and relative humidity controlled environment before and after collections of particles.

3.3.1 Hydra dual sampler – FAI Instruments

The Hydra dual sampler (Figure 3.1) is a dual channel automatic and sequential sampling system of PM that allows collecting particles on two independent filter membranes. The instrument can work with any sampling inlet (TSP, PM10, PM2.5 and PM1) within the operating flow rate range 0.8 ÷ 2.5 m^3/h, on the two independent channels.

Figure 3.2 shows the sampling unity which inside includes all Hydra sampling mechanisms and devices: the control panel is on the frontal side while communication interfaces and electrical and pneumatic connections are on the back side. The filter loader and unloader seats are on the top with the sampling line junctions.

Figure 3.1 – Hydra dual sampler (FAI-Instruments).

Figure 3.2 – Hydra (FAI – Instruments) sampling unity.

Figure 3.3 shows the Hydra sampler functioning diagram: two vacuum pumps, located downstream of the sampling unity, suck ambient air through the sampling inlets, the lines and the filter membranes.

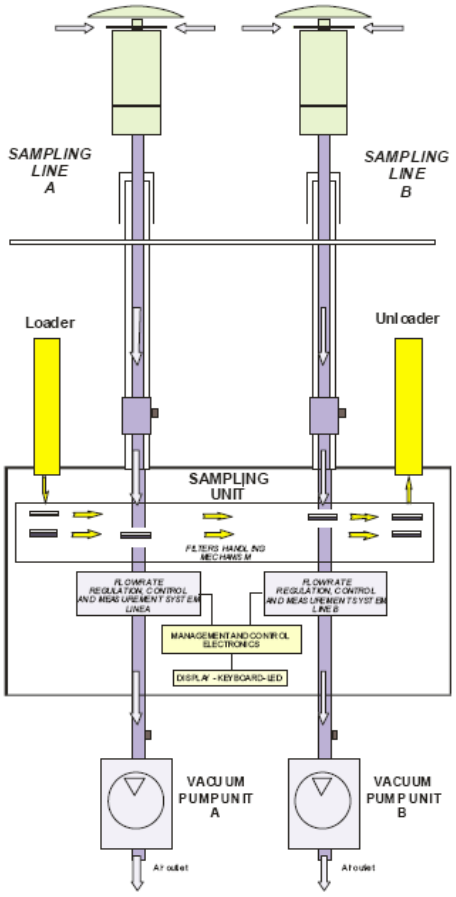

Figure 3.3 – Functioning diagram of Hydra dual sampler.

Each sampling inlet (Figure 3.4) operates as an impactor with a particular cut-off aerodynamic diameter and it is provided with anti-rain and anti-wind features. Inertial impactor operates on the principle that if particles in a moving air stream are suddenly deflected from a straight course by an impaction surface which forces the air stream to have an abrupt change direction, the inertia of the entrained particles may cause them to deviate from the streamlines of airflow and impact against the deflection surface which operates as an impaction surface.

The sampling method of Hydra dual sampler meets requirements of the norm EN 12341 Annex B1. The sampler when is equipped with a low volume PM10 inlet (model LV-PM10 – FAI Instruments) follows the requirements reported in D.L. n. 60 (02/04/2002), therefore Hydra dual sampler can be used as reference sampler. The LVS-PM10 sampling inlet of Hydra dual sampler operates at low volume condition (2.3 m^3/h) and the sampling system can automatically assure the constant flow rate.

Figure 3.4 – LSV sampling inlet (2.3 m^3/h) of Hydra dual sampler.

3.3.2 Particulate sampler FH 95 KF – Thermo ESM Andersen

The low volume (2.3 m^3/h) sampler FH 95 KF (Thermo ESM Andersen) has been designed for the manual determination of the suspended particulate mass concentration in the ambient air. The sampler has a pressure and temperature compensated probe to allow a precise measuring of the air flow rate at ambient and standard conditions; moreover the air flow rate is controlled at a stability of about 1%.

For the manual determination of the concentration of airborne particles each filter is weighed after and before the sampling. The pump is switched off automatically at the end of the sampling procedure and the accumulated volume flow is indicated and saved. The volume flow is measured and kept on a constant level by means of a variable speed pump.

Figure 3.5 shows the sampling unity of FH 95 KF. The sampler can be equipped with different low volume particulate matter inlets (TSP, PM10 and PM2.5).

Each PMx inlet (Figure 3.6) acts as a single stage impactor with integrated filter holder for use with circular filters with a diameter of 47 mm. Moreover each inlet is equipped with a special surface protection in aluminium EMATAL and includes special water separator and easily exchangeable impactor baffle plate.

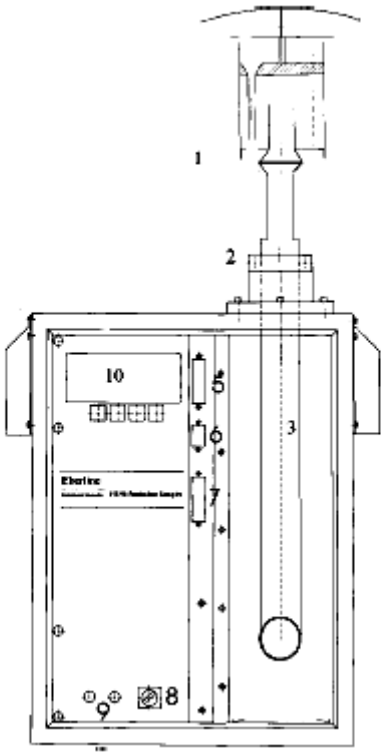

Figure 3.5 – FH 95 KF sampling unity: (1) LSV PM inlet; (2) connection for sample inlet; (3) tube; (5 - 6) data interfaces; (7) status signals; (8) power switch; (9) fuses; (10) displays for measurement data and operational menu.

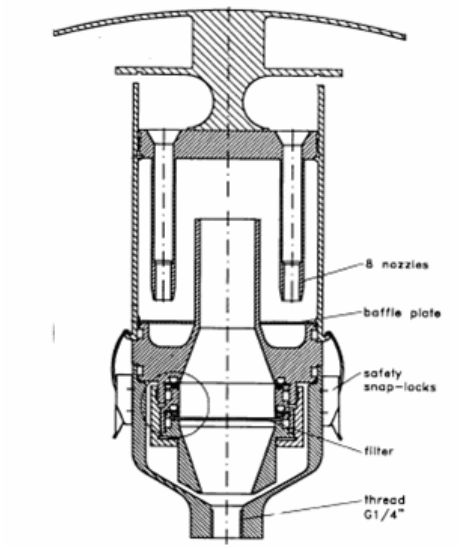

Figure 3.6 – Low volume inlet of the FH 95 KF sampler. The inlet is projected according to specification of EN 12341 Annex B1, with integrated filter holder for use with circular filters with a diameter of 47 mm.

3.3.3 Seven stage cascade impactor OH – 610 – C – Kálmán System

Size-selective sampling refers to the collection of particles below or within a specified aerodynamic diameter. Multi-stage inertial impactors provide a means of segregating particles on the basis of size; these instruments are used to separate particles into several size fractions for the determination of mass and chemical composition as a function of size.

In the impaction processes the air stream is accelerated through a small nozzle and subsequently directed on a flat plat, placed closed to the jet outlet. This surface forces the air stream to have abrupt 90° bends in the streamlines. As particles pass through the exit of the nozzle, those with sufficient inertia cross the flow stream and impact directly on the collection surface, while smaller particles remain entrained in the air (Figure 3.7).

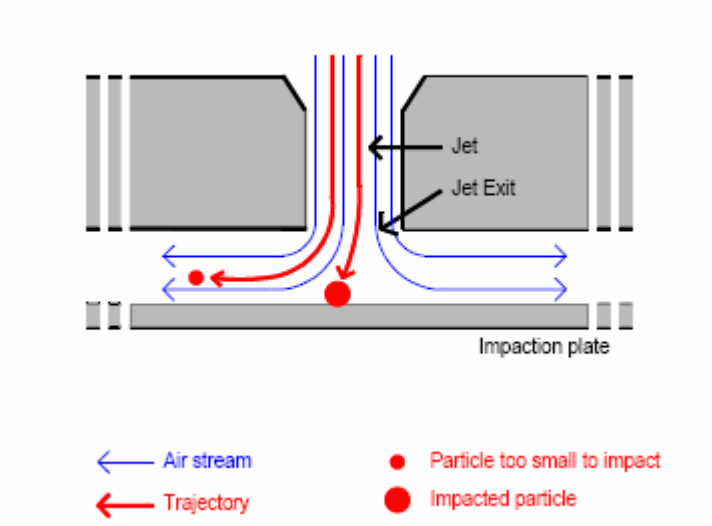

Figure 3.7 – The principle of impaction: a collection surface (the impaction plate) is placed close to the jet outlet. The particles must make an abrupt angle change of direction to follow the air stream. Larger particles with a high inertia impact, while small particles can remain in the air stream.

Inside a multi-stage impactor the aerosol is drawn from a stage to the next one: as velocity increases from stage to stage, smaller particles acquire sufficient inertia to reach the impaction surface (Figure 3.8). In this way, impactors divide an aerosol sample into a number of defined size fractions, each of which can be analyzed to determine chemical composition.

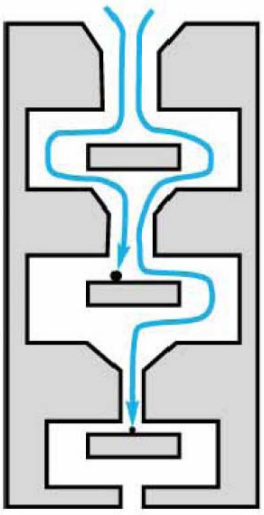

Figure 3.8 – Multistage cascade impactor: the aerosol is drawn from a stage to the next one: as velocity increases from stage to stage, smaller particles acquire sufficient inertia to reach the impaction surface.

Most of the impactors are well designed and can be assumed as ideal. Their collection efficiency is 50% meaning that the mass of the collected particles below cut-off size equals the mass of particles larger than the cut-off.

One problem involved in the use of impactors is bounce: because of coarse particles tend to be dry and solid, when they impact on a hard surface they can bounce and be carried away with the air stream (Whitby, 1978). One technique useful to minimize this effect is to use a porous substance such as a glass or quartz fiber filter. Another technique is to coat the impaction surface with adhesives such as mineral oil or grease, but this can cause problems in weighing and chemical analyses.

In this PhD work size-fractioned measurements have been performed by a 7-stage cascade impactor OH - 610 - C - Kálmán System (Figure 3.9).

The impaction scheme of the seven stages is reported in figure 3.10: each stage consists of an acceleration nozzle and an impaction surface consisting in a quartz fiber substrate. Each substrate is easily inserted and removed from a substrate base and securely transported to the laboratory for gravimetric or chemical analysis. The impactor in a disassembled state is show in figure 3.11.

The whole size-selective system is illustrated in figure 3.12 and consists of vary main sub units: indraught structure integrated with Venturi meter, 7-stage cascade impactor and end filter holder housing with connecting extension. Figure 3.13 shows

the measuring and control unit integrated with pump and motor, connection cables and electric fittings.

Figure 3.9 - The 7-stage cascade impactor OH - 610 - C - Kálmán System.

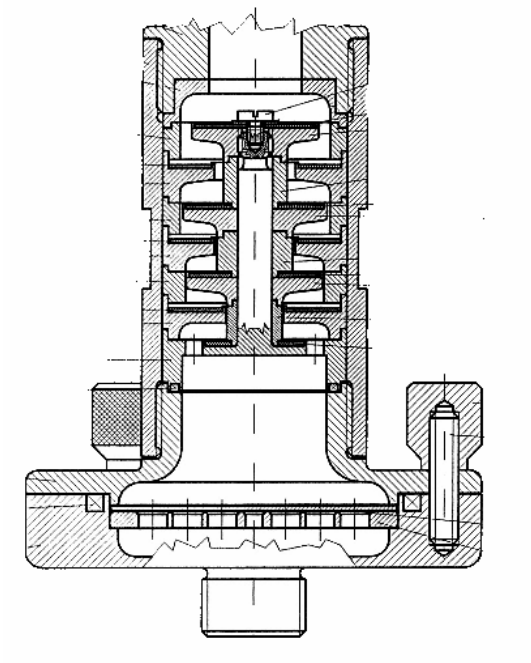

Figure 3.10 – Scheme of the seven stages of the OH-610-C cascade impactor (Kálmán System).

Figure 3.11 – The cascade impactor OH-610-C (Kálmán System) in a disassembled state. In each stage the collection surface is a quartz filter substrate.

The air flows through the sampler structure; after passing a short straight tube section and a Venturi volume flow rate meter the airborne particles are separated on interception plates of the 7-stages impactor. The particles remaining in the air stream are intercepted by a flat filter of 47 mm in diameter (end filter) accommodated in the filter housing. The high-purity air, after passing through a vacuum pump located in the measuring and control unit and a graphite particle separator, is exhausted in the atmosphere.

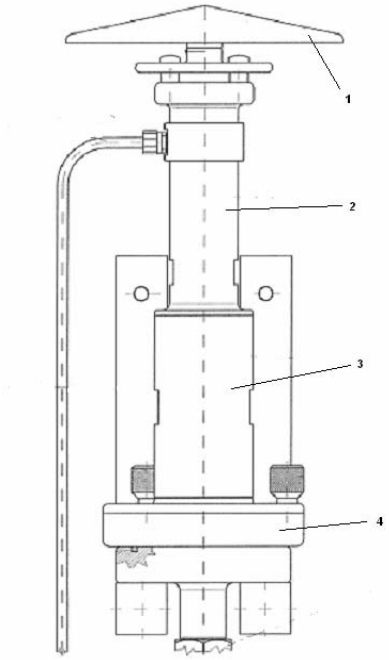

Figure 3.12 – Technical description of OH-610-C cascade impactor (Kálmán System): (1) sampler indraught structure; (2) Venturi volume flow rate meter; (3) seven-stage impactor; (4) end filter housing.

Figure 3.13 – OH-610-C impactor measuring and control unit integrated with pump and motor, connection cables and electric fittings.

The volume flow measuring system, the evaluation unit and the pressure signal of the Venturi meter measure the quantity of suctioned air (m^3/h), the total volume suctioned during the sampling (m^3) and the duration of the sampling.

The OH – 610 – C impactor can operate at different volume flow rate values; the separation characteristics of the sampler corresponding to the vary volume flow rate values are represented in table 3.3.

All size-segregated samples analyzed in this PhD work have been collected operating at a volume flow rate of 1.5 m^3/h; the 50% cut-off aerodynamic diameters corresponding to the different impactor stages are highlighted in grey in table 3.3.

Table 3.3 – OH-610-C cascade impactor 50% effective cut-off aerodynamic diameter as a function of the volume flow rate. The volume flow rate and the corresponding cut-off aerodynamic diameters considered in this PhD work are highlighted in grey.

ρ=1[kg/m³]	**Stage 1.**	**Stage 2.**	**Stage 3.**	**Stage 4.**	**Stage 5.**	**Stage 6.**	**Stage 7.**
t_i = 20 [°C]	**d_{ae} [µm]**	**d_{ae} [µm]**	**d_{ae} [µm]**	**d_{ae} [µm]**	**d_{ae} [µm]**	**d_{ae} [µm]**	**d_{ae} [µm]**
q=1,0 [m^3/h]	7	3.4	1.8	0.81	0.45	0.19	0.11
q=1,2 [m^3/h]	6.4	3.1	1.6	0.74	0.4	0.17	0.09
q=1,5 [m^3/h]	5.7	2.7	1.4	0.65	0.35	0.14	0.08
q=1,8 [m^3/h]	5.2	2.5	1.3	0.59	0.32	0.13	0.07
q=2,0 [m^3/h]	4.9	2.4	1.2	0.6	0.3	0.1	0.06

CHAPTER 4

SCANNING ELECTRON MICROSCOPY ANALYSIS

4 SCANNING ELECTRON MICROSCOPY ANALYSIS

Different analysis's techniques are generally used to properly characterize airborne particles as a consequence of the high variability of their chemical and morphological properties.

Ion Chromatography (IC), Fourier Transformed Infrared (FTIR) spectroscopy, Particle Induced X-ray Emission (PIXE), mass spectroscopy and Scanning Electron Microscopy (SEM) with an Energy Dispersive X-ray (EDX) system represent some of the most used analysis's techniques.

The SEM/EDX technique is commonly employed to get information on the size, morphology and elemental composition of individual atmospheric particles.

This chapter discusses the SEM/EDX technique and the importance of its application in environmental studies. The technique is the best suited one to properly test the performance of the 7-stage cascade impactor.

The morphological and elemental SEM/EDX analyses performed on some selected size-fractioned PM samples collected by the 7-stage cascade impactor are discussed with particular attention.

4.1 The Scanning Electron Microscopy

The scanning electron microscope (SEM) uses a focused beam of electrons to a specimen to generate a variety of signals that can provide information about the sample properties including morphology and chemical composition. In most applications data are collected over a selected area of the surface of the sample, and a two-dimensional image is generated that displays spatial variations in sample's properties. The SEM is also capable of performing analyses at selected point locations on the sample. Figure 4.1 shows a schematic diagram of a scanning electron microscope.

An electron gun with usually a tungsten filament produces electrons by thermionic emissions and accelerates them to energy between about 2 and 40 keV. The condenser lenses demagnify the electron beam until it may have a diameter of only 2-10 nm and the objective lenses focus the beam as a very fine point on the sample (Goodhew and Humphreys, 1988). The scan coils scan the fine beam of electrons across the specimen and the detector measures the signals given off from each point of the

surface. The spot of a cathode ray tube (CRT) is scanned across the screen and the brightness of the spot is modulated by the amplified current from the detector (Figure 4.2). It is important to highlight that the SEM column must always be at a high vacuum mode at a pressure of about 10^{-4} Pa.

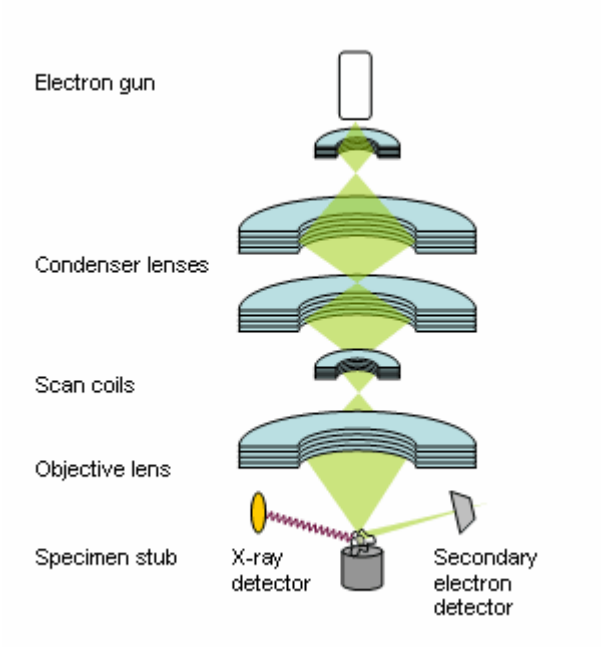

Figure 4.1 – Schematic drawing of the electron optics of a scanning electron microscope.

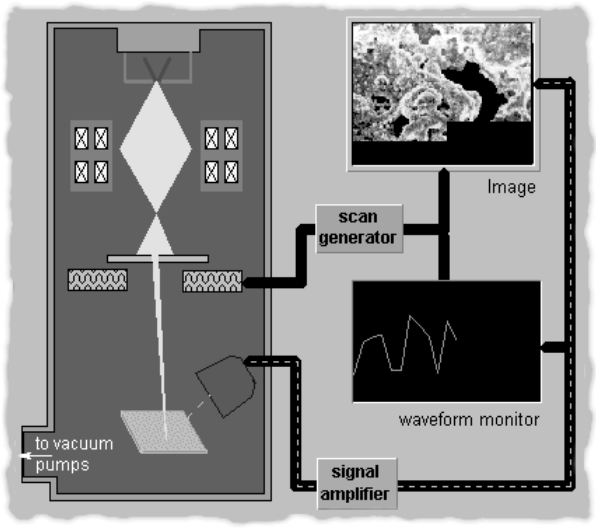

Figure 4.2 - Schematic diagram of the main components of a scanning electron microscope**.**

Electrons accelerated onto a sample can give rise to several interaction processes with the atoms of the sample. Accelerated electrons can pass through the sample without interaction, can undergo elastic scattering and/or can be inelastically scattered. Elastic and inelastic scattering result in a number of signals that are used for imaging, quantitative and semi-quantitative information of the sample and to the generation of X-rays source. Typical signals used for imaging include secondary electrons (SE), backscattered electrons (BSE), cathodoluminescence (CL), Auger electrons and characteristic X-rays. Quantitative and semiquantitative analyses of materials as well as element mapping typically utilize characteristic X-rays.

Figure 4.3 shows some of the most important signals emitted from the scanned area of the specimen.

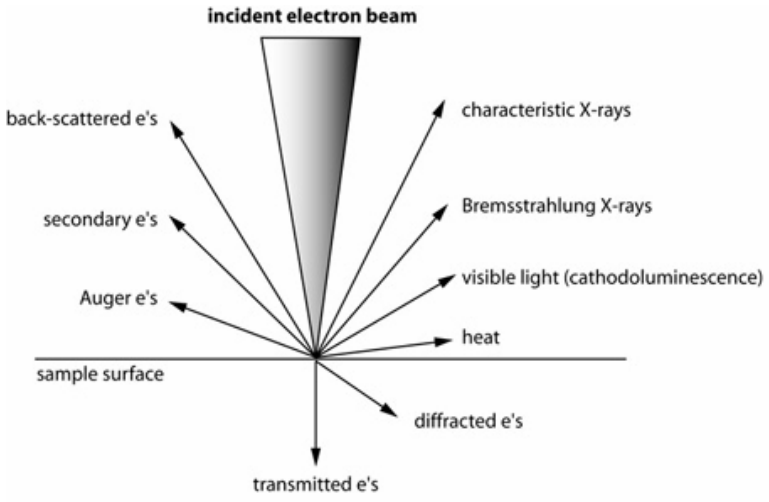

Figure 4.3 – Some of the signals which may be used in SEM analyses.

Secondary electrons are the electrons which escape from the specimen with energies below about 50 keV. They could be electrons to which a small amount of energy has been transferred (by inelastic processes) and can escape from the sample if they have sufficient energy. However they could be primary electrons that at the end of their trajectory reach the specimen surface with a small energy remaining (Goodhew and Humphreys, 1988).

Backscattered electrons are primary electrons that may leave the surface of the specimen before having given up all their energy (Goodhew and Humphreys, 1988). They are not usually as numerous as secondary electrons but most of them carry high energies.

A primary electron can knock out a localized electron of an atom of the specimen; at some later time the empty electron state will be filled and the atom will give off the excess energy. There are three ways in which the relaxation of the atom can happen. If the vacant electron state is an outer state, the atom will commonly emit a small energy in the form of a photon which may be in the visible range. This effect is known as *cathodoluminiscence*.

If the vacant state is an inner state, the energy emitted is larger and there are two main effects: a characteristic X-ray or a characteristic electron (Auger) may be emitted. If an X-ray is emitted a single outer electron jumps into the inner shell vacancy; thus the energy of the X-ray is the difference between the energies of the two excited states and it is characteristic of the particular atom species.

It is important to highlight that a primary electron can produce X-rays without knocking out inner shell electrons. This effect called *Bremsstrahlung* process (German for "braking radiation") does not produce X-rays characteristic of a particular atom, but it leads to a background of X-rays in any electron-generated X-ray spectrum (*Bremsstrahlung* spectrum). Continuum X-rays are produced when incident beam electrons are slowed down by the strong electromagnetic field of atomic nuclei in the sample. All degrees of electron braking are possible and, thus, the resulting X-rays have a continuous range of all energies. *Bremsstrahlung* radiation is a continuous spectrum of X-rays from zero to the energy of the incident electron beam, and forms a background in which characteristic X-ray must be considered.

The process which produces an ejection of an outer electron carrying the excess of energy as kinetic energy is known as *Auger emission*. In this process three electrons are involved: the original vacancy, the outer electron which jumps into it and a second outer electron which leaves the atom carrying the excess energy.

Figure 4.4 shows the *Bremsstrahlung* process and the characteristic X-rays and Auger electrons production.

When an electron beam impinges on a sample, electrons, X-rays and light emissions develop in a volume called *interaction volume*: each signal is generated from different interaction volumes and at different depths within the sample (Figure 4.5).

The volume of electron interaction may be modelled using a Monte-Carlo method (Figure 4.6), where the paths of a series of incident electrons are modelled probabilistically with equations for elastic and inelastic scattering determining the scattering angles, mean free-paths, and the rate of energy-loss. Monte-Carlo results may

be used to models not just the electron paths, but also the distribution of the resulting effects.

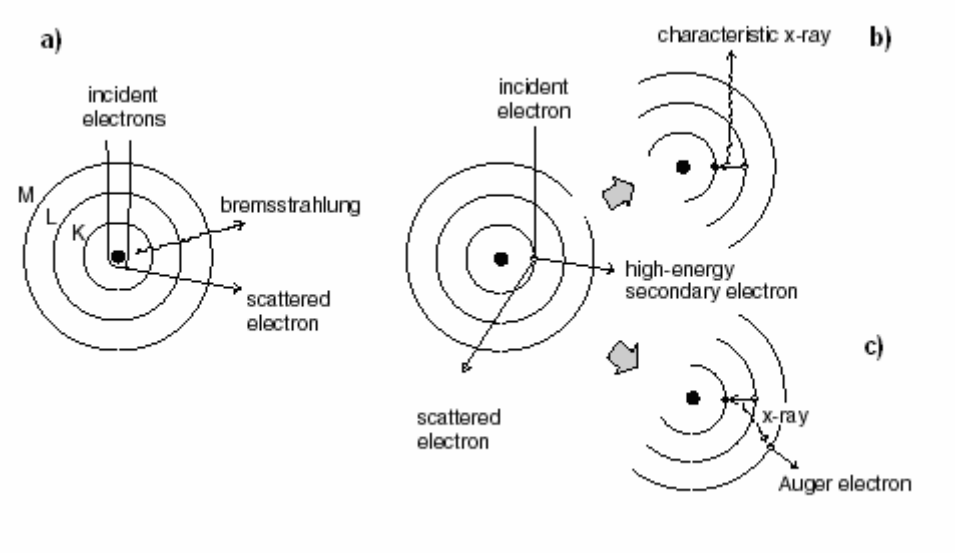

Figure 4.4 – Bremsstrahlung process and the characteristic X-rays and Auger electrons production.

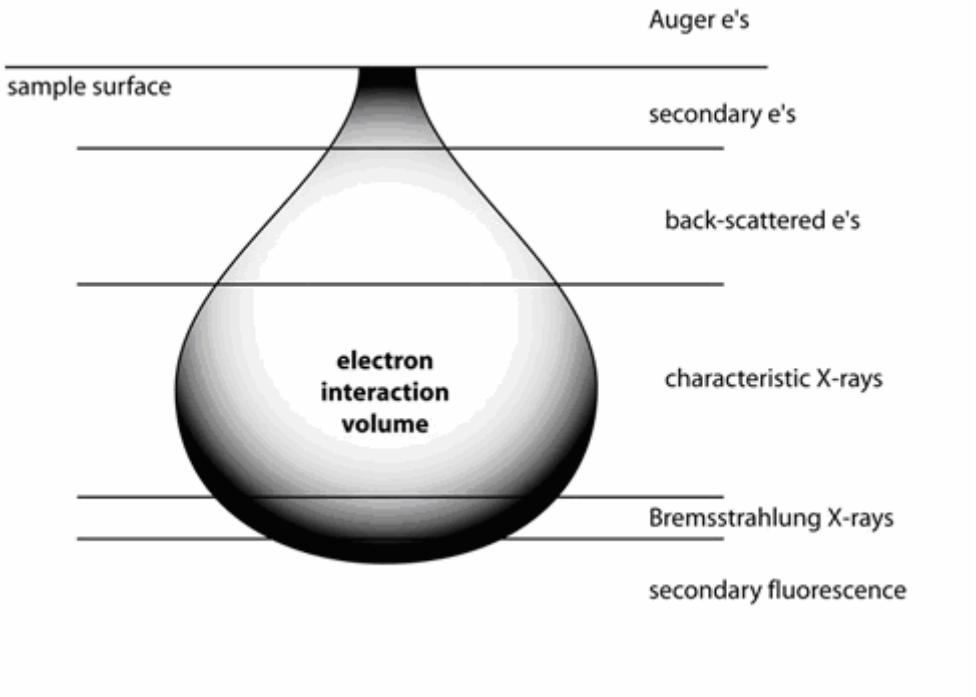

Figure 4.5 – The interaction volume and the regions from which Auger electrons, secondary electrons, backscattered electrons, characteristic X-rays, Bremsstrahlung X-rays may be detected.

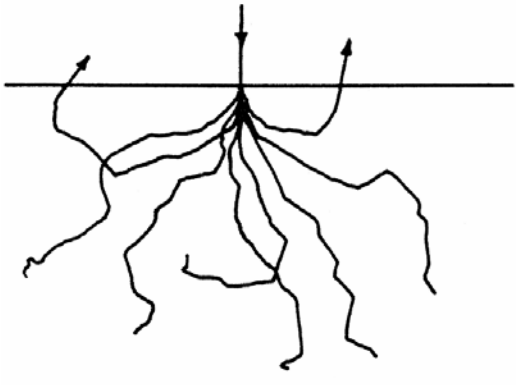

Figure 4.6 – Electron trajectories calculated by a Monte-Carlo procedure. Eight electrons are shown, only two escape and thus are backscattered.

Each signal generated by the interaction between the electron beam and the specimen has different imaging or analytical resolution. Secondary and Auger images have the best imaging resolution, being generated in the smallest volume near the surface of the sample. Backscattered electrons are generated in a larger volume resulting in images of intermediate resolution. Cathodoluminescence is generated over the largest volume resulting in images with the poorest resolution.

Image formation of the surface structures of a specimen using the SEM technique mainly depends on the production of secondary electrons, which represents the most widely used signal in the scanning electron microscope. Secondary electrons are of low energy (less than 50 keV) and when produced deeper within the interaction volume, will be absorbed by the sample. Only secondary electrons close to the surface will be able to escape the specimen. Secondary electrons are detected by a scintillator: however because of their weak energy they need to be deflected by Faraday cage surrounding the detector.

Backscattered electrons are produced deep within the sample but have a much higher energy to escape from the interaction volume. Because of their high energy, backscattered electrons will not be deflected by the Faraday Cage and only the backscattered electrons which travel in the appropriate direction can hit the scintillator, and contribute to the image formation. Therefore it is important to note that the signal collected by the scintillator is not purely due to secondary electrons as it could contain a small backscattered component.

Dedicated backscattered electron detectors are generally positioned above the sample in a "doughnut" type arrangement, concentric with the electron beam, maximising the solid angle of collection. BSE detectors are usually either of scintillator or semiconductor types.

Different numbers of secondary electrons produced at different areas of the sample will provide image contrast. If at a certain spot on the sample more secondary electrons are produced, a bright spot will appear on the image. Often many secondary electrons are produced along raised areas of the sample; therefore many electrons will be detected, producing a bright spot on the image. This effect is called “the edge effect” (Figure 4.7). The secondary electrons produced in a valley of the sample are difficult to be detected producing a dark spot on the image.

An important parameter in scanning electron microscopy analysis is the spot size which is the diameter of the electrons beam that scans the sample; a small spot size can resolve more detailed structures of the analyzed sample. The current in the condenser lens can change the spot size. However an increase in condenser lens current results in a lower beam current, the effect is that fewer electrons interact with the sample and therefore fewer secondary and backscattered electrons become available to form the images. A correct balance between spot size and beam current needs to be found.

If the electron beam is not perfectly round, incorrect information will be collected by the detector; this effect called *astigmatism* causes a reduction in resolution. The stigmator knobs on the SEM panel control distortions in the roundness of the spot that is scanned over the sample.

The working distance which is the distance between the final condenser lens and the specimen represents another crucial parameter in SEM analysis. In fact changing the working distance causes an effect on the spherical aberration of the imaging system and therefore an effect on the resolution of the final image. Spherical aberration arises when electrons passing through a lens are brought to different focal point because of the strength of the magnetic field decreases as the distance from the electromagnetic lens increases. The lens system does not image central and peripheral electrons at the same focal point, thus the spot results enlarged producing a lower resolution (Figure 4.8). When the working distance decreases, this effect of spherical aberration will become less, the spot on the specimen will become smaller and therefore will improve resolution.

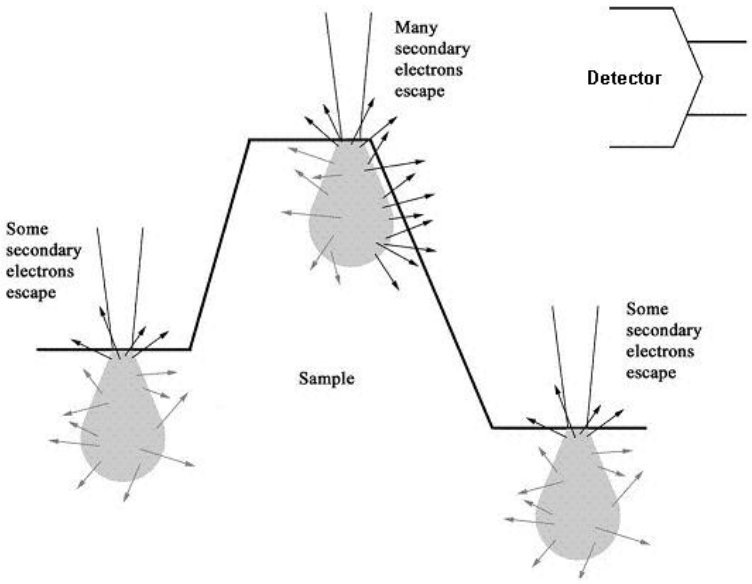

Figure 4.7 - The edge effect occurs when many electrons escape from areas with sharp edges or peaks. A low signal is detected when generated secondary electrons are deflected partially, due to the location on the sample where they are generated.

The working distance is also important in determining the depth of field of a sample, which is the depth that appears to be in focus. At a short working distance the sample will be scanned with a wide cone of electrons resulting in an image with short depth of field. At a longer working distance the sample will be scanned with a narrow cone of electrons resulting in an image with an increased depth of field (Figure 4.9).

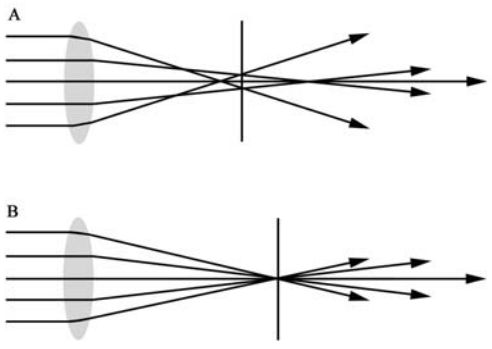

Figure 4.8 - Spherical aberration occurs when the lens system is unable to image central and peripheral electrons at the same focal point, thus the beam will scan with an enlarged spot (A); if spherical aberration is absent, the beam will scan with the sharpest spot possible (B).

Depending on the sample a correct balance between working distance and depth of field needs to be found. A sample characterized by a strong topographical variation needs to be scanned using a longer working distance to bring the image into focus as much as possible; however, the resolution will be lost. A flat sample needs to be scanned using a shorter working distance and a better resolution, since depth of field becomes less important.

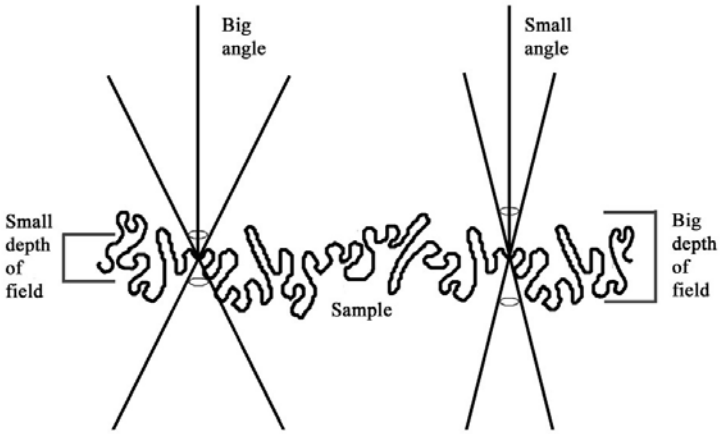

Figure 4.9 - At a short working distance little of the sample appears to be in focus. At a long working distance, more of the sample appears to be in focus because of a greater depth of field.

The depth of field is also influenced by the size of the objective aperture which is the final aperture in a SEM instrument; smaller apertures in fact result in greater depths of field. However, as expected, a reduction in the aperture size products a reduction in the number of electrons passing through it and consequently a reduction in signal strength.

The acceleration voltage applied to the filament is also a fundamental parameter in SEM analysis. In general, increasing the accelerating voltage will increase the resolution because the spherical aberration of the system decreases. However, varying the acceleration voltage will also have an effect on the beam-specimen interaction. A higher accelerating voltage products a bigger interaction volume between the beam and the specimen because of the greater energy of the beam of electrons (Figure 4.10). The secondary yield from all parts of the specimen increases due to a greater beam penetration, with a consequent reduction of the image resolution.

In SEM analysis the conductivity of the specimens is important; in fact when a specimen is nonconductive a negative charge from the electron beam tends to accumulate affecting the final image. The effects of this process include abnormal contrast and the presence of extraneous lines, shifts or breaks within the image. Nonconductive samples need to be coated with a thin layer of metal making the surface conductive. Specimens like metals and most semiconductors are conductive and can be examined without coating.

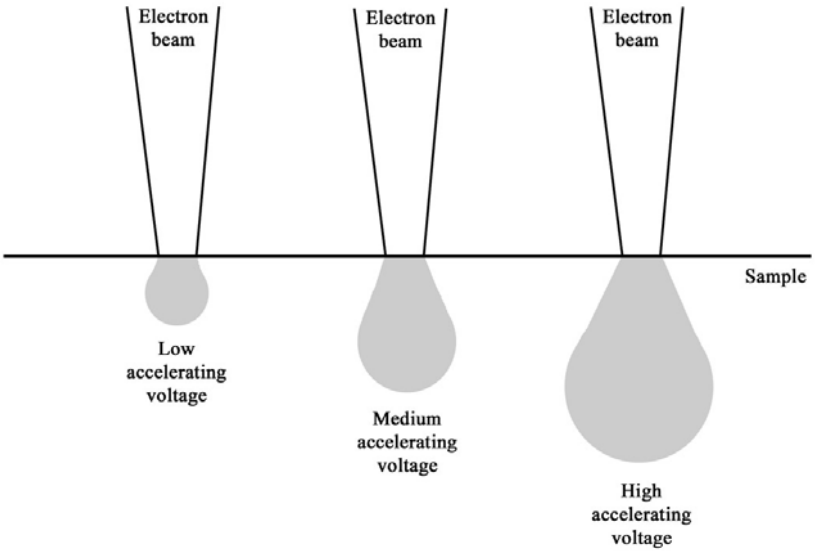

Figure 4.10 - Effect of the acceleration voltage on the interaction volume; with an increase in acceleration voltage the interaction volume becomes bigger.

4.2 Energy dispersive X-ray analysis

The energy Dispersive X-ray (EDX) analysis is a technique used for identifying the elemental composition of a specimen. An Energy Dispersive Spectrometer (EDS) is typically integrated into a SEM instrument and provides fundamental compositional information for a wide variety of materials. EDS is used to separate the characteristic X-rays of different elements into an energy spectrum, and an EDS system software is used to analyze the energy spectrum in order to determine the abundance of specific elements. The EDS can be used in semi-quantitative mode to determine chemical composition by peak height ratio relative to a standard and to create element composition maps over a selected area of the specimen.

A typical EDS spectrum is a plot of X-ray counts versus energy (in keV). Energy peaks correspond to the various elements in the sample and generally they are narrow and readily resolved, but many elements can show multiple peaks. Energy peak overlaps among different elements are frequent; particularly at higher energies individual peaks may correspond to several different elements. Moreover elements in low abundance will generate X-ray peaks that may not be resolvable from the background radiation.

The EDS detector consists of a small piece of Silicon doped with Li and covered by a thin layer (20 nm) of evaporated gold. The gold-coated outer surface is usually protected by a thin window of Beryllium. This window is necessary to prevent contaminants from the specimen chamber of the microscope. Unfortunately the window absorbs a significant part of the low-energy X-rays falling on the detector and therefore makes light elements difficult to detect.

Each incoming X-ray excites a number of electrons into the conduction band of the Silicon leaving an identical number of positively charged holes in the outer electron shells. The number of electron-hole pairs generated is proportional to the energy of X-ray photon detected.

Thin layers of gold are necessary on both surfaces of the detector so that a bias potential can be applied; however it is necessary that the layers of gold be as thin as possible so that very few X-rays are absorbed in it.

In order to preserve the detector crystal and to reduce noise in the system, the detector is kept to liquid nitrogen temperature (77 K) at all times.

One problem in an energy dispersive system is the production of spurious peaks in the spectrum: *sum peaks* and *escape peaks*.

When two identical X-ray photons enter the detector simultaneously the detector system could interpret this as being due to a single photon of twice energy and products a sum peak at an energy of twice that of X-ray detected.

An escape peak instead appears when an X-ray enters the detector and ionizes a Silicon atom in the detector crystal by knocking out a K-shell electron (1.74 keV). The original X-ray photon loses 1.74 keV in energy and releases its energy to the detector. As consequence a peak 1.74 keV below the main peak is produced.

A correct interpretation of an EDS spectrum needs to compare the height of a peak with that of the pure element acquired at the same experimental conditions. The

ratio between the two heights is known as *K-ratio* and it can be obtained by two different methods: standard and standardless technique.

The standard technique uses pure samples as standard. In this case the K-ratio must be corrected by the **ZAF** coefficient where:

- Z takes in account the atomic number effect which is related to the efficiency of an element to produces X-rays;
- A takes in account the absorption which depends closely on the elements in the sample;
- F refers to the fluorescence which is important in a sample containing several elements and negligible in a pure elemental standard.

Taking in account these three effects the concentration of an element in the sample is given by:

$$C = K \times Z \times A \times F;$$

however the accuracy of quantitative analysis is limited.

The standardless technique is the most used method for its simplicity and speed. In this technique (commonly based on the software "EDAX") the line intensity of the elements is calculated and not measured. The composition of a sample is obtained by the relation:

$$W\% = ZAF\ I_m / I_{std},$$

where W% is the weight concentration percentage of a given element in the analyzed sample, I_m is the measured intensity of the element and I_{std} is the intensity of the relative standard. For each considered element, I_{std} is unknown and the EDAX software uses calculated values. In particular I_{std} is deduced taking in account the efficiency of the detector, transition probability, absorption probability and ionization cross section of the elements.

4.3 SEM technique applications

In this PhD work some selected 7-stage impactor samples have been examined by a field-emission scanning electron microscope (JEOL, model JSM-6480LV), equipped with an Energy Dispersive X-ray (EDX) system (model EDS 2000), to characterize morphological properties of the collected particles and perform a semi-quantitative analysis of their elemental composition. The SEM-EDX system (Figure 4.11) belongs to the Physics Department of the University of Salento.

Figure 4.11 – The scanning electron microscope (JEOL, model JSM-6480LV), equipped with an energy dispersive X-ray (EDX) system (model EDS 2000) of Physics Department of University of Salento.

For each impactor filter, SEM-EDX analyses of randomly chosen areas at magnifications of 2000x have mainly been used to test the impactor fractional sampling, to analyze morphology and elemental composition of single particles and to infer their chemical composition. It is worth mentioning that EDX-spectra do not allow inferring chemical species without ambiguity. However, it may be possible to infer the presence of some chemical species when the chemical composition of particles is simple (Perrone et al., 2006).

The intensities of EDX spectrum lines have been converted to corresponding percents of weight concentrations by a standardless ZAF correction method in which ideal flat samples have been assumed (Paoletti et al., 2002), to get semi quantitative data on weight concentrations (%) of some selected elements (C, N, F, Na, Mg, Al, P, S, Cl, K, Ca, Ti, V, Mn, Fe, Cu, and Zn).

The energy resolution of the X-ray detector used for the analyses of this PhD work is 140 eV.

The spatial resolution is of about 10 nm.

The limit of detectability is about 10^{-1} % for light elements and 10^{-2} – 10^{-3} % for heavy elements.

Operating conditions for SEM analyses were as follows: accelerating voltage: 20 kV; probe current: 75 μA; working distance: 10 mm; accumulation time: 30 s for EDX spectra and 1800 s for marked images.

For each filter about 70 randomly selected single particles have been morphologically and compositionally analyzed. The X-ray semi-quantitative results referring to the individual particles analyzed in each impactor stage have been averaged in order to obtain information about the mean composition of the particulate matter sampled in the different size intervals. In addition for each stage some images have been marked selecting the most important chemical elements, in order to obtain information about the spatial distribution of the main chemical species and to identify the principal compounds constituting the collected particles.

The fibrous nature of the quartz filters used to collect the particulate matter has represented a main difficulty of these analyses. The quartz fibers of the filters (Figure 4.12) in fact are very intricate and make very complex the morphological investigation mainly on filters of impactor's stages with small cut-diameter, where the fibers particularly favor the formation of agglomerates of fine particles. In addition the chemical composition of the quartz filters interfered with semi-quantitative X-ray analyses; in fact compositional analyses showed the presence in the used matrix of some chemical elements typically constituting also the atmospheric particles. In particular Oxygen and Silicon are the main components of quartz fiber filters (Figure 4.13) but also of a wide variety of atmospheric particles, mainly of crustal origin.

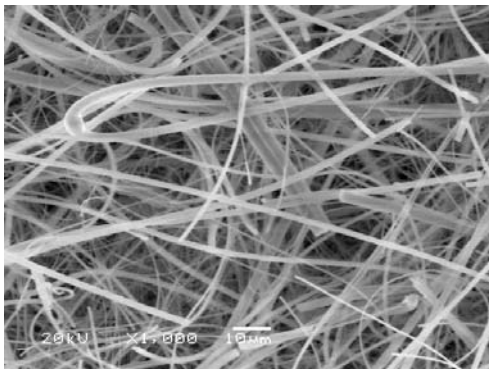

Figure 4.12 – SEM image of a randomly selected area on a quartz filter. The fibrous nature of the matrix makes difficult the morphological analyses of the collected particles.

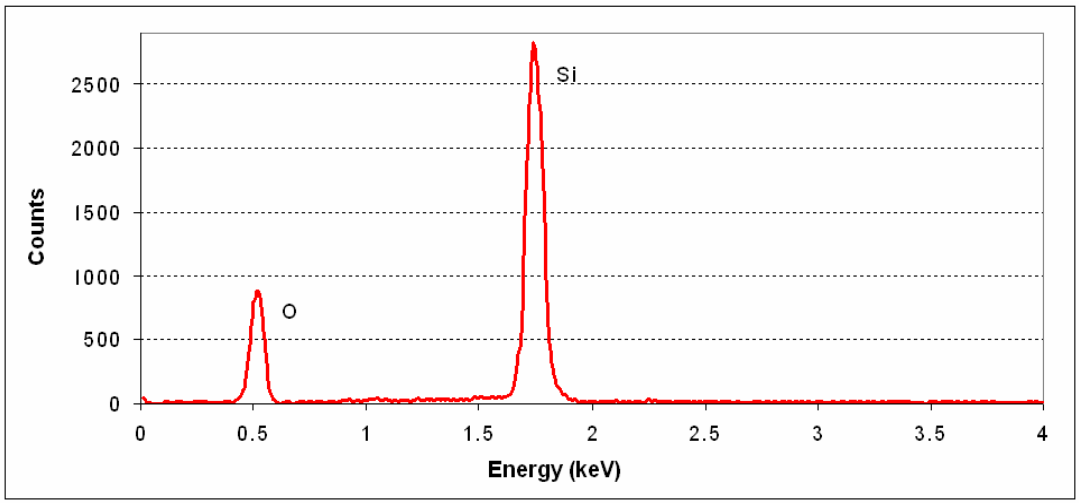

Figure 4.13 – EDX spectrum of the randomly selected area on quartz filter of figure 4.12. Silicon and Oxygen are the main components of the quartz matrix.

In this section two different sets of size-segregated samples collected by the 7-stages impactor (OH-610-C) are presented and discussed as examples. It is important to note that the two PM fractional collections have been performed in different seasons and during different advection patterns events. In fact an important objective of this study is to investigate how particle size distributions and corresponding size-segregated elemental compositions could be affected by the source regions of the air masses advected over the monitoring site.

The analyzed sets of samples are:

- Q19 collected on 30 June 2005 during a dust outbreak;
- Q33 collected on 21 November 2005 during a pollution event coming from North-Europe.

In conclusion morphological and elemental analyses performed by the SEM-EDX technique on impactor filters collected during two different advection events have clear revealed the dependence of particles' size, shape, and number on the 50%-effective-cut-diameter of the impactor filters. Nitrates, sulfates, and carbon were the main aerosol components of fine-mode particles, while sea-salts, carbonates, and minerals were the main aerosol components of larger particles. In particular, it has also been shown that dust particles mainly affect the coarse mode aerosol and that the anthropogenic fine mode particles can represent more than 50% of the aerosol load even during a dust outbreak.

The above results about these two analyzed impactor sets of filters have been presented and discussed on September 2006 at the "Particulate Matter National

Conference – PM2006", Florence (Italy) and on September 2007 at the "European Aerosol Conference", Salzburg (Austria). In addition the results referring to the Q19 samples have been published in the paper by Bellantone et al., 2008.

4.3.1 Sample Q19 (30/06/2005)

48-hour fractional measurements of particles by the 7-stage cascade impactor (OH-610-C) have been performed from 0730 UTC of 30 June 2005 till 0730 UTC of 2 July 2005. The particulate matter samples have been collected during a Saharan dust event: 7-day back-trajectories of sampled air masses and pressure levels as function of time are shown in figures 4.14–4.15. As previously discussed analytical back-trajectories provide information on the aerosol origin and on the dynamical patterns governing the air mass transport (Kazadzis et al, 2007).

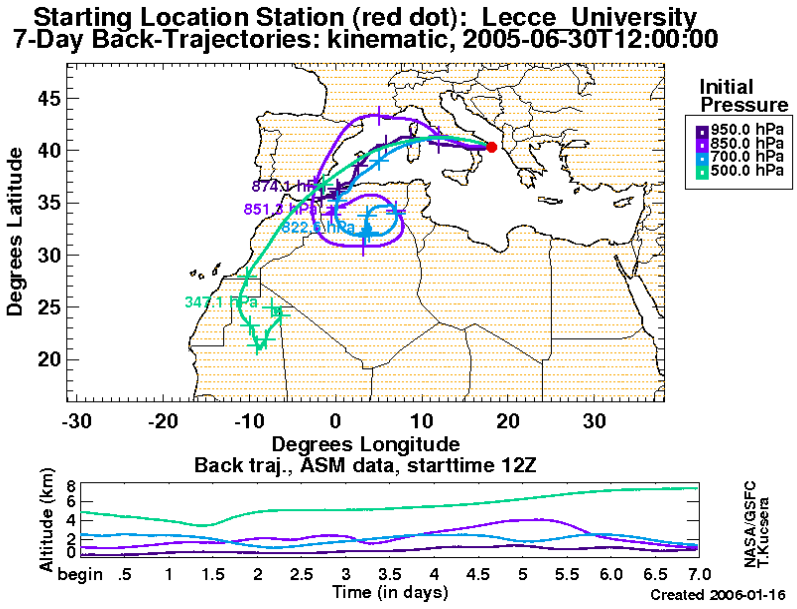

Figure 4.14 – 7-day analytical back - trajectories for the air masses reaching the observation site on 30 June 2005 (at 12:00 UTC) and pressure levels of each back trajectory as a function of time.

In particular figure 4.14 shows that on 30 June at 12 UTC the 950-500 hPa air masses advection over Lecce have their origin over North-West Africa. Conversely figure 4.15 shows that only the 950 hPa air masses are advected from North-West Africa.

The particle-mass plot as function of the 50% effective-cut-diameter of the impactor filters is shown on figure 4.16. Uncertainties on mass values are lower than 5%. Figure

4.16 reveals that the particle mass has a bimodal trend with two important peaks at the cut-diameter values 2.70 and 0.35 µm respectively.

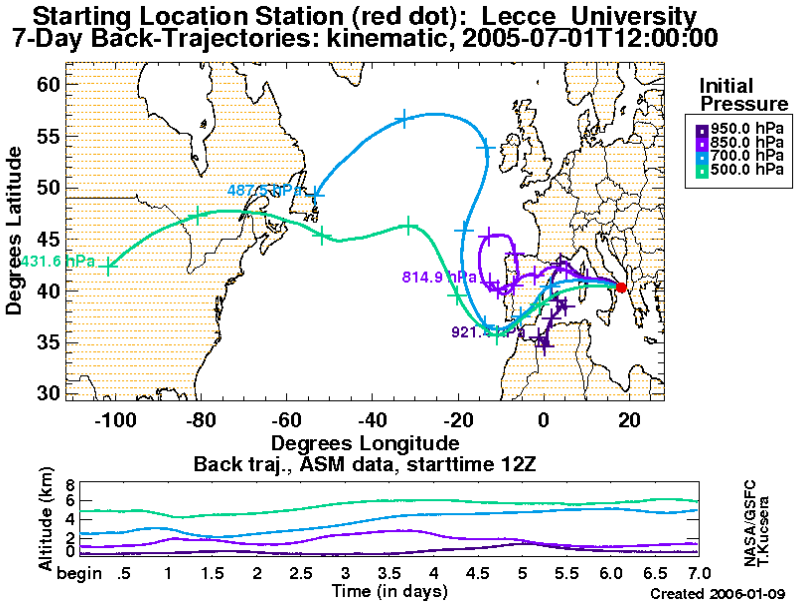

Figure 4.15 – 7-day analytical back - trajectories for the air masses reaching the observation site on 01 July 2005 (at 12:00 UTC) and pressure levels of each back trajectory as a function of time.

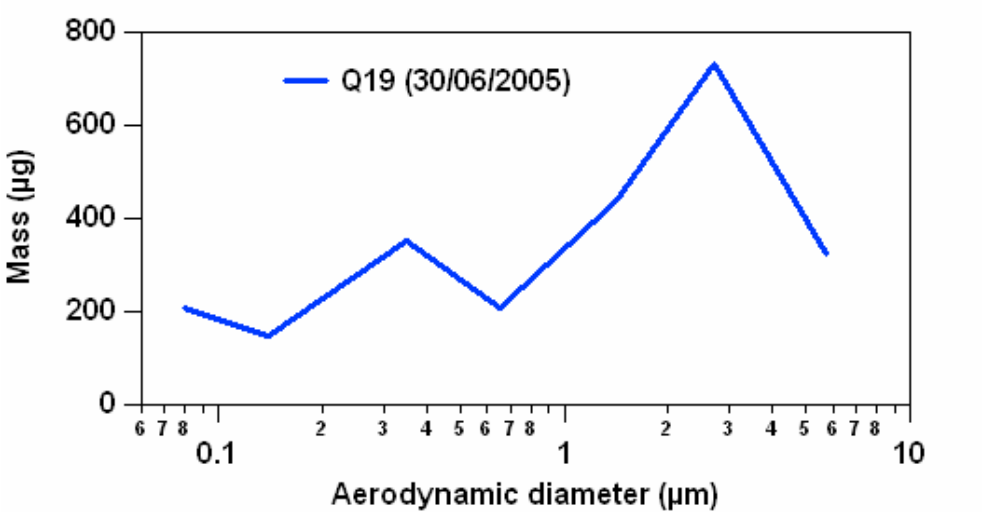

Figure 4.16 - Mass plot as function of the 50% effective-cut-diameter of the 7-stage impactor filters collected on 30 June 2005 at Physics Department of Lecce during a dust event. Uncertainties on mass values are lower than 5%.

Figures 4.17a and 4.17b show as example the SEM images of the particles collected on randomly selected areas of the impactor filters with cut-diameter 2.7 and 0.35 μm, respectively.

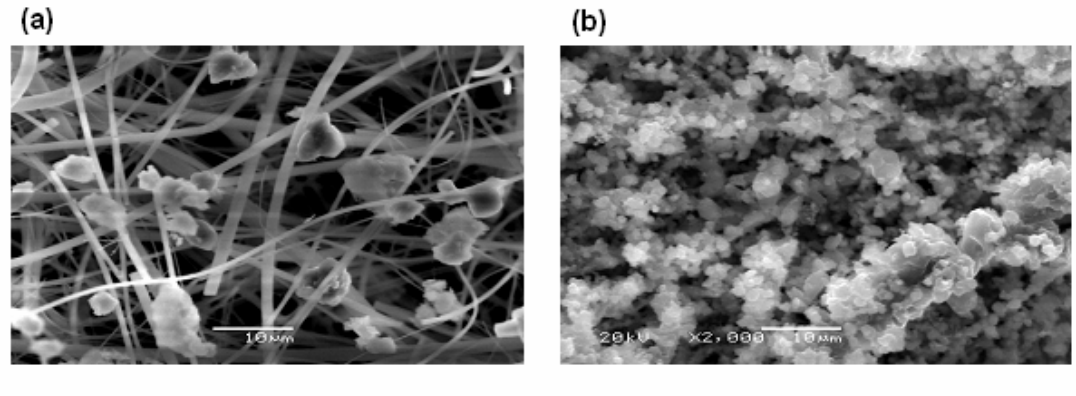

Figure 4.17 – SEM images of the particles collected on randomly chosen areas of the impactor filters with 50%-effective cut diameter of 2.7 μm (a) and 0.35 μm (b).

Both quartz filter fibers of figure 4.17 show that the shape of the collected particles, often clustered together, is quite irregular. Single particles cannot even be detected on figure 4.17 since magnifications much larger than 2000x would have been required being their number rather large and their size rather small. However it is important to highlight that the number of atmospheric particles with 0.35 μm-diameter is more than 100 times larger than that of particles with 2.7 μm-diameter.

SEM-EDX semi-quantitative analyses on the particles of Figures 4.17a and 4.17b have revealed the presence of particles containing two or more of following elements: C, N, F, Na, Mg, Al, P, S, Cl, K, Ca, Ti, Fe, and Zn. Even though Si and O have been detected, they have not been considered in the data analysis because they are major components of quartz filters. Selected elements (C, Na, Mg, Al, Cl, K, Ca, and Fe) have been marked on the SEM image of figure 4.17a and the corresponding images are shown in figure 4.18a-h.

This method allows getting the spatial distribution of the marked elements in the sample and in single particles and can allow inferring the chemical composition of particles and to know about their morphological features. We observe from figure 4.18 that Na (Figure 4.18a) and Cl (Figure 4.18b) have a rather similar spatial distribution on the selected filter area and as a consequence the marked images allow inferring the

presence, location and size of NaCl particles. The comparison of the marked areas of figures 4.18c-4.18f, allows inferring the presence of single particles or clustered particles made of elements typical of illite/smectite (Al, K, Fe, and Mg). SEM marked images have also allowed inferring the presence of elements typical of dolomite (Ca, Mg, and C), and carbonate (Ca and C) particles. Illite/smectite and dolomite are the major components of dust coming from north-west Africa (Avila et al., 1997, Blanco et al., 2003).

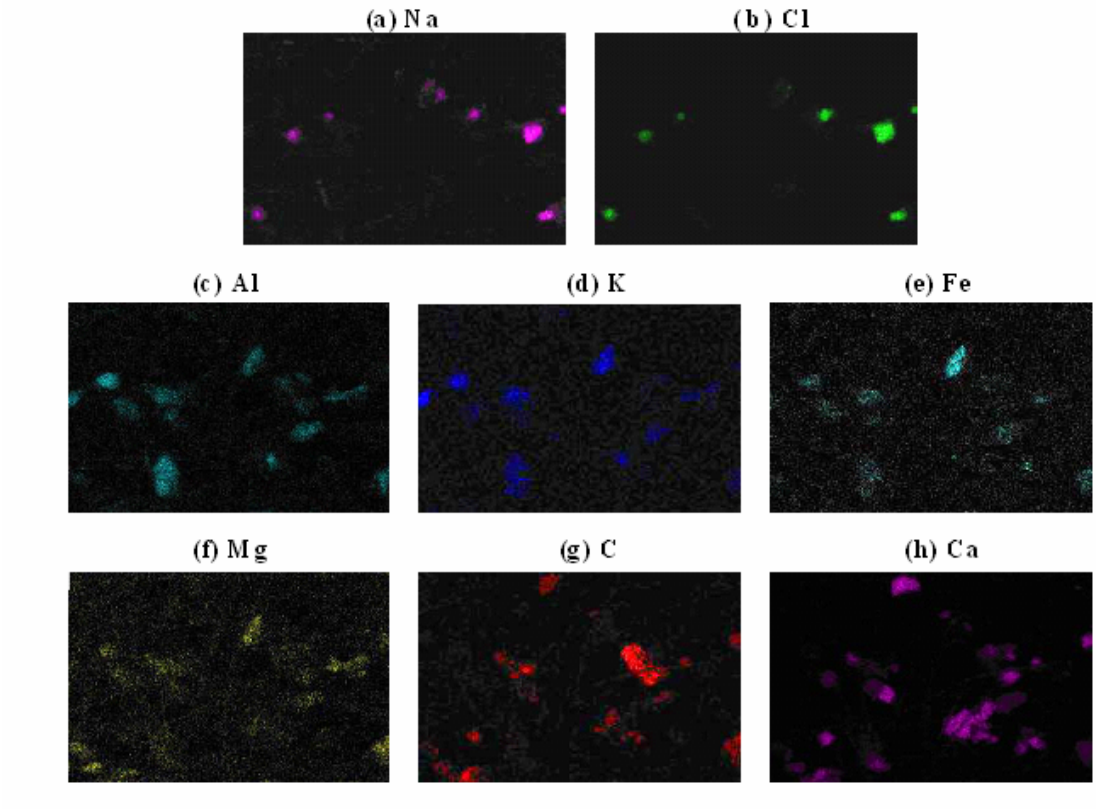

Figure 4.18 - Selected elements (C, Na, Mg, Al, Cl, K, Ca, and Fe) marked on the SEM image of figure 4.17a.

The element-marked images of figure 4.17b, shown in figure 4.19, have instead allowed inferring the presence of particles with a large content of C, S, N, and to a less extent of Ca, K and Na.

Single particle EDX-spectra have also been used to further support the above comments on the chemical composition of particles. EDX analyses have been performed on many randomly selected areas to get the mean elemental composition of the particles collected on each filter. In particular, the intensities of EDX spectrum lines have been

converted to corresponding percents of weight concentrations by a standard-less ZAF correction method in which ideal flat samples have been assumed (Paoletti et al., 2002), to get semi quantitative data on weight concentrations (%) of some selected elements (C, N, F, Na, Mg, Al, P, S, Cl, K, Ca, Ti, V, Mn, Fe, Cu, and Zn). The results referring to the 7 impactor filters are shown in figure 4.20.

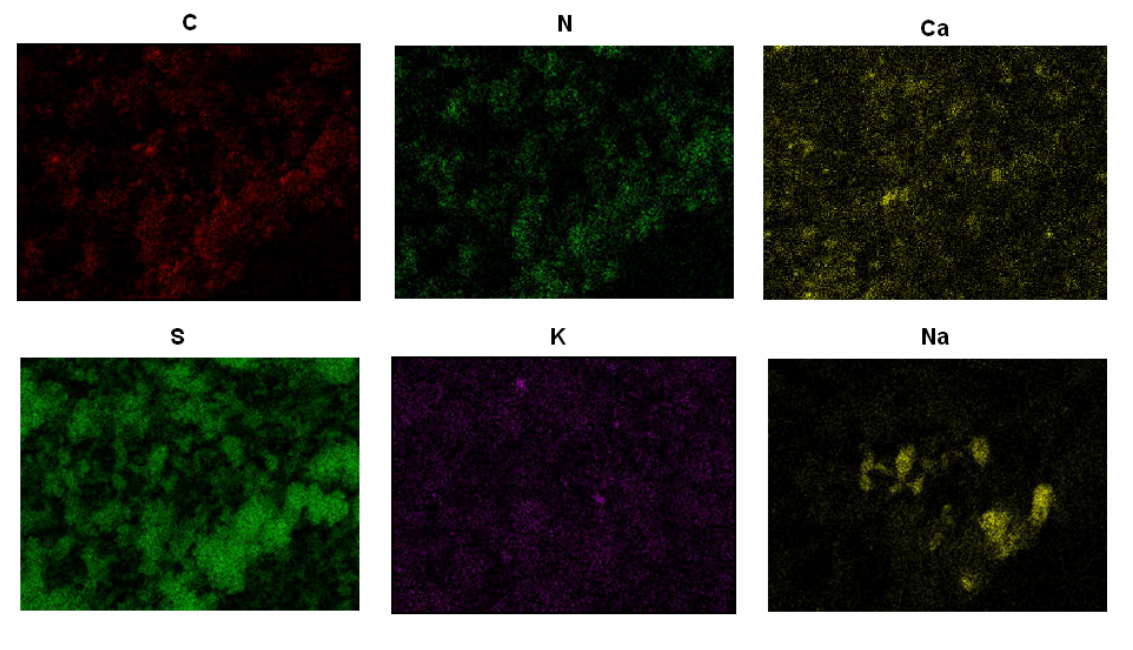

Figure 4.19 - Selected elements (C, N, Ca, S, K and Na) marked on the SEM image of figure 4.17b.

Figure 4.20 shows that both size and mean particle composition vary with the cut-diameter (d): sea-salt and particles of crustal origin (Cl, Na, Ca, Mg, K, Al, Fe) mainly affect the mass composition of the impactor filters with $d \geq 0.65$ µm, even if the percentage contribution of Ca decreases and that of S increases as d varies from 5.7 to 0.65 µm. In addition, figure 4.20 clearly shows that the mean particle composition of filters with $d \leq 0.35$ µm is significantly different than that of filters with $d \geq 0.65$ µm: the sulfur and nitrogen weight percentage is 33% on the filter with $d = 0.35$ µm, while it is 5% on the $d = 0.65$ µm filter. The aluminum weight percentage is 3% on the filter with $d = 0.35$ µm, while it is 15% on the $d = 0.65$ µm filter, and of about 14% on the filters with $d > 0.65$ µm. Hence, figure 4.20 clearly shows that SEM analyses on the impactor filters have allowed getting some information on the elemental composition of coarse and fine mode atmospheric particles, respectively: coarse particles are the ones collected on

impactor's filters with cut-diamter $d > 0.35$ µm, while fine particles are the ones collected on filters with $d < 0.35$ µm.

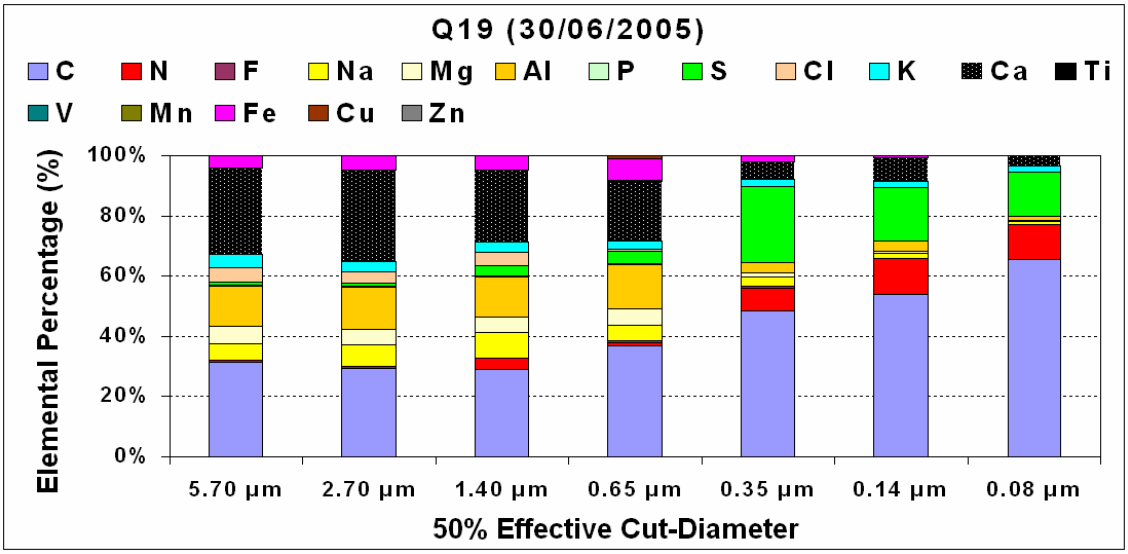

Figure 4.20 - Elemental weight concentrations (%) in the 48-h analyzed impactor filters collected during the dust event occurred on 30 June 2005.

4.3.2 Sample Q33 (21/11/2005)

24-hour size-segregated measurements of atmospheric particles have been performed from 0847 UTC of 21 November 2005 till 0847 UTC of 22 November 2005. Analytical 7-day back-trajectories analyses show that the fractionated samples have been collected using the 7-stage cascade impactor (OH-610-C) during the advection pattern event coming from North-Europe (Figure 4.21): all air masses advected from about 950 hPa to 500 hPa cross North-Europe regions before reaching Lecce.

The particle-mass plot as function of the 50% effective-cut-diameter of the impactor filters is shown on figure 4.22. Uncertainties on mass values are lower than 5%. Figure 4.22 illustrates that, as observed in the dust samples collected on June, the mass concentration has a bimodal structure with two peaks at cut-diameter values 2.7 and 0.35 µm respectively; however in this case the modes are much more less evident. Mass concentration in fact reaches the highest value in fine fraction at 0.35 µm-diameter and lower values at larger cut-diameters. The dominance of small particles in this set of size-segregated samples could be an effect of long-range transport of polluted air masses coming from industrialized countries of North-Europe, that are significant sources of anthropogenic aerosols.

In order to investigate the morphology and the elemental composition of the collected particulate matter as a function of cut-diameter, the SEM-EDX analyses have been performed on the seven impactor filters.

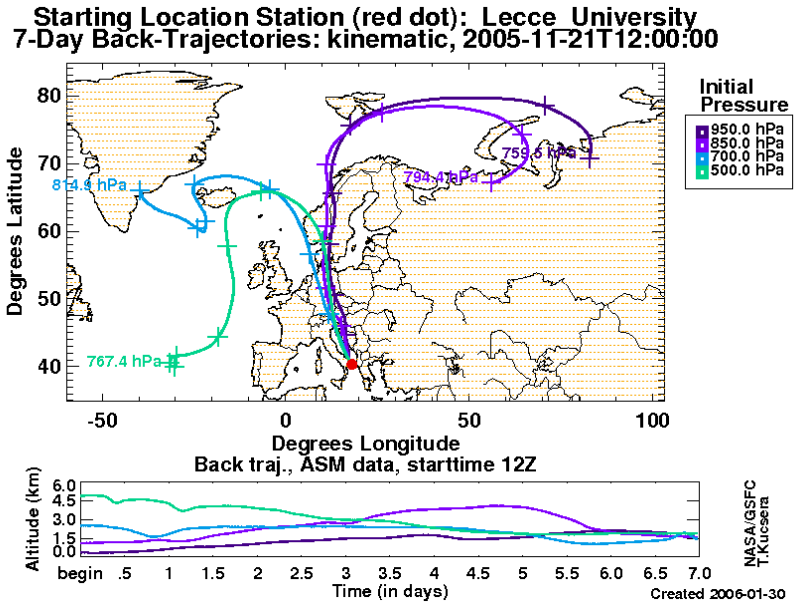

Figure 4.21 – 7-day analytical back - trajectories for the air masses reaching the observation site on 21 November 2005 (at 12:00 UTC) and pressure levels of each back trajectory as a function of time.

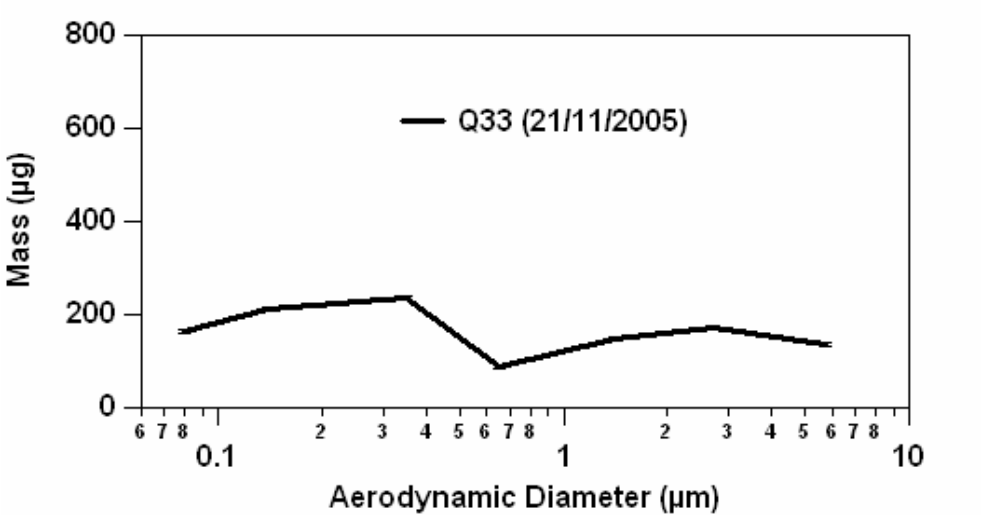

Figure 4.22 - Mass plot as function of the 50% effective-cut-diameter of the 7-stage impactor filters collected on 21 November 2005 at Physics Department of Lecce during a pollution event coming from North-Europe. Uncertainties on mass values are lower than 5%.

Figure 4.23a-d shows fours SEM images (2000x) of the particles collected on randomly selected areas of the impactor filter with cut-diameter (a) 5.7, (b) 1.4, (c) 0.35 and (d) 0.08 μm respectively. Figure 4.23 clearly illustrates that the size, the shape and the number of particles vary with impactor stage number. In particular it is evident that the number of particles increases as the cut-diameter decreases. The shape of the coarse particles collected on stage 1 (5.7 μm-diameter) is quite clear, though the presence of the intricate quartz fibers; however the morphological analysis becomes much more complex on filters with smaller cut-diameters, because of the tendency of fine particles to form clusters. Figure 4.24 shows a detail of an area of the filter with 0.08 μm-diameter analyzed at a magnification of 7000x: we can see that it is very difficult to resolve very fine particles also at high magnification; in the last impactor stage in fact we can observe only agglomerates of particles closely trusted upon the quartz fibers.

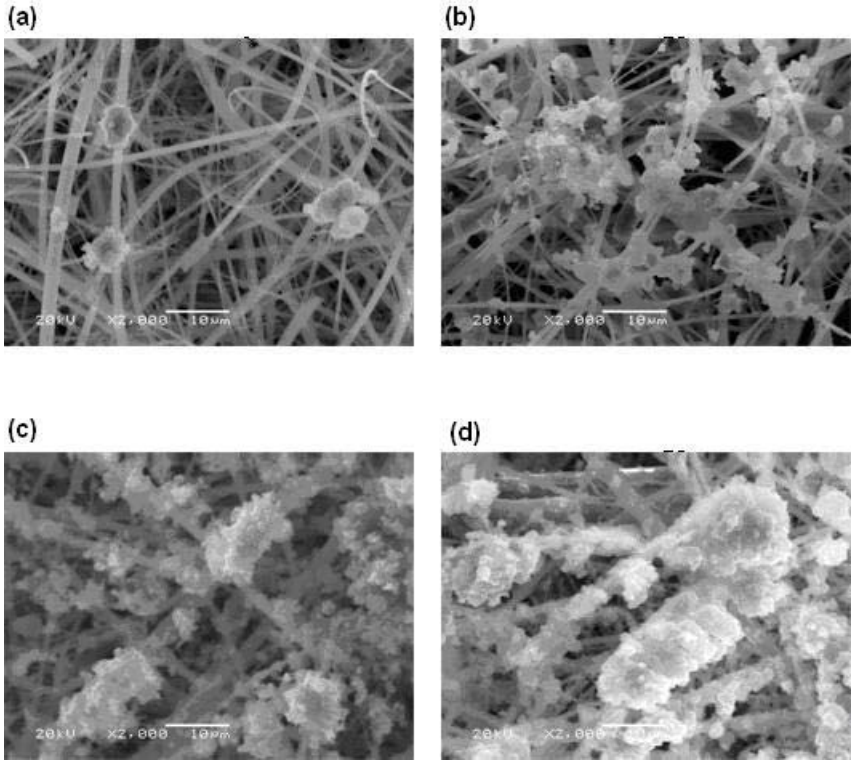

Figure 4.23 – SEM image of the particles collected on randomly chosen areas of the impactor filters with 50% effective cut diameter of 5.7 μm (a); 1.4 μm (b); 0.35 μm (c) and 0.08 μm (d).

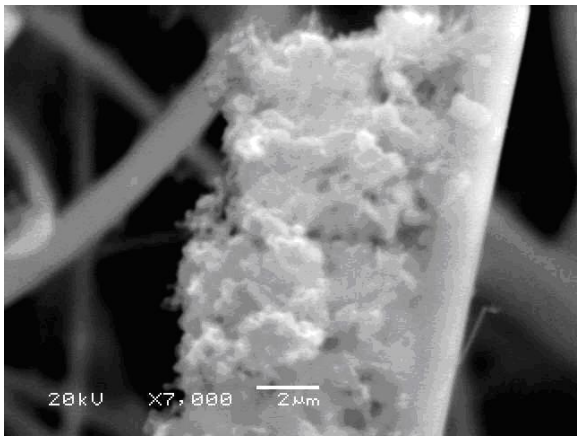

Figure 4.24 – SEM image at magnification of 7000x of the particles collected on a randomly chosen area of the impactor filter with 50% effective cut diameter of 0.08 µm.

SEM-EDX semi-quantitative analyses on the particles have revealed the presence of particles containing two or more of following elements: C, N, F, Na, Mg, Al, P, S, Cl, K, Ca, Ti, Fe, and Zn.

As previously discussed, even though Si and O have been detected, they have not been considered in the data analysis because they are major components of quartz filters. Selected elements (C, Mg, and Ca) have been marked on the SEM image of figure 4.23a and the corresponding images are shown in figure 4.25.

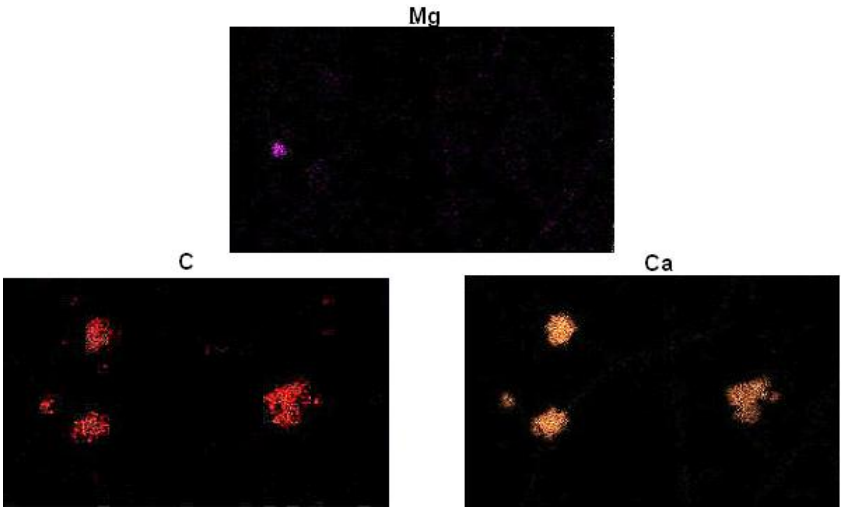

Figure 4.25 - Selected elements (C, Mg, and Ca) marked on the SEM image of figure 4.23a.

We observe from figure 4.25 that C, Mg and Ca have a rather similar spatial distribution on the selected filter area and as a consequence the marked images allow inferring the presence, location and size of Dolomite ($CaMg(CO_3)_2$) and Calcite ($CaCO_3$) particles.

The element-marked images referring to the area of the last impactor filter with a cut-diameter 0.08 μm (Figure 4.23d) have instead allowed inferring the presence of particles with a large content of C, and to a less extent of S, K and Ca (Figure 4.26). These results suggest that compounds such as $CaSO_4$, K_2SO_4 or K_2CO_3 could constitute fine particles. Aluminium and Sodium spatial distributions instead clearly reflect the texture of the quartz fibers, indicating the presence in low levels of these elements in the matrix used to collect the particles.

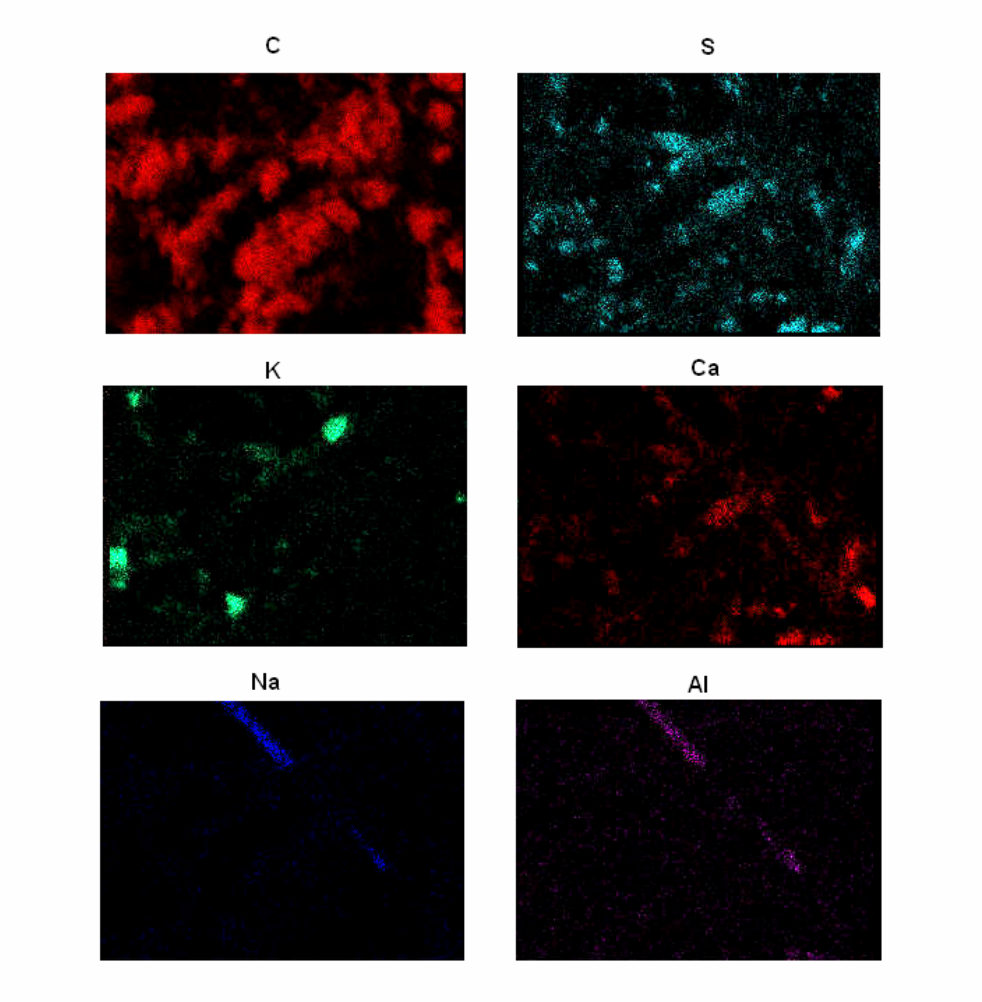

Figure 4.26 - Selected elements (S, C, Ca, K, Al, and Na) marked on the SEM image of figure 4.23d.

The elemental percentage results referring to the seven impactor filters are shown in figure 4.27 from which we can observe that the mean particle compositions vary with the cut-diameter (d). In this second example too the semi-quantitative analyses showed that the chemical composition of the particles collected in filters with $d \geq 0.65$ µm is very different from that of the particles collected in filters with $d < 0.65$ µm. In particular C and Ca are the most abundant elements in the fours filters with larger cut-diameters ($d \geq 0.65$ µm); as the particle size decreases the weight percentage of Ca drastically reduces (from about 40% to about 1%), while the C weight percentage increases until about 90%. Typical crustal origin elements such as Al, Na, Cl, Mg and Fe, found in weight percentages values 2-7 % in filters with $d \geq 0.65$ µm, become negligible in filters with smaller cut-diameters.

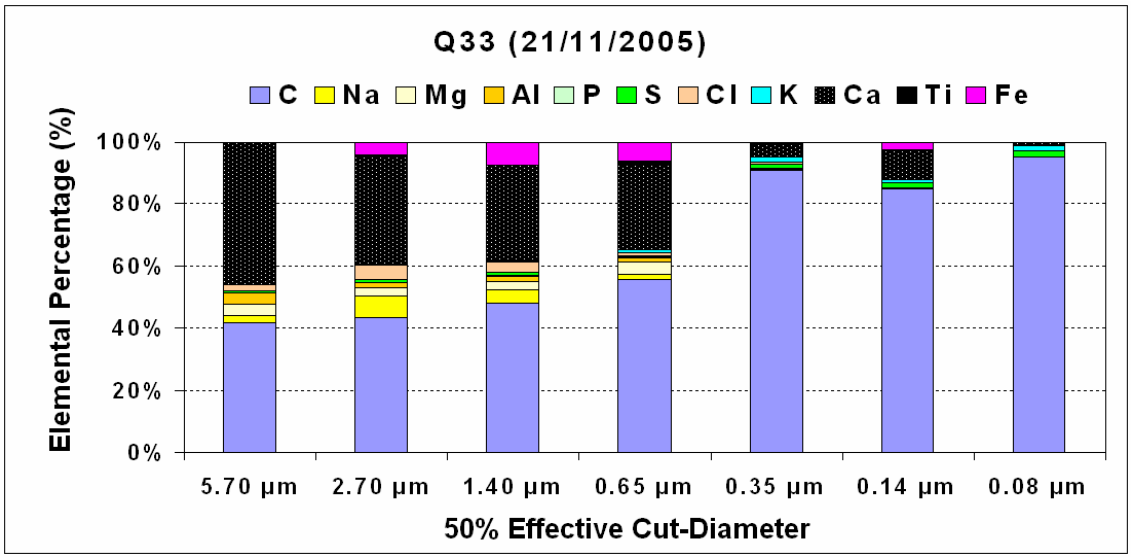

Figure 4.27 - Elemental weight concentrations (%) in the 24-h analyzed impactor filters collected during the pollution event occurred on 21 November 2005.

The composition of particles analyzed in the two sets of samples is very different. The weight concentration of typical crustal origin elements (Ca, Al, Na, Mg, Fe) are higher in larger particles of dust samples (Q19) indicating an influence on coarse fraction of the long range-transport process from Africa continent; while the lower concentration of these elements in larger-size particles of the Q33 sample set could be ascribed to the background due to local sources of primary coarse aerosols.

The composition of fine particles is also very different: in fact the particulate matter collected on the Q33 filters with smaller cut-diameter (d < 0.65 μm) is mainly made of Carbon, as above observed; while Sulphur which is one of the main components of fine particles in dust samples, reaches low weight percentage values (about 1 %) in all Q33 filters collected during the pollution event.

CHAPTER 5

ANALYSIS OF CARBONACEOUS AEROSOLS

5 ANALYSIS OF CARBONACEOUS AEROSOLS

Carbonaceous particles are a significant component of urban/industrial particulate matter and consist of organic carbon (OC), elemental carbon (EC) and carbonates. Carbonate material originates from weathering surface soils and represents a low component of PM2.5 particles (Chow and Watson, 2002). Organic carbon can be directly released into the atmosphere or produced from gas-to particle conversion processes. Elemental carbon also known as soot or black carbon represents the non-volatile, light absorption fraction which is emitted directly in the atmosphere from combustion.

Several studies of atmospheric organic carbon and elemental carbon have recently received intensive attention due to their alarming toxicological implications and their significant impact on the global radiation balance and climate change (Vedal, 1997; Jacobson, 2001; Watson, 2002). The knowledge of carbonaceous species, their fractions in the atmospheric particulate matter and partitioning between primary and secondary origin is crucial in the air quality management plans.

In this PhD work OC/EC analyses have been performed to better understand the levels of carbonaceous particulate matter in PM2.5 and PM1 samples simultaneously collected at the Physics Department. The study focuses in particular on fine fractions since anthropogenic carbon species are mainly made by small particles (Seinfeld and Pandis, 1998). In addition, as previously mentioned, PM2.5 will represent the new reference PM fraction for air quality standard in Europe.

OC/EC analyses have been performed by the Thermal-Optical Transmittance (TOT) technique which allows discriminating between the organic and elemental contributions in the total carbonaceous particulate matter collected on filter samples.

5.1 Thermal – Optical Transmittance (TOT) technique

The thermal – optical transmittance (TOT) technique is one of the most commonly used methods for OC/EC determinations in atmospheric particulate matter. In the thermal-optical technique the speciation of organic and elemental carbon is accomplished through temperature and atmosphere control. The analysis fundamentally consists in three stages (Birch and Cary, 1996):

1. In a completely pure helium atmosphere the sample is heated in four increasing temperature steps (up to 820°C) to volatilize all organic carbon from the filter. During this phase there are some organic compounds that are pyrolytically converted to elemental carbon. The pyrolytic conversion is continuously monitored by measuring through a laser He-Ne the transmittance of the filter. The volatilized carbon is catalytically oxidized to CO_2 in a bed of granular MnO_2 at about 900°. Subsequently it is reduced to CH_4 in a nickel-firebrick methanator at 450° C and quantified as CH_4 by the flame ionization detector (FID).
2. The oven temperature is lowered at 520°C, and then the pure helium eluent is switched to a 2% oxygen/helium mixture. Subsequently the temperature of the sample oven is stepped to about 860° C. The presence of the oxygen in the oven atmosphere causes the oxidation of the pyrolytically generated carbon (char) with a consequent increase of the filter transmittance. The measure of the amount of pyrolytical carbon oxidation required to return to the initial filter transmittance value allows obtaining correction for the char contribution to original elemental carbon. The "split" between the organic and elemental carbon is defined as the point at which the filter transmittance reaches the initial value. Organic carbon (including some carbonate particles) is the carbon volatilized prior to the split; the carbon evolved after the split and prior to the calibration peak is considered elemental. As in the phase 1 the carbon dioxide is then converted to methane and detected by FID.
3. When all carbon has been oxidized from the filter, a known volume and concentration of methane is injected into the sample oven. Therefore, the sample is calibrated to a known quantity of carbon. This method allows checking the operation of the instrument. On the basis of the transmittance data and the response of FID the amount of organic and elemental carbon are calculated for each sample.

In phase 1 the transition from 500°C to 700°C decomposes inorganic carbonates producing a characteristic peak (typically the fourth OC peak). An additional analysis performed on a second punch of the filter after its exposure to HCl allows verifying the presence of carbonate. The absence or diminished size of the suspect peak in the second analysis indicates the presence of carbonate in the analyzed filter.

Quartz fiber filters are required for TOT analysis because of the high temperatures employed during the analysis. For each sample a 1.0 or 1.5 cm^2 rectangular portion (punch) is analyzed and organic and elemental carbon are given as

μg/cm^2 of filter. In order to remove any residual carbon contamination the filters are pre-fired in air at 700°C for about two hours.

In this PhD work the TOT technique has been applied using a Sunset Laboratory Thermal-Optical Carbon Aerosol Analyzer (Figure 5.1). The schematic diagram of the thermal optical instrument is shown in figure 5.2.

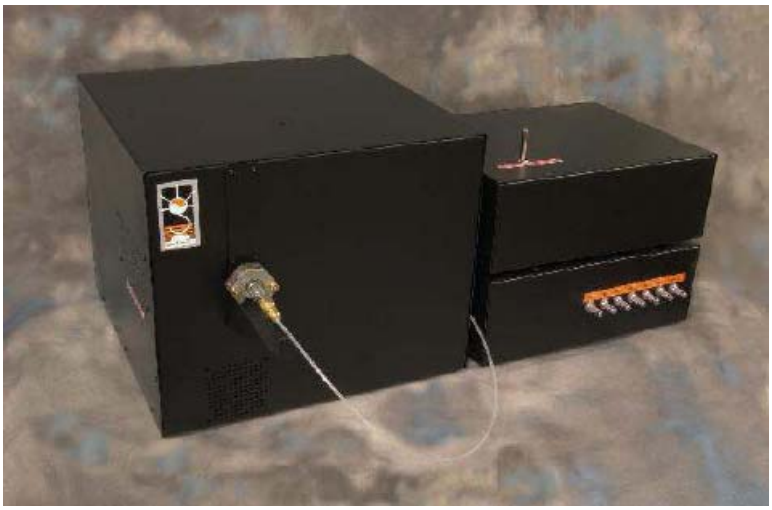

Figure 5.1 – The Sunset Laboratory Thermal-Optical Carbon Aerosol Analyzer.

The punch from a quartz filter sample is placed in a quartz boat and positioned in the path of a He-Ne diode laser, which is used to monitor the transmittance of the filter during analysis. A thermocouple at the end of the boat is used to monitor sample temperature during analysis. All carbon species evolved from the filter are converted to carbon dioxide in an oxidation oven adjacent to the primary oven, and the carbon dioxide is reduced to methane before passing into the flame ionization detector.

Figure 5.3 shows as example a thermogram obtained for a filter containing carbonaceous particles of crustal and anthropogenic origin: peaks correspond to organic carbon (OC), carbonate (CC), pyrolytic carbon (PC) and elemental carbon (EC). The final peak is the methane calibration peak.

The precision of the Sunset Laboratory method of OC/EC analysis is typically 5%, measured as a relative standard deviation (RDS).

The detection limit of the method is 0.15 μg/cm^2 for both organic and elemental carbon. This low value is the reason for which the filters are pre-cleaned as previously discussed.

It is important to highlight that the accuracy of this method for OC/EC measurements can be routinely checked: a known quantity (normally 10 μL) of OC standard solution is applied with a syringe to blank quartz fiber filter. Generally for better results the pre-cleaned filter punch is cleaned again in the sample oven prior to application. The results of the analysis of the filter with standard solution are compared to the known presence of OC. Relative standard deviation is less than 5% in a calibrated instrument.

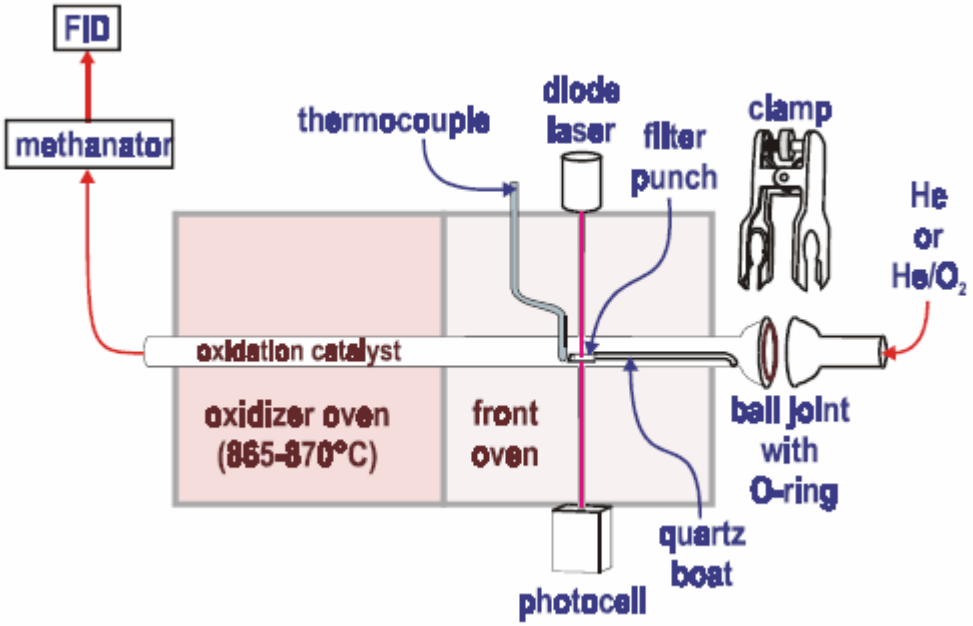

Figure 5.2 – Schematic diagram of thermal-optical instrumentation.

In general three or four quality controls standards are analyzed to ensure the instrument calibration. In this study the check for instrument calibration has routinely performed using four sucrose standard solutions with the following concentrations:

- 8.4140 μg per μL;
- 4.2060 μg per μL;
- 2.1030 μg per μL;

- 0.4206 µg per µL.

It is important to carefully inject the standard solution on the filter punch, since it is necessary to disperse the solution on the center of the filter portion in order to ensure that the standard is in laser beam.

Because of analyzer results of OC/EC are reported in µg/cm^2, to obtain the OC/EC mass in µg the reported results are multiplied by filter deposit area in cm^2. The same operation is done for blank filters. In general 10 blank filters have been analyzed to obtain an average OC/EC mass concentration for the substrate filter.

For each analyzed filter the mass concentration $C_{OC(EC)}$ in µg/m^3 of OC (EC) is calculated using the formula:

$$C_{OC(EC)} = \frac{M_{OC(EC)} - B_{OC(EC)}}{V},$$

where $M_{OC(EC)}$ is the mass in µg of OC (EC) present in the analyzed filter, $B_{OC(EC)}$ is the average mass in µg of OC (EC) in blank filters and V is the sampled air volume (m^3).

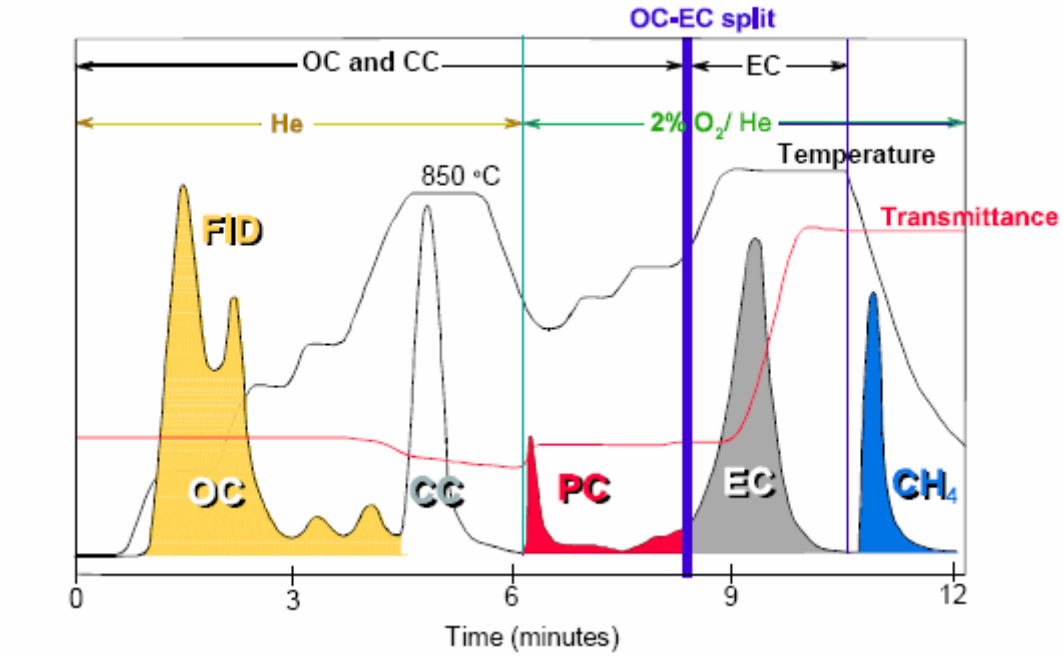

Figure 5.3 – Example of a thermogram for a filter sample containing OC, EC and carbonate (CC). The pyrolytically generated carbon or "char" is indicated as PC. The final peak is the methane calibration peak.

5.2 Sampling instrumentation

The low volume (2.3m^3/h) HYDRA-FAI dual sampler (chapter 3) has been used to simultaneously collect at the Physics Department 24-h PM2.5 and PM1 samples from July to December 2008. The sampled PM has been deposited on 47-mm-diameter quartz fibre filters, pre-cleaned (at 700° for about two hours) and conditioned before and after sampling (25°C during 48 h and 50% humidity). Particulate matter concentrations have been determined by the gravimetric method.

EC and OC mass concentrations have been determined in the collected PM2.5 and PM1 samples by the thermal/optical transmittance (TOT) technique by means of the OC/EC Sunset Analyzer of the Physics Department of Lecce.

A set of 10 blank filters have been analyzed in order to obtain an average OC/EC mass concentration characterizing the quartz fiber substrate.

5.3 PM2.5 and PM1 mass concentration results

Sampling days and corresponding 24-h mass concentration values of collected PM2.5 and PM1 samples are reported in table 5.1. Uncertainties on mass concentrations are lower than 5%. PM2.5 and PM1 mass concentrations are plotted in figure 5.4 as a function of the sampling day. PM2.5 mass concentrations vary from 41 to 7 μg/m^3 with a mean value of (21 ± 9) μg/m^3; while PM1 mass concentrations vary from 32 to 6 μg/m^3 with a mean value of (14 ± 6) μg/m^3. Within the sampling period we can observe from figure 5.4 a significant daily variation of both PM2.5 and PM1 mass concentrations; indeed both PM fractions are characterized by a rather similar seasonal trend. In fact the highest PM2.5 and PM1 mass concentration values have been recorded in summer (from July to September); conversely during October-November both sampling collections exhibit lower mass concentration values. It is important to highlight that 37% of PM2.5 samples exhibits a mass concentration value higher than the expected PM2.5 annual limit value 25 μg/m^3 (not to be exceed from January 2015).

Figure 5.5 shows the evolution with time of the mass ratio PM1/PM2.5 which varies from 0.9 to 0.3 and is characterized by significant daily variations: on average the ratio reaches larger values from July to August. Moreover, it is important to note that PM1 fraction represents on average a significant percentage (about 70%) of the total PM2.5 fraction.

Table 5.1 – Sampling days and corresponding mass concentration values of the simultaneously collected PM2.5 and PM1 samples. Uncertainties are less than 5%. The samples in bold type have been selected for OC/EC analyses.

Date	PM2.5 µg/m^3	PM1 µg/m^3
03/07/2008	**22.3**	**19.8**
07/07/2008	30.7	19.0
10/07/2008	17.2	12.8
14/07/2008	20.6	13.4
17/07/2008	**13.5**	**12.1**
21/07/2008	29.4	21.5
24/07/2008	**7.3**	**6.4**
28/07/2008	19.3	13.7
31/07/2008	**28.9**	**20.9**
04/08/2008	**37.6**	**29.4**
06/08/2008	**40.7**	**31.9**
04/09/2008	**36.5**	**12.0**
08/09/2008	**29.2**	**11.8**
11/09/2008	27.6	19.5
15/09/2008	**12.3**	**10.8**
18/09/2008	11.1	7.0
22/09/2008	11.3	7.8
29/09/2008	**28.0**	**16.8**
02/10/2008	28.5	17.5
06/10/2008	**24.2**	**16.5**
09/10/2008	26.8	17.2
03/11/2008	**22.2**	**10.7**
06/11/2008	**18.8**	**8.4**
13/11/2008	**12.1**	**6.6**
17/11/2008	**19.0**	**13.2**
20/11/2008	**27.6**	**15.6**
21/11/2008	13.7	7.5
22/11/2008	12.1	8.8
23/11/2008	12.5	9.4
24/11/2008	**14.2**	**9.5**
25/11/2008	12.3	5.8
26/11/2008	12.2	8.6
27/11/2008	21.4	13.5
28/11/2008	**25.6**	**14.1**
01/12/2008	13.5	8.3

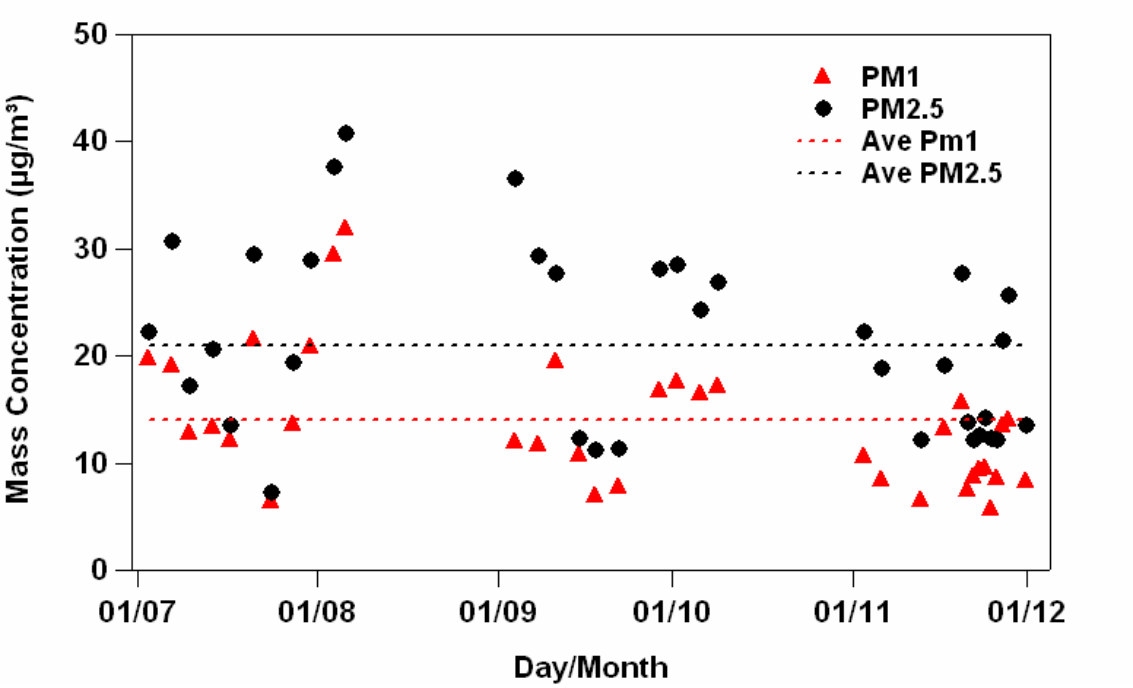

Figure 5.4 - Mass concentrations of PM2.5 (black points) and PM1 (red triangles) samples simultaneously collected from July to November 2008 at Physics Department of University of Salento. The horizontal lines represent the average values.

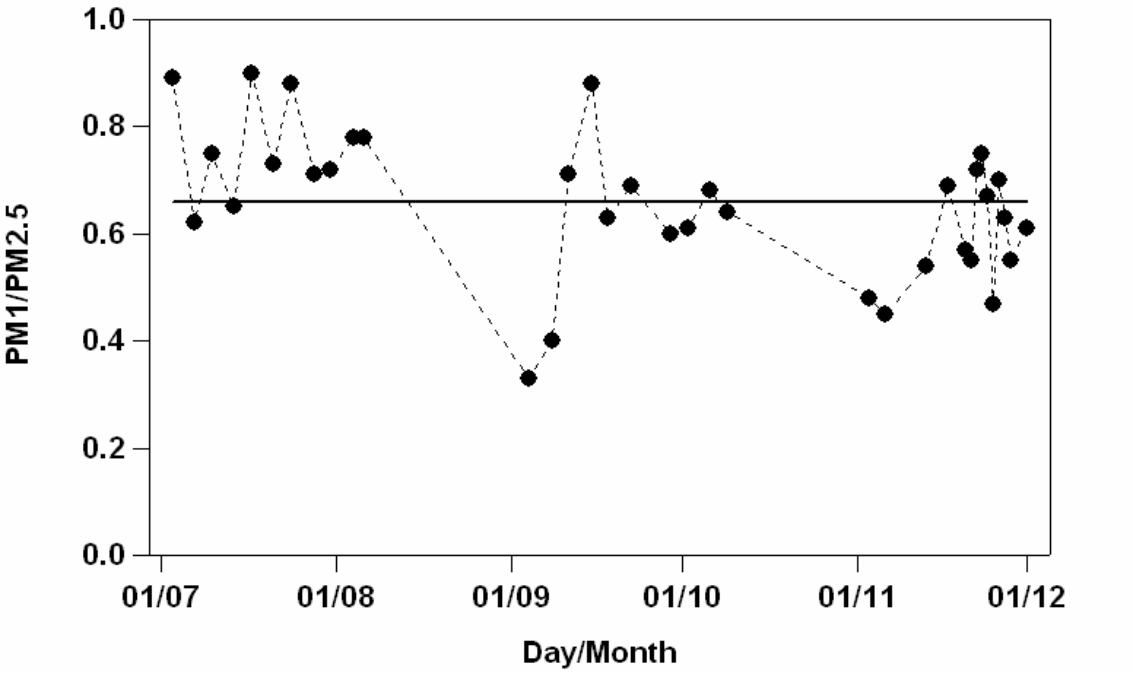

Figure 5.5 – PM1/PM2.5 mass ratios as a function of the sampling day. The horizontal line represents the average value.

5.4 OC/EC analysis results

OC/EC analyses have been performed on 18 randomly selected couples of PM1 and PM2.5 samples. The analyzed samples are highlighted in bold type in table 5.1.

Table 5.2 shows mass concentrations of organic and elemental carbon detected by thermal-optical transmittance (TOT) technique in the analyzed PM2.5 and PM1 samples.

Table 5.2 – Mass concentrations of OC and EC detected in PM2.5 and PM1 samples.

	PM2.5		PM1	
Date	**OC**	**EC**	**OC**	**EC**
	ug/m^3	**ug/m^3**	**ug/m^3**	**ug/m^3**
03/07/08	4.6	1.9	3.9	1.7
17/07/08	3.7	1.2	3.0	0.9
24/07/08	2.5	0.6	1.8	0.6
31/07/08	5.0	1.8	4.1	1.2
04/08/08	4.5	2.3	3.3	1.9
06/08/08	5.9	2.5	4.4	2.2
04/09/08	4.6	2.2	2.7	1.4
08/09/08	6.9	2.1	4.5	1.8
15/09/08	2.5	1.8	1.9	1.4
29/09/08	10.1	2.4	5.3	1.8
06/10/08	8.9	3.6	4.8	2.9
03/11/08	6.3	2.7	3.3	2.0
06/11/08	3.0	1.3	1.6	0.9
13/11/08	5.0	1.5	2.6	1.2
17/11/08	4.0	3.2	2.6	2.2
20/11/08	11.1	2.8	6.0	2.0
24/11/08	4.0	1.5	2.4	0.9
28/11/08	7.9	2.7	4.0	1.7

Figures 5.6-5.7 illustrate the evolution with time of OC and EC mass concentrations detected in PM2.5 and PM1 samples, respectively. We can observe that in both PM fractions organic and elemental carbon mass concentrations exhibit a similar trend with a significant daily variation. EC mass concentrations of PM2.5 samples vary from about 1 to 4 μg/m^3 with a mean value of (2 ± 1) μg/m^3. Conversely, OC mass concentrations vary from about 3 to 11 μg/m^3 with a mean value of (6 ± 3) μg/m^3 and reach the higher values from October to November. OC mass concentrations of PM1 samples vary from about 2 to 6 μg/m^3 with a mean value of (3 ± 1) μg/m^3. Conversely, EC mass concentrations vary in the range (1 – 2) μg/m^3 within the sampling period.

Figures 5.6 and 5.7 do not reveal any marked seasonal trend of EC and OC mass concentrations.

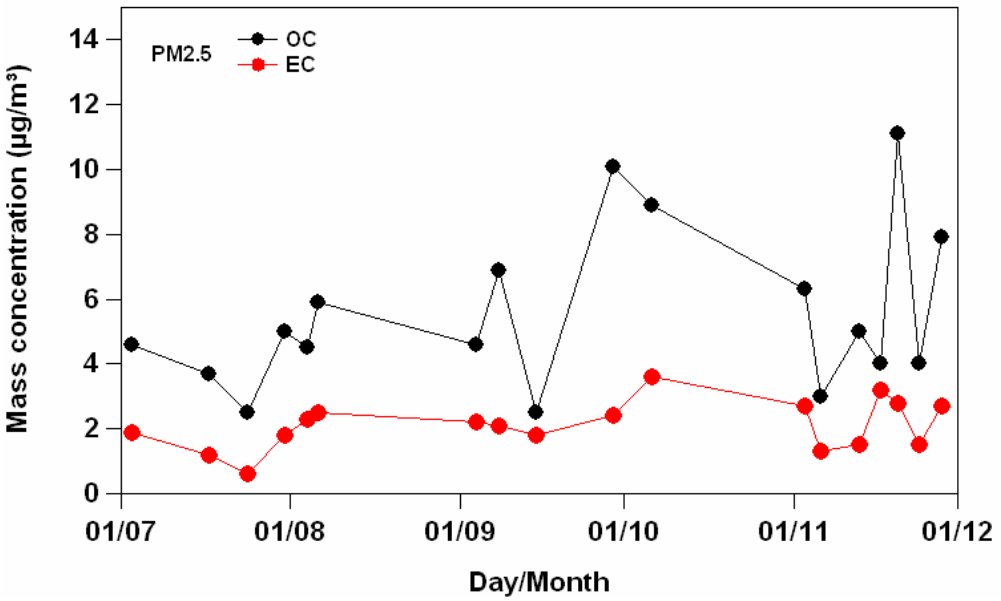

Figure 5.6 – OC and EC mass concentrations detected in PM2.5 samples as a function of the sampling day.

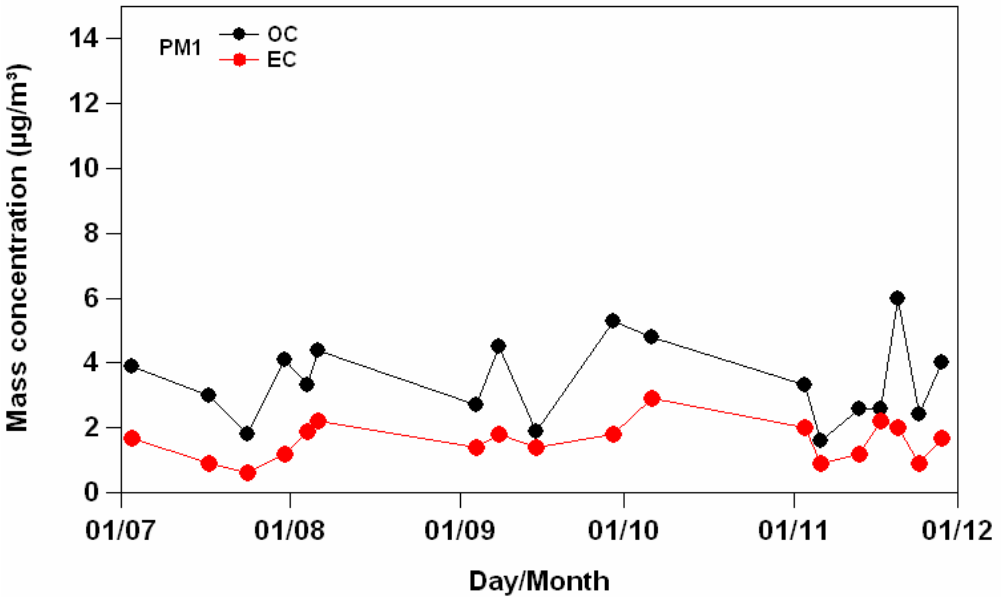

Figure 5.7 – OC and EC mass concentrations detected in PM1 samples as a function of the sampling day.

Table 5.3 provides main statistics on tested parameters for July, August, and September (JAS) and for October and November (ON). In addition to PM2.5 and PM1 mass concentrations, mean values of EC and OC mass concentrations, OC/EC mass ratios and TC/PM mass percentages are also provided in table 5.3. TC represents the total carbon mass detected in the collected particulate matter.

Table 5.3 - Average mass concentration ± 1 Standard Deviation (SD) of PM2.5, PM1, OC and EC, in addition with TC/PM mass ratio percentages and OC/EC mass ratios for JAS (July-August-September) and ON (October-November).

	PM2.5		PM1	
	JAS	**ON**	**JAS**	**ON**
PM ± 1 SD (µg/m³)	26 ± 12	20 ± 5	17 ± 8	12 ± 4
OC ± 1 SD (µg/m³)	5 ± 2	6 ± 3	3 ± 1	3 ± 1
EC ± 1 SD (µg/m³)	1.9 ± 0.6	2.4 ± 0.9	1.5 ± 0.5	1.7 ± 0.7
TC/PM (%)	30 ± 10	42 ± 10	32 ± 11	44 ± 10
OC/EC	2.7 ± 0.9	2.7 ± 0.8	2.4 ± 0.7	2.1 ± 0.6

It is worth noting from table 5.3 that about 65% and 60% of the PM2.5 mass concentration is due to PM1 particles on JAS and ON, respectively. Table 5.3 does not reveal any marked dependence on season of tested parameters, at least within ± 1 SD of mean values and within the investigated time of the year. However, as previously observed, PM2.5 and PM1 mean mass concentrations are higher on JAS; conversely TC/PM mass ratio percentages are slightly larger on October-November. In particular, the mass percentage of carbonaceous particles is about 30% and 40% of the collected mass on PM2.5 and PM1 samples on JAS and ON, respectively. These last results show that the mass contribution of carbonaceous particles is quite significant over the monitoring site.

We can also observe from table 5.3 that the OC/EC mass ratio exceeds 2.0 both in PM2.5 and PM1 samples. This last result allows inferring the significant presence in collected fine particulate matter of secondary organic particles (Cao et al. 2004).

Figures 5.8-5.9 show the good correlation ($r = 0.65$ and $r = 0.64$) between OC and EC in PM2.5 and PM1 fraction, respectively. These results may suggest that mass concentration levels of both carbonaceous species are controlled by similar atmospheric processes and that OC and EC fractions can be probably ascribed to common sources.

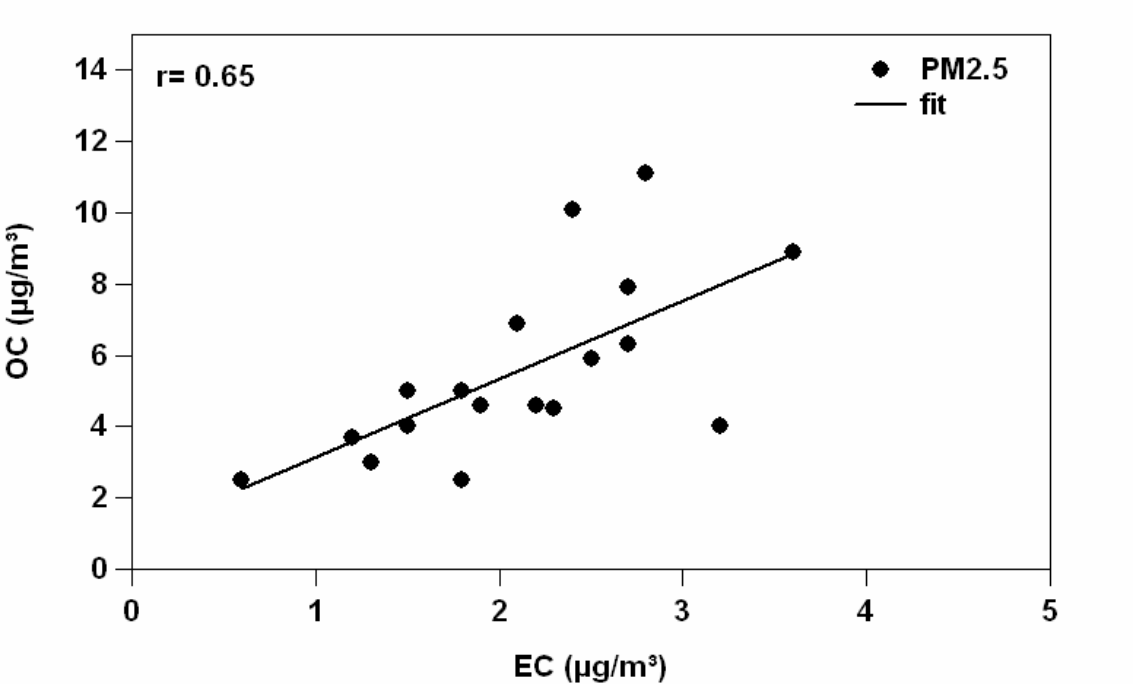

Figure 5. 8 – Scatter plot of OC-EC mass concentrations in PM2.5 samples.

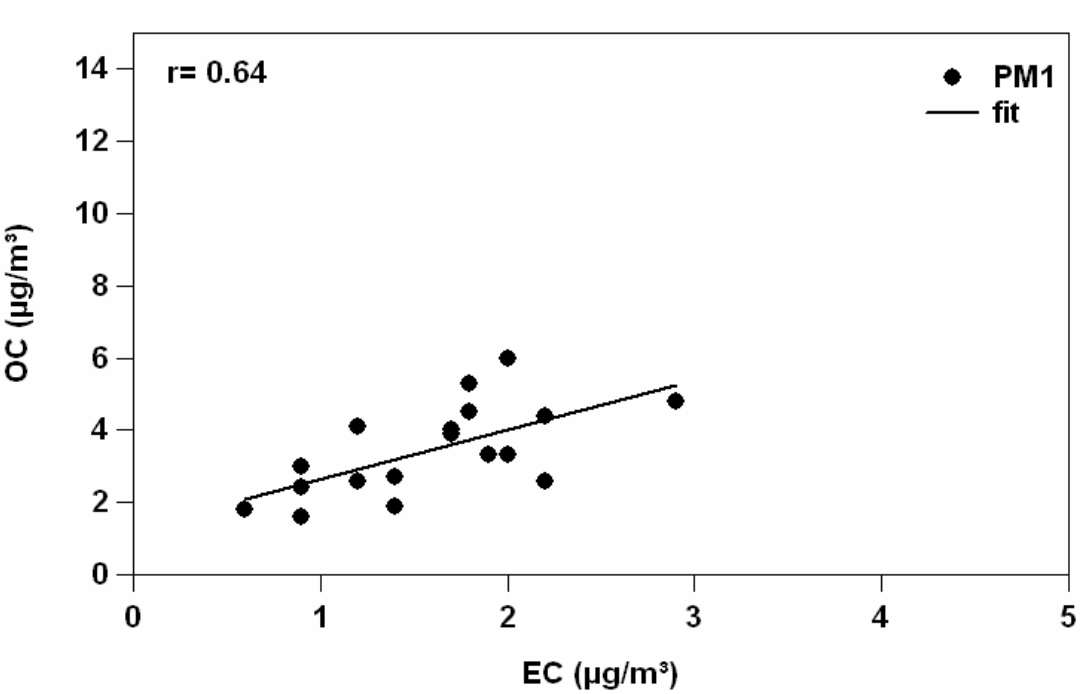

Figure 5. 9 – Scatter plot of OC-EC mass concentrations in PM1 samples.

CHAPTER 6

IONIC AND ELEMENTAL ANALYSIS OF TSP, PM10 AND PM2.5 SAMPLES

6 IONIC AND ELEMENTAL ANALYSIS OF TSP, PM10 AND PM2.5 SAMPLES

In this chapter results on mass concentrations and composition of 24-hour TSP, PM10, and PM2.5 samples collected on following day at the Physics Department of the University of Salento are presented and discussed. It is worth mentioning that sampling site is located in the Salento Peninsula, in the central Mediterranean, away from large cities and/or industrial areas, thus it is well suited to contribute to the aerosol characterization of the central Mediterranean basin which is one of the Earth regions where the aerosol climate effects are maxima, as shown by various studies (Bolle, 2003; Giorgi 2006). Due to the variety of the regions around the basin, different aerosol types can be found in the Mediterranean atmosphere: desert dust from the Sahara desert and the arid regions in the Iberian Peninsula, polluted particles from urban and industrial areas of North- and East-Europe, marine aerosols from the Mediterranean itself or transported from the Atlantic, and biomass burning particles, often produced in forest fire, mainly during the summer. Thus, the Mediterranean represents an area where aerosols from different natural and anthropogenic sources can be present. Most of the published studies on the input of natural and anthropogenic aerosols into the Mediterranean have been conducted in its western (Bergametti et al., 1989; Rodriguez et al., 2002; Querol et al., 2008) and eastern part (Levin and Lindberg, 1979; Formenti et al., 1996; Mihalopoulos et al., 1997; Ganor et al., 1998; Formenti et al., 2002; Bardouki et al., 2003). To our knowledge only few studies have been conducted to characterize the composition of aerosol particles in the background atmosphere of the central Mediterranean.

As widely discussed in the previous chapters, one the main goals of my research activities is to investigate the dependence of the particulate matter mass concentration and composition on particle size. Different complementary techniques are generally required to obtain as much information as possible. So, both Ion Chromatography (IC) and the Inductively Coupled Plasma Atomic Emission Spectroscopy (ICP-AES) have been used to determine the mass concentration of the main ionic species and metal elements, respectively in the collected TSP, PM10 and PM2.5 samples.

In particular F^-, Cl^-, NO_3^-, SO_4^{2-}, Na^+, NH_4^+, K^+, Mg^{2+}, Ca^{2+} have been analyzed as ionic species, while Ti, Al, Si, Fe, Mn, Cu, Zn, Pb, and Cd are the tested metals.

6.1 Sampling and system

24-hour TSP, PM10, and PM2.5 samples have been collected from June to October 2004, at the Physics Department of the University of Salento that, as discussed in chapter 2, is located at ~20 km away from both the Ionic and the Adriatic Sea.

The study has mainly been limited to samples collected on summer when, over the Mediterranean, the large solar irradiance favors the formation in the atmosphere of photochemical smog and the lack of raining days favor the accumulation of local and long-transported particles (De Tomasi et al., 2006).

The PM sampling has been carried out by means of the low-volume ESM Andersen sampler FH 95 KF (presented in chapter 3) that can be equipped with a TSP, or PM10, or PM2.5 inlet. The collection of PM on 47 cm-diameter nitrate cellulose filters, has been made at the top of the Physics Department building, at about 10 m from ground. Mass concentrations have been determined gravimetrically. Both blank and field filter samples have been conditioned at constant temperature (20 ± 1 °C) and relative humidity (50 ± 5 %) for at least 48 hour prior to being weighted. 13 samples of TSP, PM10, and PM2.5 respectively have randomly been selected for characterizing main ionic and elemental components. To this end, the selected samples have been punched in two portions for the separate analytical determination of the ionic and elemental species.

6.1.1 Ion chromatography analyses: methodology

A high performance ion chromatograph DIONEX model DX-500 (DIONEX, Rome, Italy) has been used to determine the mass concentration of major anions (Cl^-, F^-, Br^-, NO_3^-, SO_4^{2-}) and cations (NH_4^+, Na^+, K^+, Mg^{2+}, Ca^{2+}). A self-regenerating suppressor ASRS®-ULTRA (4 mm) at 50 mA, a guard column IONPAC® AG4A-SC (4·50 mm) and an analytical column IONPAC® AS4A-SC (4·250 mm) have been used for anions analysis. All the anions have been determined with isocratic elution at 2.0 mL min-1 of 1.8 mM Na2CO3 / 1.7 mM NaHCO3 eluent. A self-regenerating suppressor CSRS®-ULTRA (4 mm), a guard column IONPAC® CG12A (4·50 mm) at 100 mA and an analytical column IONPAC® CS12A (4·250 mm) have been used for cation analysis. All cations have been determined with isocratic elution at 1 mL min-1 of 20 mN H2SO4 eluent.

6.1.2 Metal analyses: methodology

An inductively coupled plasma atomic emission spectrometer ICP-AES Liberty 110 (Varian Inc., Palo Alto, USA) has been used to determine the mass concentration of several metals (Al, Si, Ca, Cu, Fe, Pb, Mn, Ti, Zn). The instrument was equipped with a vertical torch inert to hydrofluoric acid and an ultrasonic nebulizer CETAC U-5000AT+ (Cetac Technologies Inc., Omaha, Nebraska, USA). A microwave system MILESTONE MLS-1200 MEGA (Milestone, Bergamo, Italy) has been used to accomplish the dissolution of the samples. Details on sample preparation and analysis technique are reported elsewhere (Buccolieri et al., 2005).

Both metal and Ion Chromatography analyses have been performed by Dr. Buccolieri G. of Physics Department and Dr. Buccolieri A. of Material Science Department of the University of Salento.

6.2 Mass concentration results

Table 6.1 shows the sampling days and the corresponding mass concentration values of TSP, PM10 and PM2.5 collected samples. The randomly-selected analyzed samples are in bold type. Uncertainties on mass concentrations are lower than 5%. Daily TSP, PM10, and PM2.5 mass concentrations varied from 21 $\mu g/m^3$ to 74 $\mu g/m^3$, from 10 $\mu g/m^3$ to 83 $\mu g/m^3$, and from 17 $\mu g/m^3$ to 63 $\mu g/m^3$, respectively, without any significant dependence on the sampling month.

Mass concentrations of collected samples are plotted in figures 6a-6c as a function of the sampling day in addition to mean mass concentrations (dotted lines). Full symbols in figure 6.1 indicate the analyzed randomly-selected samples. The high daily changes in mass concentrations revealed by figure 6.1 is frequently observed in the Mediterranean area and surrounding regions (Rodriguez et al., 2002; Smolik et al., 2003; Santese et al., 2007). Changes in air mass transport arriving from different sources toward the sampling point can be responsible for these results, as several studies on advection patterns over South-East Italy have revealed (Kouyoumdjian and Saliba, 2005; Perrone et al., 2006; Bellantone et al., 2008; Santese et al., 2008).

Table 6.1 – Sampling days and mass concentration values of TSP, PM10 and PM2.5 collected samples. The samples in bold type have been selected for ionic and metal analyses.

TSP		PM10		PM2.5	
Date	**Conc. (µg m^{-3})**	**Date**	**Conc. (µg m^{-3})**	**Date**	**Conc. (µg m^{-3})**
01/06/2004	37	08/06/2004	23	**12/06/2004**	**35**
03/06/2004	43	09/06/2004	32	**20/06/2004**	**23**
04/06/2004	21	10/06/2004	10	24/06/2004	40
07/06/2004	24	**16/06/2004**	**32**	**26/06/2004**	**30**
14/06/2004	37	17/06/2004	47	01/07/2004	37
15/06/2004	44	22/06/2004	42	**03/07/2004**	**33**
28/06/2004	58	23/06/2004	47	**10/07/2004**	**38**
05/07/2004	**51**	**29/06/2004**	**36**	22/0720/04	57
06/07/2004	65	30/06/2004	40	**24/0720/04**	**48**
12/07/2004	44	**07/07/2004**	**47**	**04/09/2004**	**33**
13/07/2004	**42**	08/07/2004	83	**18/09/2004**	**33**
19/07/2004	31	**14/07/2004**	**27**	**24/09/2004**	**54**
20/07/2004	**68**	16/07/2004	27	**01/10/2004**	**52**
27/07/2004	29	21/07/2004	12	**08/10/2004**	**58**
28/07/2004	25	**02/09/2004**	**54**	**21/10/2004**	**63**
29/07/2004	**32**	**08/09/2004**	**46**	**27/10/2004**	**17**
30/08/2004	50	09/09/2004	66	28/10/2004	17
31/08/2004	**69**	**15/09/2004**	**70**		
06/09/2004	67	16/09/2004	77		
07/09/2004	**70**	**22/09/2004**	**60**		
13/09/2004	73	**29/09/2004**	**26**		
14/09/2004	**74**	**06/10/2004**	**54**		
21/09/2004	**72**	07/10/2004	72		
25/09/2004	30	13/10/2004	24		
27/09/2004	32	**14/10/2004**	**26**		
28/09/2004	**32**	15/10/2004	19		
04/10/2004	52	**20/10/2004**	**51**		
05/10/2004	**64**	22/10/2004	49		
12/10/2004	**34**	**26/10/2004**	**48**		
18/10/2004	38	29/10/2004	28		
19/10/2004	**46**				
25/10/2004	**59**				

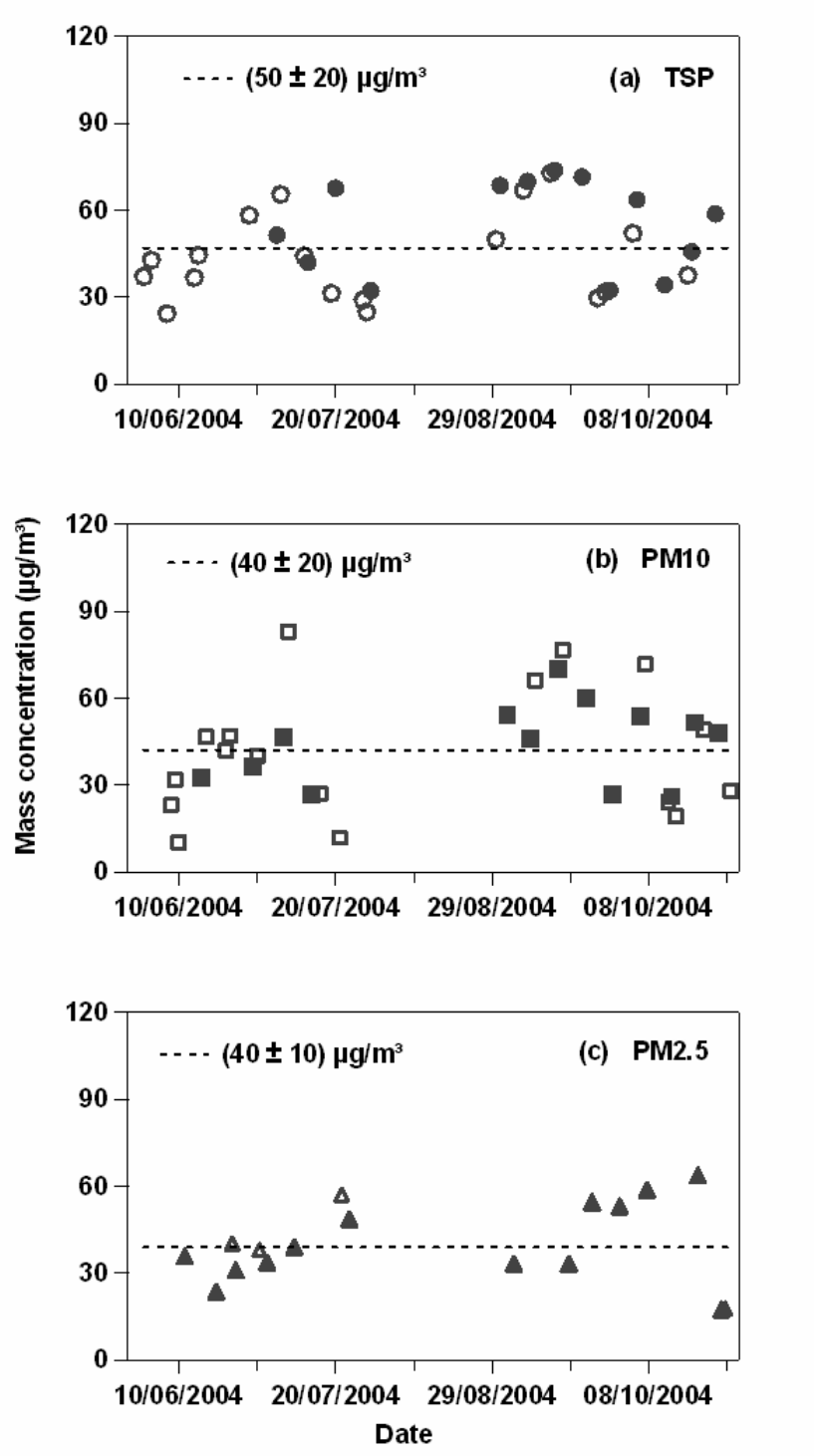

Figure 6.1 - Mass concentrations of (a) TSP, (b) PM10 and (c) PM2.5 samples as a function of the sampling day. Full symbols indicate the randomly selected samples for ionic and elemental analyses. Dashed lines represent mean values.

Figure 6.1 also shows that mean mass concentrations are not significantly affected by the PM fraction. TSP, PM10, and PM2.5 mean mass concentrations (±1 standard deviation, SD) are 50±20 µg/m^3, 40±20 µg/m^3, and 40±10 µg/m^3, respectively.

These results reveal the predominance in collected samples of particles with the aerodynamic diameter < 2.5 μm.

The PM10 limit value for human health protection established by the European Council Directive 1999/30/CE is 50 $\mu g/m^3$ for 24-hour limit value, not to be exceeded more than 35 times/year (~10%). It is worth noting from Figure 6.1b that 30% of the 30 PM10 samples have a mass concentration exceeding the 24-hour limit-value and that the mean PM10 mass concentration (40 $\mu g/m^3$) is equal to the annual limit.

The PM10 mass concentrations reported in this PhD work are in satisfactory accordance with those provided by the Regional Environmental Protection Agency ARPA-Puglia[1] for several sites of South-Eat Italy and as a consequence can be considered representative of South-East Italy.

The rather high PM10 mass concentrations and the predominance of PM2.5 particles (Figure 6.1) are likely due to the strong solar irradiance, which mainly on summer time favors in the atmosphere the secondary particle formation (photochemical smog) and to the poor renovation of air masses that, in the absence of rain, favor the accumulation of local and long-transported particles, as mentioned in the introduction. In accordance with PM ground measurements, remote sensing measurements from ground and space (Perrone et al., 2005; Santese et al., 2007) also revealed that the contribution of fine-mode particles is larger over the Mediterranean on summer.

6.3 Ion chromatography analyses results

The total analyzed ionic mass and mass concentrations of individual ionic species significantly varied from sample to sample. As a consequence, the total ionic mass can explain from 16% to 41%, from 17% to 43%, and from 18% to 43% of the PM mass in the TSP, PM10, and PM2.5 analyzed samples, respectively. In accordance with the discussion in section 6.2, changes in air mass transport arriving from different regions toward the sampling point have likely been responsible for the high variability from sample to sample of both the ionic composition and the mass concentration. Aerosol optical and microphysical properties and mass concentrations are quite dependent on source regions and pathways of the air masses advected over the monitoring site (Bellantone et al., 2008).

[1] www.arpapuglia.it

Average (±1 SD), minimum and maximum mass concentrations of tested ions in TSP, PM10, and PM2.5 samples are given in Table 6.2, to better show the dependence of the mass concentration of individual ionic species, on PM fraction. SO_4^{2-} mass concentrations have been divided into both sea-salt sulfate (ss- SO_4^{2-}) and nss- SO_4^{2-} mass concentrations to better infer the sulfate anthropogenic contribution. nss- SO_4^{2-} have been calculated by deducting the sea salt contribution to SO_4^{2-}. Assuming that all measured Na^+ had a marine origin, the sea salt contribution to SO_4^{2-} has been estimated (Keene et al., 1986) as measured Na^+ times 0.242. Table 6.2 shows that both the mean mass concentrations of tested ions and the total analyzed mean ionic mass are not significantly affected by the PM fraction, at least within ±1 SD of mean values.

Table 6.2 – Average mass concentrations (μg/m³) of ionic species and mean Ion/PM ratios in the TSP, PM10, and PM2.5 analyzed samples.

	TSP	**PM10**	**PM2.5**
	μg/m³	**μg/m³**	**μg/m³**
F^-	0.02 ± 0.02 (12)[(a)]	0.03 ± 0.02 (9)	0.02 ± 0.01 (11)
	0.003 - 0.07[(b)]	0.02 - 0.07	0.003 - 0.04
Cl^-	0.5 ± 0.4 (13)	0.3 ± 0.3 (13)	0.06 ± 0.04 (12)
	0.1 - 1.6	0.1 - 1.2	0.002 - 0.1
NO_3^-	3 ± 2 (12)	3 ± 2 (12)	1 ± 1 (13)
	0.1 - 5.4	0.2 - 6.8	0.5 - 3.7
nss-SO_4^{2-}	5 ± 2 (13)	5 ± 2 (13)	7 ± 3 (13)
	1.8 - 7.3	1.8 - 9.3	2.6 - 12.3
ss-SO_4^{2-}	0.2 ± 0.1 (13)	0.2 ± 0.1 (13)	0.08 ± 0.03 (13)
	0.02 - 1.9	0.03 - 0.2	0.05 - 0.1
Na^+	0.7 ± 0.5(12)	0.7 ± 0.3 (13)	0.3 ± 0.1 (13)
	0.1 - 1.8	0.1 - 1.0	0.2 - 0.6
NH_4^+	0.06 (1)	0.3 ± 0.3 (4)	1 ± 1 (11)
	-	0.1 - 0.8	0.01 - 2.3
K^+	0.2 ± 0.1 (13)	0.2 ± 0.1 (13)	0.3 ± 0.2 (13)
	0.04 - 0.3	0.1 - 0.5	0.1 - 0.8
Mg^{2+}	0.5 ± 0.3 (13)	0.3 ± 0.2 (13)	0.2 ± 0.1 (13)
	0.2 - 1.2	0.1 - 0.8	0.02 - 0.3
Ca^{2+}	4 ± 2 (13)	2 ± 1 (13)	1 ± 1 (13)
	1.0 - 6.9	0.9 - 3.7	0.2 - 2.3
Ion/PM (%)	24 ± 7 (13)	26 ± 7 (13)	30 ± 8 (13)
	16 - 41	17 - 43	18 - 43

[(a)]Mean ± SD (*N*); *N* represents the number of samples.
[(b)]Min – Max.

The mean ionic mass percentage (±1 SD) accounts for (24±7) %, (26±7) %, and (30±8) % of the total TSP, PM10, and PM2.5 mass, respectively. The predominance of the PM2.5 fraction in all collected samples allows understanding these results. Mean ion/PM mass concentration ratios have been plotted in Figure 6.2 to better assess the role of individual ionic species in TSP, PM10, and PM2.5 samples.

Figure 6.2 reveals that nss-SO_4^{2-}, NO_3^-, NH_4^+, and Ca^{2+} are the predominant ionic components accounting for 84%, 83%, and 91% of the total TSP, PM10, and PM2.5 ionic mass, respectively. In addition, we observe that nss-SO_4^{2-}/PM and NH_4^+/PM mass ratios are larger in PM2.5 samples: the nss-SO_4^{2-}/PM mass ratio that accounts for 9% of the measured PM mass in TSP samples accounts for 19% of the measured PM mass in PM2.5 samples. Conversely NO_3^-/PM and Ca^{2+}/PM mass ratios are larger in PM10 and TSP samples, respectively. Last results indicate that Ca^{2+} is mainly due to coarse-mode particles as those of crustal origin and that coarse-mode nitrates are predominant in the analyzed samples.

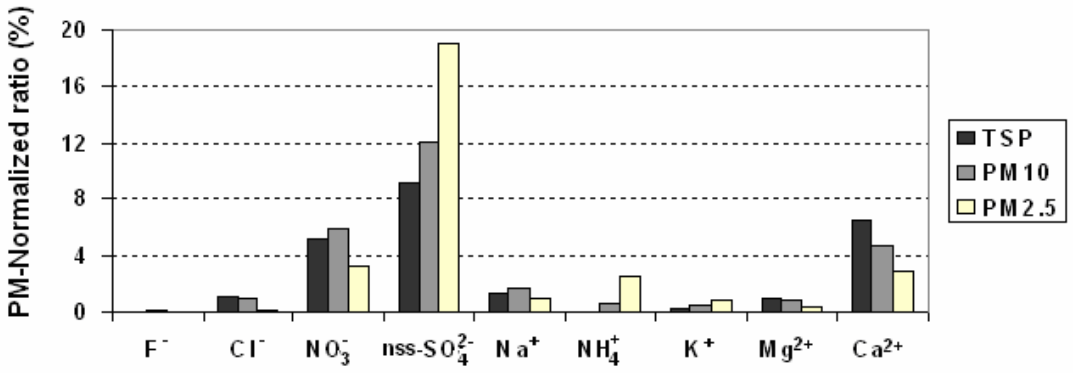

Figure 6.2 - Averaged ion/PM concentration ratios for all investigated ionic species in TSP (black bars), PM10 (grey bars), and PM2.5 (white bars) samples.

The mean mass concentration of nss-SO_4^{2-} is 1.7 larger than that of NO_3^- in TSP samples and 5 times larger than that of NO_3^- in PM2.5 samples. The predominance of sulfate to nitrate particles observed over South-East Italy and reflecting higher sulfur over nitrogen emissions has been observed mainly on summer at several coastal areas of the Mediterranean (Danalatos and Glavas, 1999; Rodriguez et al., 2002; Viana et al., 2005). Ion Chromatography analyses on PM2.5 filters collected in a densely populated area of Beirut (Kouyoumdjian and Saliba, 2005) from February 2004 to January 2005 revealed that the mean mass concentration of SO^{2-} (4.27 μg/m^3) was ~20 times larger

than that of NO_3^-. Danalatos and Glavas (1999) analyzing samples collected at the University campus of Patras also found that the particulate sulfate was 5-15 times larger than particulate nitrate. In particular, they found from all sampling period (November 1995-September 1996) that the mean sulfate concentration was 7.2 $\mu g/m^3$ and that it was similar to that observed at several coastal sites of the eastern Mediterranean (Luria et al. 1996). The high sulfate particle concentrations mainly observed in summer over coastal areas of the Mediterranean has been ascribed to long-lived particulate sulfate transported over the Mediterranean from North and East European countries (Danalatos and Glavas, 1999). The higher concentrations of sulfur containing ions observed in summer over the Mediterranean can also be ascribed to the large solar irradiance which favors the formation in the atmosphere of secondary products from the reaction of aerosol particles with sulfuric acid (Hidy, 1994). The lower contribution on summer of wet removal of SO_2, the nss-SO_4^{2-} precursor, represents a contributing factor.

Similar results were reported by Viana et al. (2005), analyzing the chemical composition of different PM fractions collected on summer in Barcelona (Spain). In particular, they also found that the NO_3^- mean mass concentration was larger in PM10 samples than in PM2.5 samples. Indeed, the large proportion of nitrate found in the coarse fraction (TSP and PM10) is peculiar of most coastal sites of the southern Mediterranean basin (Bardouki et al., 2003). The predominance of coarse-mode nitrates is probably due to the low thermal stability of NH_4NO_3 in spring-summer, when under the prevalent warm conditions of most of the Central Mediterranean sites, the formation of HNO_3 instead of NH_4NO_3 is favored (Querol et al., 2008). The presence of gaseous HNO_3 and the possible interaction of the pollutant with mineral Ca carbonate and sea salt may account for the increase of coarse nitrate proportion. Fine nitrate particles are usually the result of nitric acid/ammonia reactions for the formation of ammonium nitrates.

According to Danalatos and Glavas (1999), the low formation of ammonium nitrate over the Mediterranean coastal sites is due to low ammonia emissions (Mihalopoulos et al., 1997; Kouyoumdjian and Saliba, 2005): ammonia is first depleted by H_2SO_4 reactions to form $(NH_4)_2SO_4$ and the remaining free ammonia is depleted by reaction with HNO_3 to form NH_4NO_3 (Erisman and Schaap, 2004). Therefore, in NH_3–limited areas, HNO_3 cannot be fully neutralized by ammonia to form fine particles of ammonium nitrate, but reacts with coarse alkaline soil and/or marine particles to form coarse particulate (Kim et al., 2000; Lonati et al., 2005). However one must be aware of

the fact that NO_3^- measurements are affected by sampling artifacts: NH_4^+ associated with nitrate may evaporate during sampling (Henning et al., 2003; Marenco et al., 2006) and losses may take place in the form of gaseous HNO_3.

Correlation coefficients (r) between different ions are reported in tables 6.3-6.5 for TSP, PM10, and PM2.5 samples, respectively to infer main chemical species and hence, the natural/anthropogenic origin of sampled particles.

The high correlation between Na^+ and Cl^- mainly found in TSP (r=0.78) and PM2.5 (r=0.55) samples indicate that Na^+ and Cl^- are mainly due to sea-salt particles. The geographical location of the monitoring site supports last comment. The high correlation coefficients between Ca^{2+}, K^+, and Mg^{2+} indicate that they have a common crustal origin: soil-derived particles generally contain Ca, K, and Mg in addition to other elements (Ro et al., 2001). Conversely, nss-SO_4^{2-} and NO_3^- whose correlation is rather high in TSP (r=0.83) have a common anthropogenic origin: both anions are due to secondary products that are formed in the atmosphere from the reaction of aerosol particles with sulfuric and nitric acids, respectively (Raes et al., 2000; Kouyoumdjian and Saliba, 2005). In accordance with correlation coefficients of tables 6.3 and 6.4, nss-SO_4^{2-} and NO_3^- are mainly neutralized by K^+ in PM10 samples. These results imply that salts like K_2SO_4 and KNO_3 might be prevalent in PM10 samples. The presence of KNO_3 particles supports the previously reported comment on the low thermal stability of NH_4NO_3 that favors the formation of HNO_3.

Table 6.3 - Correlation coefficient (*r*) between sampled ions in TSP samples. Bold correlation values are significant at p-level < 0.05.

TSP	F^-	Cl^-	NO_3^-	Na^+	K^+	Mg^{2+}	Ca^{2+}	nss-SO_4^{2-}
F^-	1.00							
Cl^-	-0.30	1.00						
NO_3^-	0.16	-0.14	1.00					
Na^+	-0.12	**0.78**	0.27	1.00				
K^+	0.37	-0.27	0.47	0.22	1.00			
Mg^{2+}	-0.19	-0.07	0.42	0.28	0.47	1.00		
Ca^{2+}	0.00	-0.19	0.32	0.07	**0.63**	**0.87**	1.00	
nss-SO_4^{2-}	0.30	-0.40	**0.83**	-0.01	0.55	0.38	0.38	1.00

Table 6.4 - Correlation coefficient (*r*) between sampled ions in PM10 samples. Bold correlation values are significant at p-level < 0.05.

PM10	F^-	Cl^-	NO_3^-	Na^+	K^+	Mg^{2+}	Ca^{2+}	nss-SO_4^{2-}
F^-	1.00							
Cl^-	-0.30	1.00						
NO_3^-	0.19	-0.57	1.00					
Na^+	-0.26	0.32	0.48	1.00				
K^+	-0.13	-0.30	0.52	0.49	1.00			
Mg^{2+}	**-0.66**	0.30	-0.03	0.47	**0.56**	1.00		
Ca^{2+}	-0.03	-0.10	0.04	0.17	**0.63**	0.55	1.00	
nss-SO_4^{2-}	0.38	**-0.67**	0.55	0.04	**0.60**	-0.03	0.53	1.00

Table 6.5 - Correlation coefficient (*r*) between sampled ions in PM2.5 samples. Bold correlation values are significant at p-level < 0.05.

PM2.5	F^-	Cl^-	NO_3^-	Na^+	NH_4^+	K^+	Mg^{2+}	Ca^{2+}	nss-SO_4^{2-}
F^-	1.00								
Cl^-	0.44	1.00							
NO_3^-	0.32	**0.63**	1.00						
Na^+	0.40	**0.55**	0.26	1.00					
NH_4^+	-0.10	-0.21	0.01	-0.06	1.00				
K^+	0.11	-0.19	-0.22	0.09	0.20	1.00			
Mg^{2+}	0.08	-0.06	0.10	0.20	-0.03	**0.65**	1.00		
Ca^{2+}	0.32	-0.02	-0.12	0.38	-0.03	**0.79**	**0.82**	1.00	
nss-SO_4^{2-}	0.16	0.03	0.05	0.36	**0.82**	0.38	0.32	0.41	1.00

The high correlation ($r > 0.5$) between nss-SO_4^{2-} and Ca^{2+} in PM10 samples also suggests the presence of salts like Ca_2SO_4. Conversely, $(NH_4)_2SO_4$ and/or NH_4HSO_4 particles are expected to be significant in PM2.5 fraction, since NH_4^+ correlates very well with nss-SO_4^{2-} ($r = 0.82$) in PM2.5 samples (table 6.5). One must, however, observe that nss-SO_4^{2-} is only partially neutralized by ammonium in PM2.5 samples, since the overall average nss-SO_4^{2-}/NH_4^+ ratio is (7±3). This ratio is significantly larger than the expected ratio for pure ammonium sulfate which is 2.66 (Marenco et al., 2006). It is also worth noting that nss-SO_4^{2-} and NH_4^+ present their maximum in PM2.5 samples, in accordance with most aerosol studies (Formenti et al., 2002; Bardouki et al., 2003). In conclusion, these results show that the chemical composition of sulfate and nitrate particles is quite dependent on PM fraction and that the sulfate over nitrate mass ratio is also quite dependent on PM fraction.

NH_4^+ has been detected at mass concentrations above the detection limit in 11 of the 13 PM2.5 analyzed samples and it accounts for up to 13.5% of the total ionic mass. Conversely, NH_4^+ has been found in only one TSP sample and in 4 PM10 samples. This

result that is unexpected being PM2.5 particles a fraction of the TSP can be ascribed to artifacts during sampling (Danalatos and Glavas, 1999). Loss of material during collection may results from particulate to gaseous forms of pollutants collected on filters. In particular, overestimation of ammonia and underestimation of particulate ammonium may result from the interaction of particulate ammonium with alkaline particulate matter (Danalatos and Glavas, 1999). Figure 6.3 shows the NH_4^+ mass percentage as a function of the total mass percentage due to alkaline ions (Na^+, K^+, Mg^{2+},Ca^{2+}) in TSP (dots), PM10 (boxes), and PM2.5 (triangles) samples.

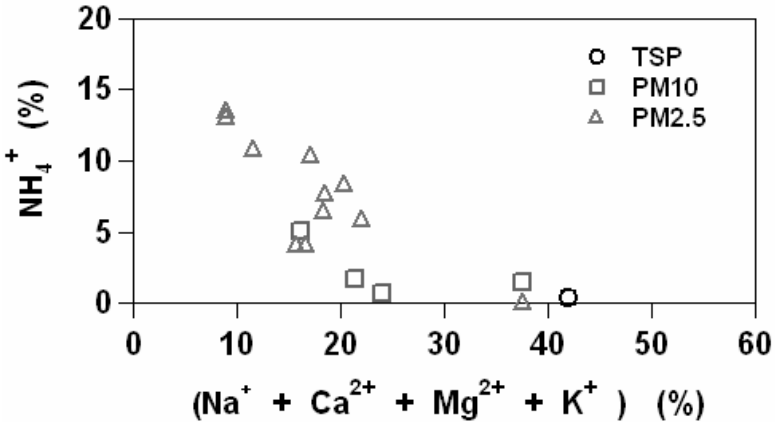

Figure 6.3 - NH_4^+ mass percentages as a function of the total mass percentage due to alkaline ions (Na^+, K^+, Mg^{2+}, and Ca^{2+}) in TSP (dots), PM10 (boxes), and PM2.5 (triangles) samples.

Mass percentages of figure 6.3 have been calculated with respect to the total detected ionic mass. We observe that the NH_4^+ mass percentage increases as the total mass percentage due to alkaline ions decreases. In particular, figure 6.3 shows that NH_4^+ mass percentages larger than 10% have only been found in samples where the mass percentage due to alkaline ions was lower than 10%. Conversely, NH_4^+ mass percentages were lower than 2% in samples with (Na^+ + K^+ + Mg^{2+} + Ca^{2+}) mass percentages larger than 25%. These last results show that the interaction of particulate ammonium with collected alkaline particulate matter may lead to significant underestimations of particulate ammonium. Na^+, K^+, Mg^{2+} and Ca^{2+} are mainly due to coarse mode particles of marine and/or crustal origin. As a consequence, mass percentages of alkaline ions are larger in TSP samples than in PM2.5 samples and the underestimation of particulate ammonium is expected to be more significant in TSP than in PM2.5 samples, as experimental results have revealed. This represents a

significant result to the best of our knowledge. Low or null NH_4^+ mass percentages in filters with high content of alkaline ions were observed in several studies (Mihalopoulos et al., 1997; Kouyoumdjian and Saliba, 2005). Grain resolved chemical characterizations of aerosol particles obtained by cascade impactor in Barcelona during warm (spring-summer) and cold (autumn-winter) seasons were reported by Rodriguez et al. (2002). Experimental results reveal that during warm and cold seasons, the NH_4^+ mass concentration was larger than 0.03 $\mu g/m^3$ only in filters collecting particles with the aerodynamic diameter within the 0.4-0.7 μm range, where the Ca^{2+} concentration was smaller than 0.006 $\mu g/m^3$. In contrast, the NH_4^+ mass concentration was smaller than 0.002 $\mu g/m^3$ in filters collecting particles with the aerodynamic diameter within the 1.5-3.0 μm range, where the Ca^{2+} mass concentration was larger than 0.02 $\mu g/m^3$. These last results, in addition to those reported in this chapter, further more indicate that a significant underestimation of particulate ammonium may result from the interaction on filters of particulate ammonium with alkaline particulate matter. Hence, the low concentrations of particulate ammonium measured over South-East Italy and at several costal sites of the Mediterranean may also result from artifacts during sampling, in addition to the thermodynamic properties of the nitric acid and/or to the low availability of ammonia coming from agricultural activities as it is generally stated (Mihalopoulos et al., 1997; Danalatos and Glavas, 1999).

6.4 Results on metal analyses

Average (±1 SD), minimum and maximum mass concentrations of tested metals in TSP, PM10, and PM2.5 samples are given in Table 6.6. Uncertainties on metal mass concentrations are lower than 5% for Al, Si, Fe, and Mn, while, are lower than 8% for Cu, Pb, and Zn. Analyzed metal mean mass percentages (±1 SD) account for (6±3)%, (7±3)%, and (7±4)% of the total TSP, PM10, and PM2.5 mass, respectively. Hence, mean metal mass concentrations that are not significantly affected by the PM fraction may suggest that tested metals were predominant in the PM2.5 fraction.

Mean Metal/PM mass concentration ratios have been plotted in figure 6.4 to investigate the role of individual metal species in TSP, PM10, and PM2.5 samples. Figure 6.4 reveals that Si is the predominant metal component, accounting for 60%, 61%, and 72% of the total TSP, PM10, and PM2.5 metal mass, respectively.

Table 6.6 - Metal mass concentrations and mean metal/PM ratios in the 24-hours TSP, PM10, and PM2.5 analyzed samples.

	TSP	PM10	PM2.5
	µg/m³	µg/m³	µg/m³
Al	0.6 ± 0.3 (13) [(a)]	0.4 ± 0.2 (13)	0.3 ± 0.2 (13)
	1.1 - 0.2 [(b)]	0.8 - 0.1	0.8 - 0.1
Cd	0.0003 ± 0.0001 (4)	0.0004 ± 0.0001 (2)	0.0004 ± 0.0002 (8)
	0.0004 - 0.0002	0.0004 - 0.0003	0.0008 - 0.0002
Cu	0.02 ± 0.01 (13)	0.02 ± 0.02 (13)	0.009 ± 0.003(13)
	0.03 - 0.01	0.1 - 0.01	0.02 - 0.003
Fe	0.5 ± 0.2 (11)	0.5 ± 0.2 (13)	0.3 ± 0.1 (13)
	0.8 - 0.1	0.9 - 0.2	0.5 - 0.2
Mn	0.01 ± 0.01 (13)	0.010± 0.004 (13)	0.006 ± 0.002 (13)
	0.02 - 0.004	0.02 - 0.004	0.01 - 0.003
Pb	0.01 ± 0.01 (11)	0.009 ± 0.005 (12)	0.02 ± 0.01 (11)
	0.03 - 0.003	0.02 - 0.002	0.04 - 0.01
Si	2.1 ± 1.5 (13)	1.8 ± 1.0 (13)	1.7 ± 0.7 (13)
	5.7 - 0.6	3.8 - 0.3	2.9 - 0.8
Ti	0.02 ± 0.01 (13)	0.02 ± 0.01 (13)	0.01 ± 0.007 (13)
	0.04 - 0.01	0.03 - 0.003	0.03 - 0.004
V	0.008 ± 0.005 (9)	0.007 ± 0.004 (10)	0.008 ± 0.003 (12)
	0.02 - 0.002	0.01 - 0.002	0.02 - 0.002
Zn	0.03 ± 0.01 (13)	0.05 ± 0.08 (13)	0.02 ± 0.01 (13)
	0.06 - 0.01	0.3 - 0.01	0.04 - 0.01
Met/PM (%)	6 ± 3 (13)	7 ± 3 (13)	7 ± 4 (13)
	11 - 2	15 - 2	14 - 3

[(a)]Mean ± SD (*N*); *N* represents the number of samples.
[(b)]Min – Max.

In order to identify the role of potential sources of natural and anthropogenic components, the enrichment factor (EF) technique has been used. Taylor's model (1964) is used to calculate EF for crustal rock with Al as reference element. The basic assumptions are that aluminum is entirely of crustal origin (Lee et al., 1994) and that the mean crustal composition represents the sampling area (Chester et al., 2000). In accordance with the suggested classification criteria (Biegalski et al., 1998) an EF value of < 3 is taken as an indication that an element in an aerosol has a significant crustal source and it is termed non-enriched element. While EF values greater than 50 are ascribed to an element of anthropogenic origin and it is termed enriched element. Figure 6.5 shows mean EF values for TSP (dots), PM10 (boxes), and PM2.5 (triangles) samples.

EF values of figure 6.5 indicate that Si, Fe, and Mn have a crustal origin, while Cd, Cu, Pb, and Zn whose mass accounts for ~ 2-3% of the total metal mass, have an anthropogenic origin. It is worth mentioning that Cd and Pb mass concentrations are lower than guide values provided by the European Council Directive 1999/30/CE.

This study has provided results on the dependence of mass concentrations and of the ionic and elemental components on PM fraction. We believe that the results presented in this chapter, as previously discussed, are in satisfactory accordance with the ones retrieved at different coastal sites of the western and eastern Mediterranean can be also considered representative of the Central Mediterranean PM.

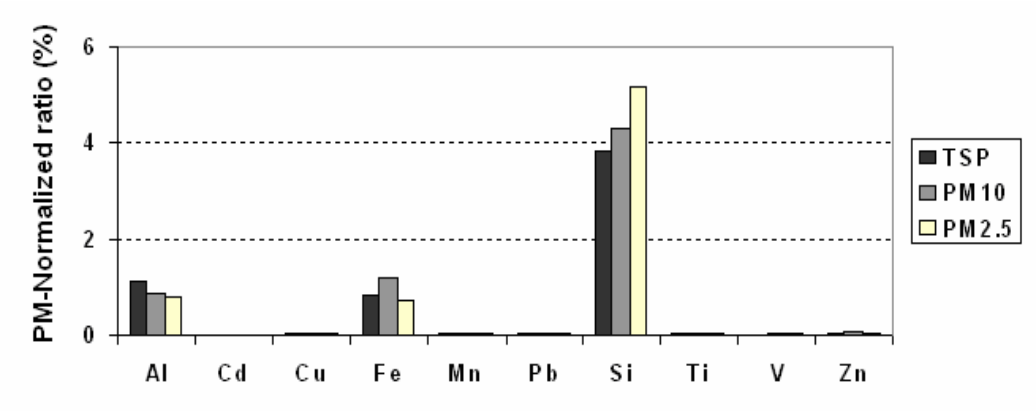

Figure 6.4 - Averaged metal/PM concentration ratios for all investigated metal elements in TSP (black bars), PM10 (grey bars) and PM2.5 (white bars) samples.

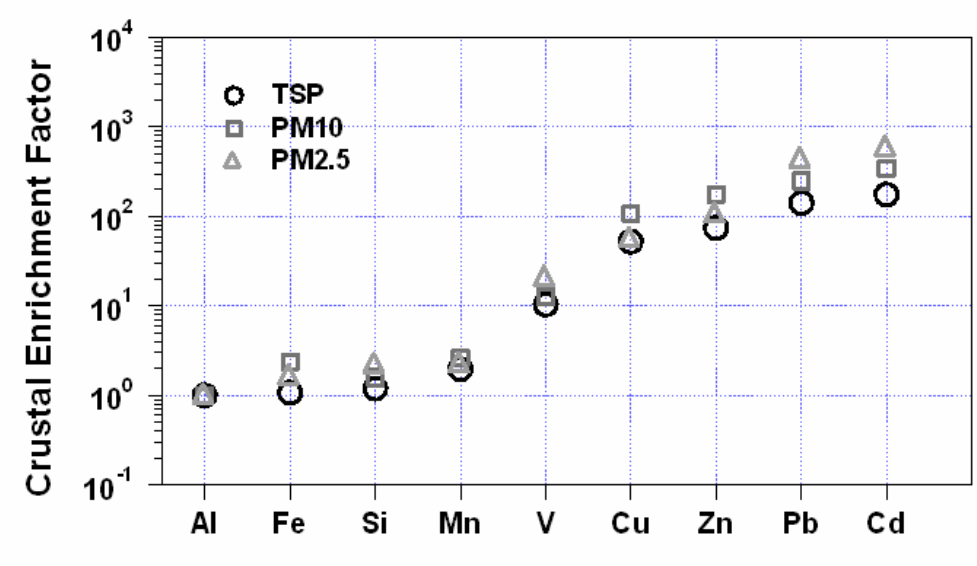

Figure 6.5 - Crustal enrichment factors (EF) for metals analyzed in TSP (dots), PM10 (boxes) and PM2.5 (triangles) samples.

CHAPTER 7

PM2.5 SAMPLES: RESULTS ON MASS CONCENTRATIONS AND IONIC AND ELEMENTAL COMPOSITION

7 PM2.5 SAMPLES: RESULTS ON MASS CONCENTRATIONS AND IONIC AND ELEMENTAL COMPOSITION

In the last years, several epidemiological studies have emphasised that adverse human health effects are mainly related to enhanced levels of fine particles (PM2.5) in the atmosphere. So, the fine particulate matter has received great attention (Dockery et al., 1993; Abbey et al., 1999; Kunzli et al., 2000; Samet et al.2000; Hoek et al., 2002; Pope et al., 2002; Stieb et al., 2002). This has led the European Commission to focus on fine atmospheric particles levels and to establish a PM2.5 annual limit of 25 μg/m³ not to be exceeded in any site of EU from 1 January 2015 (Council Directive 2008/50/EC, 2008).

In this chapter results on mass concentration and the ionic and elemental composition of 24-h PM2.5 samples collected during the year 2004 and 2005 at the Physics Department of the University of Salento are reported and discussed.

Despite the results presented in chapter 6, the principal aim of this work is to deepen the knowledge on the main composition properties of PM2.5 particles given the increasing interest to this particulate matter fraction and the scarcity of available data.

The role of different advection patterns over the sampling site and the influence of long-range transported air masses on the PM2.5 mass concentration and composition are also investigated by using the 7-day analytical back-trajectories.

7.1 Sampling and device

From June and October 2004 and from March October 2005 seventeen and thirty-two 24-h PM2.5 samples have been collected respectively at the top of the Physics Department building of the University of Salento (~ 10 m from ground). PM2.5 particles have been collected on 47 cm-diameter nitrate cellulose filters by means of the low-volume (2.3 m^3h^{-1} flow rate) FH95KF (ESM Andersen) gravimetric sampler (chapter 3) equipped with a PM2.5 cut-off inlet.

The gravimetric method has been used to determine the concentration of the collected particulate matter. The procedure for equilibration and weighting of the filters was consistent with the reference normative (Council Directive 1999/30/EC, 1999): 48-h equilibration of the filters prior the weighting, before and after the sampling, in an-air

conditioned room at (20 ± 1) °C and (50 ± 5) % relative humidity. For weighting operation a SARTORIUS digital balance with 10 μg resolution was used.

7.2 PM2.5 mass concentration results

Table 7.1 shows sampling days and the corresponding mass concentration values for both years 2004 and 2005, respectively. Uncertainties are less than 5%.

Table 7.1 - Sampling days and corresponding mass concentration values of PM2.5 samples collected during the years 2004 and 2005. The samples in bold type have been selected for ionic and metal analyses.

June – October 2004		March – October 2005	
Date	**Concentration (μg/m³)**	**Date**	**Concentration (μg/m³)**
12/06/2004	**35.2**	**23/03/2005**	**39.1**
20/06/2004	**23.0**	**30/03/2005**	**20.6**
24/06/04	39.6	**17/04/2005**	**11.5**
26/06/2004	**30.4**	**19/04/2005**	**9.8**
01/07/04	37.4	**24/04/2005**	**18.5**
03/07/2004	**33.1**	26/04/2005	11.6
10/07/2004	**38.4**	**01/05/2005**	**20.7**
22/07/04	56.5	**05/05/2005**	**19.1**
24/07/2004	**47.9**	**10/05/2005**	**12.5**
04/09/2004	**32.6**	**19/05/2005**	**9.6**
18/09/2004	**32.6**	**02/06/2005**	**15.6**
24/09/2004	**53.9**	**07/06/2005**	**10.2**
01/10/2004	**52.4**	**20/06/2005**	**19.1**
08/10/2004	**58.1**	**23/06/2005**	**26.8**
21/10/2004	**63.1**	**30/06/2005**	**33.0**
27/10/2004	**16.8**	**01/08/2005**	**50.6**
28/10/04	17.1	**09/08/2005**	**27.1**
		25/08/2005	**29.0**
		01/09/2005	**48.8**
		13/09/2005	**22.5**
		14/09/2005	**30.8**
		16/09/2005	**33.0**
		19/09/2005	19.0
		26/09/2005	**28.0**
		27/09/2005	**40.4**
		29/09/2005	**31.0**
		03/10/2005	**8.4**
		04/10/2005	**10.7**
		05/10/2005	**23.0**
		07/10/2005	**28.9**
		10/10/2005	**44.4**
		24/10/2005	37.8

Mass concentrations of all collected samples are plotted in Figure 7.1 as a function of the sampling day, in addition to the PM2.5 annual limit value 25 μg/m³

(dotted line) to be met from 1 January 2015 in accordance with the Directive 2008/50/CE of European Parliament and Council.

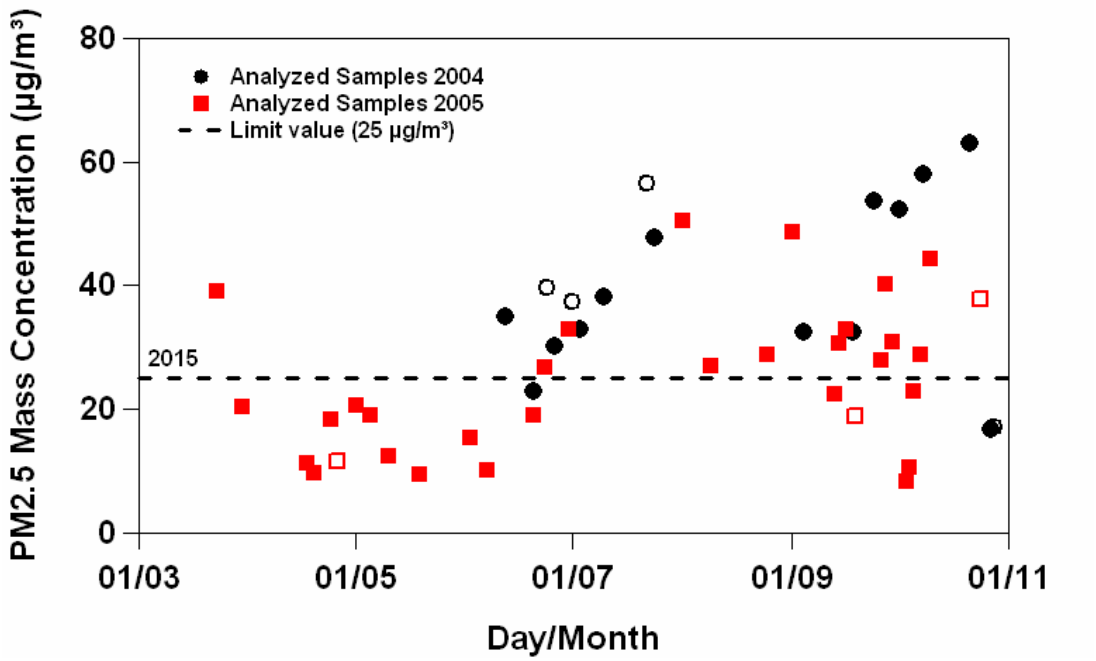

Figure 7.1 - Mass concentrations of the PM2.5 samples collected during the year 2004 (black points) and 2005 (red boxes) as a function of the sampling day, in addition to the PM2.5 annual limit value 25 µg/m³ (dotted line) fixed in the new directive (Council Directive 2008/50/EC, 2008) and to be met from 1 January 2015.

We can observe from figure 7.1 that during the year 2005 the PM2.5 mass concentration had a seasonal trend: the most mass concentration values are on average smaller than 25 µg/m^3 from March to June. Most of the PM2.5 measurements that exceed the annual limit value have been recorded in summer and autumn. It is important to highlight that we can not study the seasonal variation of the PM2.5 mass concentration during the year 2004, since the sampling collection has only been performed from June to October. However we can note that also during the year 2004 the mass concentration reaches high values in summertime and fall; in particular the 82% of the PM2.5 measurements exceed the annual limit value.

The mean statistical data referring to both sampling collections are reported in table 7.2. We can note that mean mass concentration values of both years are in accordance within ±1 standard deviation and that the highest mass concentration values are more than 2 times higher than the annual limit value (25 µg/m³) both in 2004 and 2005.

Table 7.2 – Mean statistical data referring to the PM2.5 sampling collections of the year 2004 and 2005

Year	2004	2005
Number of samples	17	32
Ave Mass Conc. (μg/m³)	39	25
St. Deviation	14	12
Max Mass Conc. (μg/m³)	63	51
Min Mass Conc. (μg/m³)	17	8

The mass concentration frequency distribution referring to the PM2.5 samples collected during both years is shown in figure 7.2. The frequency distribution exhibits a tri-modal trend with two significant peaks at mass concentration values of about 18 and 33 μg/m^3 respectively, and a lower mode peaked at about 53 μg/m^3.

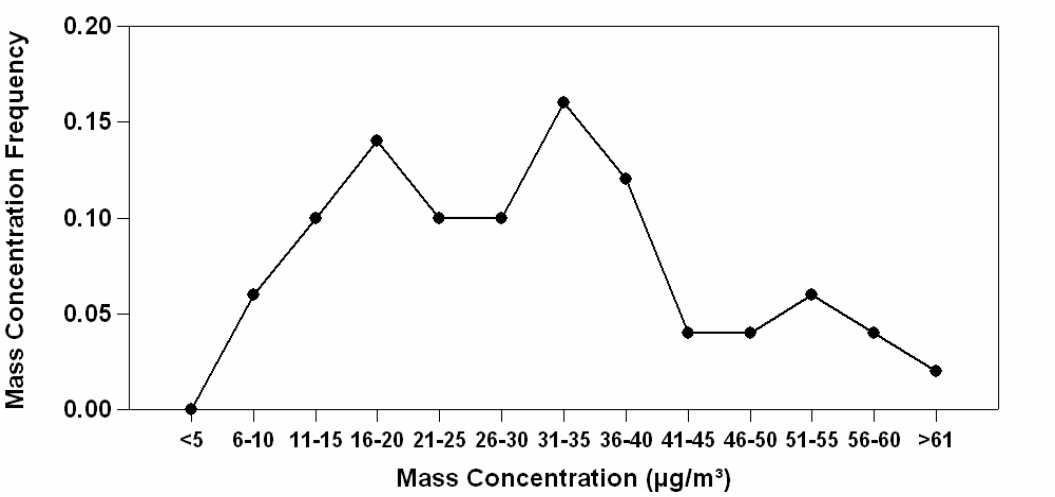

Figure 7.2 – Mass concentration frequency distribution of PM2.5 samples collected during the year 2004 and 2005.

7.3 Meteorological parameter effects on PM2.5 mass concentration

Spatial and temporal variations of PM2.5 mass concentrations can be affected by meteorological parameters. In fact, it is widely known that the weather conditions can affect air pollution levels, especially in an urban environment (Kallos et al., 1993; McGregor, 1996; Incecik, 1996; Datar et al., 1996; Cheng and Lam, 1998).

In this study, the relationship between mass concentrations and meteorological parameters (wind speed, wind direction and rainfall) is analyzed in order to better understand the evolution with time of PM2.5 mass concentrations.

Wind speed, wind direction and rainfall are the most important meteorological variables that exert an influence on PM mass concentrations. Several studies have revealed that both wind speed and wind direction affect fine and coarse particles fractions of total suspended particulate (Cheng and Lam 1998, Harrison et al. 1997, Monn et al., 1995). Precipitation is the main process responsible of the scavenging of air pollutants by falling raindrops (Elsom and Chandler, 1978, Polla-Mattiot and Scafè, 1998; Querol et al., 1998).

7.3.1 Rainfall data analysis

In order to investigate the influence of rainfall effects on PM2.5 mass concentration, the daily average rainfall data referring to the sampling collections of both years have been analyzed.

Figures 7.3-7.4 show the temporal variation of the daily average rainfall amount (mm) and the mass concentration (μg/m^3) of the PM2.5 samples collected during the year 2004 and 2005, respectively. We can observe that the amount of rainfall varies from 0.2 to 67 mm and from 0.1 to 26 mm during the year 2004 and 2005, respectively. A poor correlation between precipitation data and PM mass concentration has found in both collections: in general during both campaigns washout process was not a significant factor affecting the fine aerosol load. However, it is important to highlight that during both years a low number of raining days has been recorded and that only few samples have been collected during raining days.

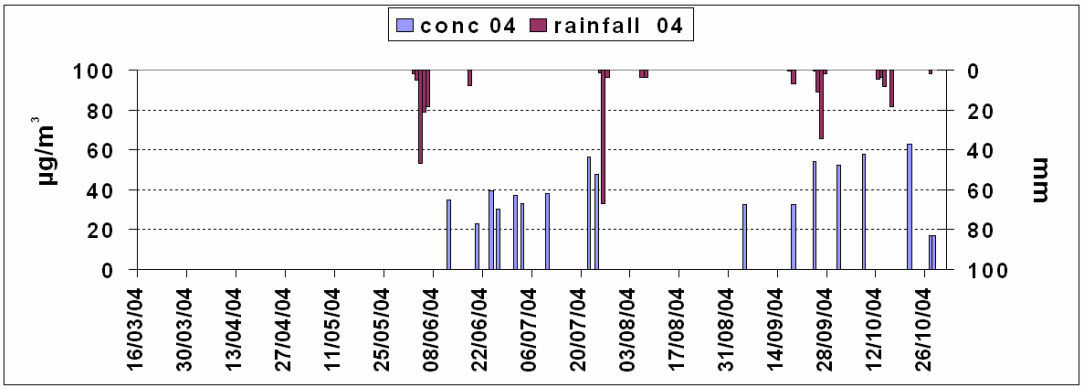

Figure 7.3 – Evolution with time of the daily average rainfall amount (mm) and the mass concentration of the PM2.5 samples collected during the year 2004.

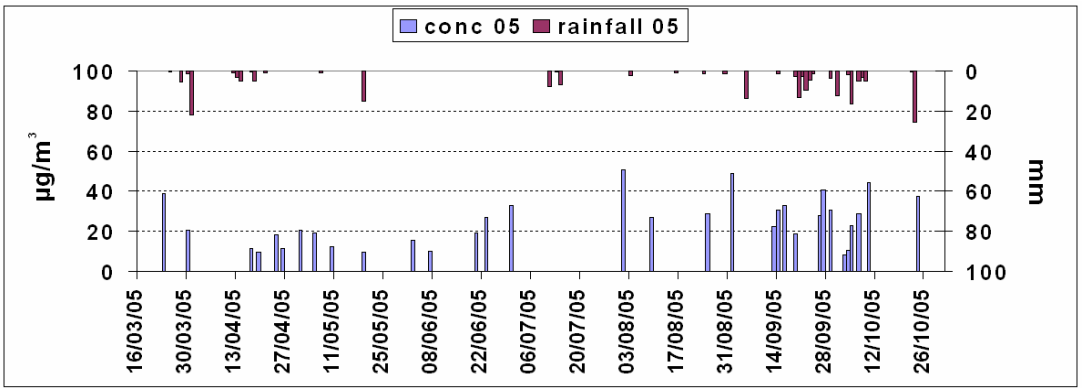

Figure 7.4 – Evolution with time of the daily average rainfall amount (mm) and the mass concentration of the PM2.5 samples collected during the year 2005.

7.3.2 Wind data analysis

Figures 7.5-7.6 show the evolution with time of the daily wind speed (m/s) and the PM2.5 mass concentration of the samples collected during the year 2004 and 2005, respectively.

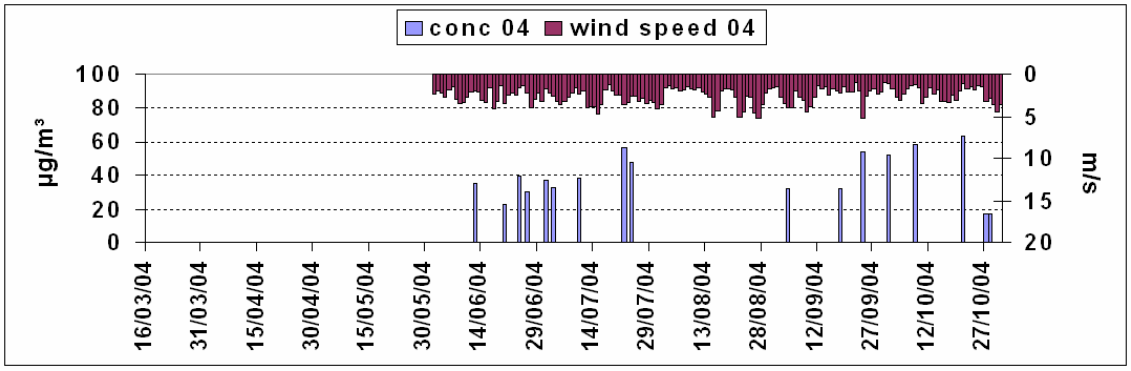

Figure 7.5 – Evolution with time of the daily wind speed (m/s) and the mass concentration of the PM2.5 samples collected during the year 2004.

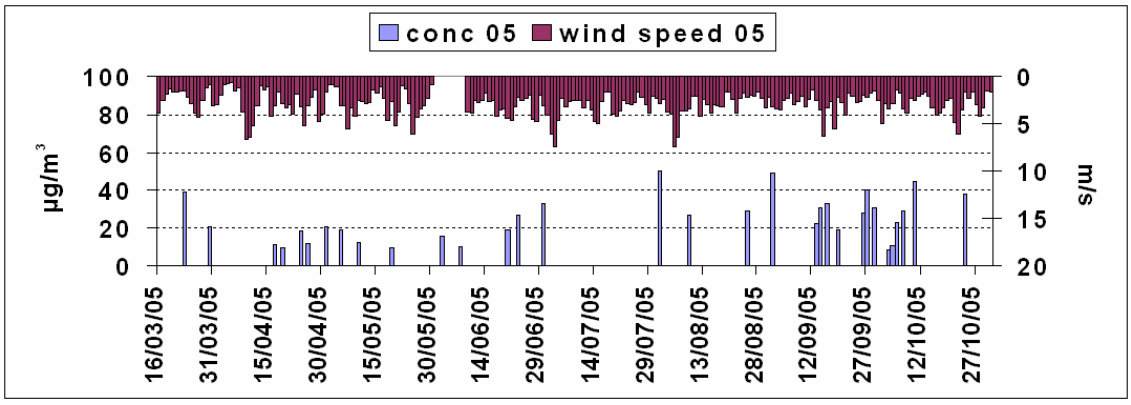

Figure 7.6 – Evolution with time of the daily wind speed (m/s) and the mass concentration of the PM2.5 samples collected during the year 2005.

Figure 7.7 shows the correlation between PM2.5 mass concentrations and daily wind speeds for the samples collected during both years: the correlation coefficient value (r = -0.05) indicates a very poor influence of wind speed on ground collected particulate matter. It is worth noting that during the year 2004 the wind speed varies from 1 to 5 m/s with a mean value of (2.5 ± 1.0) m/s and during the year 2005 from 1 to 7 m/s with a mean value of (3.0 ± 1.0) m/s. The low mean values could explain the poor influence of wind speed on PM2.5 mass concentration.

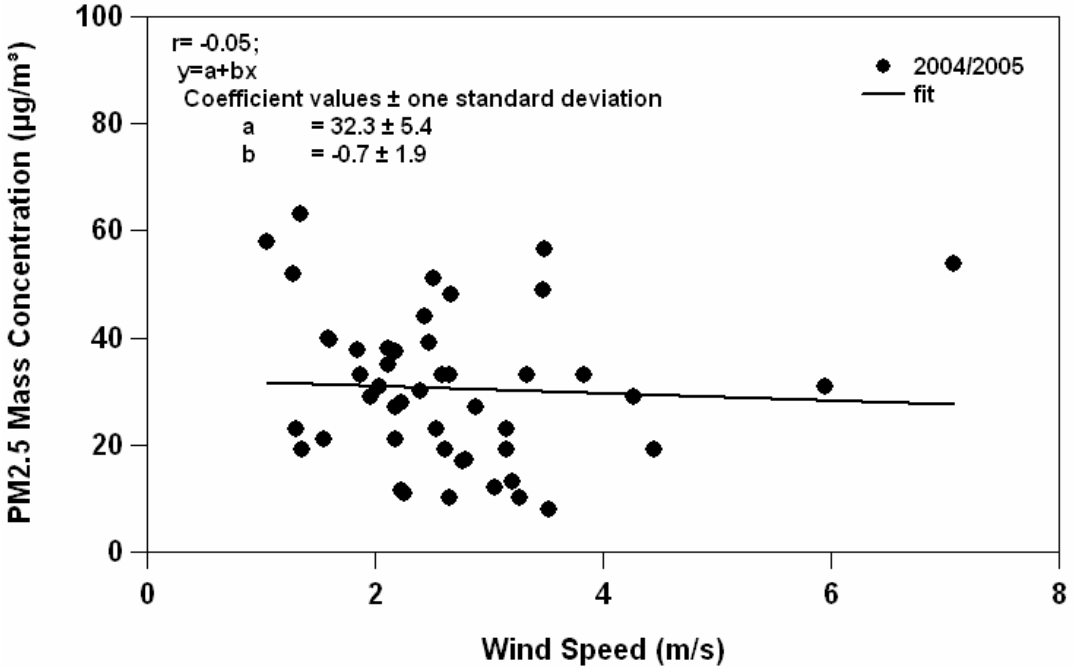

Figure 7.7 – Correlation between the PM2.5 mass concentration and the daily wind speed obtained considering the samples collected during the year 2004 and 2005.

This result has been observed in several previous investigations performed at Lecce. In particular, we have observed that the total suspended particulate (TSP) matter is typically more influenced by wind speed than the fine fraction and that the effects of a high wind speed are more easily observable on the TSP/PM2.5 ratio.

A wind sector analysis has also been performed in order to investigate the effects of different wind directions on ground collected particulate matter. Figure 7.8 shows the polar plot of the PM2.5 mass concentration measurements recorded during the year 2004 (black point) and 2005 (grey box) as a function of the wind direction, which has been calculated using the DVG method (described in the PhD thesis "Campionamneto e analisi del particolato atmosferico" of Dr. Turnone A.).

From figure 7.8 we do not observe a marked influence of wind direction on PM2.5 mass concentrations. However, we can observe that: NorthWest - NorthEast (NW-NE) and SouthEast - SouthWest (SE-SW) winds blow over the monitoring site. In particular, 32% and 49% of the PM2.5 samples have been collected during NW - NE and SE - SW winds, respectively (Figure 7.9).

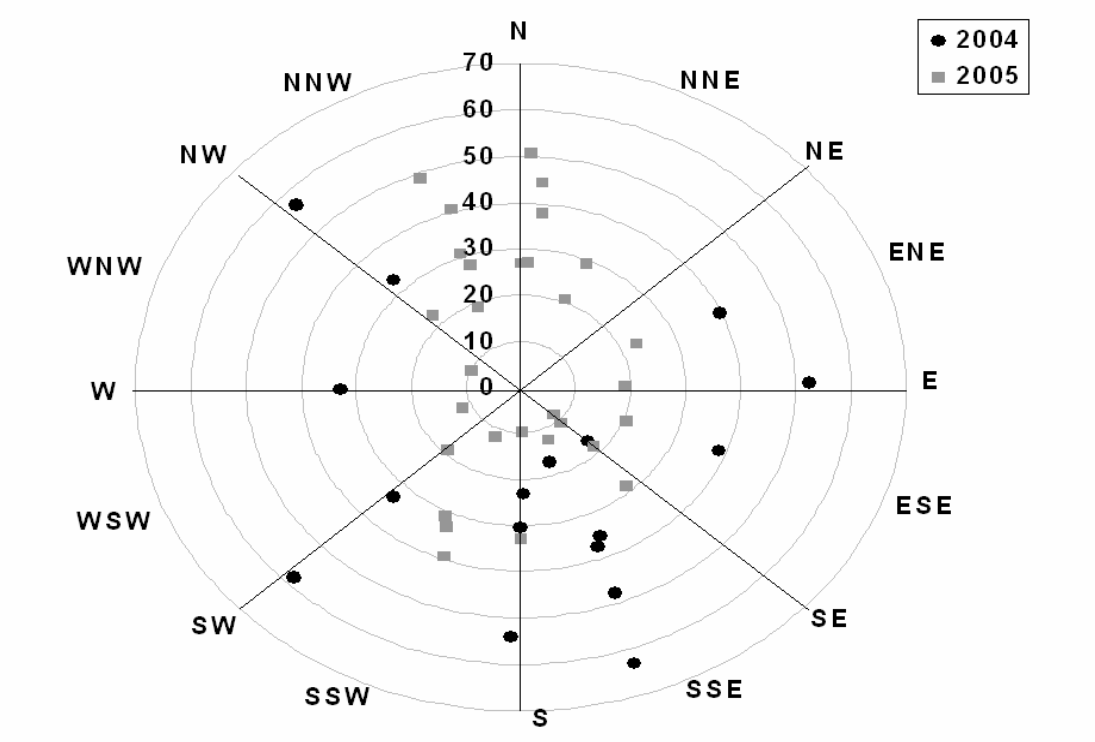

Figure 7.8 – Polar plot of the PM2.5 mass concentrations of the samples collected during the year 2004 (black points) and 2005 (grey boxes) as a function of the wind direction.

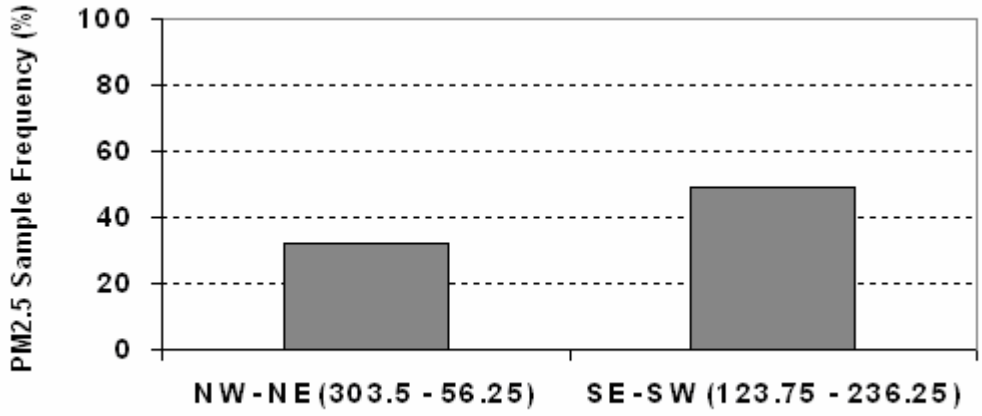

Figure 7.9 – PM2.5 sample frequency (%) for the principal wind sectors: NorthWest – NorthEast (NW – NE) and SouthEast – SouthWest (SE – SW).

7.4 PM2.5 mass characterization

In order to characterize the composition of the collected particulate matter, 13 and 29 PM2.5 randomly selected samples, of the year 2004 and 2005 respectively, have been punched in two portions for the separate analytical determination of the main ionic (F^-, Cl^-, NO_3^-, so_4^{2-}, Na^+, NH_4^+, K^+, Mg^{2+}, Ca^{2+}) and elemental (Ti, Al, Si, Fe, Mn, Cu, Zn, Pb, Cd, Cr, Ni, Pb, V, Zn) species. Ionic and metal analysis methodologies have been described in sections 6.1.1 and 6.1.2 of chapter 6. The analyzed samples have been highlighted in bold type in table 7.1. Both metal and Ion Chromatography analyses have been performed by Dr. Buccolieri G. of Physics Department and Dr. Buccolieri A. of Material Science Department of the University of Salento.

Figures 7.10-7.11 illustrate the ionic, metal and undefined mass concentrations detected in each analyzed sample of the year 2004 and 2005, respectively. Corresponding percentages found in each sample have been reported in figures 7.12-7.13.

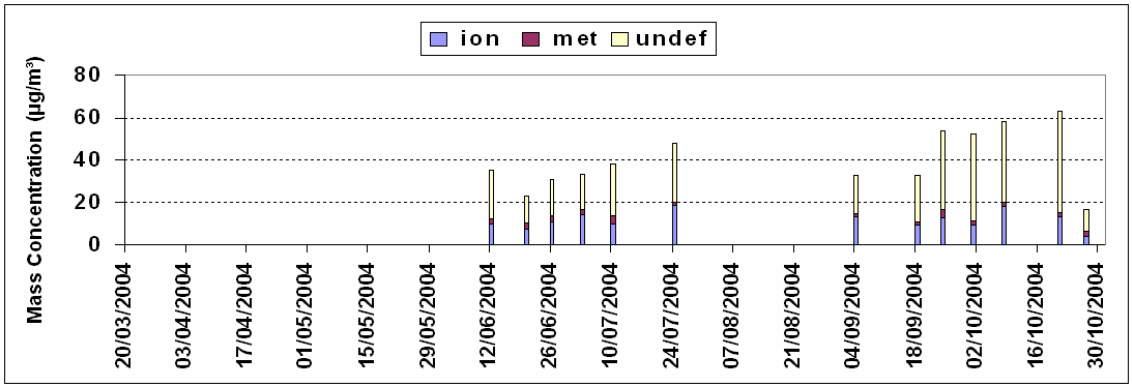

Figure 7.10 – Ionic and metal mass concentrations detected in the selected PM2.5 samples collected from June to October 2004, in addition with the undefined mass concentration**.**

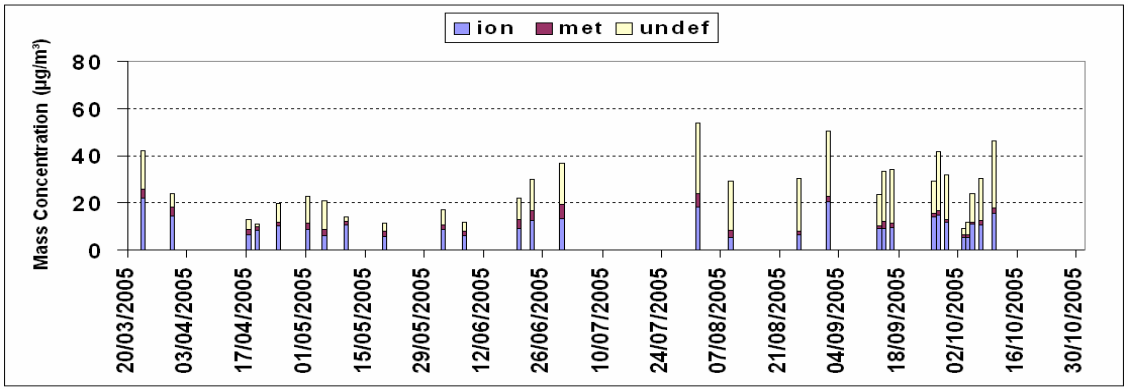

Figure 7.11 – Ionic and metal mass concentrations detected in the selected PM2.5 samples collected from March to October 2005 in addition with the undefined mass concentration**.**

We can observe that the analyzed mass percentage values vary from 22% to 51% and from 23% to 89% in the PM2.5 samples of the year 2004 and 2005, respectively. Moreover, it is important to note that in the filters of both PM2.5 series the ionic mass concentration is higher than that of metals, which represents in each sample a few percentage of the total collected particulate matter. We can also observe from figures 7.12-7.13 that in both sampling collections from June to October the analyzed mass percentage is poor dependent on the sampling time; instead from March to June 2005 the analyzed mass percentage significantly varies from sample to sample.

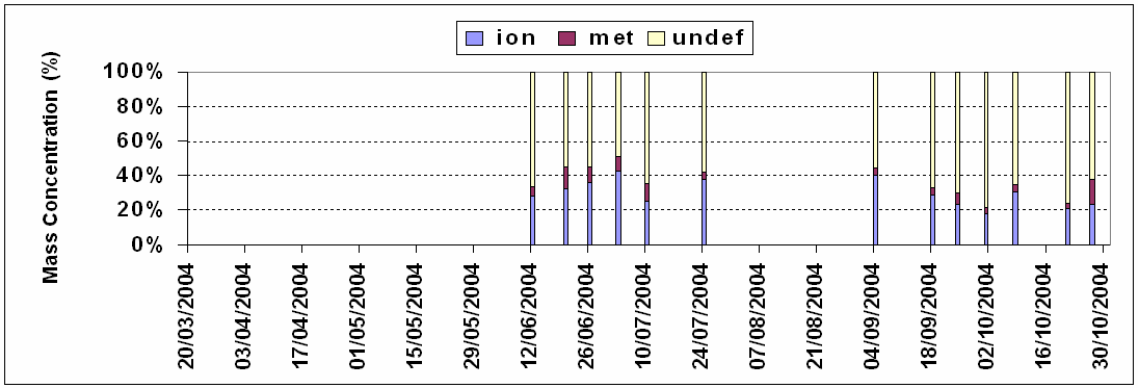

Figure 7.12 – Ionic and metal mass percentages detected in the selected PM2.5 samples collected during the year 2004 in addition with the undefined mass concentration percentage.

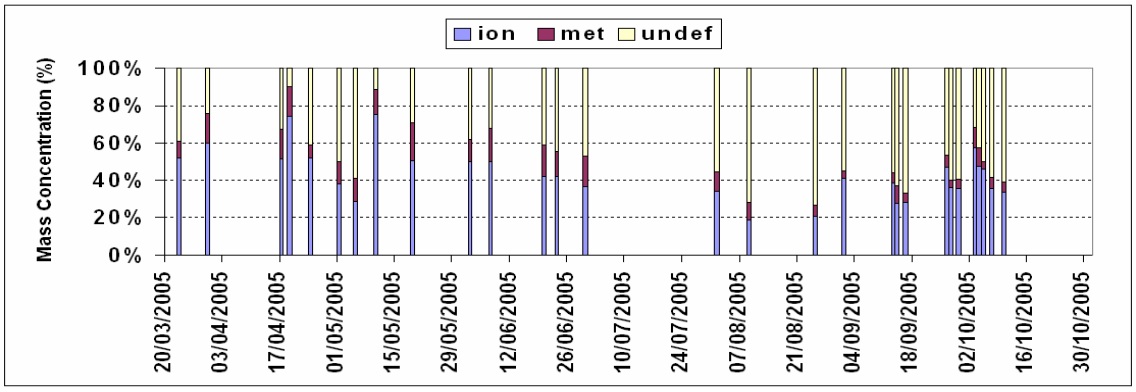

Figure 7.13 – Ionic and metal mass percentages detected in the selected PM2.5 samples collected during the year 2005 in addition with the undefined mass concentration percentage.

It is important to highlight that in both sampling collections the undefined mass percentage reaches very high values in the samples collected in summer and autumn (up to 70-80%). This result could be probably ascribed to an increase of the mass concentration of PM2.5 particles that can not be detected by Ion Chromatography or

Inductively Plasma Spectrometry (such as elemental and organic carbon). Indeed, the results presented in chapter 5 suggest that about 30-40% of the collected mass is due to organic and elemental carbon (table 5.3).

Figure 7.14 shows the scatter plot of the undefined mass concentration versus the PM2.5 mass concentration and it is worth noting the good correlation (r = 0.96) between the two parameters. This result could suggest that the undefined mass is not significantly affected by the contribution of PM due to local or long-range transported air masses of "sporadic nature" such as those due to dust events or forest fires.

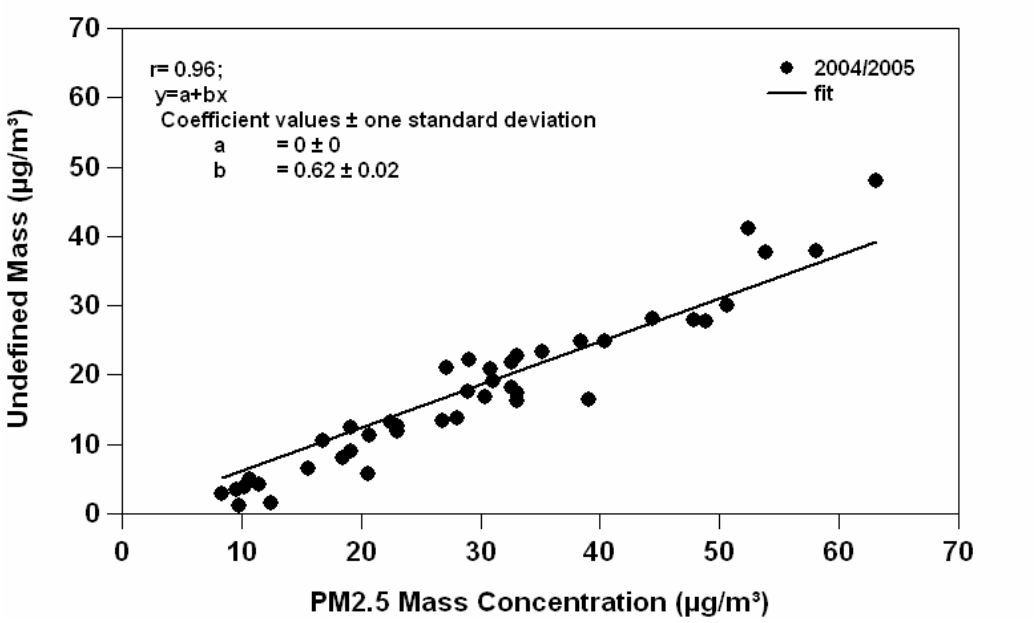

Figure 7.14 - Correlation between the undefined mass concentration and the PM2.5 mass concentration obtained for the samples collected during the year 2004 and 2005.

Tables 7.3 shows the mass concentration of the ionic species analyzed in the PM2.5 samples collected during the year 2004 and 2005. Uncertainties are less than 5%. Figures 7.15-7.16 illustrate the corresponding mass percentages calculated with respect to the total ionic mass.

We can observe from figures 7.15-7.16 that the PM2.5 ionic composition varies day by day without any marked seasonal trend. The filters collected during both years exhibit a very similar ionic composition: SO_4^{2-}, Ca^{2+}, NH_4^+, and NO_3^- are the principal ionic species of PM2.5 particles. In particular SO_4^{2-} is the predominant ionic component representing about 63% and 48% of the total ionic mass of 2004 and 2005, respectively.

Table 7.3 – Mass concentration (μg/m³) of the ionic species analyzed in the PM2.5 samples collected during the year 2004 and 2005.

2004 μg/m³										
Date	**F^-**	**Cl^-**	**Br^-**	**NO_3^-**	**SO_4^{2-}**	**Na^+**	**NH_4^+**	**K^+**	**Mg^{2+}**	**Ca^{2+}**
12/06/2004	0.003	-	-	0.8	6.3	0.2	0.8	0.3	0.2	1.3
20/06/2004	0.01	0.04	-	0.7	4.8	0.4	0.5	0.2	0.1	0.6
26/06/2004	0.01	0.01	-	0.6	7.3	0.3	0.6	0.3	0.2	1.6
03/07/2004	0.03	0.06	-	0.7	9.7	0.4	1.1	0.4	0.2	1.6
10/07/2004	0.01	0.04	-	0.7	5.4	0.4	0.01	0.8	0.2	2.3
24/07/2004	0.02	0.06	-	0.8	12.4	0.4	1.9	0.7	0.2	1.9
04/09/2004	-	0.002	-	0.5	9.7	0.4	1.4	0.2	0.1	0.9
18/09/2004	0.01	0.01	-	1.3	5.9	0.2	1.2	0.3	0.0	0.3
24/09/2004	0.03	0.15	-	2.8	7.4	0.6	-	0.1	0.1	1.4
01/10/2004	0.04	0.05	-	2.5	4.8	0.3	0.4	0.2	0.1	1.0
08/10/2004	0.01	0.09	-	2.9	11.0	0.4	2.3	0.3	0.1	0.9
21/10/2004	0.01	0.09	-	3.7	6.8	0.4	0.5	0.3	0.3	1.1
27/10/2004	-	0.09	-	0.7	2.7	0.2	-	0.1	0.02	0.2

2005 μg/m³										
Date	**F^-**	**Cl^-**	**Br^-**	**NO_3^-**	**SO_4^{2-}**	**Na^+**	**NH_4^+**	**K^+**	**Mg^{2+}**	**Ca^{2+}**
23/03/2005	0.11	0.3	-	4.5	10.8	1.0	3.7	0.6	0.2	0.9
30/03/2005	0.15	0.4	-	6.2	4.6	1.1	0.8	0.4	0.2	0.6
17/04/2005	0.04	0.4	-	1.8	2.6	0.8	0.4	0.2	0.1	0.4
19/04/2005	0.04	0.4	-	2.0	3.6	0.6	1.1	0.2	0.1	0.3
24/04/2005	0.08	0.3	-	2.2	4.4	0.8	1.6	0.5	0.1	0.3
01/05/2005	0.05	0.1	0.06	1.7	4.0	0.4	0.9	0.2	0.2	1.1
05/05/2005	0.05	0.3	-	1.1	2.3	0.6	0.0	0.2	0.2	1.3
10/05/2005	0.05	0.2	-	1.9	5.5	0.7	1.4	0.2	0.2	0.6
19/05/2005	0.05	0.3	-	1.4	2.3	0.6	-	0.1	0.2	0.9
02/06/2005	0.04	0.1	-	1.4	4.5	0.5	1.0	0.2	0.1	0.7
07/06/2005	0.04	0.1	-	1.3	2.8	0.4	0.0	0.1	0.2	0.9
20/06/2005	0.04	0.1	-	1.1	4.3	0.5	0.2	0.1	0.5	2.3
23/06/2005	0.04	0.1	-	1.4	6.3	0.4	1.1	0.3	0.5	2.5
30/06/2005	0.04	0.2	-	1.5	6.8	0.6	1.1	0.3	0.3	2.7
01/08/2005	0.04	0.1	-	2.2	11.0	0.6	1.3	0.4	0.5	2.2
09/08/2005	0.04	0.2	-	0.9	2.0	0.2	-	0.1	0.3	1.8
25/08/2005	0.04	0.1	-	2.2	2.6	0.5	-	0.1	0.1	0.5
01/09/2005	0.06	0.3	0.08	1.4	13.6	0.8	3.3	0.3	0.1	0.6
13/09/2005	0.05	0.3	-	2.4	4.4	0.8	0.5	0.2	0.1	0.2
14/09/2005	0.05	0.3	-	1.0	4.5	0.7	-	0.1	0.5	1.9
16/09/2005	0.04	0.2	0.07	2.0	5.3	0.6	0.7	0.2	0.1	0.5
26/09/2005	0.04	0.2	-	2.4	7.5	0.5	2.6	0.3	0.1	0.5
27/09/2005	0.04	-	-	2.5	8.5	0.5	2.6	0.4	0.1	0.3
29/09/2005	0.03	0.1	-	2.1	6.2	0.5	1.8	0.2	0.1	0.4
03/10/2005	0.04	0.3	0.20	1.3	2.4	0.5	0.4	0.1	0.05	0.1
04/10/2005	0.04	0.2	-	1.8	2.5	0.5	0.2	0.1	0.04	0.05
05/10/2005	0.03	0.2	-	1.8	5.9	0.5	2.2	0.1	0.03	0.1
07/10/2005	0.04	0.5	-	1.3	5.5	0.9	1.7	0.4	0.1	0.2
10/10/2005	0.04	0.3	-	1.7	8.8	0.6	2.7	0.5	0.1	0.8

Table 7.4 shows the mass concentration of the metal species analyzed in the selected samples of the year 2004 and 2005. Uncertainties are less than 5%. Corresponding percentages, calculated with respect to the total metal mass are shown in figures 7.17-7.18 respectively. We can observe that the metal composition too is very similar in both sampling collections. In each analyzed sample the predominant metal species are Si, Al and Fe constituting about 96% and 94% of the total metal mass analyzed in samples of the year 2004 and 2005, respectively. The remaining elements are present in each filter in very low mass percentages.

The average mass concentration of all analyzed species in addition with the undefined mass concentration, Ion/PM and Met/PM mass ratio percentages referring to 2004 and 2005 samples and to all samples (2004/2005) have been reported in tables 7.5-7.7, respectively. N represents the number of samples where the ionic and metal species were at levels higher than the detection limit.

As explained in the previous chapter, also in this case SO_4^{2-} mass concentrations have been divided into both sea-salt sulfate (ss-SO_4^{2-}) and nss-SO_4^{2-} mass concentrations to better investigate the sulfate anthropogenic contribution. Assuming that all measured Na^+ had a marine origin, the sea salt contribution to SO_4^{2-} has been estimated (Keene et al., 1986) as measured Na^+ times 0.242; thus nss-SO_4^{2-} have been calculated by deducting the sea salt contribution to SO_4^{2-}.

Average mass percentages of the analyzed species in addition with the average undefined mass percentages calculated with respect to the total PM2.5 mass referring to 2004 and 2005 samples and to all samples (2004/2005) are shown in figure 7.19, which clearly illustrates that the PM2.5 particulate collected during the two campaigns has quite similar average composition.

It is important to highlight that in accordance to previous studies (Kouyoumdjian and Saliba, 2005), SO_4^{2-} is the main ionic component of fine mode particles representing the 51%, 46% and 47% of the total analyzed mass for the year 2004, 2005 and for both years together respectively.

The correlations between the main ionic/metal components and the total collected particulate matter have been studied in order to better investigate main peculiarities of the PM2.5 particles chemical composition.

Table 7.4 - Mass concentration (μg/m³) of the metal species analyzed in the PM2.5 samples collected during the year 2004 and 2005.

2004 μg/m³												
Date	**Al**	**Cd**	**Cr**	**Cu**	**Fe**	**Mn**	**Ni**	**Pb**	**Si**	**Ti**	**V**	**Zn**
12/06/2004	0.2	0.0003	0.002	0.010	0.2	0.007	0.003	0.01	1.6	0.008	0.007	0.02
20/06/2004	0.2	-	0.001	0.015	0.2	0.004	-	0.01	2.5	0.007	0.004	0.01
26/06/2004	0.3	0.0002	0.001	0.010	0.2	0.007	0.003	0.01	2.1	0.010	0.008	0.01
03/07/2004	0.3	-	0.001	0.009	0.2	0.006	0.004	0.01	2.0	0.012	0.011	0.01
10/07/2004	0.8	0.0002	0.005	0.009	0.5	0.012	-	0.01	2.4	0.030	0.006	0.02
24/07/2004	0.4	0.0006	0.005	0.008	0.3	0.009	0.004	0.01	0.9	0.013	0.012	0.03
04/09/2004	0.2	0.0002	0.006	0.006	0.2	0.006	0.004	0.01	0.8	0.010	0.008	0.02
18/09/2004	0.3	0.0002	0.004	0.005	0.2	0.005	-	0.01	0.9	0.009	0.006	0.02
24/09/2004	0.3	-	0.018	0.010	0.3	0.006	-	-	2.9	0.013	-	0.02
01/10/2004	0.1	-	0.012	0.009	0.3	0.005	-	0.01	1.5	0.004	0.009	0.03
08/10/2004	0.2	0.0005	0.017	0.010	0.3	0.008	-	0.04	1.6	0.006	0.009	0.04
21/10/2004	0.3	0.0008	0.014	0.011	0.4	0.007	-	0.04	1.2	0.013	0.015	0.02
27/10/2004	0.1	-	0.020	0.003	0.2	0.003	-	-	2.1	0.005	0.002	0.01

2005 μg/m³												
Date	**Al**	**Cd**	**Cr**	**Cu**	**Fe**	**Mn**	**Ni**	**Pb**	**Si**	**Ti**	**V**	**Zn**
23/03/2005	0.03	-	-	0.021	0.13	-	-	-	0.48	-	-	0.02
30/03/2005	0.02	-	-	0.026	0.17	-	0.026	-	0.21	-	-	-
17/04/2005	0.06	-	-	0.005	0.10	-	-	-	0.40	-	-	0.01
19/04/2005	0.04	-	-	0.005	0.04	-	-	-	0.25	-	-	0.09
24/04/2005	0.02	-	-	-	0.04	-	-	-	0.17	-	-	0.02
01/05/2005	0.14	-	-	0.006	0.14	-	-	-	0.43	-	-	0.02
05/05/2005	0.13	-	-	-	0.15	-	-	-	0.38	-	-	-
10/05/2005	0.06	-	-	0.005	0.08	-	0.005	-	0.15	-	0.010	0.01
19/05/2005	0.07	-	-	-	0.10	-	-	-	0.29	-	-	0.01
02/06/2005	0.13	-	-	0.014	0.10	-	-	-	0.31	-	-	0.01
07/06/2005	0.08	-	-	0.006	0.08	-	-	-	0.29	-	-	-
20/06/2005	0.17	-	-	0.008	0.14	0.006	-	-	0.52	0.01	-	0.01
23/06/2005	0.18	-	-	0.013	0.17	0.005	0.007	-	0.47	0.01	0.008	0.01
30/06/2005	0.54	-	-	0.014	0.40	0.009	0.005	-	1.23	0.01	0.005	0.02
01/08/2005	0.46	-	-	0.008	0.30	0.008	0.009	-	1.38	0.01	0.016	0.01
09/08/2005	0.12	-	-	0.007	0.12	-	-	-	0.43	-	-	-
25/08/2005	0.12	-	-	0.014	0.11	-	-	-	0.43	-	-	0.01
01/09/2005	0.09	-	-	0.005	0.09	0.005	0.006	-	0.33	-	0.007	0.01
13/09/2005	0.05	-	-	0.005	0.06	-	0.005	-	0.14	-	0.007	0.01
14/09/2005	0.15	-	-	-	0.10	0.005	-	-	0.60	-	-	0.01
16/09/2005	0.07	-	-	0.006	0.08	-	-	-	0.29	-	-	0.01
26/09/2005	0.04	-	-	0.020	0.05	-	-	-	0.24	-	0.005	0.01
27/09/2005	0.07	-	-	0.014	0.11	0.005	0.006	-	0.32	-	0.007	0.01
29/09/2005	0.05	-	-	0.007	0.07	-	-	-	0.19	-	-	0.01
03/10/2005	0.02	-	-	-	0.02	-	-	-	0.05	-	-	0.01
04/10/2005	-	-	-	0.005	0.06	-	-	-	0.23	-	-	0.01
05/10/2005	0.01	-	-	0.006	0.06	-	-	-	0.12	-	0.005	0.01
07/10/2005	0.05	-	-	0.018	0.05	-	0.005	-	0.35	-	-	0.02
10/10/2005	0.06	-	-	0.017	0.16	0.005	0.005	-	0.50	-	-	0.02

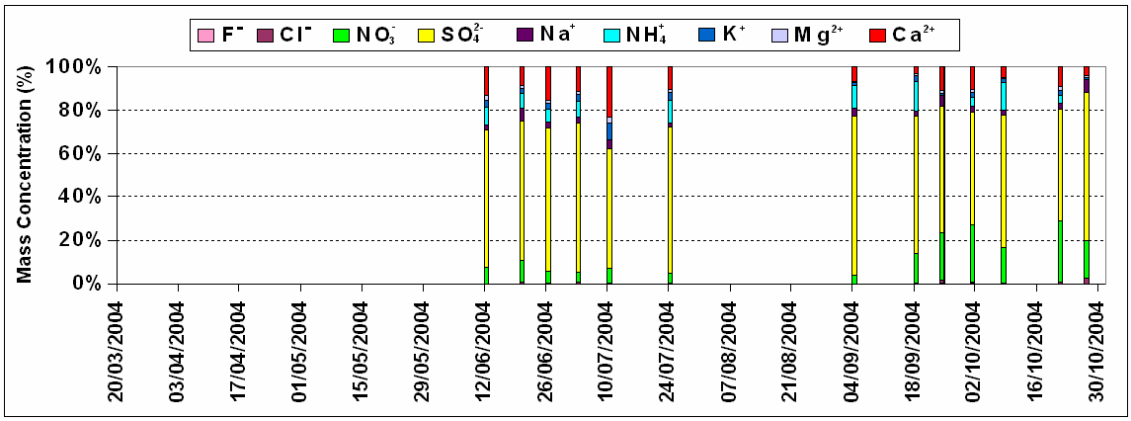

Figure 7.15 – Mass percentages of the ionic species detected in the PM2.5 samples collected from June to October 2004.

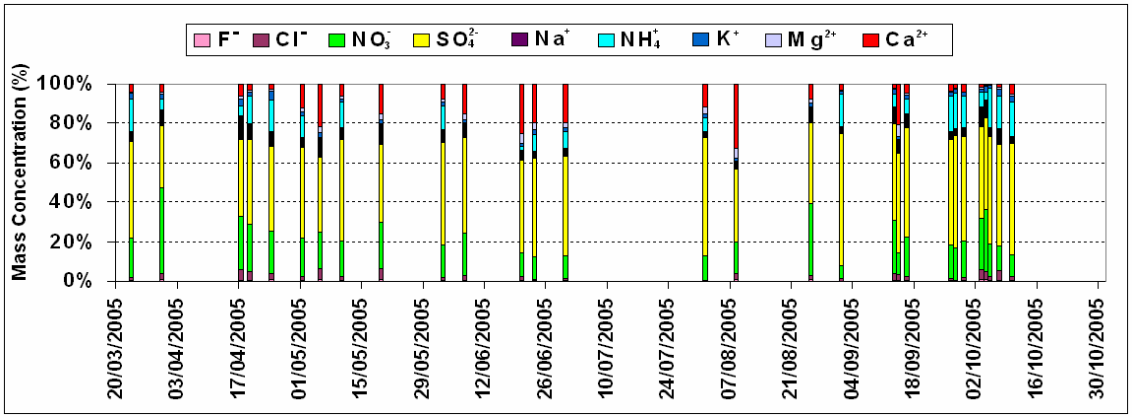

Figure 7.16 – Mass percentages of the ionic species detected in the PM2.5 samples collected from March to October 2005.

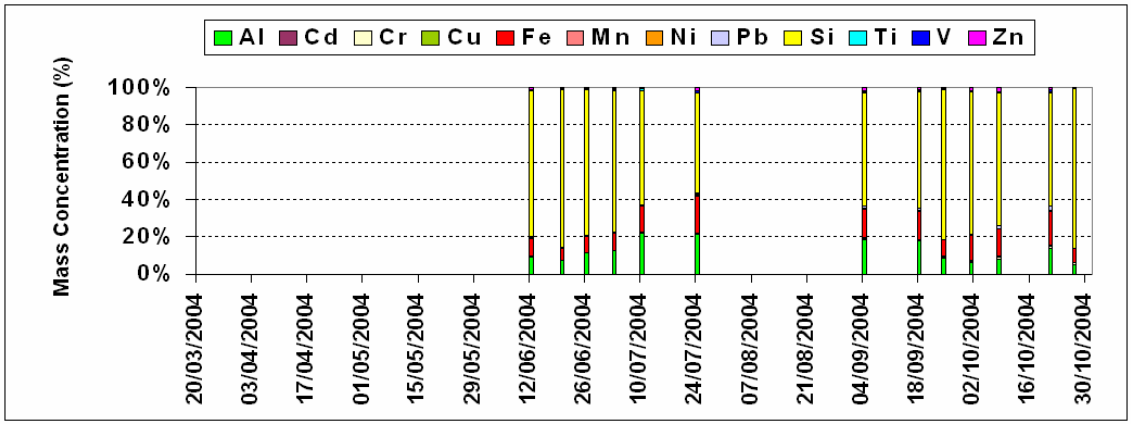

Figure 7.17 – Mass percentages of the metal species detected in the PM2.5 samples collected from June to October 2004.

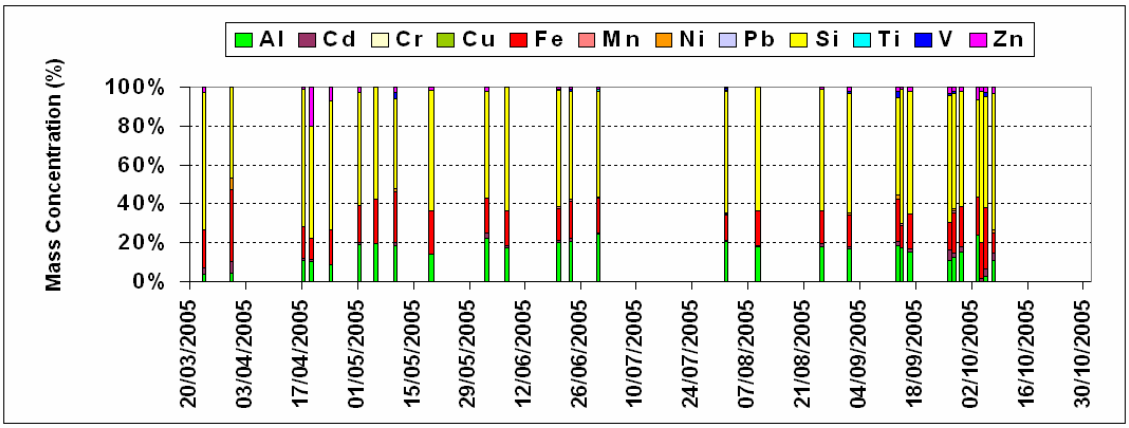

Figure 7.18 – Mass percentages of the metal species detected in the PM2.5 samples collected from March to October 2005.

Table 7.5 – Average mass concentrations (μg/m^3) of the species analyzed in the PM2.5 samples collected during the year 2004, in addition with mean Ion/PM2.5 and Met/PM2.5 ratios and the undefined mass concentration.

	2004 μg/m^3				
PM2.5	**Ave**	**St. Dev.**	**Max**	**Min**	**N**
F^-	0.02	0.01	0.04	0.003	11
Cl^-	0.06	0.04	0.15	0.002	12
Br^-	-	-	-	-	-
NO_3^-	1.4	1.1	3.7	0.5	13
nss-SO_4^{2}	7.1	2.8	12.3	2.6	13
ss-SO_4^{2-}	0.08	0.03	0.14	0.05	13
Na^+	0.3	0.1	0.6	0.2	13
NH_4^+	1.0	0.7	2.3	0.01	11
K^+	0.3	0.2	0.8	0.1	13
Mg^{2+}	0.2	0.1	0.3	0.02	13
Ca^{2+}	1.2	0.6	2.3	0.2	13
Al	0.3	0.2	0.8	0.1	13
Cd	0.0004	0.0002	0.001	0.0002	8
Cr	0.008	0.007	0.020	0.001	13
Cu	0.01	0.003	0.01	0.003	13
Fe	0.3	0.1	0.5	0.2	13
Mn	0.01	0.002	0.01	0.003	13
Ni	0.004	0.0004	0.004	0.003	5
Pb	0.02	0.01	0.04	0.01	11
Si	1.7	0.7	2.9	0.8	13
Ti	0.01	0.01	0.03	0.004	13
V	0.01	0.003	0.01	0.002	12
Zn	0.02	0.01	0.04	0.01	13
Undef	25.9	11.8	47.9	10.5	
Ion/PM2.5 (%)	30	8	43	18	
Met/PM2.5 (%)	7	4	14	3	

Table 7.6 – Average mass concentrations (μg/m^3) of the species analyzed in the PM2.5 samples collected during the year 2005, in addition with mean Ion/PM2.5 and Met/PM2.5 ratios and the undefined mass concentration.

	2005 μg/m^3				
PM2.5	**Ave**	**St. Dev.**	**Max**	**Min**	**N**
F^-	0.05	0.02	0.15	0.03	29
Cl^-	0.2	0.1	0.5	0.08	28
Br^-	0.10	0.07	0.20	0.06	4
NO_3^-	1.9	1.1	6.2	0.9	29
nss-SO_4^2	5.2	2.9	13.5	2.0	29
ss-SO_4^{2-}	0.15	0.05	0.27	0.05	29
Na^+	0.6	0.2	1.1	0.2	29
NH_4^+	1.3	1.0	3.7	0.01	25
K^+	0.2	0.1	0.6	0.1	29
Mg^{2+}	0.2	0.1	0.5	0.03	29
Ca^{2+}	0.9	0.8	2.7	0.05	29
Al	0.1	0.1	0.5	0.01	28
Cd	-	-	-	-	-
Cr	-	-	-	-	-
Cu	0.01	0.01	0.03	0.005	24
Fe	0.1	0.1	0.4	0.02	29
Mn	0.01	0.00	0.01	0.005	8
Ni	0.01	0.01	0.03	0.005	10
Pb	-	-	-	-	-
Si	0.4	0.3	1.4	0.05	29
Ti	0.01	0.005	0.01	0.01	4
V	0.01	0.004	0.02	0.005	9
Zn	0.01	0.02	0.09	0.01	25
Undef	13.6	8.6	30.0	1.1	29
Ion/PM2.5 (%)	47	16	85	20	
Met/PM2.5 (%)	3	2	7	1	

Figures 7.20-7.28 show the correlation between PM2.5 mass concentration and SO_4^{2-}, NH_4^+, NO_3^-, Ca^{2+}, Mg^{2+}, K^+, Cl^-, Na^+, Si mass concentration, respectively obtained using the samples of both PM2.5 series. Only sulphates, which represent the main components of the fine particulate matter collected during both years, exhibit a good correlation (r = 0.73) with PM2.5 mass concentration. Ca^{2+}, Mg^{2+}, K^+, NH_4^+, NO_3^- and Si show a low correlation; while Na^+ and Cl^- mass concentrations exhibit an anti-correlation (r =-16 and r = -38 respectively).

NH_4^+ has been detected at mass concentrations above the detection limit in 11 of the 13 analyzed samples of the year 2004 and in 25 of 29 analyzed samples of the year 2005. As widely discussed in chapter 6, loss of material during collection may results from particulate to gaseous forms of pollutants collected on filters. In particular, we

observed that underestimation of particulate ammonium may result from the interaction of particulate ammonium with alkaline particulate matter (Danalatos and Glavas, 1999).

Table 7.7 – Average mass concentrations ($\mu g/m^3$) of the species analyzed in the PM2.5 samples collected during the year 2004 and 2005, in addition with mean Ion/PM2.5 and Met/PM2.5 ratios and the undefined mass concentration.

	2004/2005 $\mu g/m^3$				
PM2.5	**Ave**	**St. Dev.**	**Max**	**Min**	**N**
F^-	0.04	0.03	0.15	0.003	40
Cl^-	0.2	0.1	0.5	0.002	40
Br^-	0.10	0.07	0.20	0.06	4
NO_3^-	1.8	1.1	6.2	0.5	42
nss-SO_4^2	5.8	3.0	13.5	2.0	42
ss-SO_4^{2-}	0.13	0.05	0.27	0.05	42
Na^+	0.5	0.2	1.1	0.2	42
NH_4^+	1.2	0.9	3.7	0.01	36
K^+	0.3	0.2	0.8	0.05	42
Mg^{2+}	0.17	0.13	0.53	0.02	42
Ca^{2+}	1.0	0.7	2.7	0.05	42
Al	0.2	0.2	0.8	0.01	41
Cd	0.0004	0.0002	0.001	0.0002	8
Cr	0.008	0.007	0.020	0.001	13
Cu	0.01	0.01	0.03	0.003	37
Fe	0.2	0.1	0.5	0.02	42
Mn	0.01	0.00	0.01	0.003	21
Ni	0.01	0.01	0.03	0.003	15
Pb	0.02	0.01	0.04	0.006	11
Si	0.8	0.8	2.9	0.05	42
Ti	0.01	0.01	0.03	0.004	17
V	0.01	0.00	0.02	0.002	21
Zn	0.02	0.01	0.09	0.01	38
Undef	17.4	11.2	47.9	1.1	42
Ion/PM2.5 (%)	42	16	85	18	
Met/PM2.5 (%)	4	3	14	1	

Figure 7.29 shows the NH_4^+ mass percentage as a function of the total mass percentage due to alkaline ions (Na^+, K^+, Mg^{2+} and Ca^{2+}) for all PM2.5 samples. Mass percentages of figure 7.29 have been calculated with respect to the total detected ionic mass.

A result similar to that one discussed in chapter 6 is revealed by figure 7.29: the NH_4^+ mass percentage increases as the total mass percentage due to alkaline ions decreases. In particular, figure 7.29 shows that the NH_4^+ mass percentages larger than 10% have been found mainly in samples where the mass percentage due to alkaline ions

was lower than about 15%. Conversely, the very low NH_4^+ mass percentages values (about 2%) are in samples with ($Na^+ + K^+ + Mg^{2+} + Ca^{2+}$) mass percentages larger than 25%. As consequence, this study in addition with the analysis conducted in chapter 6 for different PM fractions confirms that a significant underestimation of particulate ammonium may frequently result from artifacts during sampling.

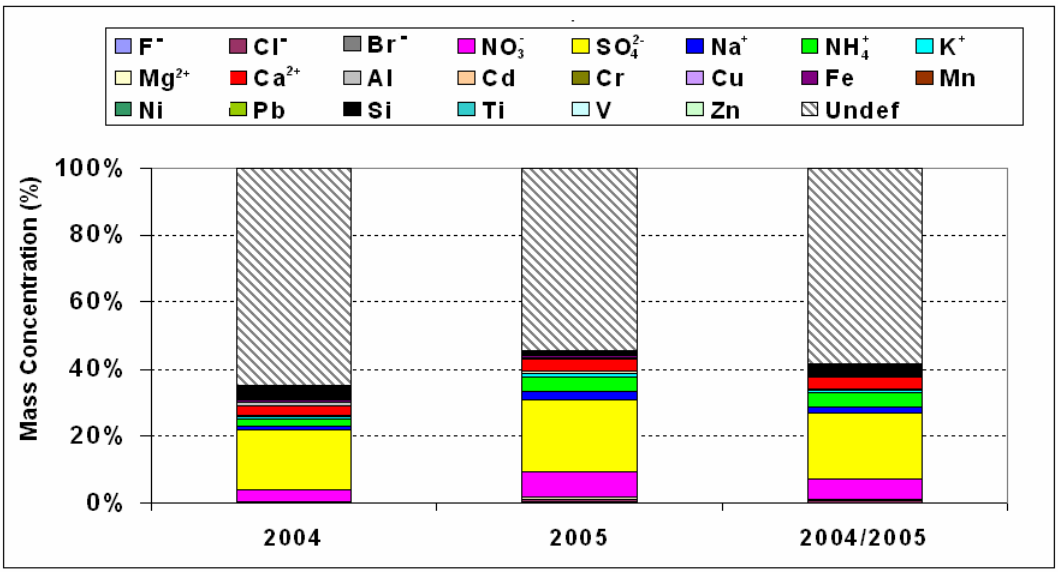

Figure 7.19 – Mean mass concentration percentages of the analyzed species and undefined mass calculated using the PM2.5 samples collected during the year 2004 and 2005 separately and all samples collected during both years.

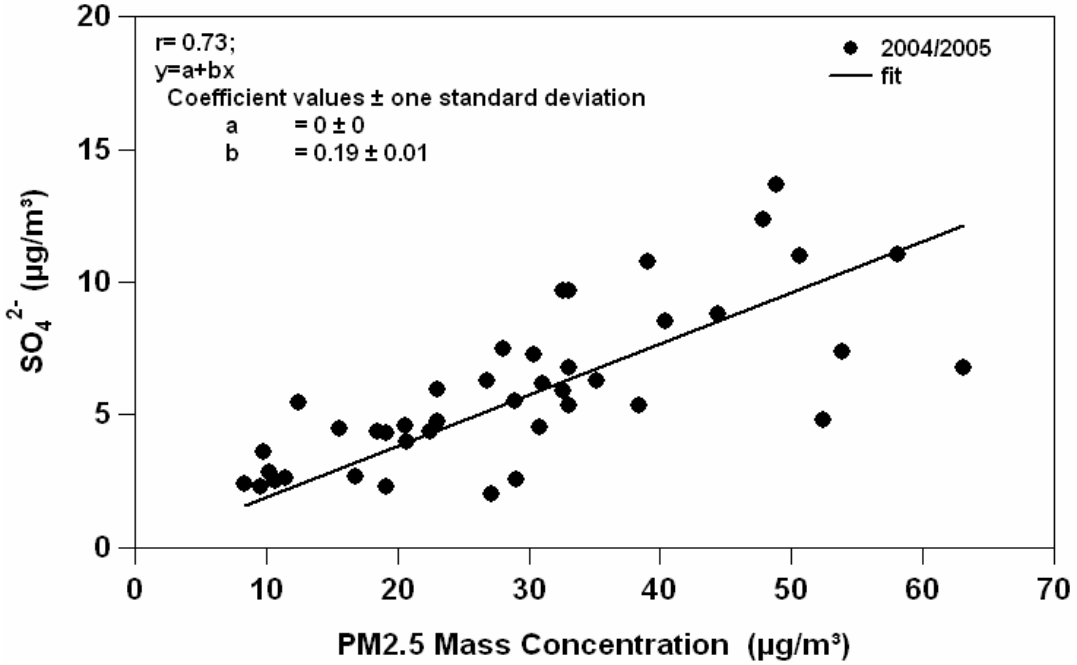

Figure 7.20 – Correlation between SO_4^{2-} and PM2.5 mass concentration obtained using the samples collected during the year 2004 and 2005.

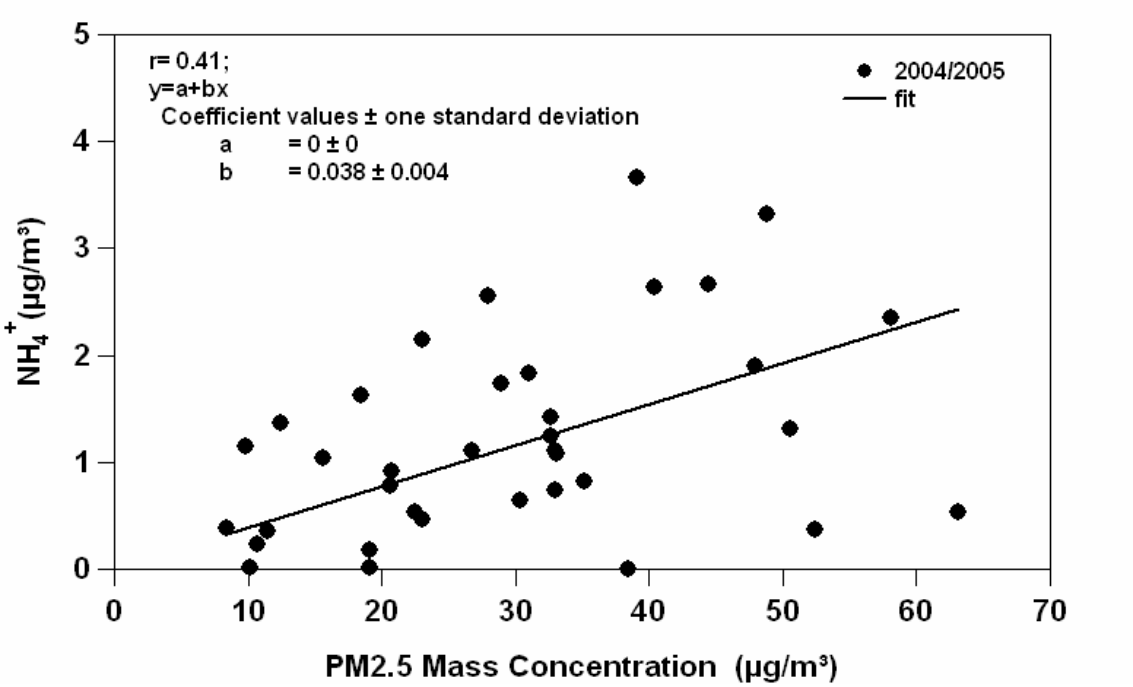

Figure 7.21 – Correlation between NH_4^+ and PM2.5 mass concentration obtained using the samples collected during the year 2004 and 2005.

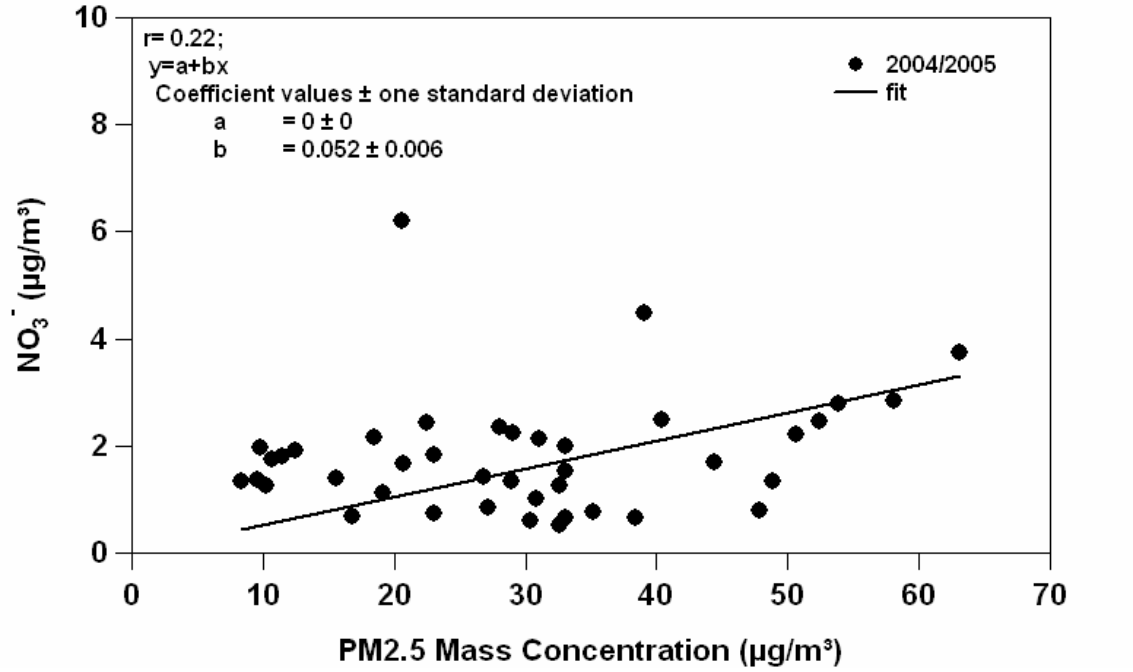

Figure 7.22 – Correlation between NO_3^- and PM2.5 mass concentration obtained using the samples collected during the year 2004 and 2005.

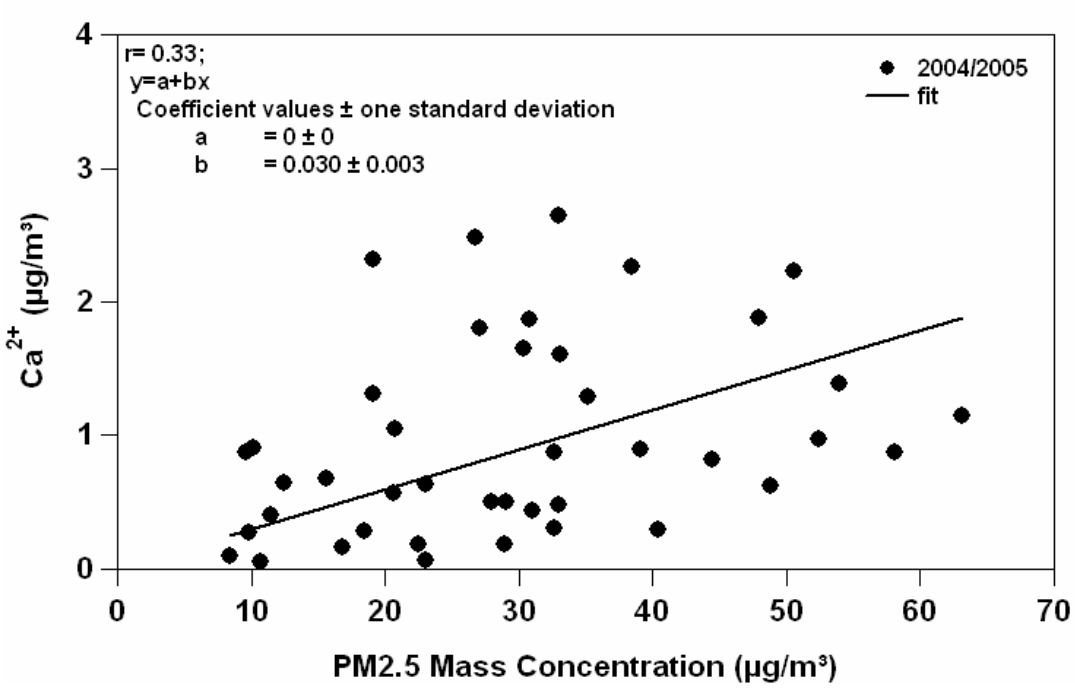

Figure 7.23 – Correlation between Ca^{2+} and PM2.5 mass concentration obtained using the samples collected during the year 2004 and 2005.

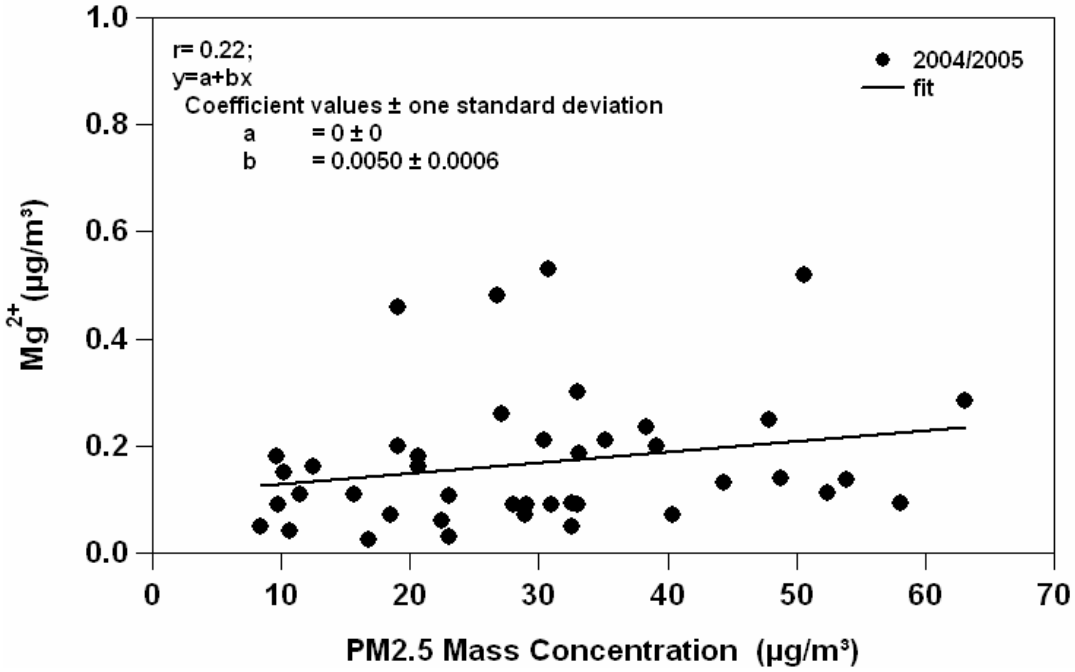

Figure 7.24 – Correlation between Mg^{2+} and PM2.5 mass concentration obtained using the samples collected during the year 2004 and 2005.

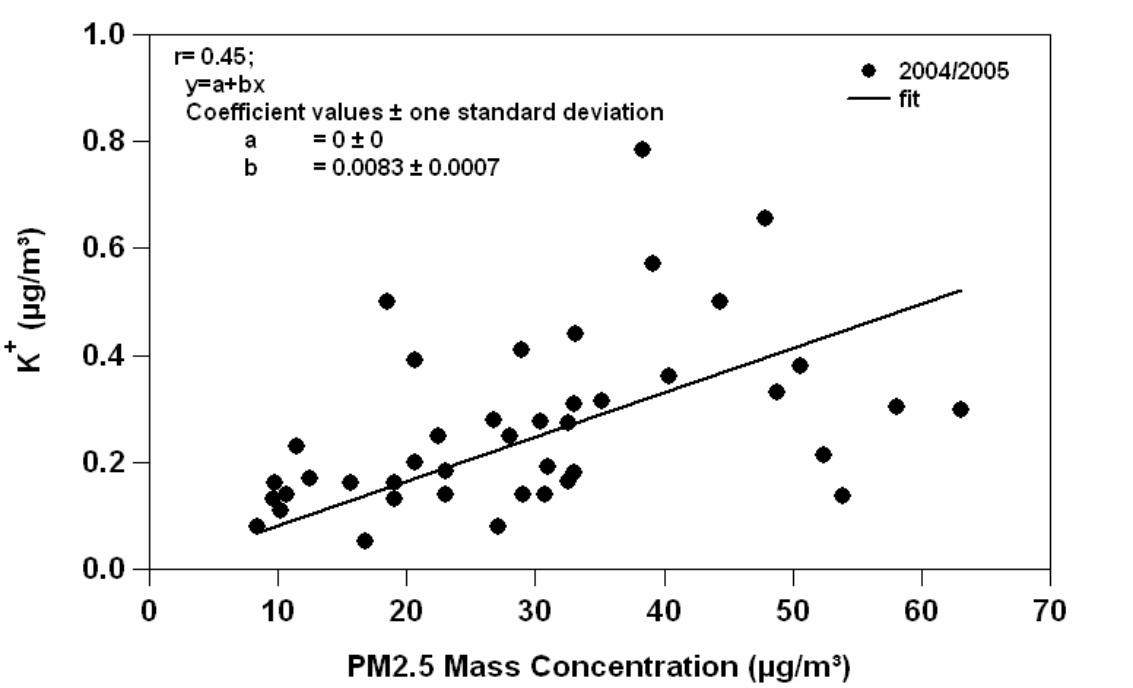

Figure 7.25 – Correlation between K^+ and PM2.5 mass concentration obtained using the samples collected during the year 2004 and 2005.

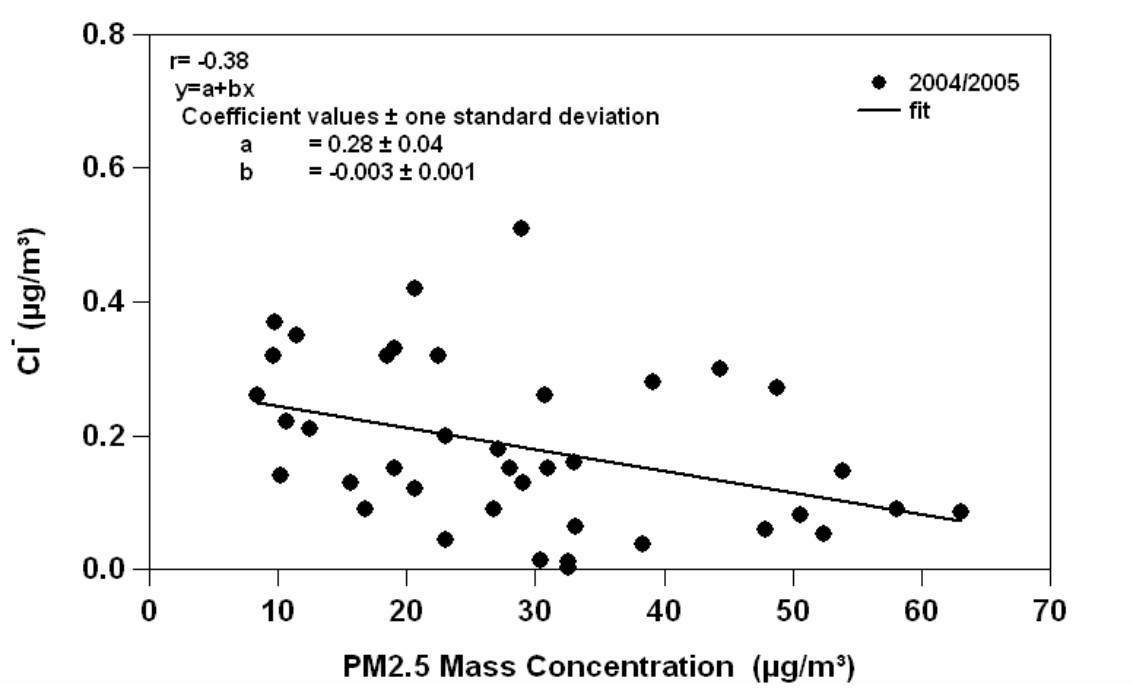

Figure 7.26 – Correlation between Cl^- and PM2.5 mass concentration obtained using the samples collected during the year 2004 and 2005.

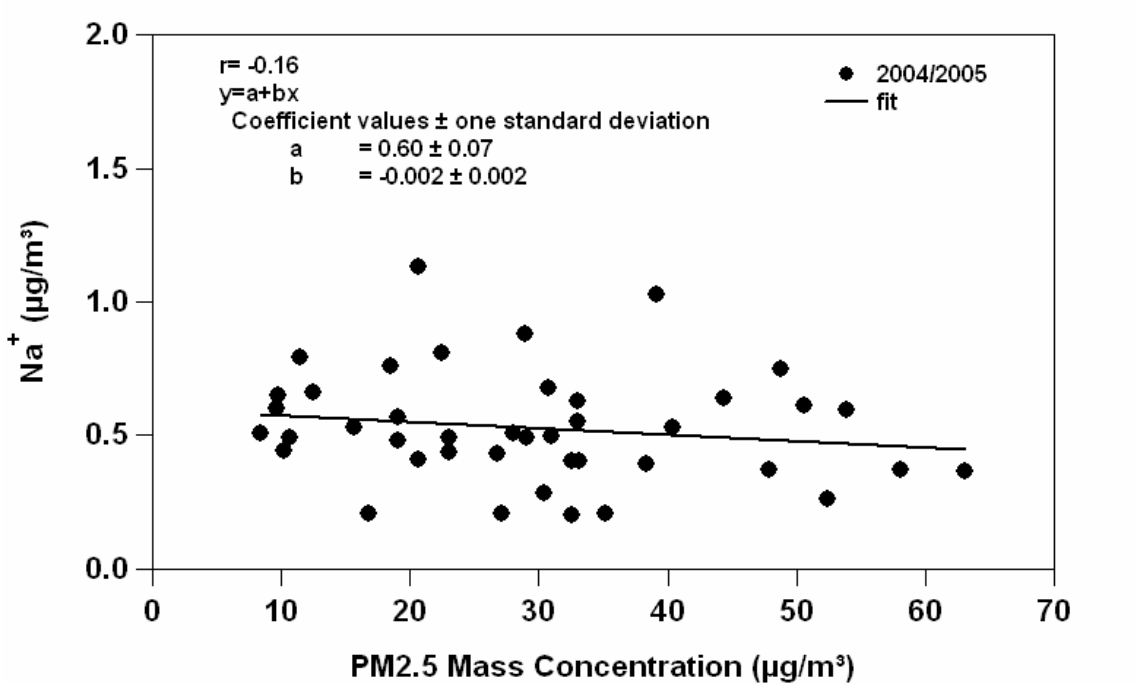

Figure 7.27 – Correlation between Na^+ and PM2.5 mass concentration obtained using the samples collected during the year 2004 and 2005.

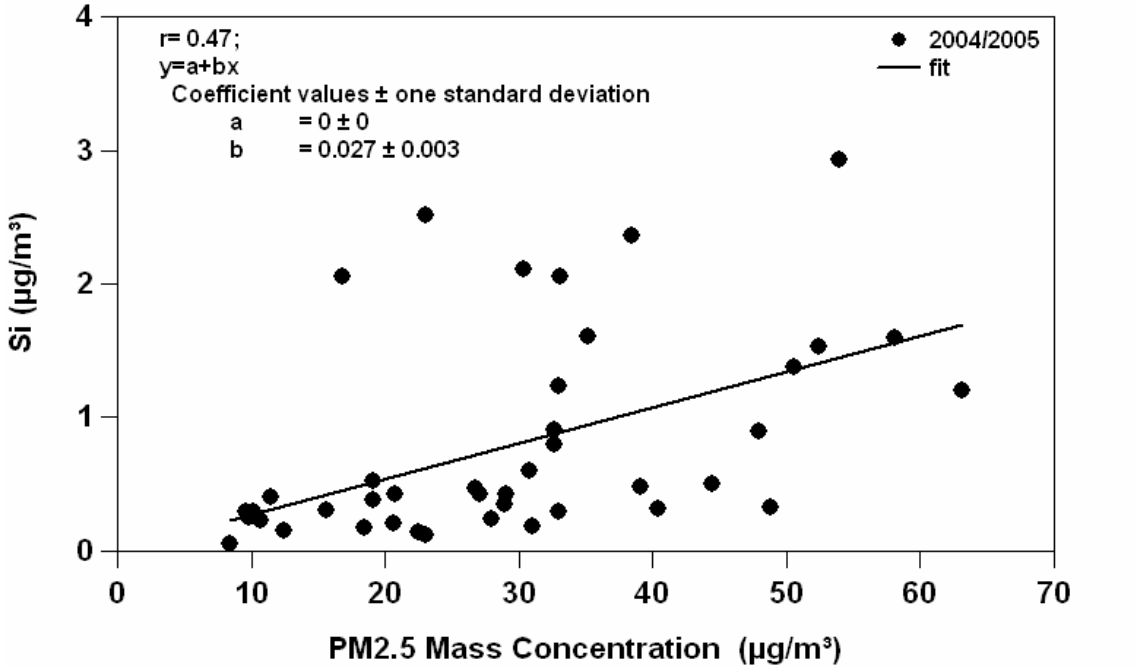

Figure 7.28 – Correlation between Si and PM2.5 mass concentration obtained using the samples collected during the year 2004 and 2005.

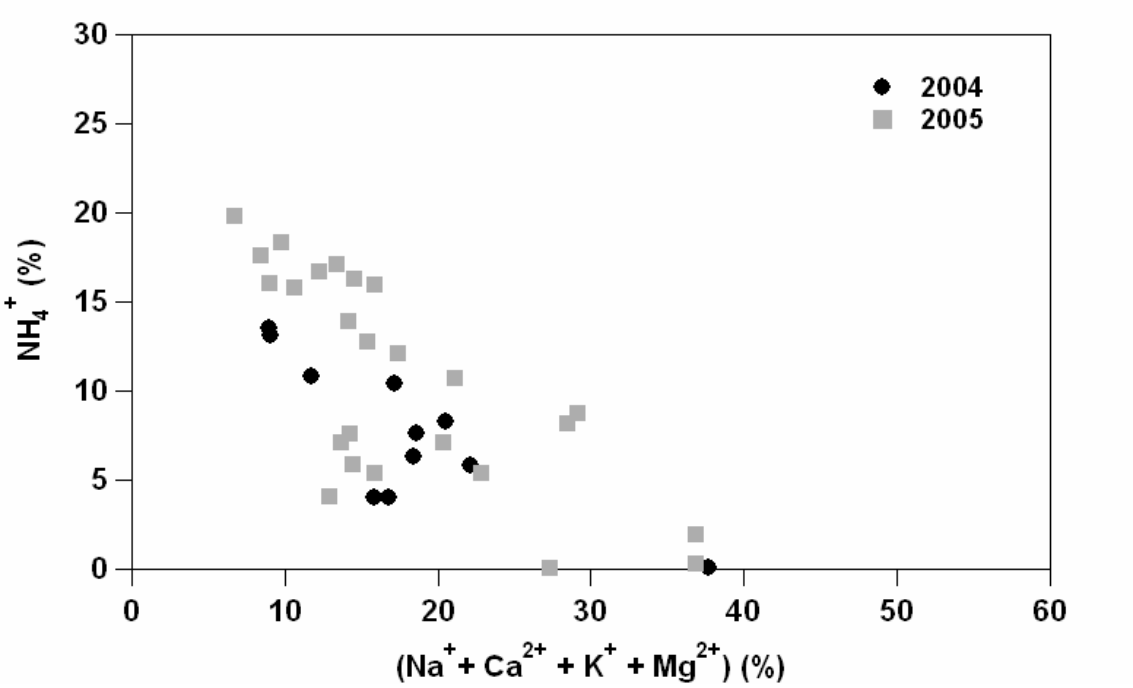

Figure 7.29 - NH_4^+ mass percentages as a function of the total mass percentage due to alkaline ions (Na^+, K^+, Mg^{2+}, and Ca^{2+}) in PM2.5 samples collected during the year 2004 (black points) and 2005 (grey boxes).

The correlation among the main PM2.5 ionic and metal components has been analyzed in order to better identify the main fine fraction chemical compounds and hence, the natural/anthropogenic origin of collected particles.

Figure 7.30 shows the correlation between NH_4^+ and nss-SO_4^{2-} obtained considering all samples collected during the year 2004 and 2005. NH_4^+ well correlates with nss-SO_4^{2-} ($r = 0.72$), thus $(NH_4)_2SO_4$ and/or NH_4HSO_4 particles are expected to be significant in PM2.5 fraction. However, we can observe that nss-SO_4^{2-} is only partially neutralized by ammonium in PM2.5 samples, since the overall average nss-SO_4^{2-}/NH_4^+ ratio is (4.0 ± 0.3). This ratio is significantly larger than the expected ratio for pure ammonium sulfate which is 2.66 (Marenco et al., 2006).

In order to investigate to what extent the possible losses of ammonia due to the interaction with alkaline particulate responsible for the high nss-SO_4^{2-}/NH_4^+ ratio, a second analysis has been performed considering only the samples characterized by high NH_4^+ mass percentages and low levels of alkaline matter. In particular the study focuses on 8 samples in which NH_4^+ mass percentages are larger than 15% and the alkaline ions percentage is lower than 15%; this selection has been performed in order to analyze the

correlation between NH_4^+ and nss-SO_4^{2-} considering only the filters in which the effects of the interaction between ammonia and alkaline ions could be considered minimum.

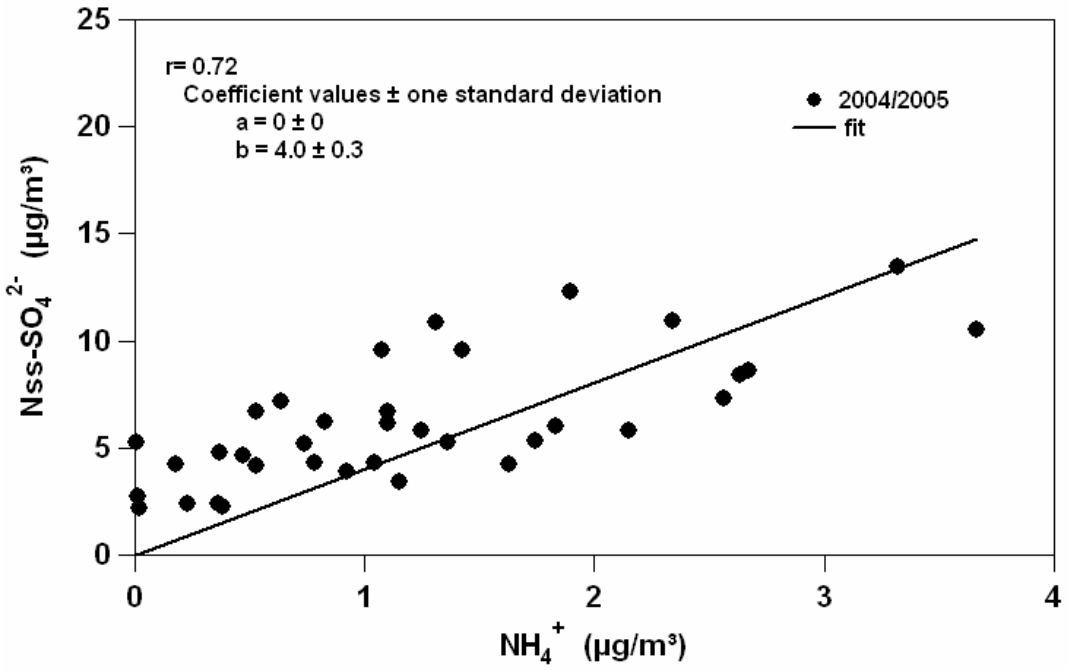

Figure 7.30 – Correlation between nss-SO_4^{2-} and NH_4^+ mass concentration obtained using the PM2.5 samples collected during the year 2004 and 2005.

Figure 7.31 shows the correlation between nss-SO_4^{2-} and NH_4^+ obtained using the 8 selected samples which have been highlighted in figure 7.32 (red boxes). Figure 7.31 reveals that the correlation coefficient is higher (r = 0.89) and that the overall average ratio nss-SO_4^{2-}/NH_4^+ is lower (3.2 ± 0.2). This result further more seems to suggest that the loss of ammonia is less important in filters characterized by lower level of alkaline particulate matter; however the volatilization of NH_4^+ is usually significant in our filters and needs appropriate examinations.

Figure 7.33 shows the high correlation (r = 0.79) between Cl^- and Na^+ obtained for the samples collected during both years; this result indicates that in the analyzed particulate matter Na^+ and Cl^- are mainly due to sea-salt particles. However the Cl^-/Na^+ ratio (0.35 ± 0.02) is significantly lower than the expected seawater ratio 1.18 (Keene et al., 1986). This result suggests that chloride depletion processes due to HNO_3–sea salt particle reactions (Perrone et al., 2006) are responsible for the low Cl^-/Na^+ ratio.

Figure 7.34 shows that K^+ well correlates with nss-SO_4^{2-} (r = 0.56) indicating that nss-SO_4^{2-} are also neutralized by K^+ in the collected fine fraction; this result implies

that salts like K_2SO_4, prevalent in PM10 as observed in the analysis discussed in the previous chapter, might be present in significant levels also in PM2.5 particulate matter.

Finally we can observe in figures 7.35-7.38 the good correlation between the ions Ca^{2+} and Mg^{2+} (r = 0.86), Si and Fe (r = 0.74), Si and Al (r = 0.68) and Al and Fe (r = 0.89). These results indicate the presence of crustal and alumino-silicate particles.

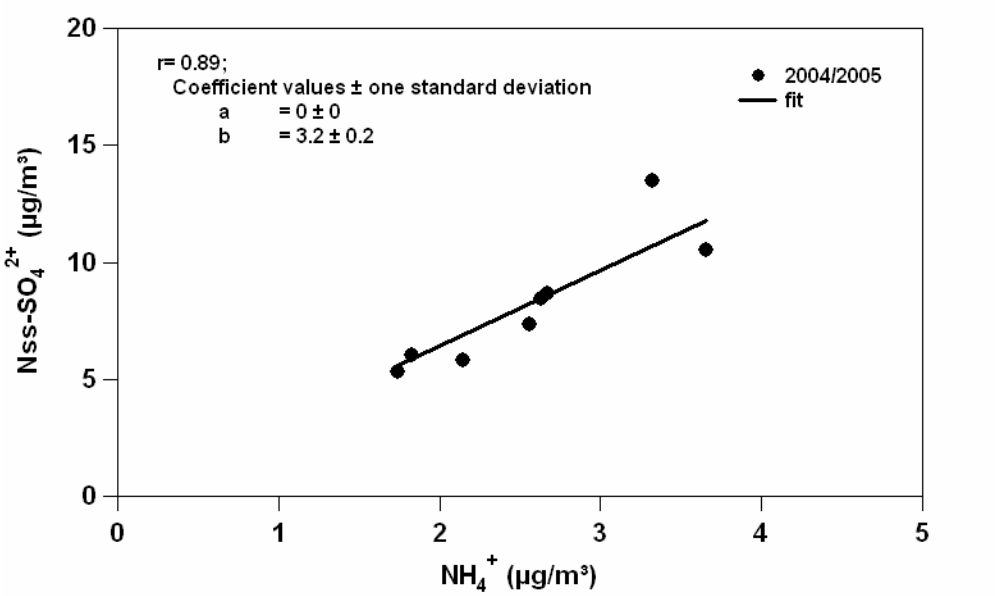

Figure 7.31 - Correlation between nss-SO_4^{2-} and NH_4^+ mass concentration obtained considering only the 8 samples in which the ammonium percentages are higher than 15% and the alkaline ions mass percentages are lower than 15%.

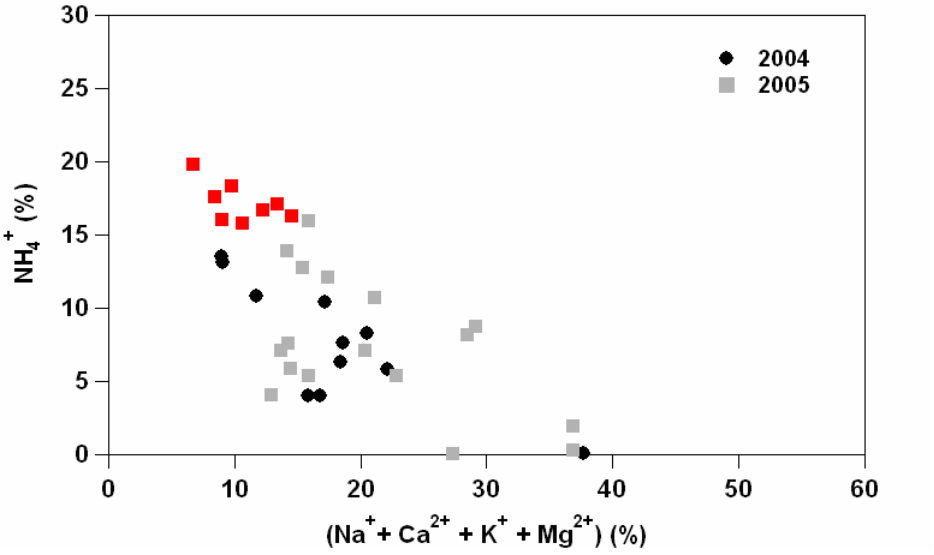

Figure 7.32 - NH_4^+ mass percentages as a function of the total mass percentage due to alkaline ions (Na^+, K^+, Mg^{2+}, and Ca^{2+}) for PM2.5 samples collected during the year 2004 (black points) and 2005 (grey boxes). Red boxes indicate the 8 samples in which NH_4^+ mass percentages are higher than 15% and alkaline ions percentages are lower than 15 %.

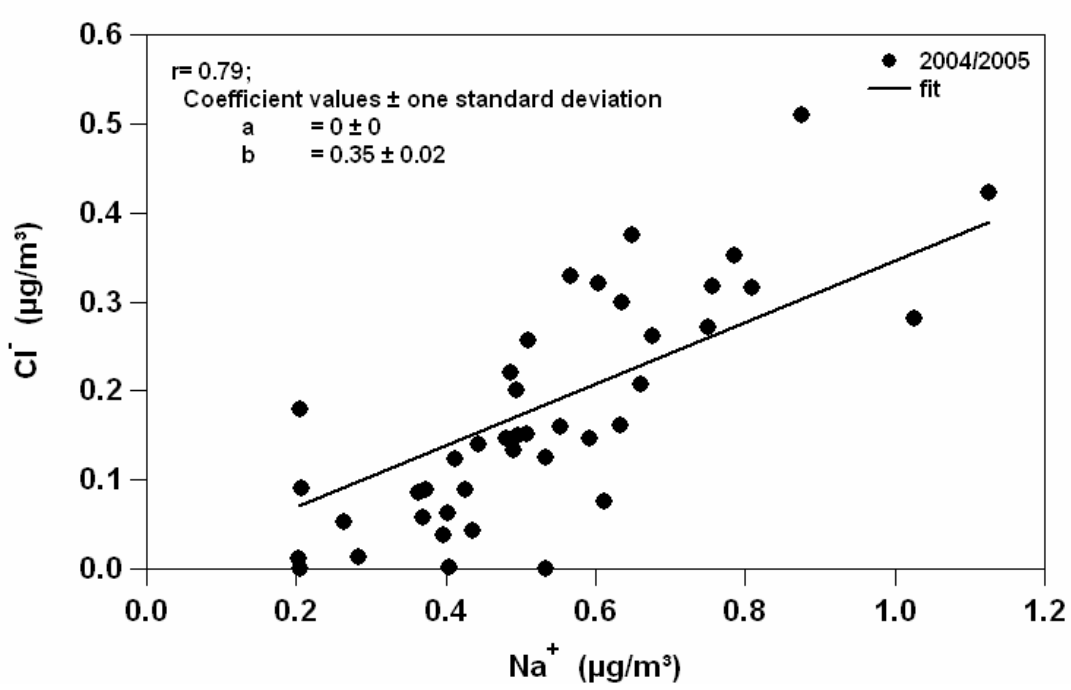

Figure 7.33 – Correlation between Cl^- and Na^+ mass concentration obtained using the PM2.5 samples collected during the year 2004 and 2005.

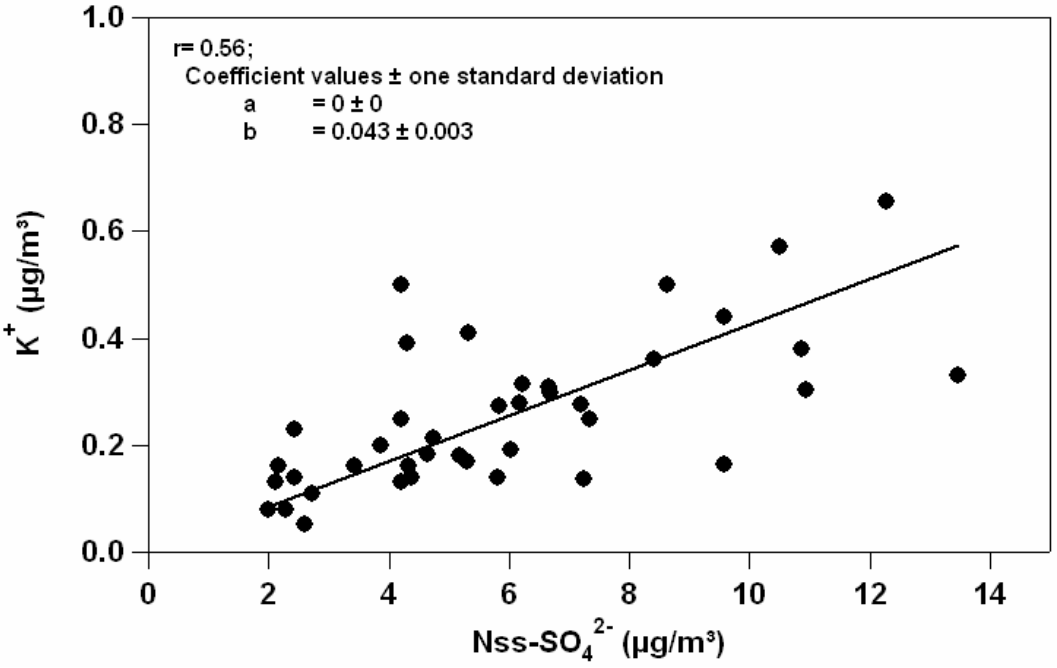

Figure 7.34 – Correlation between K^+ and nss-SO_4^{2-} mass concentration obtained using the PM2.5 samples collected during the year 2004 and 2005.

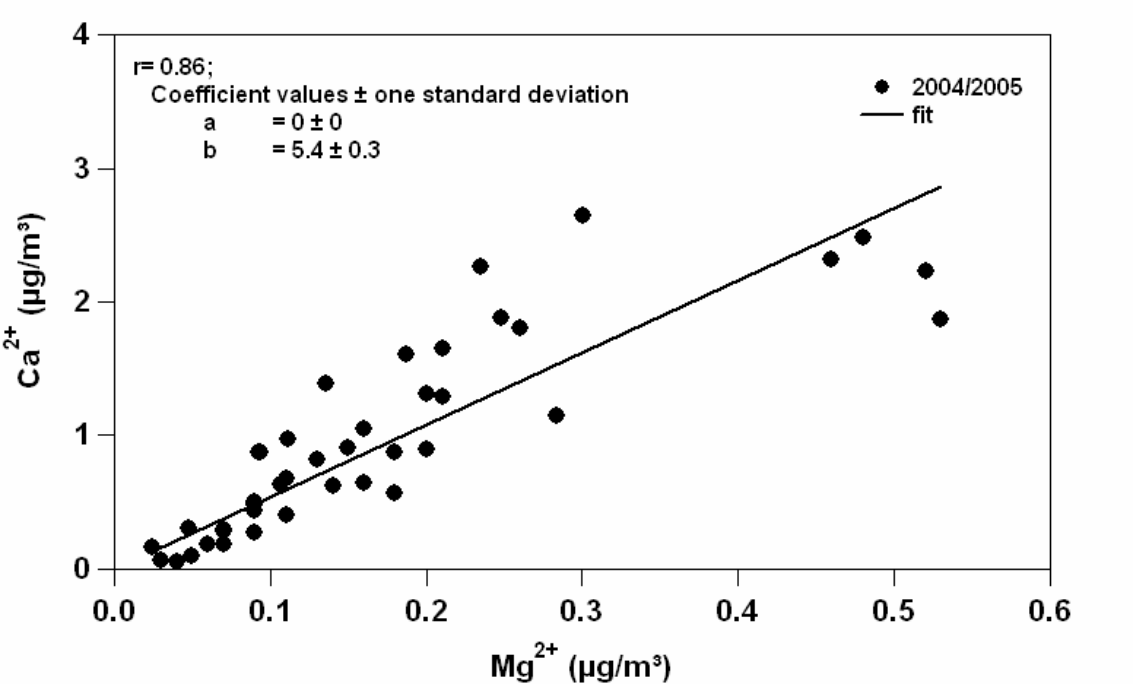

Figure 7.35 – Correlation between Ca^{2+} and Mg^{2+} mass concentration obtained using the PM2.5 samples collected during the year 2004 and 2005.

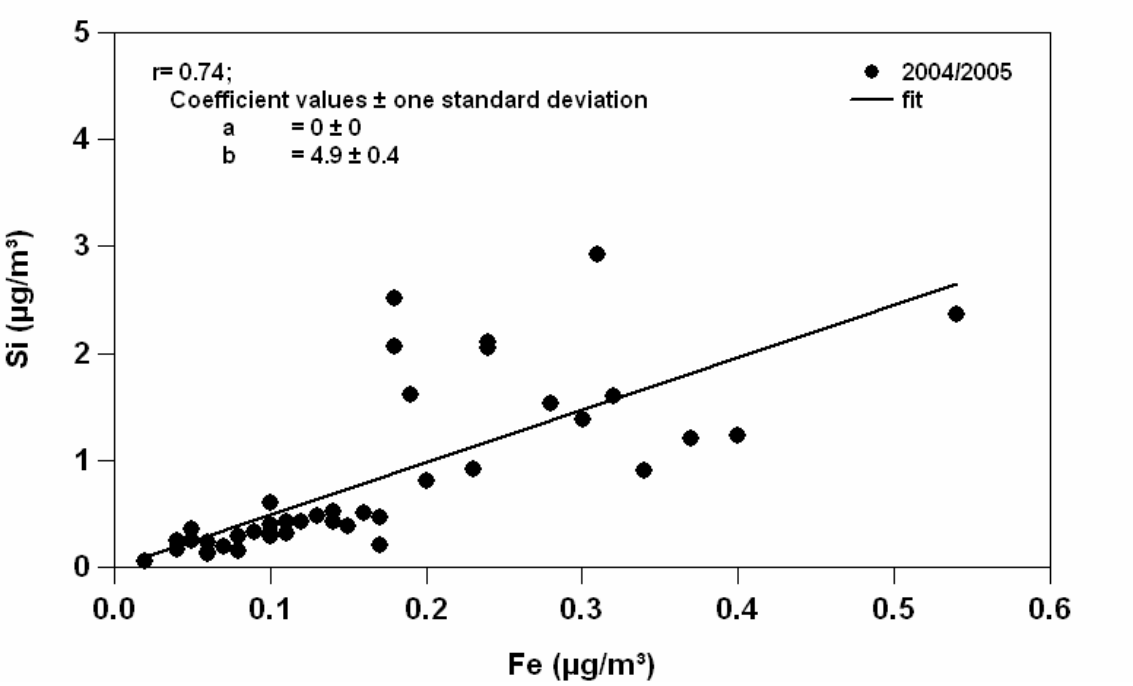

Figure 7.36 – Correlation between Si and Fe mass concentration obtained using the PM2.5 samples collected during the year 2004 and 2005.

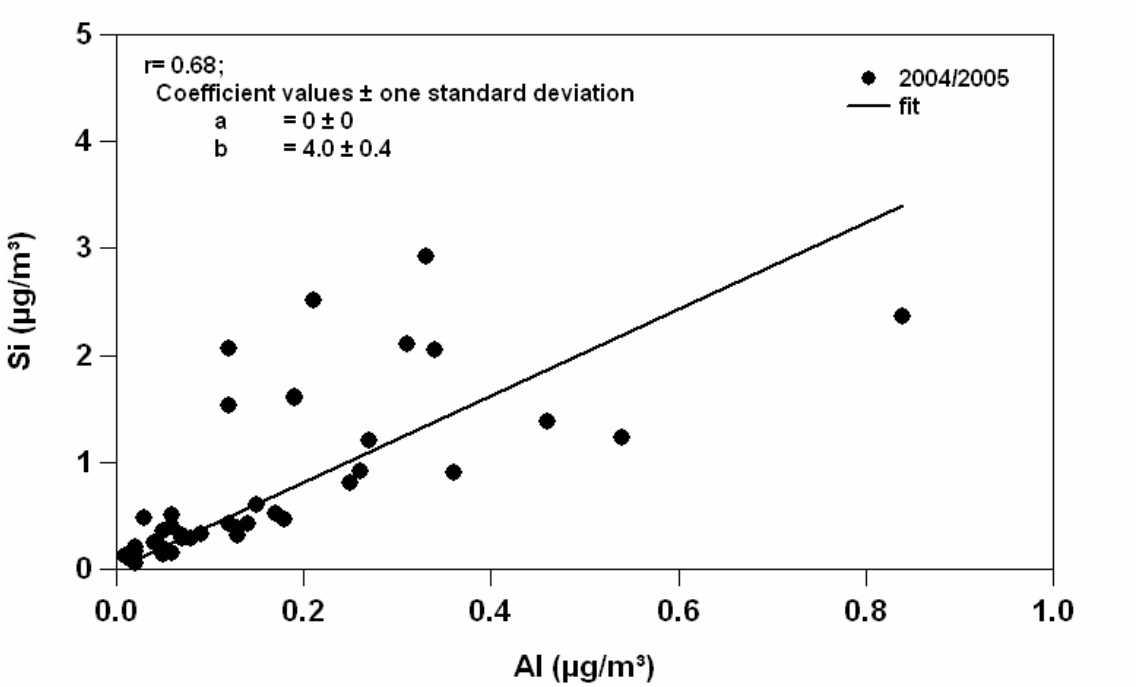

Figure 7.37 – Correlation between Si and Al mass concentration obtained using the PM2.5 samples collected during the year 2004 and 2005.

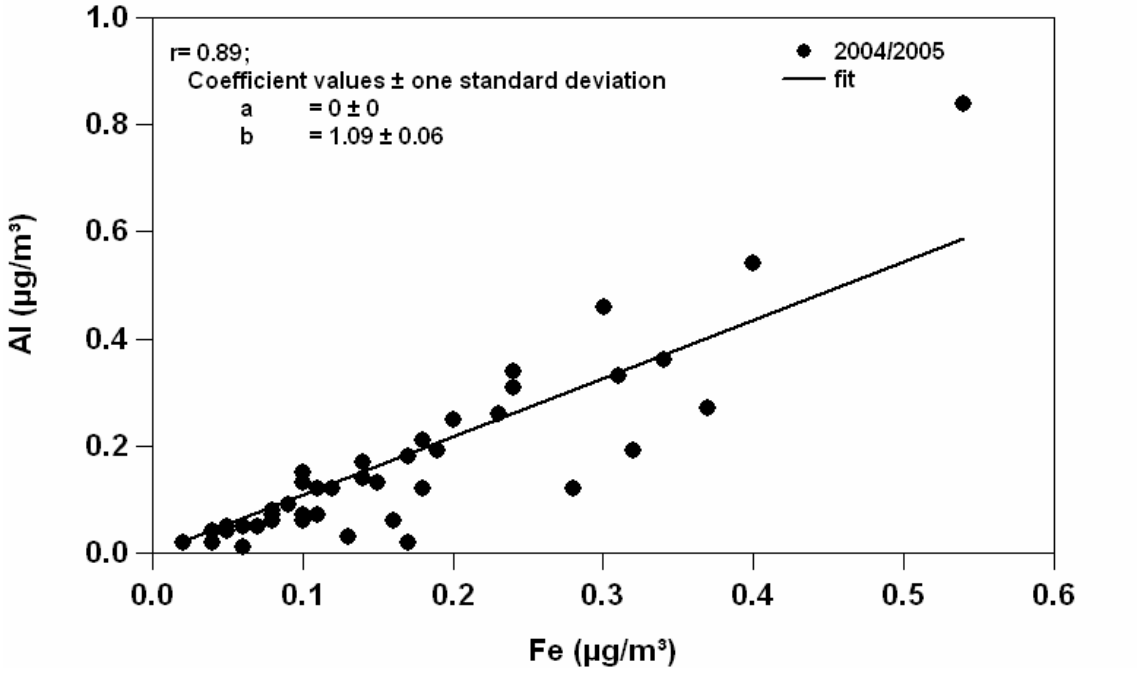

Figure 7.38 – Correlation between Al and Fe mass concentration obtained using the PM2.5 samples collected during the year 2004 and 2005.

7.5 Back-trajectories analysis results

The impact of long-range transported air masses on the concentration and composition of PM2.5 samples collected during the year 2004 and 2005 has also been investigated.

As previously discussed analytical back-trajectories provide information on the aerosol origin observed at a particular location (Kazadzis et al., 2007). In this study 7-day analytical back-trajectories have been used to characterize main advection patterns over Lecce.

Figure 7.39 shows the 7-day analytical back-trajectories characterized by arrival pressure levels of 950 and 850 hPa and referring to the measurement days of the year 2004 and 2005 selected for the ionic and metal analyses on 24-hour samples.

We can observe from figure 7.39 that the air masses pathways uniformly distribute over the regions surrounding the sampling site, as consequence it is not possible to identify a preferential geographical sector.

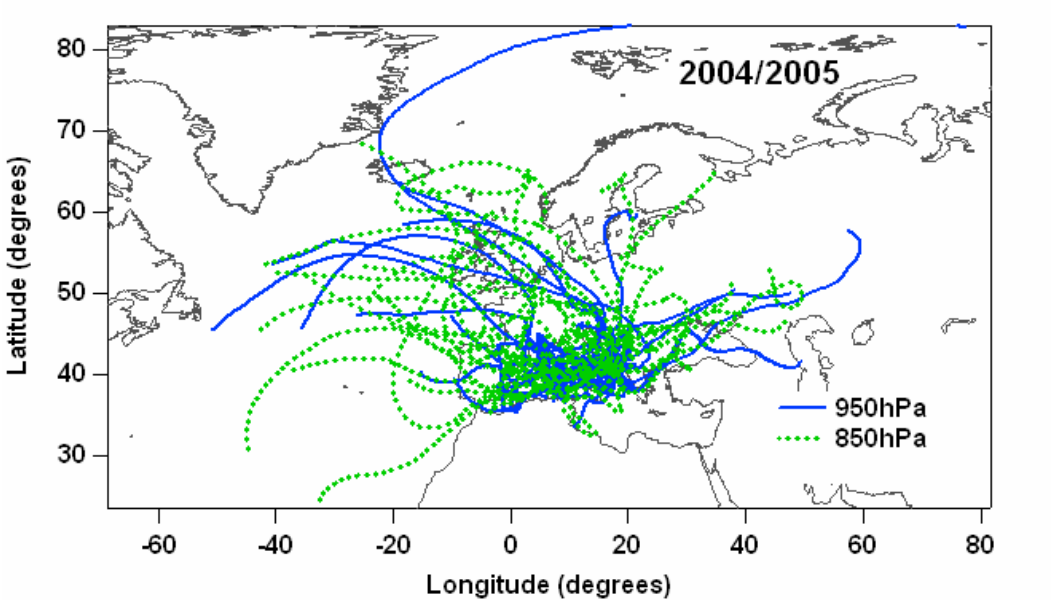

Figure 7.39 – 7-day analytical back-trajectories referring to the measurement days of the year 2004 and 2005 selected for ionic and metal analyses. In this study only the back-trajectories characterized by arrival pressure levels of 950 and 850 hPa have been considered.

In accordance with previous studies (Perrone et al., 2005; De Tomasi et al., 2006; Santese et al., 2008) four broad geographical sectors (Figure 7.40) can be considered as potential source regions of the aerosol advected over South-East Italy: Sector North and

East which include the industrialized countries of North and East Europe respectively, Sector South which includes the Southern Mediterranean and Africa continent, and Sector West which includes the Western Mediterranean, the Iberian Peninsula and the Atlantic Ocean.

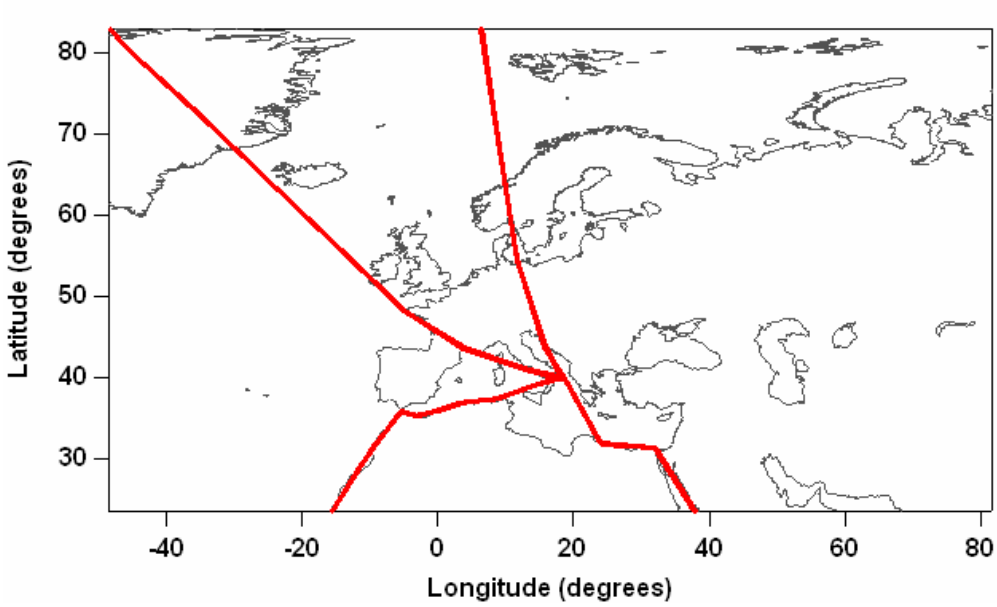

Figure 7.40 – Broad geographical sectors defined as potential source regions of the aerosol advected over South-East Italy.

The time spent by each back-trajectory in a particular Sector up to the sampling day has also been considered to better identify aerosol source regions. In particular, we have assumed that a Sector is an aerosol source area if both the 950 hPa and the 850 hPa-pressure level back-trajectories have spent at least 70% the time within the Sector before reaching the sampling site. Figures 7.41-7.44 show the back-trajectories which have spent at least 70% of the time in sector East, South, North and West, respectively before arriving to Lecce. We can observe that 15 of 42 sampling days exhibit the back-trajectories in Sector West, 11 in Sector East, 4 in Sector North and only 2 in Sector South; 10 of 42 analyzed days were characterized by a mixed advection pattern (Figure 7.45).

In order to investigate the impact of different advection patterns on ground collected particulate matter, the mass concentration and ionic composition of the PM2.5 samples of the year 2004 and 2005 have been analyzed as a function of geographical source sector.

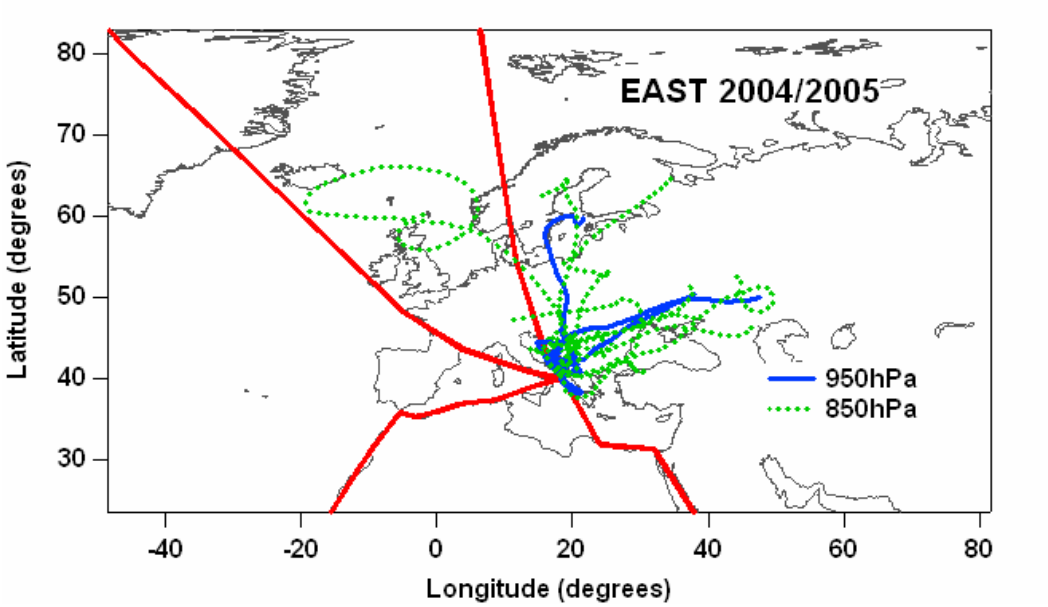

Figure 7.41 – 7-day analytical back-trajectories which spend the most of the time in Sector East before arriving to the sampling site.

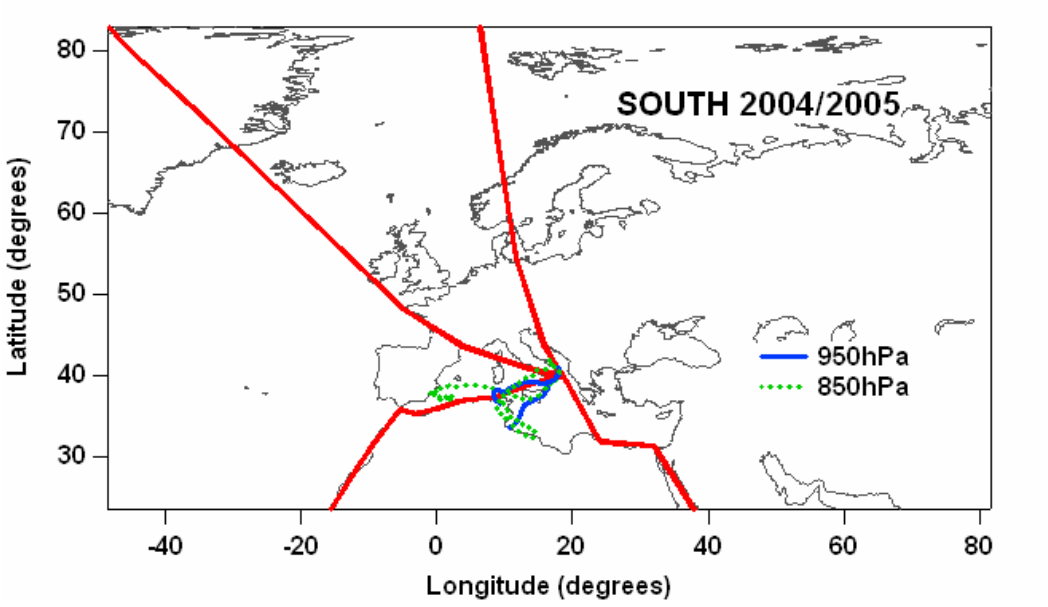

Figure 7.42 – 7-day analytical back-trajectories which spend the most of the time in Sector South before arriving to the sampling site.

The averaged PM2.5 mass concentration of the samples collected during 2004 and 2005 has been plotted in figure 7.46 as a function of aerosol source sector. The numbers in brackets indicate the samples considered in calculations for each geographical region. We can observe from figure 7.46 that the PM2.5 mass concentrations of both years are poorly dependent on the aerosol source sector.

In contrast, we have found that the ionic composition of the analyzed PM2.5 samples was quite dependent on advection patterns.

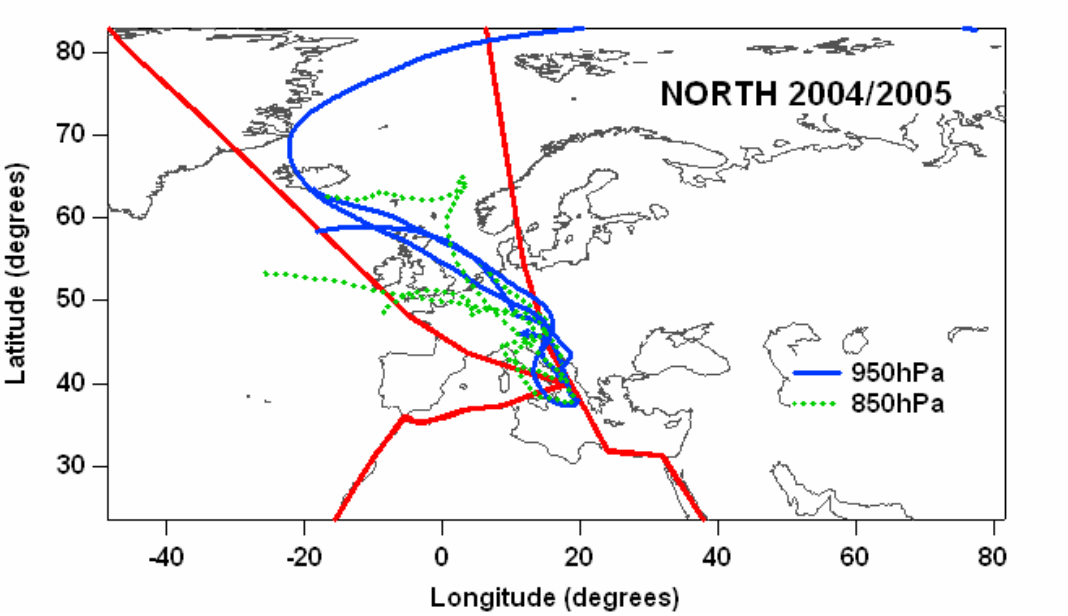

Figure 7.43 – 7-day analytical back-trajectories which spend the most of the time in Sector North before arriving to the sampling site.

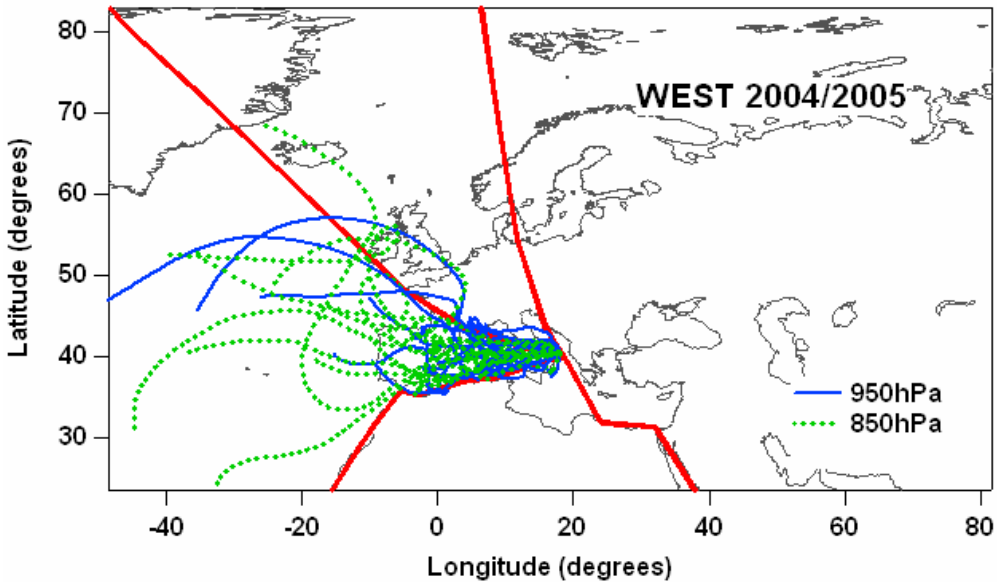

Figure 7.44 – 7-day analytical back-trajectories which spend the most of the time in Sector West before arriving to the sampling site.

Figure 7.47 shows the SO_4^{2-} mass percentages as a function of the source geographical sector; we can observe that the SO_4^{2-} mass percentages trend is similar in both PM2.5 collections; in particular the percentages are highest in samples collected

during advection pattern events from East-Europe. This result may indicate a significant influence on the ground collected PM2.5 composition of polluted air masses advected from industrialized East-European countries. Sulphates in fact, as widely observed, are the main components of fine anthropogenic particulate matter.

Figure 7.48 shows the Na^+ mass percentages as a function of the source geographical sector.

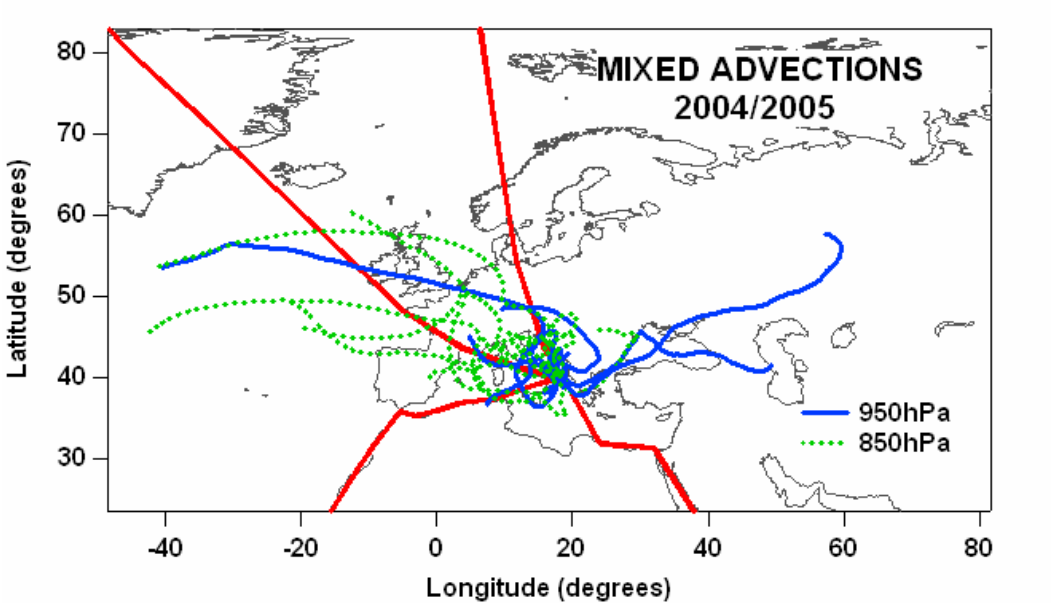

Figure 7.45 – 7-day analytical back-trajectories referring to mixed advection sampling days.

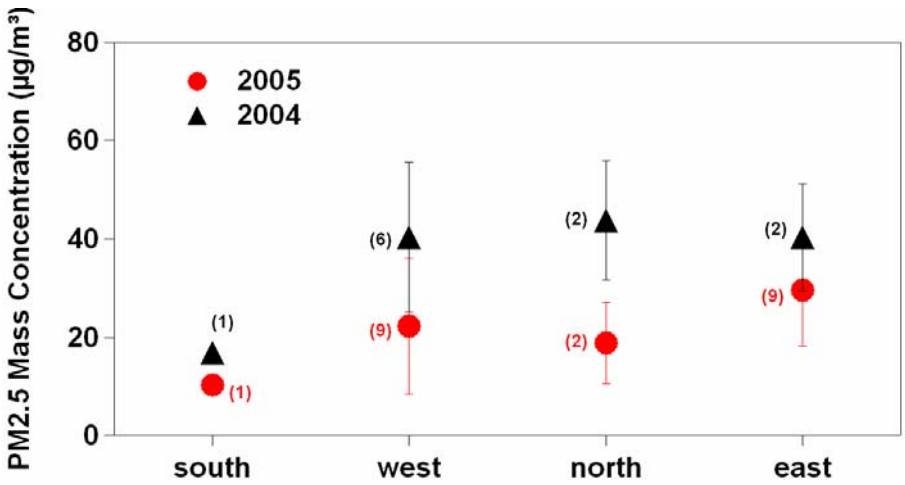

Figure 7.46 – PM2.5 mass concentration values as a function of selected geographical Sector.

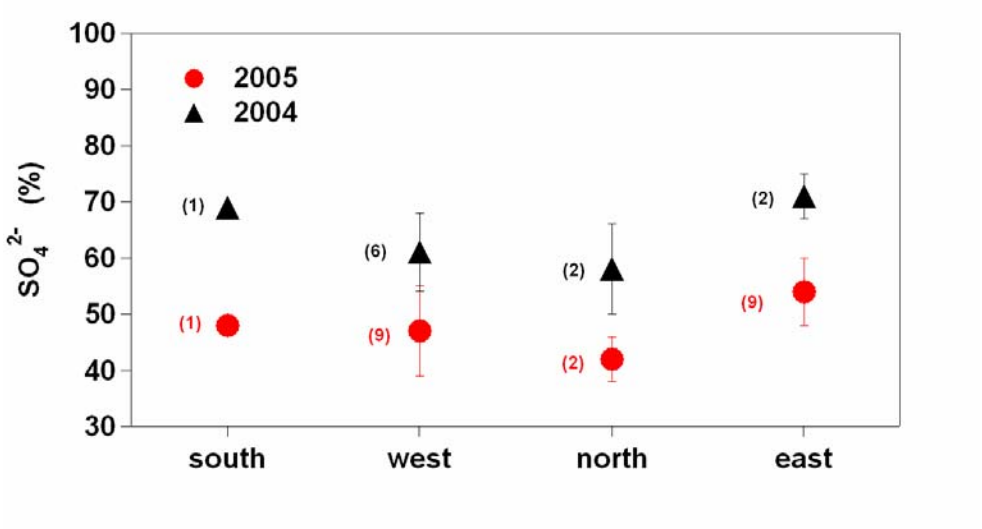

Figure 7.47 – SO_4^{2-} mass percentages values as a function of selected geographical Sector. Mass percentages have been calculated with respect to the total ionic mass.

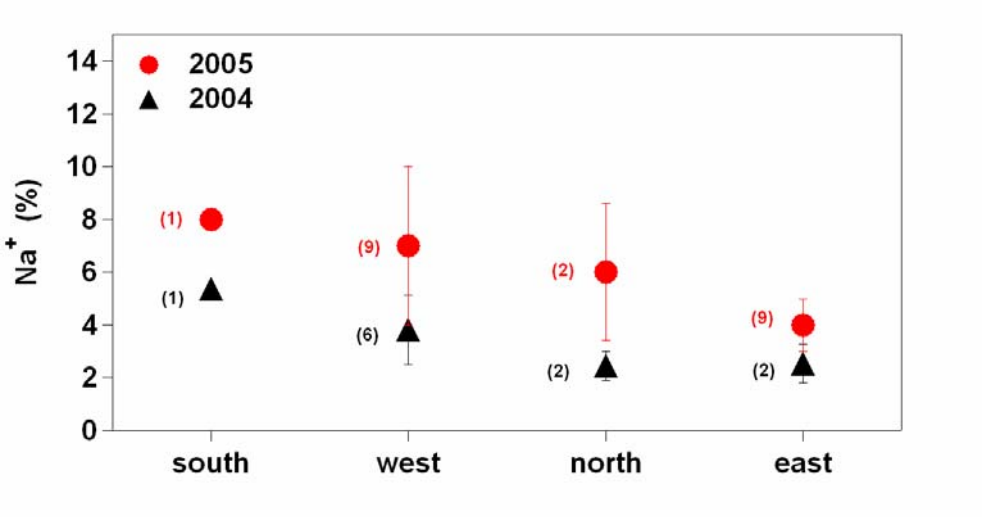

Figure 7.48 - Na^+ mass percentages values as a function of selected geographical Sector. Mass percentages have been calculated with respect to the total ionic mass.

It is worth noting from figure 7.48 that the higher Na^+ mass percentages have been found in samples collected during the advection of air masses coming from Sector West and hence from the western Mediterranean and the Atlantic Ocean. Therefore, sea salt particles can be responsible for the higher mass percentages of Na^+ ion. Conversely the air masses advected from Sector East which includes several industrialized eastern countries are characterized by lower Na^+ mass percentages; in fact Sector East air masses spend less time over the Mediterranean Sea being South-East Italy about 100 km away from the Balkan Peninsula coast.

Ca^{2+} and NO_3^- mass percentages show a poor dependence on aerosol source sector (figures 7.49-7.50): we can only note that the mass percentages of both ions reach the lowest values in correspondence of Sector East. The typical primary coarse nature of Ca^{2+} ion and the bivalent role of NO_3^- ion which is generally a secondary product but frequently found in coarse particles can explain this result.

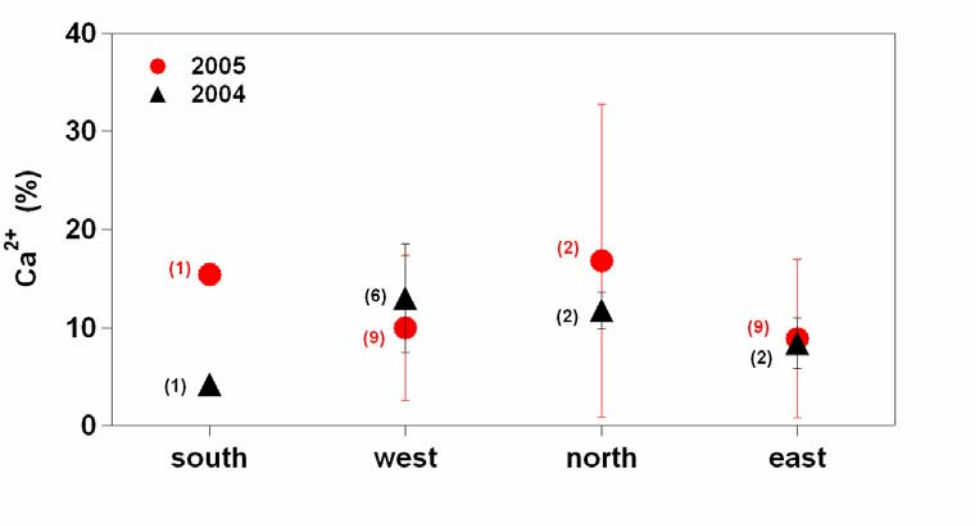

Figure 7.49 – Ca^{2+} mass percentages values as a function of selected geographical Sector. Mass percentages have been calculated with respect to the total ionic mass.

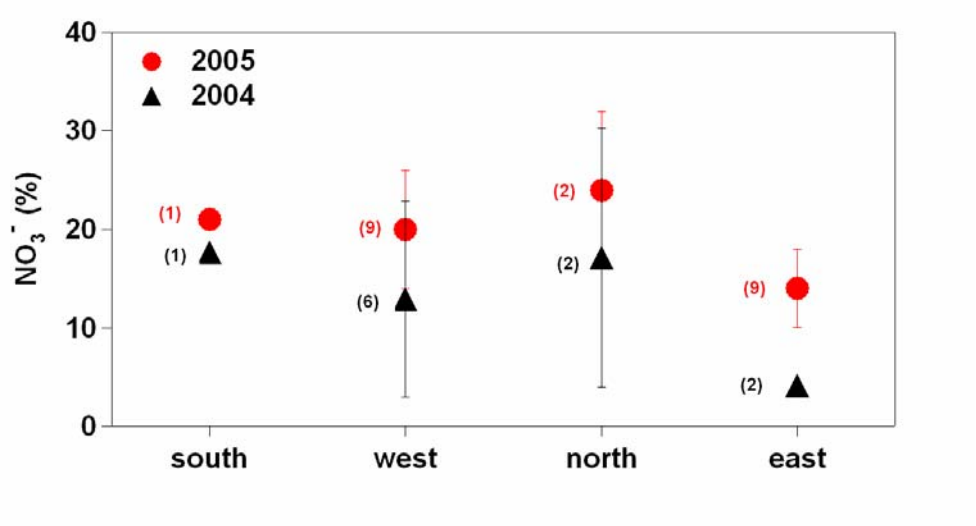

Figure 7.50 – NO_3^- mass percentages values as a function of selected geographical Sector. Mass percentages have been calculated with respect to the total ionic mass.

7.5.1 Sample (30/06/2005) composition results

As observed and discussed in chapter 4 a dust outbreak occurred at Lecce on 30 June 2005 and the results of SEM/EDX analyses performed on the size-fractioned

particles collected by the 7-stage cascade impactor (set Q19) during this advection event have been widely presented and discussed in section 4.3.1

The ionic and elemental composition of a PM2.5 sample collected during the dust outbreak is analyzed in this section.

Figure 7.51 illustrates the mass percentages of all species detected in the dust sample collected on 30 June 2005 in addition with the undefined mass percentage. We can observe from table 7.3 and figure 7.51 that NO_3^-, SO_4^{2-}, and Ca^{2+} are the main ion components: their mass represents 70% of the total analyzed mass. This result further more shows the significant contribution of sulfates and nitrates to the fine fraction of the aerosol load even during a dust event, in accordance to SEM analyses on impactor filters discussed in chapter 4 (Figure 4.20).

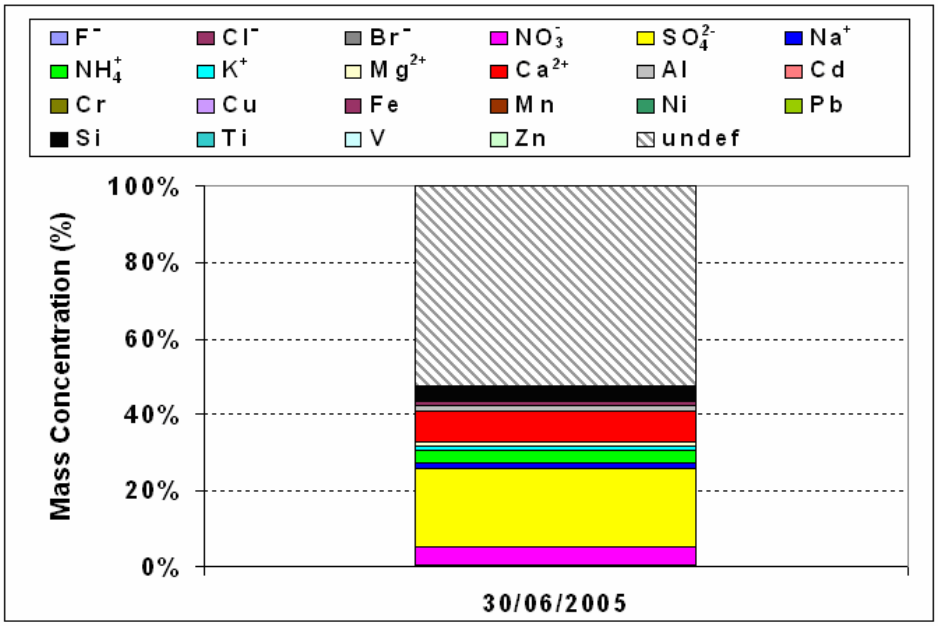

Figure 7.51 - Mass percentages of all species detected in the PM2.5 sample collected on 30 June 2005.

The high mass concentrations of K^+, Mg^{2+}, and Ca^{2+} reported in table 7.3, are due to the Sahara dust particles collected on 30 June, being K^+, Mg^{2+}, and Ca^{2+} elements of illite/smectite and dolomite particles. Moreover, the high mass concentration values of Si, Fe and Al (Table 7.4) could be ascribed to alumino-silicate particles typically present in coarse particulate matter of crustal origin.

7.5.2 Sample (10/05/2005) composition results

The influence of long-range transported air masses on the ground level collected PM composition is also evident in the sample collected on 10 May 2005. The analytical 7-day back-trajectories referring to the measurement day (Figure 7.52) show that the sampled air masses crossed wide marine regions over the Atlantic Ocean before arriving to the sampling site.

Tables 7.3-7.4 show the mass concentrations of the ionic and metal species detected in the filter sampled on 10 May 2005, and figure 7.53 shows the corresponding mass percentages of all analyzed species. We can observe that SO_4^{2-}, NO_3^- and NH_4^+ are the dominant ionic species. The sea salt particles influence can be considered responsible for the significant percentages of Na^+ and Cl^-, which with Ca^{2+} ion can be considered among the principal ionic species constituting the collected particulate matter.

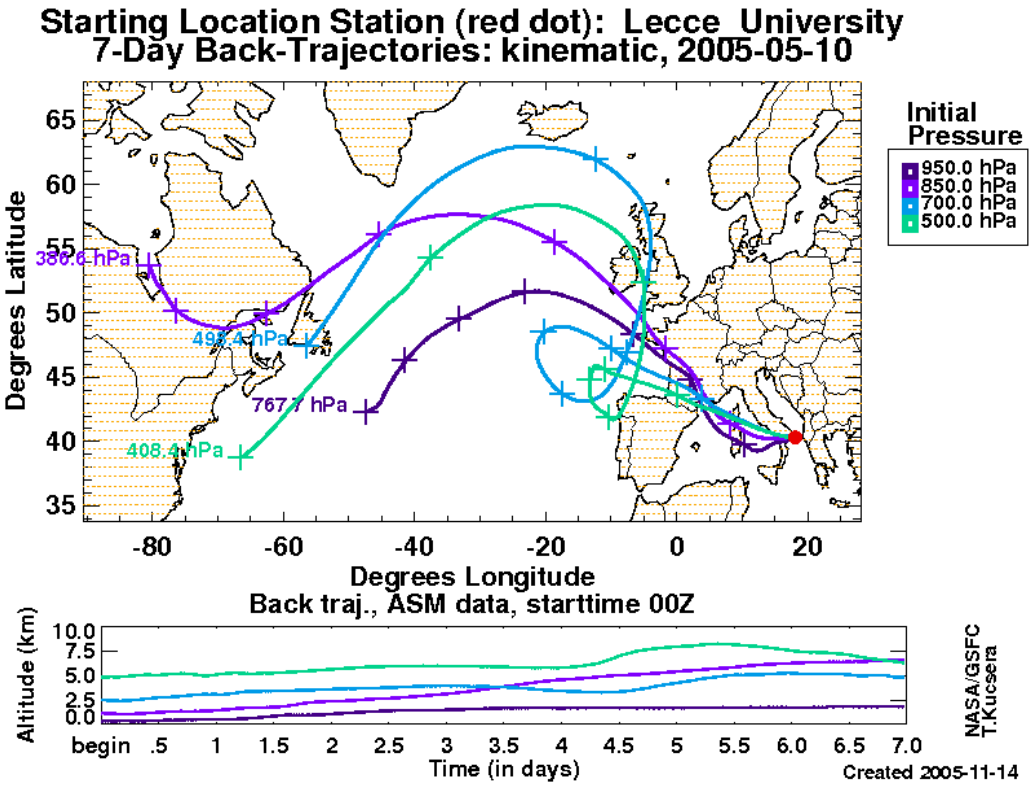

Figure 7.52 – 7-day analytical back - trajectories for the air masses reaching the observation site on 10 May 2005 at 00:00 UTC and pressure levels of each back trajectory as a function of time.

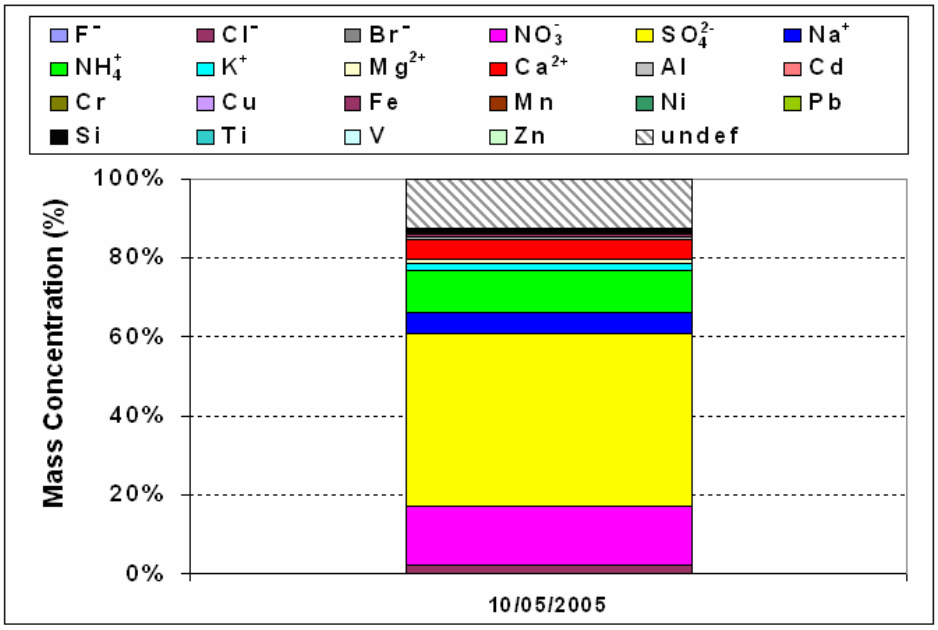

Figure 7.53 – Mass percentages of all species detected in the PM2.5 sample collected on 10 May 2005.

7.5.3 Sample (27/09/2005) composition results

Figure 7.54 shows the 7-day analytical back-trajectories for the air masses reaching the sampling site on 27 September 2005 at 00:00 UTC.

We can observe that the back-trajectories characterized by lower pressure levels cross East-Europe.

Tables 7.3-7.4 show the mass concentrations of the ionic and metal species analyzed in the PM2.5 sample collected on 27 September 2005 and figure 7.55 illustrates the corresponding mass percentages. We can observe that also in this case SO_4^{2-}, NO_3^- and NH_4^+ are the main ionic components but the contribution of coarse mode species is low.

It is important to highlight that the undefined mass percentage found in this PM2.5 sample represents about 62% of the total mass. This percentage value is close to that found in dust sample (of about 52%) but very different from that detected in the sample collected on 10 May 2005 (about 13%).

A major contribution of particles that can not be detected by Ion Chromatography or Inductively Plasma Spectrometry in the PM2.5 samples collected on 30 June and 27 September could be responsible for this result.

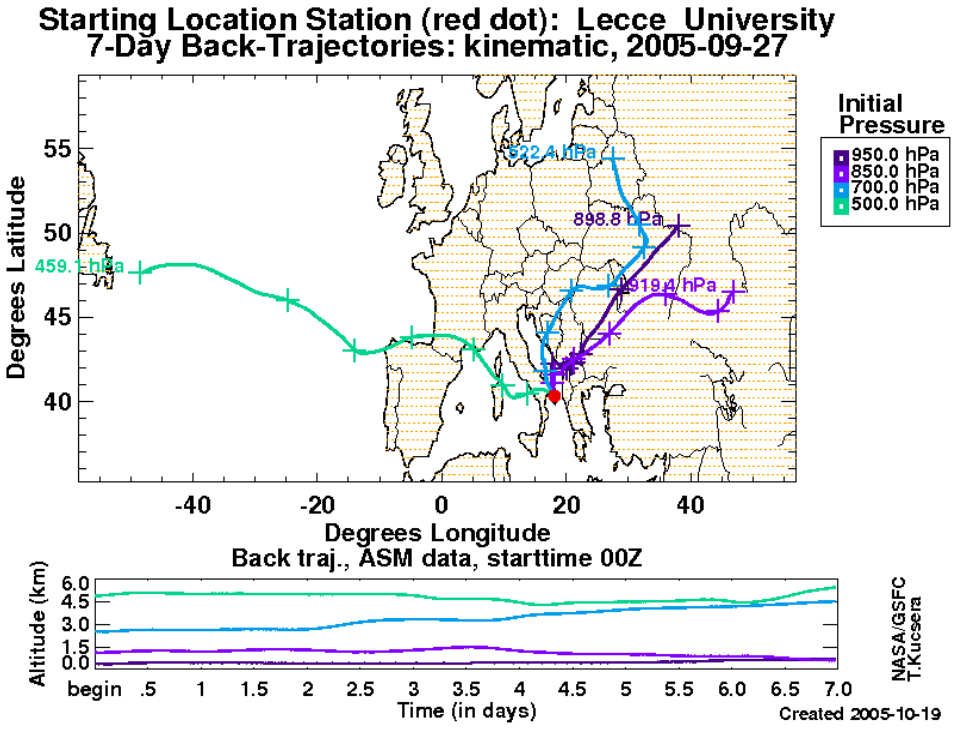

Figure 7.54 – 7-day analytical back - trajectories for the air masses reaching the observation site on 27 September 2005 at 00:00 UTC and pressure levels of each back trajectory as a function of time.

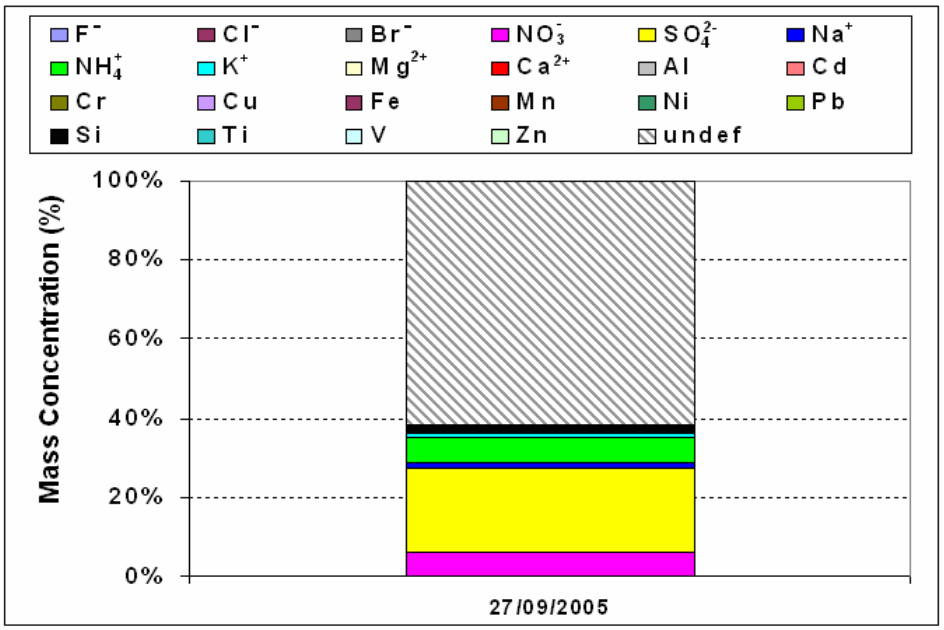

Figure 7.55 – Mass percentages of all species detected in the PM2.5 sample collected on 27 September 2005.

7.6 Ionic composition of 7-stage cascade impactor filters

This section discusses the ionic composition results of two size-fractioned samples collected at the Physics Department of Lecce on 10 May (Q16) and on 27 September 2005 (Q30) by the 7-stage cascade impactor. The aim of this study is to show how PM ionic composition varies with the impactor cut-off diameter.

As previously observed, 7-day analytical back-trajectories analyses have shown that the long-range transported air masses crossed the Atlantic Ocean and East-Europe before arriving to the sampling site on 10 May and 27 September 2005, respectively.

Ion Chromatography analyses have been performed on the collected size-fractioned samples in order to characterize the main composition of the particles collected in each size interval.

Figure 7.56 shows the mass percentages of the ionic species detected in each filter collected on 10 May 2005. We can observe that the particles collected in the stages with cut-off diameter ≥ 0.65 μm have a similar composition with a high contribution of coarse species: Ca^{2+}, Mg^{2+}, Na^{+}, Cl^{-}, K^{+} and NO_3^{-}. It is important to highlight the significant percentages of nitrates (up to about 40% of the total ionic mass) in the filters with a cut-off diameter ≥ 0.65 μm indicating an important contribution of nitrates in coarse fraction. NO_3^{-} percentages drastically decrease in the particles of the filters with cut-off diameter < 0.65 μm.

Sulphates represent the dominant ionic species constituting the fine mode particles; in fact SO_4^{2-} mass percentages increase as particle size decreases, reaching high values (about 80%) in filters with cut-off diameter ≤ 0.35 μm.

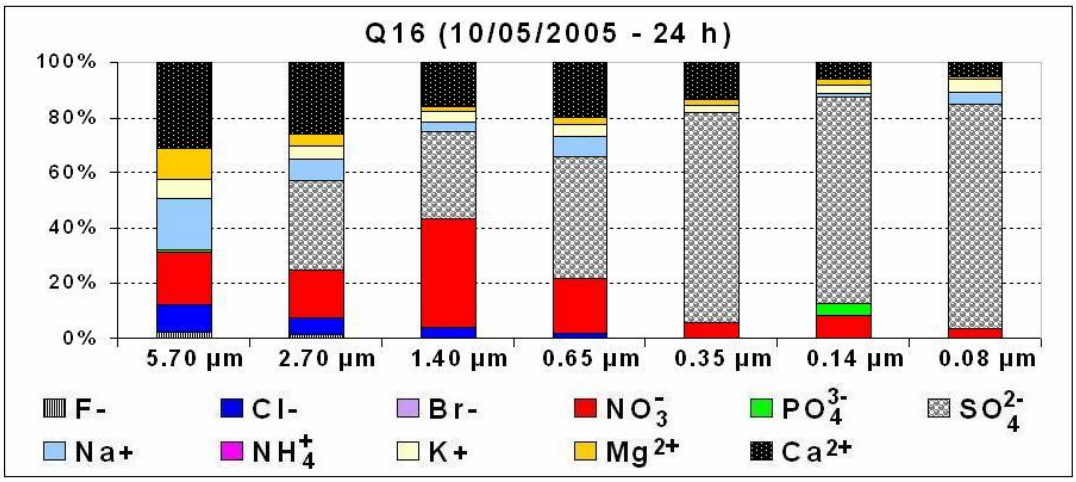

Figure 7.56 – Mass percentages of the ionic species detected in the filters collected by the 7-stage cascade impactor on 10 May 2005.

Figure 7.57 shows the ionic mass percentages of the species detected in each filter collected by the 7-stage cascade impactor on 27 September 2005 during an advection event from East-Europe. We can observe that sulphates are the dominant components in each stage. The coarse-mode ionic species Ca^{2+}, Na^{+}, Cl^{-}, Mg^{2+}, K^{+} and NO_3^{-} have higher mass percentages in the filters with cut-off diameter ≥ 0.65 μm and their values decrease with size particles.

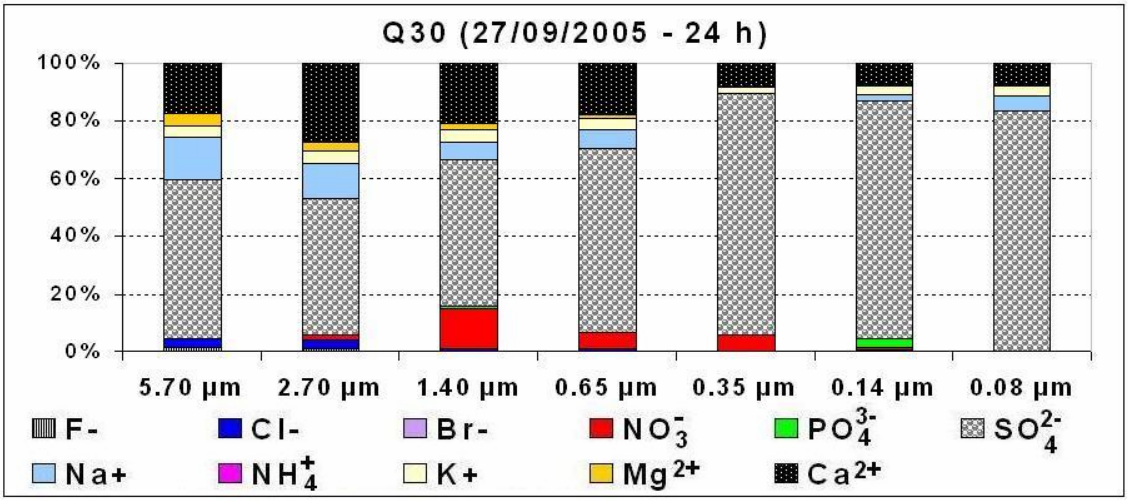

Figure 7.57 – Mass percentages of the ionic species detected in the filters collected by 7-stage cascade impactor on 27 September 2005.

It is worth noting that fine fraction is poorly dependent on long-range transport processes; in fact in both analyzed samples the ionic composition of the particles collected on the filters with cut-off diameter ≤ 0.35 μm is similar. The different advection patterns have clearly affected the coarse-mode particulate matter collected on the filters with cut-off diameter ≥ 0.65 μm. In particular sea salt particles advected from the Atlantic Ocean influenced the coarse mode fraction of the sample collected on 10 May increasing in particular the mass percentages of Na^{+} and Cl^{-}. Conversely, the anthropogenic fine aerosols transported from East Europe on 27 September could be considered responsible of the higher SO_4^{2-} mass percentages in each filter.

CHAPTER 8

ADVECTION PATTERNS AND COMPOSITION OF TSP AND PM2.5 SAMPLES

8 ADVECTION PATTERNS AND COMPOSITION OF TSP AND PM2.5 SAMPLES

A main objective of this study is to investigate both how TSP and PM2.5 mass concentrations vary with the time of the year and how mass concentrations and the chemical composition of TSP and PM2.5 samples are affected by long-range transported air masses.

In the current study, 7–day analytical back-trajectories have been used to characterize main advection patterns over the monitoring site. Analytical back trajectories in fact provide information on the aerosol origin observed at a particular location and on the dynamical patterns governing the air mass transport (Kazadzis et al, 2007).

In order to asses the relative contribution of natural and anthropogenic sources to the ground collected PM, Ion Chromatography and OC/EC analyses have been performed on some randomly selected TSP and PM2.5 samples, respectively. This study reports in particular results on the IC and OC/EC analyses performed on two couples of TSP and PM2.5 samples, which have simultaneously been collected on 15 March 2007 during the advection of air masses from East Europe and during a Saharan dust event occurred on 25 June 2007 (Carofalo et al., 2008).

8.1 Measurements

24-h Total Suspended Particulate (TSP) matter and PM2.5 samples have simultaneously been collected by the low volume Hydra (FAI) dual sampler (chapter 3) at the Physics Department of Lecce from March to December 2007.

The sampled particulate matter has been deposited on 47-mm-diameter quartz fibre filters, pre-cleaned (at 700° for about two hours) and conditioned before and after sampling (25°C during 48 h and 50% humidity). Gravimetric method allows assessing the mass concentration of the collected particulate matter.

Ion Chromatography and OC/EC analyses have been performed on some selected TSP and PM2.5 samples to determine mass concentrations of the main ionic species (F^-, Cl^-, NO_3^-, SO_4^{2-}, Na^+, NH_4^+, K^+, Mg^{2+}, Ca^{2+}) and of organic/elemental carbon.

8.1.1 Chemical analysis

Anions analyses were carried out by means an Ion Pac AS14A (Dionex) column using 8 mM Na2CO3/1mM NaHCO3 as eluent at 1mL/min flow rate and, for the detection, a conductivity system equipped with a ASRS-ULTRA suppression mode (Dionex). Cations determination was performed by means of a CS12A (Dionex) column using 20 mM MSA (Methanesulphonic Acid) as eluent at 1mL/min flow rate and, for the detection, a conductivity system equipped with a CSRS-ULTRA suppression mode (Dionex). The extraction procedure is reported in Fermo et al., 2006a.

8.1.2 OC/EC analysis

Elemental and organic carbon mass concentrations have been determined in the selected TSP and PM2.5 samples by the thermal/optical transmittance (TOT) technique by means of an OC/EC Sunset Analyzer (chapter 5).

Both ionic and EC/OC analyses have been performed by Dr. Fermo P. and Dr. Piazzalunga A. of the Department of "Chimica Inorganica, Metallorganica e Analitica" of University of Milano.

8.2 TSP and PM2.5 mass concentration results

Mass concentrations by the gravimetric method of TSP and PM2.5 samples, collected from March to December 2007 at Physics Department of Lecce are shown in figure 8.1 as a function of the sampling day. Uncertainties on mass concentrations are lower than 5%.

We can observe from figure 8.1 that both TSP and PM2.5 mass concentrations significantly vary day by day. Changes in air mass transport arriving from different source regions toward the sampling point have mainly been considered responsible for these results. Figure 8.1 highlights that TSP and PM2.5 mass concentrations take larger values on July and August. Conversely, November and December are the months during which TSP and PM2.5 mass concentrations take smaller values. Figure 8.1b in particular shows that 23% of the PM2.5 collected samples exceed the European reference annual limit value 25 $\mu g/m^3$ (not to be exceeded from 1 January 2015).

The TSP mass concentrations higher than 80 μg/m^3 that have been monitored on 25 June and 30 August are due to dust events. It is important to highlight that the dust events have also affected PM2.5 mass concentrations, which reached the highest values: about 40 - 45 μg/m^3.

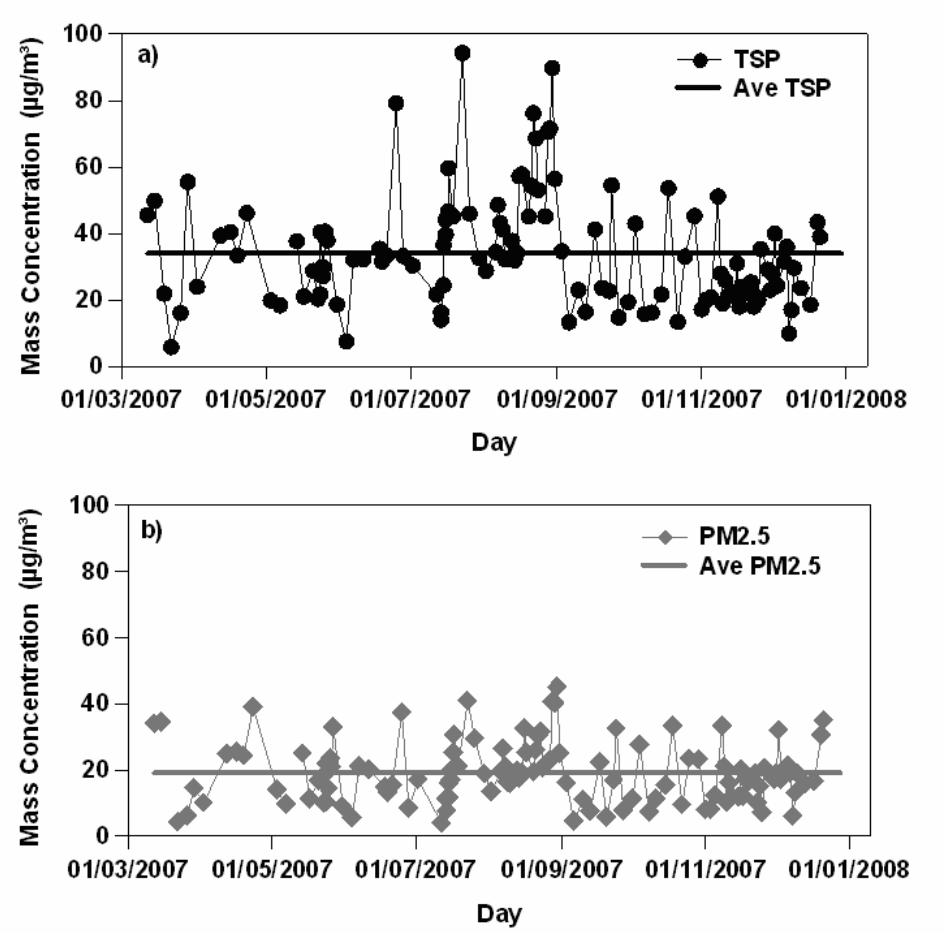

Figure 8.1 – Mass concentrations of TSP (a) and PM2.5 (b) samples simultaneously collected at Physics Department of Lecce as a function of the sampling day. The horizontal lines represent the average values.

Mean statistical data referring to both sampling collections are reported in table 8.1, from which we can observe that TSP mass concentrations vary within the 6 – 94 μg/m^3 range and are characterized by a mean value ± 1 SD of (34 ± 17) μg/m^3. PM2.5 mass concentrations vary within the sampling period between 4 and 45 μg/m^3, with a mean value of (19 ± 9) μg/m^3.

Table 8.1 – Mean statistical data referring to the PM2.5 and PM1 sampling collections.

	TSP	PM2.5
Number of samples	117	117
Ave Mass Conc. (μg/m³)	34	19
St. Deviation	17	9
Max Mass Conc. (μg/m³)	94	45
Min Mass Conc. (μg/m³)	6	4

The mass ratio between the two PM fractions (PM2.5/TSP), shown in figure 8.2, varies between 0.2 and 0.9 with an average value of 0.6. It is evident that PM2.5 particles represent a substantial fraction of the total suspended particulate matter.

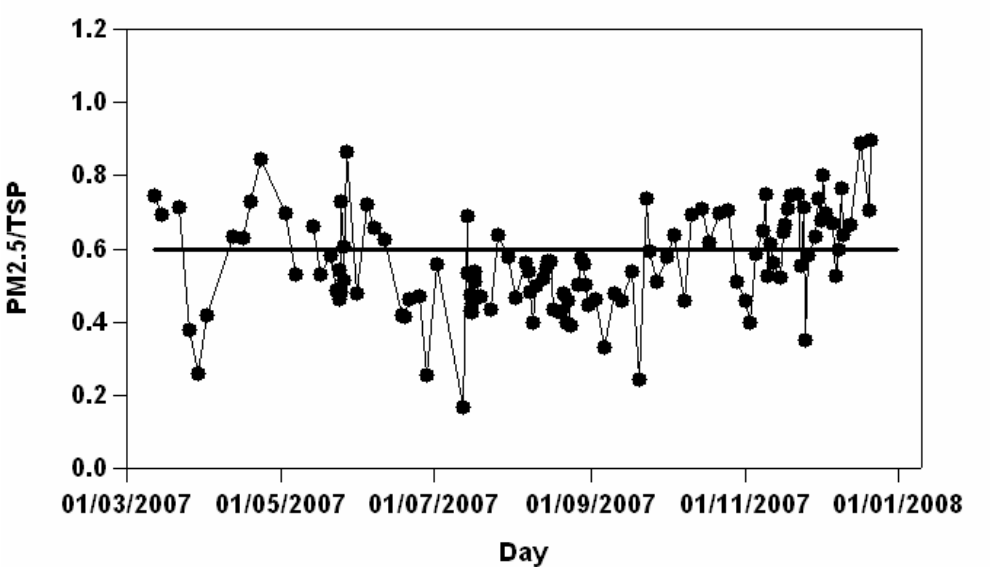

Figure 8.2 - PM2.5/TSP mass ratios as a function of the sampling day. The horizontal line represents the average value.

Like the temporal series of TSP and PM2.5 mass concentrations, also the PM2.5/TSP mass ratios showed significant daily variations. A slight seasonal dependence is also revealed by figure 8.2. In particular, the smaller PM2.5/TSP mass ratios recorded from June to September indicate that mass concentrations due to coarse-mode particles were larger during summer. This result can probably be ascribed to dust events.

8.3 Results on Ion Chromatography and OC/EC analyses

Ion chromatography (IC) and Organic Carbon/Elemental Carbon (OC/EC) analyses have been performed on 10 randomly selected couples of PM2.5 and TSP simultaneous samples, in order to determine mass concentrations of the main ionic species and of EC and OC, respectively.

Figures 8.3-8.4 illustrate the mass percentages of the ionic species, OC and EC detected in TSP and PM2.5 analyzed samples respectively, in addition with the undefined mass percentages.

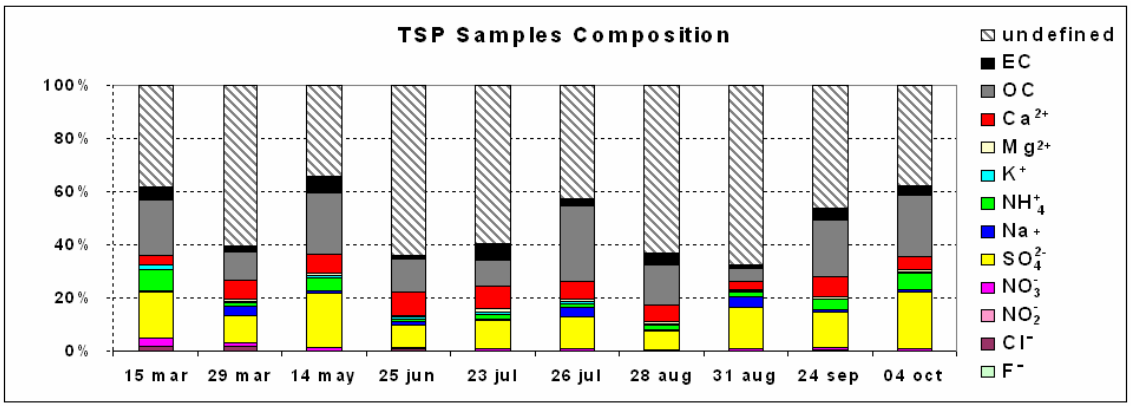

Figure 8.3 – Mass percentages of the ionic species and OC/EC investigated in TSP samples, in addition with undefined mass percentages.

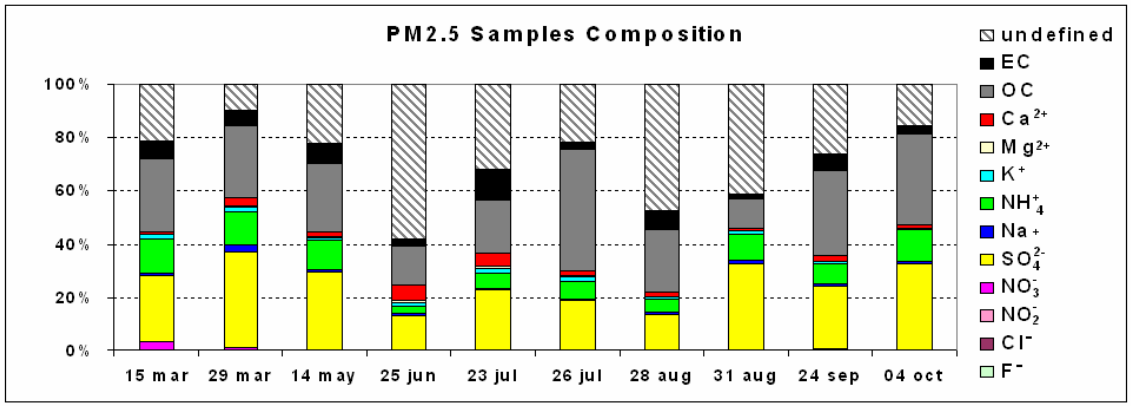

Figure 8.4 – Mass percentages of the ionic species and OC/EC investigated in PM2.5 samples, in addition with undefined mass percentages.

In accordance with TSP and PM2.5 mass concentrations and PM2.5/TSP ratios, Ion Chromatography and OC/EC analyses have revealed that both ionic species and OC/EC concentrations significantly varied from sample to sample, as a consequence of

the significant dependence of aerosol properties on regional sources and pathways of the air masses advected over the monitoring site.

SO_4^{2-}, NH_4^+ and OC represent the main components of the PM2.5 particulate; SO_4^{2-} and OC mass percentages decrease in TSP samples, instead Ca^{2+} and Na^+ levels increase. Elemental carbon mass percentages are similar in both sampling collections.

Tables 8.2-8.3 show the average mass concentration values of the species investigated in TSP and PM2.5 selected samples respectively, in addition with the undefined mass concentrations, Ion/PM and TC/PM mass percentage ratios. We can observe from figures 8.3-8.4 and tables 8.2-8.3 that the undefined mass percentage values are higher in TSP samples; this result suggests the presence of some coarse mode PM components that can not be detected by the IC and TOT technique, such as insoluble alumino-silicate particles.

Table 8.2 – Average mass concentrations ($\mu g/m^3$) of the ionic species and organic and elemental carbon detected in TSP selected samples, in addition with undefined mass concentration, Ion/PM and TC/PM mass percentage ratios. N is the number of samples used for calculations.

	TSP				
	Ave	**SD**	**Max**	**Min**	**N**
	$\mu g/m^3$				
F-	0.03	0.04	0.09	0.002	9
Cl^-	0.7	0.2	0.9	0.4	3
NO_2^-	0.02	0.01	0.03	0.002	10
NO_3^-	0.6	0.4	1.7	0.3	10
SO_4^{2-}	7.4	1.7	10.1	4.8	10
Na^+	1.0	0.7	2.2	0.3	10
NH_4^+	1.6	1.0	3.9	0.7	10
K^+	0.4	0.2	0.8	0.2	10
Mg^{2+}	0.5	0.2	0.9	0.2	10
Ca^{2+}	3.8	2.2	8.3	1.4	10
OC	9.2	2.9	13.1	2.9	10
EC	2.3	1.6	6.2	0.6	10
Undef.Mass	31.6	15.3	56.1	12.9	10
Ion/PM (%)	28	6	36	17	
TC/PM (%)	21	8	31	6	

Figures 8.5-8.11 show the mass concentrations of the species SO_4^{2-}, OC, EC, Ca^{2+}, Na^+, NO_3^-, and $NH4^+$ detected in both investigated PM fractions as a function of the sampling day. It is important to note that Ca^{2+} and Na^+ mass concentrations are

higher in TSP samples indicating a coarse mode nature (figures 8.8-8.9); instead SO_4^{2-}, OC and EC (figures 8.5-8.7) exhibit mass concentration values similar in both TSP and PM2.5 samples suggesting a dominant presence in the fine fraction.

Table 8.3 – Average mass concentrations ($\mu g/m^3$) of the ionic species and organic and elemental carbon detected in PM2.5 selected samples, in addition with undefined mass concentration, Ion/PM and TC/PM mass percentage ratios. N is the number of samples used for calculations.

	PM.5				
	Ave	**SD**	**Max**	**Min**	**N**
	$\mu g/m^3$				
F^-	0.04	0.04	0.10	0.003	10
Cl^-	-	-	-	-	-
NO_2^-	0.02	0.02	0.07	0.003	9
NO_3^-	0.2	0.4	1.0	0.0	7
SO_4^{2-}	7.0	1.7	9.1	4.7	10
Na^+	0.3	0.1	0.4	0.2	10
NH_4^+	2.4	0.9	4.4	1.0	10
K^+	0.4	0.2	0.9	0.2	10
Mg^{2+}	0.1	0.1	0.2	0.0	10
Ca^{2+}	0.8	0.8	2.2	0.2	10
OC	7.9	3.2	13.4	2.8	10
EC	1.8	1.3	4.7	0.5	10
Undef.Mass	9.7	6.5	21.7	1.4	10
Ion/PM (%)	39	11	57	22	
TC/PM (%)	32	10	48	13	

Nitrates are found both in TSP and PM2.5 samples (Figure 8.10); however mass concentrations reach higher values in TSP samples. This result, also observed in other studies (Henning et al., 2003, Putaud et al., 2004., Marenco et al., 2006), could be ascribed to the possible interaction of HNO_3 with coarse-mode particles.

Figure 8.11 shows that the NH_4^+ mass concentrations found in TSP samples are lower than that detected in PM2.5 filters. This result is unexpected since the total suspended particulate matter includes fine fraction. In chapter 6 we observed that underestimation of particulate ammonium may result from the interaction of particulate ammonium with alkaline particulate matter (Danalatos and Glavas, 1999). Thus the effect observed in figure 8.11 could be ascribed to an artefact due to volatilization of ammonium.

Figure 8.12 shows NH_4^+ mass percentage reported as a function of the total mass percentage due to alkaline ions (Na^+, K^+, Mg^{2+} and Ca^{2+}). Mass percentages of figure 8.12 have been calculated with respect to the total analyzed mass. In both analyzed fractions the NH_4^+ mass percentage decreases as the mass percentage due to alkaline ions increases. The effect is more evident in total suspended particulate matter supporting the hypothesis of underestimation of ammonium in TSP samples.

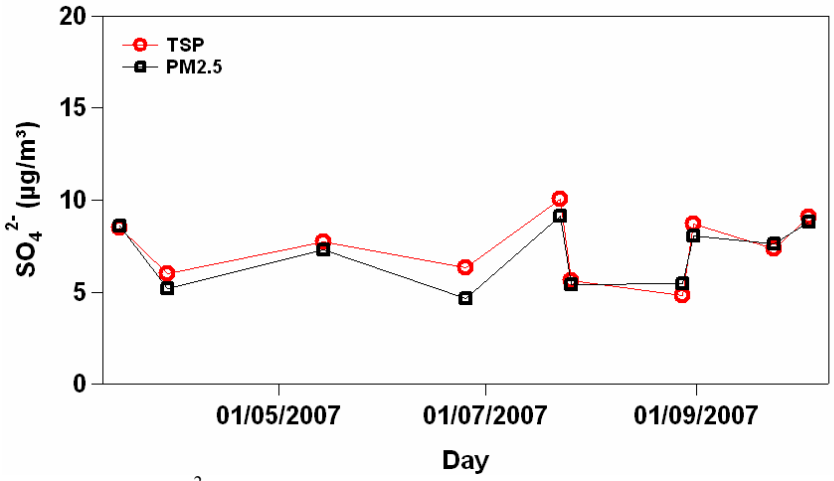

Figure 8.5 – SO_4^{2-} mass concentrations detected in TSP and PM2.5 selected samples as a function of the sampling day.

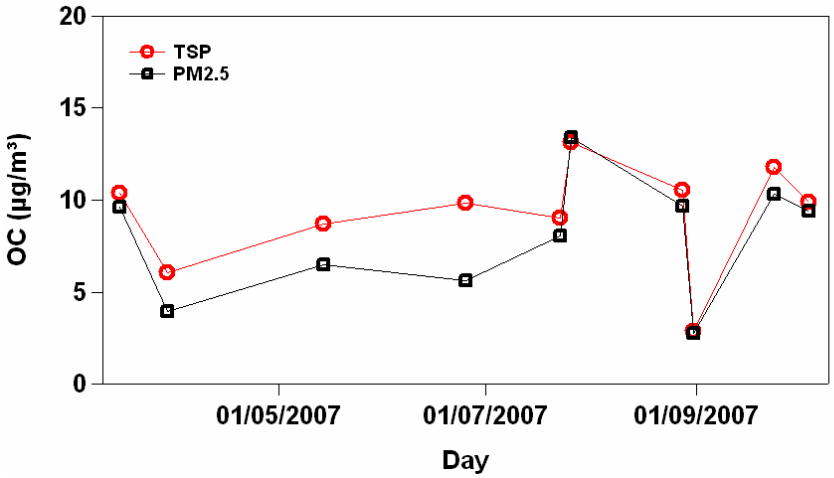

Figure 8.6 – OC mass concentrations detected in TSP and PM2.5 selected samples as a function of the sampling day.

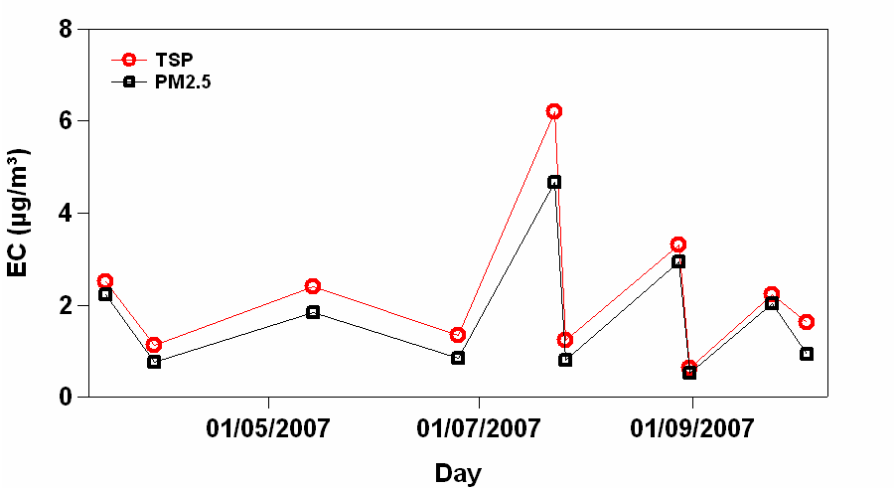

Figure 8.7 – EC mass concentrations detected in TSP and PM2.5 selected samples as a function of the sampling day.

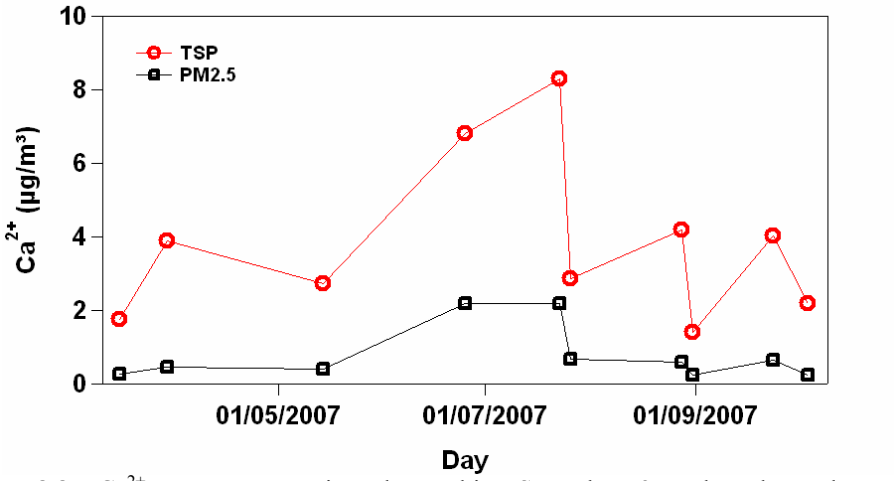

Figure 8.8 – Ca^{2+} mass concentrations detected in TSP and PM2.5 selected samples as a function of the sampling day.

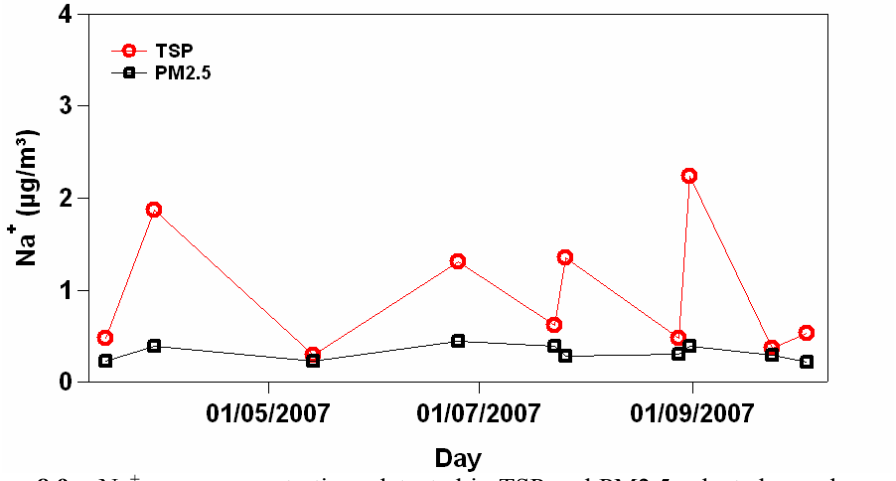

Figure 8.9 – Na^{+} mass concentrations detected in TSP and PM2.5 selected samples as a function of the sampling day.

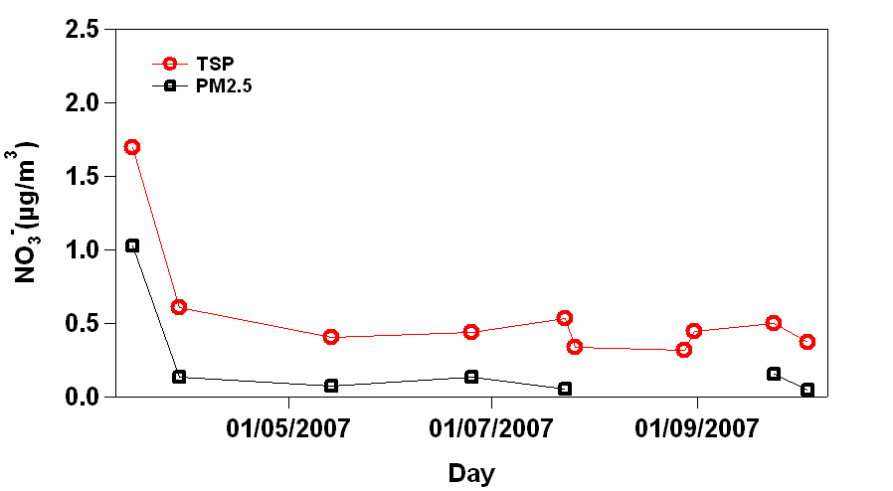

Figure 8.10 – NO_3^- mass concentrations detected in TSP and PM2.5 selected samples as a function of the sampling day.

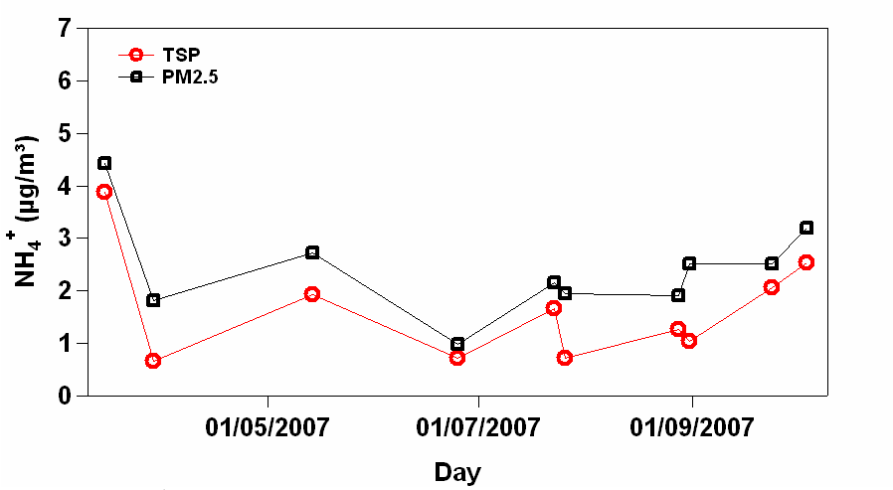

Figure 8.11 – NH_4^+ mass concentrations detected in TSP and PM2.5 selected samples as a function of the sampling day.

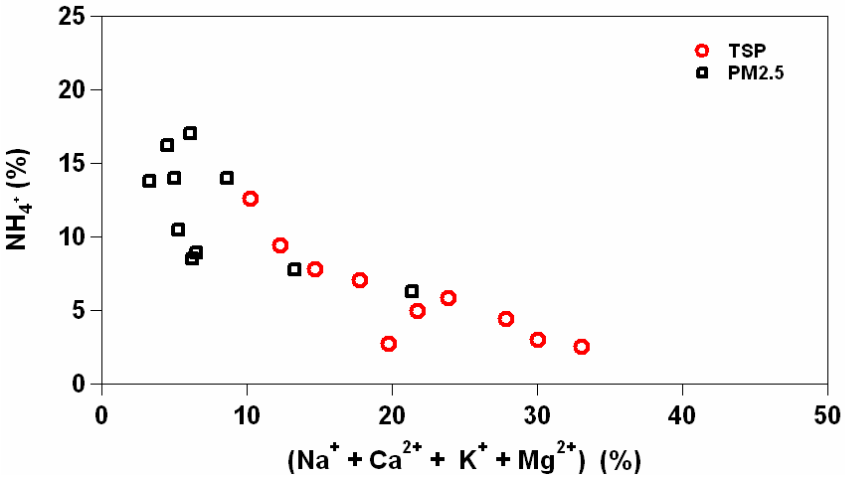

Figure 8.12 - NH_4^+ mass percentage as a function of the total mass percentage due to alkaline ions (Na^+, K^+, Mg^{2+}, and Ca^{2+}) in TSP and PM2.5 selected samples.

8.4 Results on Ion Chromatography and OC/EC analyses of two couples of TSP and PM2.5 samples

This study focuses in particular on Ion Chromatography and OC/EC analyses performed on two couples of TSP and PM2.5 samples, which have simultaneously been collected during a pollution event from East Europe occurred on 15 March 2007 and a Saharan dust event occurred on 25 June 2007.

TSP and PM2.5 mass concentrations and PM2.5/TSP ratios referring to both sampling days are marked in figure 8.13 and 8.14 respectively by a square and a circle.

Figure 8.15a shows the pathways of the 950, 850, 700, and 500 hPa analytical back-trajectories that reached the monitoring site on 15 March. Pressure levels of each back-trajectory as a function of time are shown on figure 8.15b.

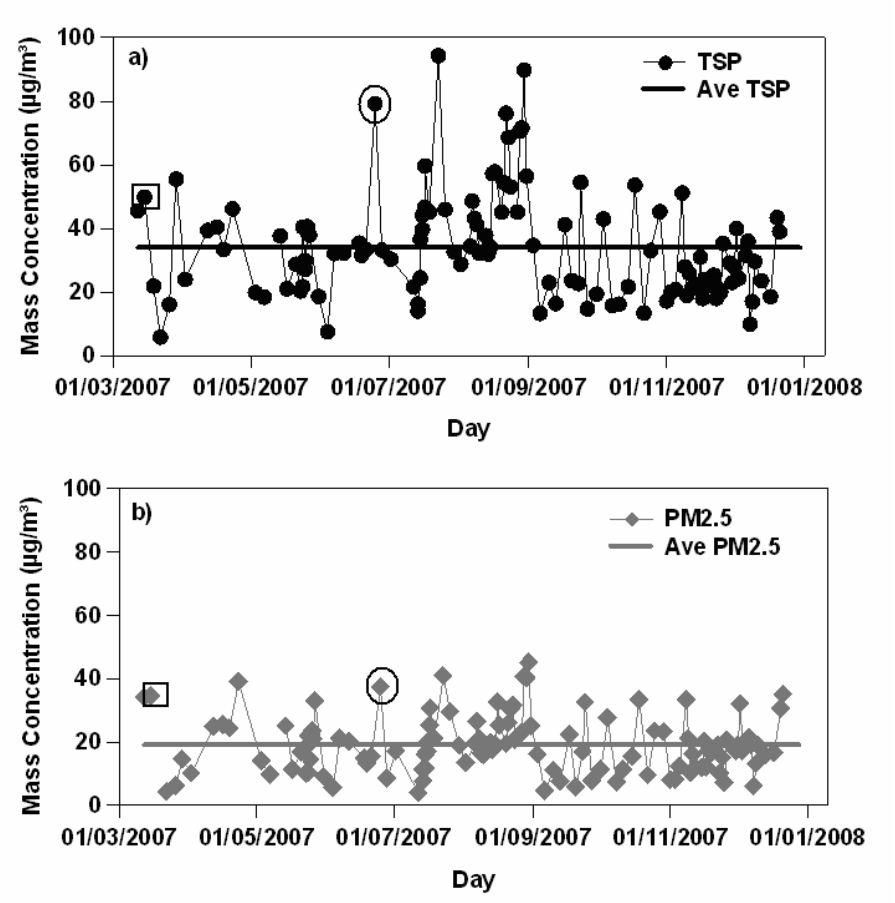

Figure 8.13 –Mass concentrations of (a) TSP and (b) PM2.5 ground collected samples as a function of the sampliung day. The horizontal lines represent average mass concentrantion values. Square and circle markers indicate the East-European pollution event occurred on 15 March 2007 and the Saharan dust event occurred on 25 June 2007, respectively.

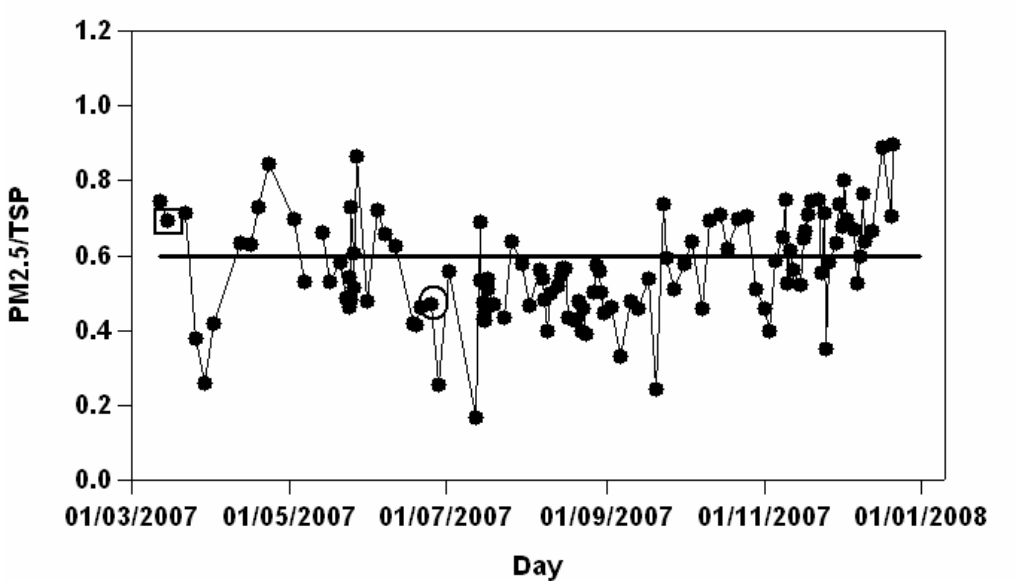

Figure 8.14 - PM2.5/TSP mass ratios as a function of the sampling day. The horizontal line represents the average value. Square and circle markers indicate the East-European pollution event occurred on 15 March 2007, and the Saharan dust event occurred on 25 June 2007, respectively.

We can observe from figure 8.15 that all back-trajectories travelled over Eastern Europe before reaching the monitoring site. As a consequence, they can be responsible for the advection over the monitoring site of anthropogenic polluted air masses.

Figures 8.16a and 8.16b report the 7-days back-trajectories and corresponding pressure levels, respectively for the air masses arrived at the sampling site on 25 June, after spending most of travelling time over northwestern Africa.

TSP and PM2.5 mass concentrations of the main ionic species and organic and elemental carbon referring to the two sampling days are reported in table 8.4. Uncertainties for ions and for OC and EC are of 5%. Beside the compositional results table 8.4 gives also the total sampled mass (S-M), the total analyzed mass (A-M) and the analyzed mass percentage (A-M)/(S-M). It is worth observing from table 8.4, that on 15 March, 79% and 62% of the total sampled PM2.5 and TSP, respectively has been analyzed. Conversely, on 25 June, IC and OC/EC analyses have allowed characterizing only 42% and 36% of the total PM2.5 and TSP sampled mass, respectively. This last result shows that more than 55% of the PM collected during the dust event, was made of particles, such as alumino-silicate particles, that could not be analyzed by the techniques used in this study.

Figures 8.17 and 8.18 report mass percentages of investigated species in TSP and PM2.5 samples collected on 15 March, and 25 June, respectively. We can observe

from table 8.4 and both figures that compositional properties of the sampled PM are quite dependent on advection patterns. Mass percentages of coarse ionic species (Ca^{2+}, Mg^{2+} and Na^{+}) are higher in dust event samples; whereas mass percentages of fine components (NH_4^{+}, SO_4^{2-}, NO_3^{-}, OC and EC) are larger in anthropogenic polluted samples. Moreover, for each day, it can be seen that Ca^{2+}, Mg^{2+} and Na^{+} mass percentages decrease with particulate matter cut-off diameter. Conversely, mass percentages of NH_4^{+}, SO_4^{2-}, NO_3^{-}, OC and EC reach higher values in the fine fraction.

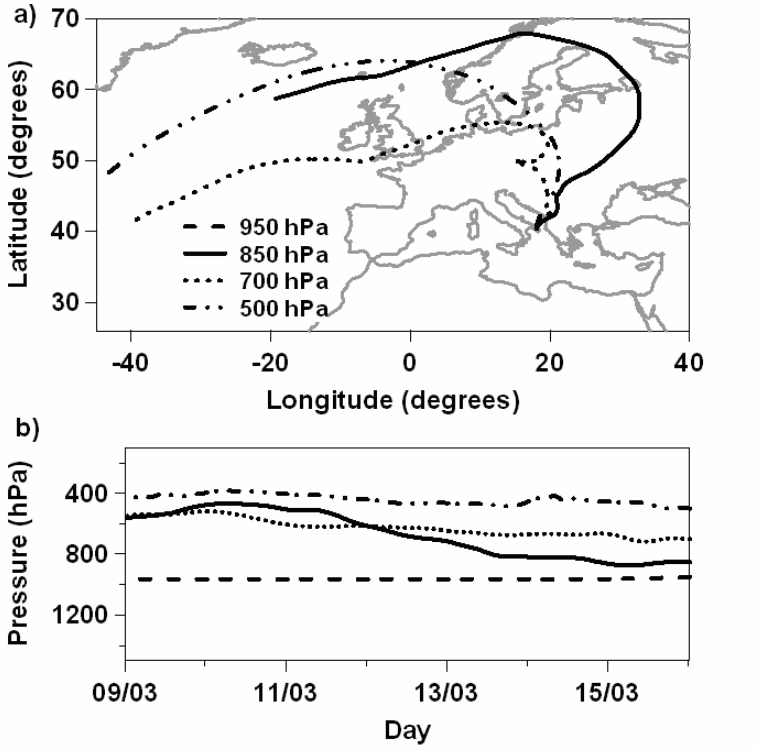

Figure 8.15 - (a) 7-days analytical back-trajectories for the air masses reaching the sampling site on 15 March 2007. (b) Pressure levels of each back-trajectory as a function of time.

Chlorine depletion reactions due to HNO_3–sea salt particle reactions (Perrone et al., 2006), are responsible for the lack of Cl^{-} ions in the PM2.5 samples of both sampling days.

As previously discussed, artefacts during sampling leading to ammonium volatilization processes as a consequence of the interaction of ammonium particulate with alkaline particulate matter might partially be responsible for the minor presence of ammonium particulate in TSP samples.

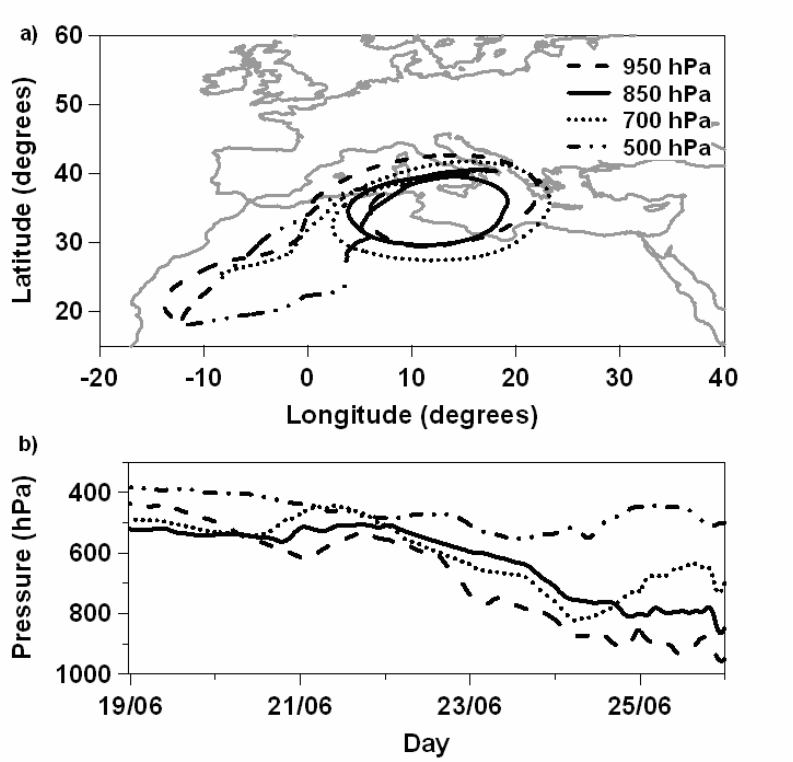

Figure 8.16 - (a) 7-days analytical back-trajectories for the air masses reaching the sampling site on 25 June 2007. (b) Pressure levels of each back-trajectory as a function of time.

Table 8.4 - Mass concentrations (μg/m^3) of the analyzed species in TSP and PM2.5 samples collected on 25 June 2007 and 15 March 2007. A-M is the total analyzed mass, S-M is the total sampled mass and (A-M)/(S-M) is the ratio between the analyzed and the sampled mass. Uncertainties for ions and for OC and EC are of 5%.

	25/06/2007		**15/03/2007**	
	TSP	**PM2.5**	**TSP**	**PM2.5**
F^-	0.1	0.005	0.004	0.1
Cl^-	0.4	-	0.7	-
NO_2^-	0.002	0.01	0.03	0.04
NO_3^-	0.4	0.1	1.7	1.0
SO_4^{2-}	6.4	4.7	8.5	8.6
Na^+	1.3	0.4	0.5	0.2
NH_4^+	0.7	1	3.9	4.4
K^+	0.5	0.5	0.7	0.7
Mg^{2+}	0.9	0.2	0.2	0.04
Ca^{2+}	6.8	2.2	1.8	0.3
OC	9.8	5.6	10.4	9.6
EC	1.3	0.8	2.5	2.2
A -M	28.7	15.6	30.9	27.3
S -M	79.2	37.3	49.9	34.6
(A-M)/(S -M) %	36	42	62	79

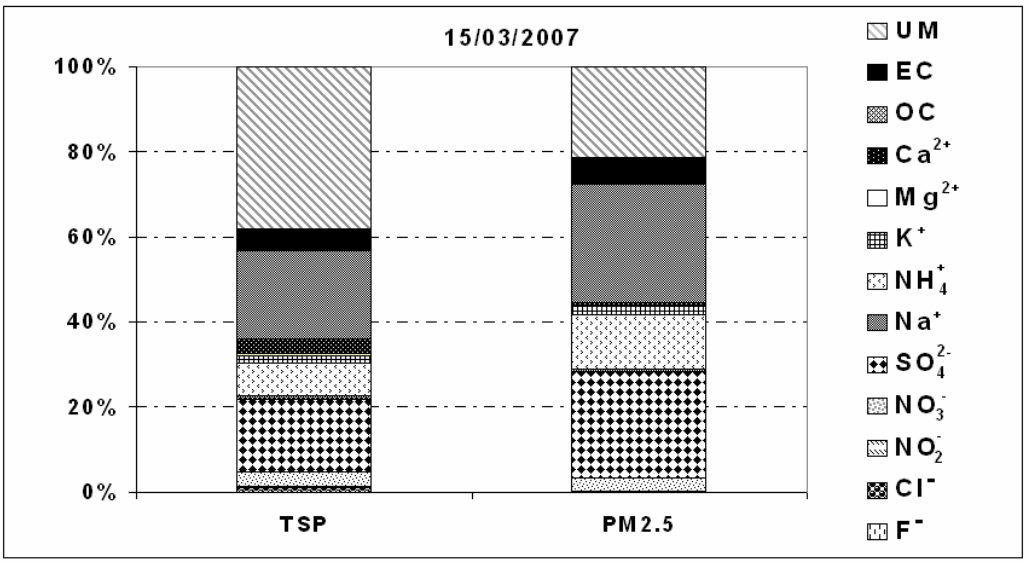

Figure 8.17 – Mass concentration percentages of all investigated species and undefined mass (UM) in the TSP and PM2.5 samples collected during the pollution event occurred on 15 March 2007.

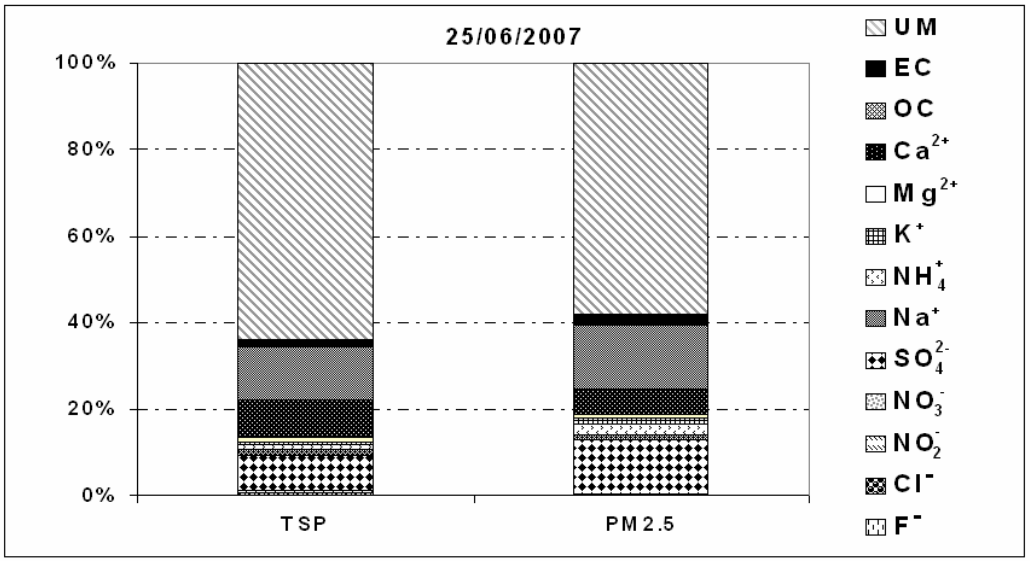

Figure 8.18 – Mass concentration percentages of all investigated species and undefined mass (UM) in the TSP and PM2.5 samples collected during the dust event occurred on 25 June 2007.

CONCLUDING REMARKS

The impact of aerosols on human health, reduction of visibility, global energy balance and climate change has motivated environmental scientists to conduct analyses of the microphysical aerosol properties over the past decades. The size and composition characterization of individual atmospheric particles is of relevance for modeling of atmospheric processes and for environmental control purposes.

The Mediterranean basin is one of the Earth regions where the aerosol climate effects are maxima. Studies performed in the Mediterranean basin suggest that both anthropogenic and natural sources significantly affect the composition of atmospheric particles mainly by means of long-range transport processes from the different regions around the basin: Europe, Africa, Atlantic Ocean and the Mediterranean itself.

The results of this PhD research contributes to the characterization of the central Mediterranean aerosol load providing results on the dependence of mass concentration and composition on particle size.

Several in situ mass concentration measurements have been performed at the Physics Department of University of Salento using different devices and the collected atmospheric particles have been characterized by vary techniques in order to define the main aerosol compositional properties in each particulate matter fraction.

Aerosol size distribution has been investigated by means an Aerosol Particle Sizer (APS) spectrometer presented and discussed in Chapter 2.

The particle size distribution of airborne particulate matter was also determined in this PhD work by a sampling system equipped with a 7-stage cascade impactor that separates the particulate matter during sampling on the basis of the particle size. This second method (reported in Chapter 3) has been used in this thesis to obtain additional results and to perform the chemical characterization of atmospheric size-fractionated particles by the scanning electron microscopy (SEM) technique.

APS analyses and cascade impactor mass concentration results have shown that aerosol size distribution generally exhibits a bimodal trend with a mode in fine fraction (particles with aerodynamic diameter < 1 μm) and a second peak in coarse size range (particles with aerodynamic diameter > 1 μm). Local emissions and the advection of long-range transported air masses have been considered responsible for the properties of the collected PM.

Morphological and elemental analyses by SEM/EDX technique on the size-fractioned samples collected by the 7-stage cascade impactor (discussed in Chapter 4) have revealed the significant dependence of particles' size, shape, and number on the 50% effective-cut-diameter. In addition the analyses have allowed inferring that nitrates, sulfates, and carbon were the main aerosol components of fine-mode particles, while sea-salts, carbonates, and minerals were the main aerosol components of coarse-mode particles. In particular, it has also been shown that dust particles mainly affect the coarse mode aerosol and that the anthropogenic fine mode aerosol can represent a significant fraction of the aerosol load even during a dust outbreak.

Particulate matter mass concentration results obtained for several sampling collections carried out during different years (2004, 2005, 2007 and 2008) have shown a significant daily variation of the PM mass concentration and composition. We have found that in all PM fractions the mass concentration and composition vary from sample to sample in the investigated periods. Changes in air mass transport arriving from different sources toward the sampling point have been considered responsible for these results, as several studies on advection patterns over South-East Italy have revealed (Kouyoumdjian and Saliba, 2005; Perrone et al., 2006; Bellantone et al., 2008; Santese et al., 2008).

The results reported in Chapter 6 referring to the year 2004 have shows in particular that mean mass concentrations are not significantly affected by the PM fraction. TSP, PM10, and PM2.5 mean mass concentrations (±1 standard deviation, SD) are 50±20 $\mu g/m^3$, 40±20 $\mu g/m^3$, and 40±10 $\mu g/m^3$, respectively. These results reveal the predominance in all collected samples of particles with the aerodynamic diameter < 2.5 μm.

The analyses performed on PM2.5 samples collected from June to October 2004 and from March to October 2005 (Chapter 7) have shown that 82% and 47% of the samples collected during 2004 and 2005 respectively exceeded the European reference annual limit value for the PM2.5 fraction, which is of 25 $\mu g/m^3$ (not to be exceeded from 1 January 2015).

PM2.5 mass concentration results referring to the year 2007 (Chapter 8) have shown that 23% of 117 samples collected from March to December exceeded the PM2.5 annual limit value. Finally, the PM2.5 mass concentration analysis performed during the year 2008 (Chapter 5) shown that 37% of PM2.5 samples collected from July

to November exhibits a mass concentration value higher than the PM2.5 reference annual limit value.

Mass percentages of ionic and elemental components tested in all analyzed PM collections were found to significantly vary from sample to sample. The different transfrontier advection events over the sampling site can be responsible for these results.

Ion Chromatography analyses have revealed that SO_4^{2-}, NO_3^-, NH_4^+, and Ca^{2+} are the predominant ionic components in all analyzed fractions.

In particular SO_4^{2-} and NH_4^+ are dominant species in fine fraction; instead Ca^{2+}, K^+, Mg^{2+} and Na^+ mass percentages are higher in coarse mode particles. NO_3^- can be present in both fine and coarse fractions.

The predominance of sulfate to nitrate particles has also been observed in all samples. This last result that has also been found at several coastal sites of the eastern and western Mediterranean, can be ascribed either to larger sulfur over nitrogen emissions and to long-lived particulate sulfates transported over the Mediterranean from the industrialized areas of north- and east-Europe. The formation in the atmosphere of secondary products from the reaction of aerosol particles with sulfuric acid that is favored in summer by the large solar irradiance and the poor occurrence of SO_2 wet removal processes also contribute to the predominance of sulfate to nitrate particles.

The results of this PhD research have also revealed that the sulfate/nitrate mass ratio was quite dependent on particulate matter fraction since coarse nitrates were predominant. The possible interaction of HNO_3 with crustal and marine particles may account for the increase of the coarse nitrate particulate.

The study has also shown that the mean NH_4^+ mass concentration was quite dependent on PM fraction: the NH_4^+ mass percentage increases as the total mass percentage due to alkaline ions decreases. Artefacts during sampling, as a consequence of the interaction of ammonium particulate with alkaline particulate matter, have been considered responsible for the minor presence of ammonium particulate in TSP and PM10 samples, respectively.

Elemental analyses have revealed that Si, Al, and Fe, which are of crustal origin, are prevalent metal components.

Organic/elemental carbon analyses performed in particular on fine fraction (PM2.5 and PM1), reported in Chapter 5, have revealed that the mass contribution of both carbonaceous species is significant over the monitoring site mainly in small particles. The analysis performed on TSP and PM2.5 simultaneously sampling

collections of the year 2007 (Chapter 8) supported this result. OC/EC analyses have shown in fact that organic and elemental carbon species are among the main component of fine fraction

Analytical back-trajectories analyses widely used in this PhD work have illustrated that the transport pathways from different regions can have different effects on aerosol size distribution and composition.

The anthropogenic components mainly present in the fine fraction, consist of nitrates, sulphates, and carbonaceous particles, especially originated from urban and industrial sources of European countries. Conversely, air masses coming from Sahara desert are predominantly responsible for the transport of coarse type mineral and crustal aerosols. Long-range transported polluted air masses from the Atlantic Ocean and from the Mediterranean itself may instead cause the advection of marine aerosols.

The results provided in this PhD thesis that are in satisfactory accordance with the ones retrieved at different coastal sites of the western and eastern Mediterranean can be considered representative of the central Mediterranean particulate matter. As a consequence they are of large interest, being the Mediterranean a climatically sensitive region where the aerosol climate effects are maxima. Hence, they can constitute a reference point for central Mediterranean transport modeling studies and local regulatory and policy makers.

REFERENCES

Abbey D., Nishino N., McDonnell W., Burchette R., Knustsen S., Beeson W. and Yang J., 1999. Long-term inhalable particles and other air pollutants related to mortality in non-smokers. American Journal of Respiratory Critical Care Medicine, 159, 373-382.

Atkinson R. and Lloyd A.C., 1984. Evaluation of kinetic and mechanistic data for modelling of photochemical smog. Journal of Physical and Chemical Reference Data, 13, 315-444.

Avila A., Queralt-Mitjans I. and Alarc M., 1997. Mineralogical composition of African dust delivered by red rains over the northeastern Spain. Journal of Geophysical Research, 102, 21977–21996.

Bardouki H., Liakakou H., Economu C., Sciare J., Smolik J., Zdimal V., Eleftheriadis K., Lazaridis M., Dye C. and Mihalopoulos N., 2003. Chemical composition of size-resolved atmospheric aerosols in the eastern Mediterranean during summer and winter. Atmospheric Environment, 37, 195–208.

Bashurova V.S., Dreiling V., Hodger T.V., Jaenicke R., Koutsenogii K.P., Koutsenogii P.K., Kraemer M., Makarov V.I., Obolkin V.A., Potjomkin V.L. and Pusep A.Y., 1992. Measurements of atmospheric condensation nuclei size distributions in Siberia. Journal of Aerosol Science, 23, 191–199.

Bellantone V., Carofalo I., De Tomasi F., Perrone M.R., Santese M., Tafuro A.M. and Turnone A., 2008. In situ samplings and remote sensing measurements to characterize aerosol properties over South-East Italy. Journal of Atmospheric and Oceanic Technology, 25(8), 1341-1356.

Bergametti G., Dutot A.L., Buat-Menard P., Losno R. and Remoudaky E., 1989. Seasonal variability of the elemental composition of atmospheric aerosol particles over North western Mediterranean atmosphere. Tellus, 41B, 353-361.

Biegalski S.R, Landsberger S. and Hoff R.M., 1998. Source-Receptor modeling using trace metals in aerosols collected at three rural Canadian great lakes sampling stations. Journal of Air and Waste Management Association, 48, 227-237.

Birch M.E. and Cary R.A., 1996. Elemental carbon-based method for monitoring occupational exposures to particulate diesel exhaust. Aerosol Science and Technology, 25, 221-241.

Blanchard D.C. and Woodcock A.H., 1957. Bubble formation and modification in the sea and in its meteorological significance. Tellus, 9, 145-152.

Blanco, A., De Tomasi F., Filippo E., Manno D., Perrone M.R., Serra A., Tafuro A.M. and Tepore A., 2003. Characterization of African dust over southern Italy. Atmospheric Chemistry and Physics, 3, 1-13.

Bolle, H.J., 2003. Mediterranean Climate, Climate, Climate variability and impacts in the Mediterranean area: an Overview. Springer-Verlag, Berlin.

Buccolieri A., Buccolieri G., Cardellicchio N., Dell'Atti A. and Florio E.T., 2005. PM10 and heavy metals in particulate matter of the province of Lecce (Apulia, Southern Italy). Annali di Chimica, 95, 15-25.

Calvert J.G. and Stockwell W.R., 1983. Acid generation in the troposphere by gas-phase chemistry. Environmental Science and Technology, 17, 430A.

Cao J.J., Lee S.C., Ho K.F., Zou S.C., Chow J.C., Fung K., Watson J.G. and Li Y., 2004. Spatial and seasonal variations of atmospheric organic carbon and elemental carbon in Pearl River Delta Region, China. Atmospheric Environment, 38, 4447-4456.

Carofalo I., Fermo P., Perrone M.R. and Piazzalunga A., 2008. Advection patterns and composition of TSP and PM2.5 samples over south-east Italy. Proceeding in: Chemical Engineering Transactions, 18, 185-192.

Cheng S. and Lam K.C., 1998. An analysis of winds affecting air pollution concentrations in Hong Kong. Atmospheric Environment, 32, 2559-2567.

Chester R., Nimmo M., Alarcon M., Saydam C., Murphy K.J.T., Sanders G.S. and Corcoran P., 1993. Defining the chemical character of aerosols from the atmosphere of the Mediterranean-sea and surrounding regions. Oceanologica Acta, 16**,** 231–246.

Chester J.C, Nimmo M., Fones G.R., Keyse S. and Zhang Z., 2000. Trace metal chemistry of particulate aerosols from the UK mainland coastal rim of the NE Irish Sea. Atmospheric Environment, 34, 949-958.

Chow J.C., 1995. Critical review: Measurement methods to determine compliance with ambient air quality standards for suspended particles. Journal of the Air and Waste Management Association, 45, 320-382.

Chow J.C. and Watson J.G., 2002. PM2.5 carbonate concentrations at regionally representative Interagengy Monitoring of Protected Visual Environment Sites. Journal of Geophysical Research, 107 (D21), ICC6-1-ICC6-9.

Clarke W.E. and Whitby K.T., 1967. Concentration and size distribution measurements of atmospheric aerosols and a test of the self-preserving size distribution. Journal of Atmopsheric Sciences, 24, 677-687.

Council Directive 1999/30/EC, 1999. Relating to limit values for sulphur dioxide, nitrogen dioxide and oxides of nitrogen, particulate matter and lead in ambient air. Official Journal European Communities. Legis 163, 41-60.

Council Directive 2008/50/EC, 2008. Of the European Parliament and of the Council of 21 May 2008 on ambient air quality and cleaner air for Europe. Official Journal European Communities. Legis 152, 1–44.

d'Almeida G.A. and Schutz L., 1983. Number, mass and volume distributions of mineral aerosol and soils of the Sahara. Journal of Climate and Applied Meteorology, 22, 233-243.

Danalatos D., and Glavas S., 1999. Gas phase nitric acid, ammonia and related particulate matter at a Mediterranean coastal site, Patras, Greece. Atmospheric Environment, 33, 3417–3425.

Datar S.V., Mukhopadhyay B. and Srivastava H.N., 1996. Trends in background air pollution parameters over India. Atmospheric Environment, 30, 3677-3682.

Deepak A. and Gali G., 1991. The International Global Aerosol Program (IGAP) Plan. Deepak Publishing, Hampton, VA.

De Leeuw G., 1986. Vertical profiles of giant particles close above the sea surface. Tellus, 38B, 51-61.

Dentener F., Carmichael G.R., Zhang Y., Lelieveld J. and Crutzen P.J., 1996. Role of mineral aerosol as a reactive surface in the global troposphere. Journal of Geophysical Research, 101, 22869-22889.

De Tomasi F., Tafuro A.M and Perrone M.R., 2006. Height and seasonal dependence of aerosol optical properties over south-east Italy. Journal of Geophysical Research, 111, D10203, doi: 10.1029/2005JD006779.

Dockery D.W., Pope C.A., Xu X., Spengler J.D., Ware J.H., Fay M.E., Ferris Jt. B.G. and Speizer F.E., 1993. An association between air pollution and mortality in six US cities. New England Journal of Medicine, 329, 1753-1759.

Elsom D.M. and Chandler T.J., 1978. Meteorological controls upon ground level concentrations of smoke and sulphur dioxide in two urban areas of United Kingdom. Atmospheric Environment, 12, 1543-1554.

Englert N., 2004. Fine particles and human health – a review of epidemiological studies. Toxicology Letters, 149, 235-242.

Erisman, J.W. and Schaap, M., 2004. The need for ammonia abatement with respect to secondary PM reduction in Europe. Environmental Pollution, 129, 159-163.

European Standard EN 481, 1993. Workplace atmospheres – Size fraction definitions for measurement of airborne particles. CEN, Brussels, Belgium.

European Standard EN 12341, 1999. Air quality-Determination of the PM10 fraction of suspended particulate matter. Reference method and field test procedure to demonstrate reference equivalence of measurement methods. CEN, Brussels, Belgium.

Fermo P., Piazzalunga A., Vecchi R. And Valli G., 2006a. Set-up of Extraction Procedures for Ions Quantification in Aerosol Samples. Proceeding in: Chemical Engineering Transactions, 10, 203-208.

Fermo P., Piazzalunga A., Martino F., Vecchi R., Valli G. and D'Alessandro A., 2006b. Assessment of Organic and Elemental Carbon in Atmospheric Aerosol Samples. Proceeding in: Chemical Engineering Transactions, 10, 83-88.

Fitzgerald J.W., 1991. Marine aerosols: a review. Atmospheric Environment, 25A, 533-545.

Formenti P., Prati P., Zucchiatti A., Lucarelli F. and Mando P.A., 1996. Aerosol study in the town of Genova with a PIXE analysis. Nuclear Instruments and Methods in Physics Research B, 113, 359-362.

Formenti P., Boucher O., Reiner T., Sprung D., Andreae M.O., Wendisch M., Wex H., Kindred D., Tzortziou M., Vasaras A. and Zerefos C., 2002. STAARTE-MED 1998 summer airborne measurements over Aegean Sea. 2. Aerosol scattering and absorption, and radiative calculations. Journal of Geophysical Research, 107, D21, doi:10.1029/2001JD001536.

Ganor E., Levin Z. and Van Grieken R., 1998. Composition of individual aerosol particles above the Israelian Mediterranean coast during the summer time. Atmospheric Environment, 32, 1631-1642.

Giorgi, F., 2006. Climate change hot-spots. Geophysical Research Letters, 33, L08707, doi:10.1029/2006GL025734.

Goodhew P.J. and Humphreys F.J., 1988. Electron microscopy and analysis. Taylor and Francis.

Haaf W. and Jaenicke R., 1980. Results of improved size distribution measurements in the Aitken range of atmospheric aerosols. Journal of Aerosol Science, 11, 321-330.

Harrison R.M., Deacon A.R., Jones M.R. and Appleby R.S., 1997. Sources and process affecting concentrations of PM10 and PM2.5 particulate matter in Birmingham UK. Atmospheric Environment, 24, 4103-4117.

Henning S., Weingartner E., Schwikowski M., Gaggeler H.W., Gehring R., Hinz K.P., Trimborn A., Splengler B. and Baltensperger U., 2003. Seasonal Variation of Water-Soluble Ions of the Aerosol at the High-Alpine Site Jungfraujoch (3580 m asl). Journal of Geophysical Research, 108(D1) doi: 10.1029/2002JD002439.

Hidy G.M., 1994. Atmospheric sulphur and nitrogen oxides. Academic Press, San Diego, California.

Hlavay J., Polyak K. and Wesemann G., 1992. Particle size distribution of mineral phases and metals in dusts collected at different workplaces. Fresenius Journal of Analytical Chemistry, 344, 319-321.

Hobbs P.V., Bowdle D.A. and Radke L.F., 1985. Particles in the lower troposphere over the high plains of the United States. 1. Size distributions, elemental compositions, and morphologies. Journal of Climate and Applied Meteorology, 24, 1344-1356.

Hoek G., Brunekreef B., Goldbohm S., Fisher P. and Van den Brant P., 2002. Association between mortality and indicators of traffic-related air pollution in the Netherlands: a cohort study. The Lancet, 360 (9341), 1203-1209.

Hoppel W.A., Fitzgerald J.W., Frick G.M., Larson R.E. and Mack E.J., 1989. Atmopsheric aerosol size distribution and optical properties in the marine boundary layer over the Atlantic Ocean. NRL Report 9188, Washington, DC.

Husar R.B., Prospero J.M. and Stowe L.L., 1997. Characterization of tropospheric aerosol over the ocean with the NOAA Advanced Very High Resolution Radiometer optical thickness operational product. Journal of Geophysical research, 102, 16889-16909.

Incecik S., 1996. Investigation of atmospheric conditions in Istanbul leading to air pollution episodes. Atmospheric Environment, 30, 2739-2749.

Jacobson M. Z., 2001. Strong radiative heating due to the mixing state of black carbon in atmospheric aerosols. Nature, 409, 695-697.

Jaenicke R and Schutz L., 1978. Comprehensive study of physical and chemical properties of the surface aerosol in the Cape Verde Islands region. Journal of Geophysical Research, 83, 3583-3599.

Jaenicke R., 1993. Troposheric aerosols, in Aerosol-Cloud-Climate Interactions. Edited by Hobbs P.V. Academic Press, San Diego, CA, 1-31.

Kalivitis N., Gerasopoulos E., Vrekoussis M., Kouvarakis G., Kubilay N., Hatzianastassiou N., Vardavas I. and Mihalopoulos N., 2007. Dust transport over the eastern Mediterranean derived from Total Ozone Mapping Spectrometer, Aerosol Robotic Network, and surface measurements. Journal of Geophysical Research, 112, D03202, doi:10.1029/2006JD007510.

Kallos G., Kassomenos P. and Pielke R.A., 1993. Synoptic and mesoscale weather conditions during air pollution episodes in Athens. Boundary Layer Meteorology, 62, 163-164.

Kazadzis S., Bais A., Amindis V., Balis D., Meleti C., Kourementi N., Zerefos C.S., Rapsomanikis S., Petrakakis M., Kelesis A., Tzoumaka P. and Kelektsoglou K., 2007. Nine Years of UV aerosl optical deph measurements at Thessaloniki, Greece. Atmospheric Chemistry and Physics, 7 (8), 2091-2101.

Keene W.C., Pszenny A.A.P., Galloway J.N. and Hawley M.E., 1986. Sea-Salt corrections and interpretation of constituent ratios in marine precipitation. Journal of Geophysical Research, 91, 6647-6658.

Khemani L.T., Momin G.A., Naik M.S., Vijaya Kumar R. and Ramanamurthy V., 1982. Chemical composition and size distribution of atmospheric aerosols over the Deccan Plateau, Inda. Tellus, 34, 152-158.

Kiehl J.T. and Rodhe H., 1995. Modeling geographical and seasonal forcing due to aerosols. Aerosol Forcing of Climate. Edited by Charlson R.J.and Heintzenberg J., Wiley, New York, 281-296.

Kim M.K., Teffera S., and Zeldin M.D., 2000. Characterization of PM2.5 and PM1 in the South Coast Air Basin of Southern California: part 1-spatial variations. Journal of the Air and Waste Management Association, 50, 2034-2044.

Kloster S., Feichter J., Maier-Reimer E., Six K.D., Stier P. and Wetzel P., 2006. DMS cycle in the marine ocean-atmosphere system – a global study. Biogeosciences, 3, 29-51.

Koutsenogii P.K., Bufetov N.S. and Drosdova V.I., 1993. Ion composition of atmospheric aerosol near Lake Baikal. Atmospheric Environment, 27A, 1629-1633.

Koutsenogii P.K. and Jaenicke R., 1994. Number concentration and size distribution of atmospheric aerosol in Siberia. Journal of Aerosol Science, 25, 377-383.

Kouyoumdjian, H. and Saliba N.A., 2005. Ion concentrations of PM10-2.5 and PM2.5 aerosols over the eastern Mediterranean region: seasonal variation and source identification. Atmospheric Chemistry and Physics Discussions, 5, 13053-13073.

Kunzli N., Kaiser R., Medina S., Studnicka M., Chanel O., Filliger P., Hery M., Horak F., Puybonnieux-Texier V. and Quénel P., 2000. Public impact of outdoor and traffic-related air pollution: a European assessment. The Lancet, 356, 795-801.

Lee D.S., Garland J.A. and Fox A.A., 1994. Atmospheric concentrations of trace elements in urban areas of the United Kingdom. Atmospheric Environment, 28(16), 2691-2713.

Levin Z. and Lindberg J.D., 1979. Size distribution, chemical composition and optical properties of urban and desert aerosols in Israel. Journal of Geophysical Research, 84, 6941-6950.

Li X., Maring H., Savoie D., Voss K. and Prospero J.M., 1996. Dominance of mineral dust in aerosol light scattering in the North Atlantic trade winds. Nature, 380, 416-419.

Lippmann M., 1978. Filter media for air sampling. In: Air Sampling Instruments for Evaluation of Atmospheric Contaminants, Section N. Proceeding of: American Conference of Governmental Industrial Hygienists, Cincinnati.

Lonati, G., Giugliano, M., Butelli, P., Romele, L. And Tardivo, R., 2005. Major Chemical components of PM2.5 in Milian (Italy). Atmospheric Environment, 39, 1925-1934.

Luria M., Peleg M., Sharf G., Siman Tov-Alper D., Spitz N., Ben Ami Y., Gawii Z., Lifschitz B., Yitzchachi A. and Seter I., 1996. Atmospheric sulfur over the Eastern Mediterranean region. Journal of Geophysical Research, 101, 25917-25930.

Marenco F., Bonasoni P., Calzolari F., Ceriani M., Chiari M., Cristofanelli P., D'Alessandro A., Fermo P., Lucarelli F. , Mazzei F., Nava S., Piazzalunga A., Prati P., Valli G. and Vecchi R., 2006. Characterization of Atmospheric Aerosols at Monte Cimone, Italy, During Summer 2004: Source Apportionment and Trasport Mechanism. Journal of Geophysical Research, 111, D24202, doi:10.1029/2006JD007145.

McGregor G.R., 1996. Identification of air quality affinity areas in Birmingham, UK. Applied Geography, 16, 109-122.

McMurry, P.H., 2000. A review of atmospheric aerosol measurements. Atmospheric Environment, 34(12-14), 1959-1999.

Medeiros B., Hall A. and Stevens B., 2005. What control the mean depth of PBL. Journal of Atmospheric Science, 62, 3157-3172.

Mészaros A. and Vissy K., 1974. Concentration, size distribution and chemical nature of atmospheric particles in remote ocean areas. Journal of Aerosol Science, 5, 101-109.

Mihalopoulos, N., Stephanou, E., Kanakidou, M., Pilitsidis, S. and Bousquet P., 1997. Tropospheric aerosol ionic composition in the Eastern Mediterranean region. Tellus, 49B, 314-326.

Monahan E.C., Fairall C.W., Davidson K.L. and Jones-Boyle P., 1983. Observed inter-relationships amongst 10-m-elevation winds, oceanic whitecaps, and marine aerosols. The Quarterly Journal of the Royal Meteorological Society, 109, 379-392.

Monahan, E.C., Spiel D.E. and Davidson K.L., 1986. A model of marine aerosol generation via whitecaps and wave disruption, Oceanic whitecaps and their role in air-sea exchange processes. Edited by Monahan E.C. and MacNiocaill G. Reidel D. Publishing, Dordrecht.

Monn Ch., Braendli O., Schaeppi G., Chandler Ch., Ackermann-Liebrich U., Leunberger Ph. and Team S., 1995. Particulate matter < 10 μm (PM10) and total suspended particulates (TSP) in urban, rural and alphine air in Switzerland. Atmospheric Environment, 29, 2565-2573.

Moorthy K.K., Nair P.R. and Murthy B.V.K., 1991. Size distribution of coastal aerosols: effects of local sources and sinks. Journal of Applied Meteorology, 30, 844-852.

Paoletti L., De Berardis B., and Diociaiuti M., 2002. Physicochemical characterisation of the inhalable particulate matter (PM10) in an urban area: an analysis of the seasonal trend. Science of the Total Environment, 292, 265–275.

Penner J.E., Eddleman H. and Novakov T., 1993. Towards the development of a global inventory for black carbon emissions. Atmospheric Environment, 27A, 1277-1295.

Penner J.E., Chuang C.C. and Grant K., 1998. Climate forcing by carbonaceous and sulphate aerosols. Climate Dynamics, 14(12), 839-852.

Perrone M.R., Santese M., Tafuro A.M., Holben B. and Smirnov A., 2005. Aerosol load characterization over South-East Italy by one year of AERONET sun-photometer measurements. Atmospheric Research, 75, 111–133.

Perrone M.R., Turnone A., Buccolieri A., and Buccolieri G., 2006. Particulate matter characterization at a coastal site of south east Italy. Journal of Environmental Monitoring, 8, 183–190.

Polla-Mattiot F. and Scafe E., 1998. The effect of rain on suspended particulate matter and other pollutants in an urban area. Edited by Brebbia C.A., Ratto C.F. and Power H. Air Pollution VI, WIT Press, CMP Southampton, UK.

Pope C.A., Burnet R.T., Thun M.J., Calle E.E., Krewski D., Ito K. and Thurston G.D., 2002. Lung cancer, cardiopulmonary mortality, and long term exposure to fine particulate air pollution. Journal of Air and Waste Management Association, 287, 1132-1141.

Pui D.Y.H., 1996. Direct-reading instrumentation for workplace aerosol measurements. A Review. Analyst, 121, 1215-1224.

Putaud J. P., Van Dingenen R., Dell'Acqua A., Raes F., Matta E. Decessari S., Facchini M.C. and S. Fuzzi, 2004. Size-segregated aerosol mass closure and chemical composition in MonteCimone (I) during MINATROC. Atmospheric Chemistry and Physics, 4, 889-902.

Querol X., Alastuey A., Puicercus J.A., Mantilla E., Miro J.V., Lopez-Soler A., Plana F. and Artinano B., 1998. Seasonal evolution of suspended particles around a large coal-fired power station: particulate levels and sources. Atmospheric Environment, 32, 1963-1978.

Querol X., Alastuey A., Moreno T., Viana M.M, Castillo S., Pey J., Rodriguez S., Artinano B., Salvador P., Sanchez M., Garcia Dos Santos S., Herce Garraleta M.D., Fernandez-Patier R., Moreno-Graud S., Negral L., Minguillon M.C., Monfort E., Sanz M.J., Palomo-Marin R., Pinilla-Gil E., Cuevas E., de la Rosa J. and Sanchez de la Campa A., 2008. Spatial and temporal variations in airborne particulate matter (PM10 and PM2.5) across Spain 1999-2005. Atmospheric Environment, 42, 3964-3979.

Raes F., Dingenen R.V., Vignati E., Wilson J., Putaud J.P., Seinfeld J.H. and Adams P., 2000. Formation and cycling of aerosols in the global troposphere. Atmospheric Environment, 34, 4215-4240.

Rodriguez S., Querol X., Alastuey A. and Mantilla E., 2002. Origin of high summer PM10 and TSP concentrations at rural sites in Eastern Spain. Atmospheric Environment, 36, 3101-3112.

Ro C.U., Oh K.Y., Kim H., Chun Y., Osan J., de Hoog J. and Van Grieken R., 2001. Chemical speciation of individual atmospheric particles using low-Z electron probe X-ray microanalysis: characterizing "Asian Dust" deposited with rainwater in Seoul, Korea. Atmospheric Environment, 35, 4995-5005.

Samet M.J., Dominici F., Curriero F.C., Coursac I. and Zeger S.L., 2000. Fine particulate air pollution and mortality in 20 US cities, 1978-1994. New England Journal of Medicine, 343, 1742-1749.

Santese M., De Tomasi F. and Perrone M.R., 2007. AERONET versus MODIS aerosol parameters at different spatial resolutions over southeast Italy. Journal of Geophysical Research, 112, D10214, doi:10.1029/2006JD007742.

Santese M., De Tomasi F. and Perrone M.R., 2008. Advection patterns and aerosol optical and microphysical properties by AERONET over south-east Italy in the Central Mediterranean. Atmospheric Chemistry and Physics, 8, 1881-1896.

Saxena P. and Seigneur C., 1987. On the oxidation of SO_2 to sulphate in the atmospheric aerosols. Atmospheric Environment, 21, 807-812.

Seinfeld J.H. and Pandis S.N., 1998. Atmopsheric Chemistry and Physics – From Air pollution to climate change. John Wiley, New York.

Smirnov A., Royer A., O'Neill N.T. and Tarussov A., 1994. A study of the link between synoptic airmass type and atmospheric optical parameters. Journal of Geophysical Research, 99, 20967-20982.

Smolik J., Zdimal V., Schwarz J., Lazarinis M., Havranek V., Eleftheriadis K., Mihalopoulos N., Bryant C. and Colbeck I., 2003. Size resolved mass concentration and elemental composition of atmospheric aerosols over Eastern Mediterranean area. Atmospheric Chemistry and Physics, 3, 2207-2216.

Spurny, K.R., 1999. Analytical chemistry of aerosol. Lewis Publishers.

Stieb M.D., Stan J. and Burnett R.T., 2002. Meta-analysis of time series studies of air pollution and mortality: effects of gases and particles and the influence of cause of death, age and season. Journal of Air and Waste Management Association, 52, 470-484.

Stull R.B., 1988. An introduction to boundary layer meteorology. Lower Academic Publishers, the Netherlands.

Taylor S.R.,1964. Geochimica and Cosmochimica Acta.

Turnone A. PhD thesis: Campionamento e analisi del particolato atmosferico. Department of Scienza dei Materiali. University of Salento.

US – EPA, 1986. Second addendum to air quality criteria for particulate matter and sulphur oxides (1982): assessment of newly available health effects information. US Environmental Protection Agency, Washington, DC.

US – EPA, 1997. Mercury Study Report to Congress. U.S. Environmental Protection Office of Air Quality Planning and Standard and Office of Research and Development. US Environmental Protection Agency, Washington, DC.

US – EPA, 1999. Compendium method TO-9A: method for the determination of polychlorinated, polybrominated and brominated/chlorinated dibenzo-*p*-dioxins and dibenzofurans in ambient air. US Environmental Protection Agency, Washington, DC.

Van Vaeck L. and Van Cauwenberghe K., 1978. Cascade impactor measurements of the size distribution of the major classes of organic pollutants in atmospheric particulate matter. Atmospheric Environment, 12, 2229-2239.

Vedal S., 1997. Critical review: ambient particles and health: lines that divide. Journal of air and Waste Management Association, 47(5), 551-581.

Venkataraman C. and Friedlander S.K., 1994. Size distributions of polycyclic aromatic hydrocarbons and elemental carbon. 2. Ambient measurements and effects of atmospheric processes. Environmental Science and Technology, 28, 563-572.

Viana, M., Pérez, C., Querol, X., Alasuey, A., Nickovic, S. and Baldasano, J.M., 2005. Spatial and temporal variability of PM levels and composition in a complex summer atmospheric scenario in Barcelona (NE Spain). Atmospheric Environment, 39, 5343-5361.

Wall S.M., John W. and Ondo J.L., 1988. Measurement of aerosol size distributions for nitrate and major ionic species. Atmospheric Environment, 22, 1649-1656.

Wang C.S. and Street R.L., 1978. Measurements of spray at an air-water interface. Dnamics of Atmosphere and Oceans, 2, 141-152.

Warneck P., 1988. Chemistry of the Natural Atmosphere. Academic Press, San Diego, CA.

Watson J.G., 2002. Visibility: science and regulation. Journal of the Air and Waste Management Association, 52 (6), 628-713.

Whitby K.T. and Cantrell B., 1976. Fine particles. Proceeding of: International Conference on Environmental Sensing and Assessment. Las Vegas, NV, Institute of Electronic Engineers.

Whitby K.T., 1978. The physical characteristic of sulphur aerosol. Atmospheric Environment, 12, 135-159.

WHO, 2003. Health aspects of air pollution with particulate matter, ozone and nitrogen dioxide, report on a WHO working group, 13-15 January 2003, Bonn Germany. WHO, Regional Office for Europe, Copenhagen.

Woolf D.K., Monahan E.C. and Spiel D.E., 1988. Quantification of the marine aerosol produced by whitecaps. American Meteorological Society, Boston M.A., 182-185.